Stefan Koch, MSc

Analysis and Synthesis of Discrete-Time Sliding Mode Controllers and Observers

DOCTORAL THESIS

to achieve the university degree of
Doktor der technischen Wissenschaften

submitted to
Graz University of Technology

Supervisor
Univ.-Prof. Dipl-Ing. Dr.techn. Martin Horn

Co-Supervisor
Assoc.Prof. Dipl.-Ing. Dr.techn. Markus Reichhartinger

Institute of Automation and Control

Faculty of Electrical and Information Engineering

Graz, July 2019

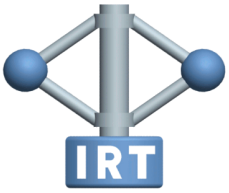

Institute of Automation and Control
Graz University of Technology
Inffeldgasse 21/B
8010 Graz, Austria
https://www.tugraz.at/institute/irt

Affidavit

I declare that I have authored this thesis independently, that I have not used other than the declared sources/resources, and that I have explicitly indicated all material which has been quoted either literally or by content from the sources used. The text document uploaded to TUGRAZonline is identical to the present doctoral thesis.

Graz, _____ _____

Date Signature

Abstract

Feedback loops designed using the ideas of sliding mode control are known to exhibit a number of appealing features. A very prominent characteristic is their insensitivity against bounded matched disturbances and model uncertainties. However, it is well-known that improper discrete-time realizations of sliding mode based algorithms cause so-called discretization chattering, i.e., undesired oscillations in the control signal. These oscillations typically deteriorate the closed-loop performance or even cause damages.

This thesis deals with the analysis and development of tools for the characterization of chattering effects as well as with the development of discretization schemes that entirely avoid this effect. The theoretical results are supported by simulations and experiments.

For the characterization of chattering effects, i.e., the determination of frequency and amplitude of oscillations, frequency domain techniques such as the describing function method and the locus of perturbed relay system approach and their extension to the sampled data configuration are studied. The so-called sampled describing function approach is revisited and a formula for the computation of the locus of perturbed relay system approach is derived. In contrast to the describing function method, the locus of perturbed relay system approach yields exact results for the oscillation frequency. Stability properties of limit cycles and the basin of attraction of periodic solutions are discussed.

Then, novel discrete-time variants of the super-twisting algorithm are presented. In contrast to the commonly employed explicit Euler discretized super-twisting dynamics, the proposed schemes are exact in the sense that in the unperturbed case the controllers ensure convergence to the origin. Discretization chattering effects are avoided whilst the robustness properties are preserved. The approach is extended to a family of homogeneous differentiators, including the well-known arbitrary-order robust exact differentiator.

Finally, exploiting the notion of homogeneous eigenvalues, a new family of continuous-time arbitrary-order homogeneous state feedback controllers is derived. A formula that allows to design controllers for all combinations of the system's relative degree and the desired homogeneity degree of the closed-loop system is presented. The structure of the resulting controllers permits realization in a discrete-time environment straightforwardly using the developed ideas.

Kurzfassung

Strukturvariable Regelkreise mit Gleitzustand (engl.: *Sliding Mode*) zeichnen sich durch eine Reihe attraktiver Merkmale aus. Ein wesentlicher Vorteil ist ihre Unempfindlichkeit gegenüber beschränkten Störungen und Modellunsicherheiten. Eine unsachgemäße zeitdiskrete Realisierung von Gleitzustandsreglern führt jedoch zu sogenanntem "Diskretisierungs-Rattern" (engl.: *Chattering*). Das sind unerwünschte hochfrequente Schwingungen der Stellgröße. Diese wirken sich negativ auf die erreichbare Regelgüte aus und können im schlimmsten Fall sogar zu Schäden führen.

Die vorliegende Arbeit beschäftigt sich mit der Analyse und Entwicklung von Methoden zur Beschreibung von Rattern und dessen Einfluss auf die Regelgüte, sowie mit der Entwicklung von Diskretisierungsmethoden, die diesen negativen Effekt vollständig vermeiden. Die theoretischen Ergebnisse werden durch Simulationen und experimentelle Ergebnisse validiert.

Für die Charakterisierung von Rattern hinsichtlich der Schaltfrequenz und Amplitude werden Frequenzbereichsmethoden betrachtet. Konkret sind dies die Methode der harmonischen Linearisierung und die sogenannte LPRS (Locus of Perturbed Relay System) Methode. Für beide wird eine Erweiterung auf den Abtastregelkreis diskutiert wobei eine Formel für die Berechnung der Ortskurve nach der LPRS Methode abgeleitet wird. Im Gegensatz zur Analyse mithilfe von Beschreibungsfunktionen liefert die LPRS Methode ein exaktes Ergebnis für die Schwingungsfrequenz. Weiters werden die Stabilitätseigenschaften von Grenzzyklen und die Berechnung des Einzugsbereichs von periodischen Lösungen diskutiert.

Anschließend werden neue zeitdiskrete Varianten des sogenannten Super-Twisting Algorithmus vorgestellt. Im Gegensatz zu dem üblicherweise verwendeten Vorwärts-Euler Verfahren sind die vorgeschlagenen Varianten insofern exakt, dass die Lösungen im ungestörten Fall zur Ruhelage konvergieren. Rattern aufgrund der Diskretisierung wird vermieden, während die Robustheitseigenschaften erhalten bleiben. Der Ansatz wird auf eine Klasse von homogenen Differenzierern erweitert, welche den bekannten robusten exakten Differenzierer beliebiger Ordnung einschließt.

Unter Ausnutzung sogenannter homogener Eigenwerte wird dann eine Klasse von zeitkontinuierlichen homogenen Zustandsreglern vorgeschlagen. Es wird eine Formel hergeleitet, welche den Entwurf von Reglern für beliebige Relativgrade der Strecke und beliebige Homogenitätsgrade des geschlossenen Regelkreises erlaubt. Die Struktur der erhaltenen Regelgesetze erlaubt dabei eine geradlinige zeitdiskrete Umsetzung basierend auf den zuvor gezeigten Ideen.

Acknowledgments

This thesis was developed in the course of my activity as a university project assistant at the Institute of Automation and Control at Graz University of Technology. Several persons have contributed in their own particular way to this thesis.

First and foremost I wish to thank my supervisor Prof. Martin Horn for providing me the opportunity to work on this thesis. I am grateful for his guidance, advice and support during the planning and development of this research work.

The present document would not have been possible without the guidance and help of my co-supervisor Assoc. Prof. Markus Reichhartinger. Many thanks for the insightful discussions and suggestions and the patience when reading draft after draft of every paper.

I also wish to thank Prof. Franck Plestan for his interest in my work and his participation in my thesis committee.

I also had great pleasure of working with Prof. Leonid Fridman whose suggestions and advice were invaluable.

I am also grateful to Prof. Wolfgang Werth for drawing my attention to control systems engineering by his excellent lectures and for encouraging me to pursue my interests in this field.

Many thanks to the staff of the Institute of Automation and Control for the friendly working atmosphere, the numerous interesting discussions and their help, whenever I needed it.

I am extremely grateful to my family and friends for the support throughout my years of study and for giving me the necessary distraction from work. Finally, very warm thanks go to my love Daniela and my daughter Olivia for their daily patience, encouragements and the unconditional support.

Graz, July 2019 Stefan Koch

Contents

1 Introduction

Model-based control relies on a mathematical model that describes the behavior of the plant to be controlled. A model-based approach usually allows designing more sophisticated and generic controllers when compared to, e.g., PID controllers. However, there is always a mismatch between the model and the system which, e.g., arises from uncertain plant parameters, unknown external disturbances, and unmodeled dynamics. The controller usually needs to be designed such that it guarantees desired performance of the closed-loop system despite these uncertainties. So-called robust control techniques explicitly deal with such model uncertainties and unknown external disturbances.

Sliding mode control (SMC) is one particular nonlinear robust control technique that exhibits a number of appealing features. The most striking feature is its robustness with respect to bounded matched uncertainties, see [1, 2, 3, 4]. The design of a sliding mode (SM) controller aims for the finite-time stabilization of a sliding variable which in consequence ensures a predefined dynamic behavior of the feedback loop. Once in a sliding mode, the dynamics are insensitive to the above mentioned perturbations. A first-order sliding mode (FOSM) controller achieves this insensitivity by means of a discontinuous control law, [5, 6]. However, the discontinuous nature of the control law often is considered as the major drawback of sliding mode control as an improper application or realization may lead to the so-called chattering effects [7, 8]. The chattering effects, although not uniquely defined in literature, are usually described as self-sustaining high frequency oscillations in the control signal, in the plant output and in the system states [9, 10]. These oscillations do not *only* lower the control accuracy but also cause actuator wear or even damage the system. There are various root causes for chattering effects. The sources are usually grouped into two categories: the discretization chattering, which comprises effects related to the discrete-time realization of the controller and the control chattering which embodies the effects designated to model imperfections.

In recent years much attention has been paid to the reduction of the chattering effects which led to concept of higher-order sliding mode (HOSM) control. The main idea of higher-order sliding mode algorithms is to reduce the chattering effects by substituting the discontinuous control signal by a continuous one while maintaining certain robustness features [11, 12, 13, 14, 15]. The continuous control signal entails some restrictions regarding the rate of change of the disturbance. A HOSM controller which generates a continuous control signal cannot anymore compensate discontinuous disturbances, but is capable to reject, e.g., Lipschitz continuous disturbances. If applied properly, HOSM controllers are basically able to reduce the chattering effects and ensure more accurate control of the sliding variable. However, recent analysis, which aimed to quantify and compare the chattering effects in systems controlled by continuous and discontinuous sliding mode controllers of certain orders brought some interesting insights on the continuous HOSM controllers. Other than originally assumed, the chattering effects

are not reduced in any case when replacing a discontinuous controller with a continuous one. Depending on the characteristics of the plant, and in particular the actuator dynamics, performance may even be worsened (see [16]).

Over and above the appropriate choice of the controller order also its proper discrete-time realization plays a crucial role in the chattering mitigation. Due to its nonlinear nature, it is common to design sliding mode controllers in the continuous-time domain. The control algorithms are then discretized and implemented in a digital environment, either for simulation purposes or for real-time execution on control hardware. Besides model uncertainties and external disturbances, also the discrete-time realization of the control algorithm introduces imperfections to the closed-loop system and hence, contributes to chattering. Therefore, the discretization of continuous-time algorithms is an important step in the controller synthesis, see, e.g., [17] and the references provide there in.

Analysis of chattering effects and the development of strategies reducing chattering effects forms an important field of research in sliding mode control. In this work, the chattering effects, and their impacts on the closed-loop performance, play a central role, too. It is emphasized that chattering effects are unavoidable in real systems regulated by sliding mode controllers. Chattering free sliding mode control, as sometimes promoted in literature, is not feasible.

In the following Section, the sliding mode control concept will be briefly introduced and the chattering effects caused by the different sources are explained by examples. Based on these discussion and a literature review the objective of the thesis will be formulated.

1.1 Sliding Mode Control

It is noteworthy, that the application of sliding mode algorithms is not limited to the controller design but is also applicable to the design of state observers as well as parameter and disturbance estimators. In the following examples, however, only sliding mode controllers are discussed. In most cases the observer design can be done in the same manner and all demonstrated effects remain the same. As mentioned above, it is common to design sliding mode algorithms in the continuous-time domain. In fact, if dealing with discrete-time systems, the design can also be carried out in the discrete-time domain. This approach usually is called *discrete-time sliding mode control* design, which, however, is not subject of this work. It is assumed, that the system studied is a continuous-time system, the control or observation algorithm, however will be implemented in a discrete-time environment.

1.1.1 Continuous-Time Sliding Mode Control

For the purpose of analysis consider the nonlinear affine input system

$$\begin{aligned} \frac{\mathrm{d}\boldsymbol{x}}{\mathrm{d}t} &= \boldsymbol{f}(\boldsymbol{x}) + \boldsymbol{g}(\boldsymbol{x})\left[u(t) + d(t,\boldsymbol{x})\right], \\ \sigma(t) &= h(\boldsymbol{x}), \end{aligned} \tag{1.1}$$

where $\boldsymbol{x}(t) \in \mathbb{R}^n$ denotes the state vector, $u(t) \in \mathbb{R}$ is the control input and $d : \mathbb{R}_{\geq 0} \times \mathbb{R}^n \to \mathbb{R}$ represents external disturbances and/or model uncertainties. Furthermore, the known vector fields $\boldsymbol{f} : \mathbb{R}^n \to \mathbb{R}^n$ and $\boldsymbol{g} : \mathbb{R}^n \to \mathbb{R}^n$ are assumed to be continuous and smooth, $h : \mathbb{R}^n \to \mathbb{R}$

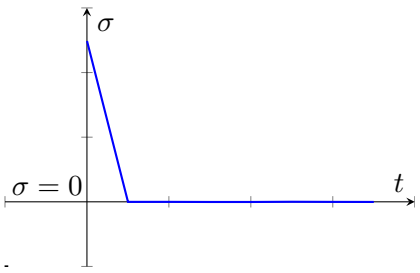

Figure 1.1: Trajectory reaching a first-order sliding mode. The sliding variable $\sigma(t)$ converges to zero in finite time.

represents a smooth known output function. Assume that the constant relative degree ρ of the output (sliding-variable) $\sigma(t) \in \mathbb{R}$ w.r.t. the input u is $1 \leq \rho \leq n$. The constraint $h = 0$ defines an $n - \rho$ dimensional surface in the n-dimensional state space and the set

$$\mathcal{S} = \{\sigma \in \mathbb{R} \,:\, \sigma(t) = 0\}$$

is called a 1-sliding set. A sliding mode controller aims to drive the system state to the sliding surface $\mathcal{S}$ and maintain $\sigma = 0$ for all future times despite the unknown perturbation $d(t, \boldsymbol{x})$. Note that driving the states to the sliding surface $\mathcal{S}$ and keeping $\sigma = 0$ afterwards despite $d(t, \boldsymbol{x})$ requires a discontinuous control. If the the disturbance $d(t, \boldsymbol{x})$ is discontinuous and the relative degree $\rho = 1$ then the discontinuous control law that achieves this goal is called a first-order sliding mode (FOSM) controller. An example for such a motion is given Figure 1.1. Under the assumption that

$$|\tilde{d}| \leq \bar{d}, \quad \forall t, \boldsymbol{x} \quad \text{with} \quad \tilde{d} := \frac{\partial h}{\partial \boldsymbol{x}} \boldsymbol{g}(\boldsymbol{x}) d(t, \boldsymbol{x})$$

and if $\frac{\partial h}{\partial \boldsymbol{x}} \boldsymbol{g} \neq 0$, the control law

$$\begin{cases} u &= \left(\frac{\partial h}{\partial \boldsymbol{x}} \boldsymbol{g}\right)^{-1} \left(u_\mathrm{d} - \frac{\partial h}{\partial \boldsymbol{x}} \boldsymbol{f}\right) \\ u_\mathrm{d} &= -k_1 \mathrm{sign}(\sigma), \quad k_1 > \tilde{d} \end{cases} \tag{1.2}$$

represents a FOSM controller for system (1.1). The input-output behavior of the the plant (1.1) with controller (1.2) is governed by

$$\dot{\sigma} = u_\mathrm{d} + \tilde{d}(t, \boldsymbol{x}),$$

i.e., a differential equation with discontinuous right hand side. Its solutions are understood in the sense of Filippov [18], i.e., its solutions are absolutely continuous functions that satisfy the differential inclusion

$$\dot{\sigma} \in -k_1 \mathrm{sign}(\sigma) + [-\bar{d}, \bar{d}], \tag{1.3}$$

where the sign function $\mathrm{sign}(y)$ is multivalued and defined by

$$\mathrm{sign}(\sigma) = \begin{cases} \{1\}, & \sigma > 0, \\ [-1, 1], & \sigma = 0, \\ \{-1\} & \sigma < 0. \end{cases}$$

The global asymptotic stability of the equilibrium $\sigma = 0$ is verified with the help of the Lyapunov function candidate

$$V = \frac{1}{2}\sigma^2. \tag{1.4}$$

Taking the time derivative of V along the trajectories of (1.3) yields the inequality

$$\dot{V} \leq -(k_1 - \bar{d})|\sigma|, \tag{1.5}$$

i.e., if the condition $(k_1 - \bar{d}) > 0$ holds, $\dot{V}$ is globally negative definite. Furthermore, the inequality

$$\dot{V} \leq -\sqrt{2}(k_1 - \bar{d})\sqrt{V},$$

obtained by substituting (1.4) into (1.5) shows that σ converges to the origin in a finite time, see, e.g., [19, 4]. In order to achieve asymptotic stability of the origin of the original system (1.1), it is required that $\sigma = 0$ describes a sliding surface with asymptotically stable dynamics. Once in sliding mode, the dynamics (1.3) reduce to

$$u_\mathrm{d} = -\tilde{d}(t, \boldsymbol{x}), \tag{1.6}$$

i.e., the set-valued part of the control law (1.2) compensates the perturbation and the closed-loop system is said to be insensitive to the perturbation. The control signal (1.6), or more generally, the control signal that is required to maintain the sliding motion is usually termed as *equivalent control* in literature [7].

The FOSM controller was introduced in the mid sixties by Prof. Vadim I. Utkin and published in Russian language. The first English publications appeared in the 1970's, see, e.g., [5, 20] and the references given there in. One of the main advantages of FOSM control is, that it renders the compensated dynamics insensitive to the perturbation without requiring an exact plant model as well as its simplicity concerning its implementation. The FOSM controller might be implemented as a simple relay controller, i.e., as a switching element. In order to confine the trajectories in such an configuration to the sliding surface requires theoretically infinite switching frequency. However, in a real system imperfections always lead to a limitation of the switching frequency. Such imperfections like unmodeled actuator dynamics, time delay or hysteresis, evoke the *chattering* phenomenon which, as already mentioned in the introduction, are oscillations with finite frequency and amplitude in the system output, its input and in the state variables. The system trajectories are not further confined to $\sigma = 0$. However, they converge to a neighborhood of $\sigma = 0$. Such a motion is typically referred to as real sliding motion.

In modern control systems, even such relatively simple control laws, are commonly implemented in a discrete-time environment. In such a closed-loop system, the measured signals are obtained by sampling the continuous-time signal and the control signal is usually fed to the system input via a reconstruction element such as, e.g., a zero-order holder (ZOH). These elements, the sampler and the ZOH element, add additional imperfections to the closed-loop system which also diminish the control accuracy and contribute to the chattering phenomenon.

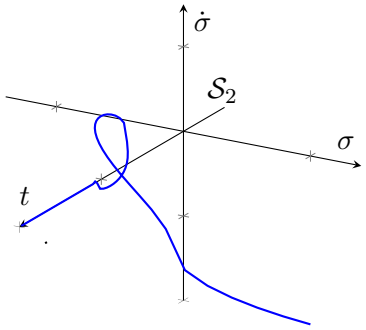

Figure 1.2: Trajectory reaching a 2-sliding set. The sliding variable σ and its first derivative converge to zero in finite time.

HOSM control was introduced to reduce the chattering effects. First results on HOSM controller have been published in the former Soviet Union, see [21] and, e.g., [14, 15, 13, 12, 22, 2] for more recent results, or a collection of results.

The HOSM concept generalizes the FOSM approach. The set

$$\mathcal{S}_r = \{\boldsymbol{\sigma} \in \mathbb{R}^r \,:\, \sigma(t) = \dot{\sigma}(t) = \ldots = \sigma^{r-1}(t) = 0\}$$

with $\boldsymbol{\sigma} := \begin{bmatrix}\sigma & \dot{\sigma} & \ldots & \sigma^{r-1}\end{bmatrix}^{\mathrm{T}}$ is called a r-sliding set. Every controller that drives the system states, despite the perturbation, on $\mathcal{S}_r$ and maintains them on $\mathcal{S}_r$ for all subsequent times is called an r-sliding mode algorithm. The r^{th} derivative of σ is discontinuous. For $r = 2$ such a controller is called a second-order sliding mode controller. A formal definition is given in e.g. [13]. Figure 1.2 illustrates a motion imposed by a second-order sliding mode controller. The sliding variable σ and its first derivative converge to zero in finite time.

Since the introduction of the so-called twisting algorithm, the super-twisting algorithm and the suboptimal algorithm, which can be considered as the first second-order sliding mode algorithms, a number of HOSM algorithms have been introduced. Apart from the specific algorithms which are available in literature, focus has recently been placed on the generalization of the HOSM concept for arbitrary values of r as well as on providing tools that facilitate the design and tuning of such controllers. A central role in this advancement plays the notion of homogeneity and weighted homogeneity. See, e.g., [23] for details on the classical homogeneity property and [24] for weighted homogeneity and its application in SMC. The homogeneity notion is explained in more detail in Section 4.1.

Table 1.1 gives a selection of sliding mode controllers related to the relative degree ρ of the output σ. The super-twisting algorithm (STA) is one of the most deployed and established algorithms in the field of robust nonlinear control and observation [13, 25, 14]. Besides its robustness, its remarkable properties are the structural simplicity, high control precision, and finite time convergence of the sliding variable and its derivative to zero. It is a second-order SMC applicable to systems with relative degree one output subject to Lipschitz perturbations,

r	ρ	Name	Control Law
1	1	1-sliding	$u_\mathrm{d} = -k_1 \mathrm{sign}(\sigma)$
2	1	Super-Twisting	$u_\mathrm{d} = -k_1\sqrt{\lvert\sigma\rvert}\mathrm{sign}(\sigma) - k_2 \int_0^t \mathrm{sign}(\sigma)\,\mathrm{d}s$
2	2	Twisting	$u_\mathrm{d} = -k_1 \mathrm{sign}(\sigma) - k_2 \mathrm{sign}(\dot{\sigma})$
2	3	Continuous-Twisting	$u_\mathrm{d} = -k_1\lvert\sigma\rvert^{\frac{1}{3}}\mathrm{sign}\,(\sigma) - k_2\lvert\dot{\sigma}\rvert^{\frac{1}{2}}\mathrm{sign}\,(\dot{\sigma}) + \nu$ $\dot{\nu} = -k_3 \mathrm{sign}\,(\sigma) - k_4 \mathrm{sign}\,(\dot{\sigma})$
3	3	Nested	$u_\mathrm{d} = -k\mathrm{sign}\left(\ddot{\sigma} + 2(\lvert\dot{\sigma}\rvert^3 + \lvert\sigma\rvert^2)^{\frac{1}{6}}\mathrm{sign}\left(\dot{\sigma} + \lvert\sigma\rvert^{\frac{2}{3}}\mathrm{sign}(\sigma)\right)\right)$
	$\vdots$		
$r \geq \rho$		arbitrary-order (Nested, Quasi-Continuous)	$u_\mathrm{d}(t) = -k_1 \mathrm{sign}\left(f(k_2, \ldots, k_r, \sigma, \dot{\sigma}, \ldots, \sigma^{(r-1)})\right)$

Table 1.1: A selection of $r-$sliding controllers sorted by the relative degree of the output.

e.g. to systems represented by[1]

$$\begin{aligned} \dot{\sigma} &= u_\mathrm{d} + d \\ \dot{d} &\in [-L,\, L], \end{aligned} \tag{1.7}$$

where L denotes the Lipschitz constant of d. The STA is given by

$$\begin{aligned} u_\mathrm{d} &= -\,k_1\lvert\sigma\rvert^{\frac{1}{2}}\mathrm{sign}\,(\sigma) + \nu, \\ \dot{\nu} &= -\,k_2 \mathrm{sign}\,(\sigma). \end{aligned} \tag{1.8}$$

where k_1 and k_2 denote the positive (constant) controller gains. Applying the control law (1.8) to system (1.7) and introducing the new coordinates $\sigma_1 := \sigma$ and $\sigma_2 := \nu + d$ yields the closed-loop dynamics

$$\begin{aligned} \dot{\sigma}_1 &= -\,k_1\lvert\sigma_1\rvert^{\frac{1}{2}}\mathrm{sign}\,(\sigma_1) \;\; + \sigma_2, \\ \dot{\sigma}_2 &\in -\,k_2 \mathrm{sign}\,(\sigma_1) + [-L,\, L]. \end{aligned}$$

Choosing the gains k_1 and k_2 as discussed in [13, 28, 29] will render the equilibrium $\sigma_1 = \sigma_2 = 0$ finite time stable. In contrast to the control signal produced by the FOSM controller (1.2), the STA provides an continuous control signal. The twisting algorithm is applicable to systems of the form

$$\begin{aligned} \dot{\sigma}_1 &= \sigma_2, \\ \dot{\sigma}_2 &\in u_\mathrm{d} + [-L,\, L], \end{aligned}$$

[1] This corresponds to the case when the control gain equals one or is known perfectly. This assumption is in general not necessary for the applicability of the STA, see, e.g., [26]. Time-dependent uncertainties will only translate in the choice of the control gains. State-dependent uncertainties in the control gain require some special attention, see [27] for a more detailed discussion on this issue.

i.e., to systems with a relative degree two output. Obviously, rendering the origin $\sigma_1 = \sigma_2 = 0$ of the closed-loop system finite time stable despite the possibly discontinuous perturbation requires a discontinuous control action. The twisting algorithm, which achieves this goal, is given by the static feedback controller

$$u_{\mathrm{d}} = -k_1 \mathrm{sign}\,(\sigma_1) - k_2 \mathrm{sign}\,(\sigma_2).$$

The resulting closed-loop system is

$$\begin{aligned} \dot{\sigma}_1 &= \sigma_2, \\ \dot{\sigma}_2 &\in -k_1 \mathrm{sign}\,(\sigma_1) - k_2 \mathrm{sign}\,(\sigma_2) + [-L,\, L]. \end{aligned} \tag{1.9}$$

On the other hand, the twisting algorithm might also be applied to systems of the form (1.7) by introducing an integrator in the controller, i.e.,

$$\begin{aligned} u_{\mathrm{d}} &= \nu, \\ \dot{\nu} &= -k_1 \mathrm{sign}\,(\sigma) - k_2 \mathrm{sign}\,(\dot{\sigma}). \end{aligned} \tag{1.10}$$

Applying control law (1.10) to (1.7) and introducing the new coordinates $\sigma_1 := \sigma$ and $\sigma_2 := \dot{\sigma} = \nu + d$, as in the case of the STA, allows to represent the closed-loop dynamics in the same form as given in (1.9). The integrator in the controller ensures a Lipschitz continuous control signal u_{d} with Lipschitz constant $k_1 + k_2$. Driving the system state variables to the sliding surface requires gains satisfying the inequalities $k_2 > L$, $k_1 > L + k_2$.

As seen in the example of the twisting algorithm, the introduction of additional dynamics (e.g. an integrator) in the control channel, as well as the choice of the system output, i.e., the design of the sliding variable offers a certain freedom in the choice of the control algorithm. However, the presence of perturbations usually narrows this choice. In the last decades a number of sliding mode control laws, as well as algorithms which allow to generate controllers, for theoretically arbitrary $\rho > 1$ have been introduced in literature. Almost all these controllers require full state information, i.e., the output σ as well as its $\rho - 1$ derivatives w.r.t. to time need to be available from measurements or at least estimates obtained from a state observer need to be incorporated into the control law. Some of the algorithms, discussed so far, especially the STA, may also be exploited as a state observer. The STA forms the basis for the so-called arbitrary-order Robust Exact Differentiator (RED) proposed by Levant in [14], which, in terms of structure, looks very similar to the STA. The differentiator is capable to provide the derivative of a large class of functions theoretically exact in a finite time.

In combination with the arbitrary-order RED, the HOSM controllers are applicable to a wide class of uncertain systems. Theoretically, they are capable to solve the Black Box control problem, as only the relative degree of the output w.r.t. to the input needs to be known, see [30]. The relative degree determines the order of the controller and this in turn gives the order of the state estimator/differentiator. The choice of the appropriate controller order is crucial as the application of a controller of too low order will evoke the control chattering effects.

1.1.2 Control Chattering

The control chattering effects are demonstrated by a simple example. Consider the nonlinear unity feedback configuration depicted in Figure 1.3. The feedback loop consists of a linear

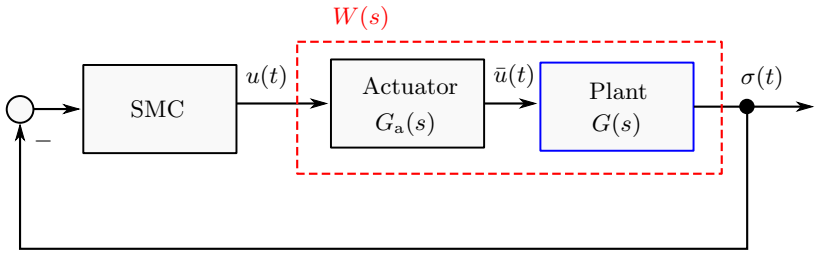

Figure 1.3: Nonlinear unity feedback system. The feedback loop is composed of a linear plant, actuator dynamics and a sliding mode controller.

plant controlled by a sliding mode algorithm. The plant dynamics is described by its transfer function

$$G(s) = \frac{\mathscr{L}\{\sigma(t), s\}}{\mathscr{L}\{\bar{u}(t), s\}} = \frac{K_\mathrm{p}}{s(T_\mathrm{p}s + 1)}, \quad K_\mathrm{p}, T_\mathrm{p} > 0$$

where $\mathscr{L}\{\cdot, s\}$ denotes the Laplace transform. The relative degree of the output σ w.r.t. to the input $\bar{u}$ is $\rho = 2$. For the following analysis the twisting algorithm

$$u = -k_1 \mathrm{sign}\,(\sigma) - k_2 \mathrm{sign}\,(\dot{\sigma})$$

is chosen as a control algorithm, hence $r = 2$. The control goal is to steer the output σ as well as its derivative $\dot{\sigma}$ to zero in finite time. In the absence of the actuator dynamics $G_\mathrm{a}(s)$, $r = \rho$ holds. Hence, a proper choice of gains k_1 and k_2 ensures the existence of an *ideal* second-order sliding mode. The trajectory plotted on the left hand side in Figure 1.4 illustrates such an ideal sliding motion. However, in the presence of a first-order actuator dynamics, e.g.,

$$G_\mathrm{a}(s) = \frac{\mathscr{L}\{\bar{u}(t), s\}}{\mathscr{L}\{u(t), s\}} = \frac{1}{T_\mathrm{a}s + 1},$$

there is a mismatch in the relative degree and the controller order. Hence, as $r < \rho$, it is not possible anymore to achieve $\sigma = 0$, $\forall t > T$. This can be seen in the right plot given in Figure 1.4. The trajectory eventually exhibits a limit cycle in the phase plane $(\sigma, \dot{\sigma})$ around $\sigma = \dot{\sigma} = 0$, i.e., the control chattering effects are present. The control chattering effects are characterized by self-sustaining oscillations with high frequency and nonzero amplitude [2]. These effects are generally evoked not only by unmodeled actuator dynamics but also by parasitic dynamics like a time delay, additional nonlinearities or hysteresis.

Chattering effects are commonly analyzed with the help of the describing function method (method of harmonic balance). For the purpose of this analysis, the sign function in the controller is supposed to be realized by an ideal relay. Then the describing function of the twisting algorithm is

$$N(A) = \frac{4}{\pi A}(k_1 + jk_2), \tag{1.11}$$

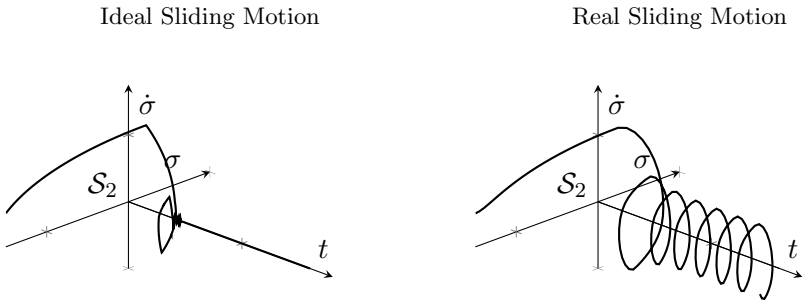

Figure 1.4: Ideal vs. real sliding mode. In the absence of parasitic dynamics the order of the controller is equal to the relative degree of the plant output and an ideal sliding motion is achieved (left plot). The actuator dynamics increases the relative degree of the plant which eventually results in control chattering effects (right plot). The motion is called real sliding mode.

Figure 1.5: Chattering analysis using the describing function technique. Graphical solution of the harmonic balance equation with and without actuator dynamics.

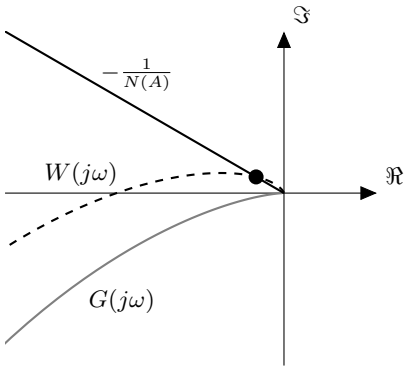

where A represents the amplitude of the oscillation, see, e.g., [2]. With the gain selection k_1, $k_2 > 0$ the negative reciprocal of the describing function $-1/N(A)$ lies entirely in the second quadrant of the complex plane, see Figure 1.5. The Nyquist plot of $G(s)$, however lies in the third quadrant. Hence, no intersection exists. In contrast to that, the Nyquist plot of

$$W(s) = \frac{\mathscr{L}\{\sigma(t), s\}}{\mathscr{L}\{u(t), s\}} = G_{\mathrm{a}}(s)G(s)$$

intersects with the negative reciprocal describing function, i.e., an oscillation in the nonlinear unity feedback system is predicted. The intersection point of the negative reciprocal describing function with the Nyquist plot of the linear part, characterized by the harmonic balance equation

$$N(A)W(j\omega) = -1$$

provides estimations of the chattering amplitude A and frequency ω. The describing function method succeeds if the filtering hypothesis is fulfilled, i.e., the plant has low-pass characteristics. An alternative approach, that allows to analyze also plants for which the filtering hypothesis is *not* satisfied, is the so-called Locus of Perturbed Relay System (LPRS) approach, see [9]. This method provides better accuracy than the DF and additionally allows to analyze the input-ouput problem, i.e., forced motions. However, it is restricted to relay systems only.

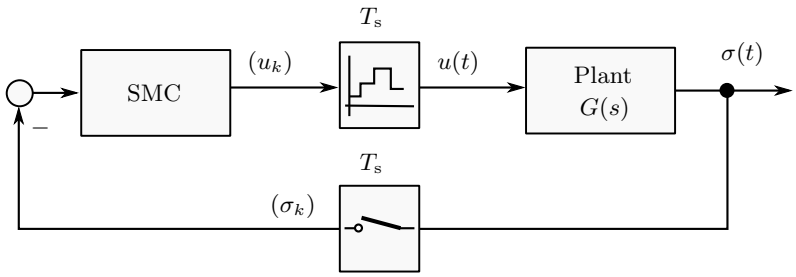

Figure 1.6: Nonlinear unity feedback system with sample and hold element.

Under the assumption that the controller is realized by ideal relays, an ideal sliding motion demands theoretically infinite high switching frequency. A limitation of the switching frequency results in chattering, i.e., a *real* sliding motion. In addition to the above mentioned chattering sources also the realization of the controller in a digital environment and the associated limitation of the switching frequency results in chattering, the so-called discretization chattering.

1.1.3 Discretization Chattering

Nowadays control algorithms are predominantly implemented in a digital environment which usually leads to a closed-loop system as illustrated in Figure 1.6. The continuous-time output signal $\sigma(t)$ of the plant is converted to a sequence $(\sigma_k) = (\sigma_0, \sigma_1, \sigma_2, \ldots)$ where $\sigma_k = \sigma(kT_\mathrm{s})$, T_s denotes the sampling period, $k = 0, 1, 2, \ldots$, which then is processed by the control algorithm. The control algorithm, generates the input sequence $(u_k) = (u_0, u_1, u_2, \ldots)$ which is converted by a reconstruction element to a continuous-time signal $u(t)$. A realization of the controller in a digital environment requires a discrete-time version of the control algorithm. Basically, there are two fundamental approaches to obtain a discrete-time controller for a plant under sampling. The first approach, often referred to as direct discrete-time design, aims to design a controller in discrete-time domain. This approach requires a discrete-time model of the plant. However, for nonlinear plants there is generally no closed-form solution that could be discretized and thus an exact sampled-data model for the continuous-time plant description is not available. The second approach is the so-called emulation design [31]. In this approach the controller design is carried out in the continuous-time domain and sampling is ignored in the first step. In the second step, the continuous-time controller is discretized and finally implemented in a digital environment.

When dealing with discontinuous control laws the first choice in terms of the discretization scheme often is the forward (explicit) Euler scheme. The application of this discretization scheme to sliding mode based algorithms results in closed-loop systems which have certain beneficial properties. For the first-order sliding mode it has been shown that the origin of the forward Euler discretized closed-loop system (1.3) is practically stable. The steady state accuracy of the state variable of the closed-loop system is proportional to the discretization

time T_s, i.e., the trajectories converge to the real sliding set

$$\mathcal{R}_1 = \{\sigma \in \mathbb{R} : |\sigma| \leq \mu_0 T_\mathrm{s}\}, \tag{1.12}$$

where μ_0 is a positive constant. When applying a r-sliding mode controller, the trajectories converge to the real sliding set

$$\mathcal{R}_r = \{\boldsymbol{\sigma} \in \mathbb{R}^r : |\sigma| \leq \mu_0 T_\mathrm{s}^r, |\dot{\sigma}| \leq \mu_1 T_\mathrm{s}^{r-1}, \ldots, |\sigma^{(r-1)}| \leq \mu_{r-1} T_\mathrm{s}\},$$

where $\mu_0, \ldots, \mu_{r-1} > 0$. However, even in the nominal case ($r = \rho$) it is in general not possible to achieve an ideal sliding motion in the presence of perturbations. Even in the unperturbed case the explicit discretization scheme evokes the discretization chattering i.e., implementation of the control law in a digital environment, and the associated limitation of the switching frequency leads to similar effects as discussed in the previous paragraph.

Consider for example a linear time invariant system in controllable canonical form regulated by the FOSM controller, i.e.,

$$\begin{aligned} \dot{\boldsymbol{x}} &= \boldsymbol{A}\boldsymbol{x} + \boldsymbol{b}u, \\ \sigma &= \boldsymbol{c}^\mathrm{T}\boldsymbol{x}, \\ u &= -\boldsymbol{c}^\mathrm{T}\boldsymbol{A}\boldsymbol{x} - k_1 \mathrm{sign}\,(\sigma), \end{aligned} \tag{1.13}$$

where $\boldsymbol{x} \in \mathbb{R}^n$, $u, \sigma \in \mathbb{R}$ and $\boldsymbol{A}$, $\boldsymbol{b}$, $\boldsymbol{c}$ are matrices of appropriate dimensions. The entries in the vector $\boldsymbol{c}$ are scaled s.t. $\boldsymbol{c}^\mathrm{T}\boldsymbol{b} = 1$ holds. The dynamics of the sliding variable then is given by

$$\dot{\sigma} = -k_1 \mathrm{sign}\,(\sigma).$$

Before dealing with the configuration depicted in Figure 1.6 the forward Euler discretization of the closed-loop system (1.13) is studied. The forward Euler discretization of (1.13) yields the recursion

$$\boldsymbol{x}_{k+1} = (\boldsymbol{I} + T_\mathrm{s}\boldsymbol{A}_\mathrm{c})\boldsymbol{x}_k - T_\mathrm{s}k_1\boldsymbol{b}\mathrm{sign}(\sigma_k), \quad \sigma_k = \boldsymbol{c}^\mathrm{T}\boldsymbol{x}_k \tag{1.14}$$

where $\boldsymbol{A}_\mathrm{c} = (\boldsymbol{I} - \boldsymbol{b}\boldsymbol{c}^\mathrm{T})\boldsymbol{A}$, $\boldsymbol{I}$ denotes the identity matrix and $\boldsymbol{x}_k = \boldsymbol{x}(kT_\mathrm{s})$. The dynamics of the sliding variable take the form

$$\sigma_{k+1} = \sigma_k - T_\mathrm{s}k_1 \mathrm{sign}\,(\sigma_k).$$

In the continuous-time system (1.13) the existence of a FOSM is ensured by positive choice of the parameter k_1. The trajectory obtained with $\boldsymbol{x}_0 = [0.5 \quad 1]^\mathrm{T}$, $k_1 = 1$ and

$$\boldsymbol{A}_\mathrm{c} = \begin{bmatrix} 0 & 1 \\ 0 & -c_1 \end{bmatrix}, \, c_1 > 0$$

is illustrated in the phase plane in the upper left plot in Figure 1.7. The plot on the r.h.s. shows the sliding variable $\sigma(t)$. It monotonically decreases towards zero and once it reaches the sliding surface, $\sigma = 0$ is kept for all subsequent time. A simulation of the discrete-time system (1.14) is provided in the lower two plots. In this example $T_\mathrm{s} = 0.15$ s. The sliding variable σ_k exhibits a zigzagging motion around zero, i.e., the discretization chattering effect. The trajectory in

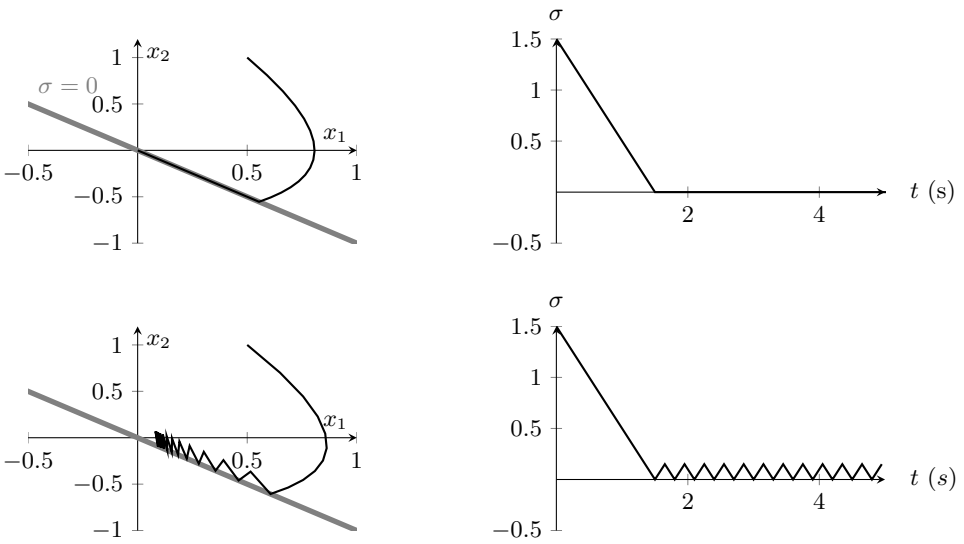

Figure 1.7: First-order sliding mode in a continuous-time system compared to the forward Euler discretized closed-loop system. The trajectory of the discretized system shows the chattering effects characterized by a zigzagging motion around $\sigma = 0$.

the $x_1 - x_2$ plane is confined to a real sliding set as given in (1.12). The solution (σ_k), plotted in Figure 1.7, is connected by piecewise linear functions. The chattering amplitude depends on the discretization time T_s as well as on the gain k_1. The value of the offset of the oscillation will depend on the initial conditions $\boldsymbol{x}_0$. The motions occurring in explicit Euler discretized FOSM systems have been studied extensively in literature, see [32, 33]. The chattering effects in higher-order sliding modes are in general much more complex than the motions observed in the FOSM system and the analysis is far more complex [34, 35].

Recently an implicit scheme for the discretization of the FOSM controller has been proposed in [36]. The basic idea of this approach is explained with the help of the following example. Let the control signal as well as a perturbation enter the continuous-time system via a ZOH element, i.e., $u(t) = u_k$, $d(t) = d_k$ in the interval $[kT_\mathrm{s}, (k+1)T_\mathrm{s})$. Then an exact discretization of a LTI system is given by

$$\boldsymbol{x}_{k+1} = \boldsymbol{A}_\mathrm{d}\boldsymbol{x}_k + \boldsymbol{b}_\mathrm{d}(u_k + d_k)$$

where $\boldsymbol{A}_\mathrm{d} = e^{\boldsymbol{A}T_\mathrm{s}}$ is the state transition matrix evaluated at $t = T_\mathrm{s}$ and the input vector $\boldsymbol{b}_\mathrm{d}$ is computed as $\boldsymbol{b}_\mathrm{d} = \int_0^{T_\mathrm{s}} e^{\boldsymbol{A}s}\boldsymbol{b}\,\mathrm{d}s$. The perturbation d_k is assumed to be bounded by a known value, i.e., $|d_k| < \bar{d}$, $\forall k$ and the linear sliding variable

$$\sigma_k = \boldsymbol{c}^\mathrm{T}\boldsymbol{x}_k$$

is introduced. Then

$$\sigma_{k+1} = \boldsymbol{c}^\mathrm{T}\boldsymbol{A}_\mathrm{d}\boldsymbol{x}_k + \boldsymbol{c}^\mathrm{T}\boldsymbol{b}_\mathrm{d}(u_k + d_k),$$

and the control

$$u_k = \frac{1}{\boldsymbol{c}^\mathrm{T}\boldsymbol{b}_\mathrm{d}}(-\boldsymbol{c}^\mathrm{T}\boldsymbol{A}_\mathrm{d}\boldsymbol{x}_k + \sigma_k) - k_1 u_{\mathrm{s},k}, \tag{1.15}$$

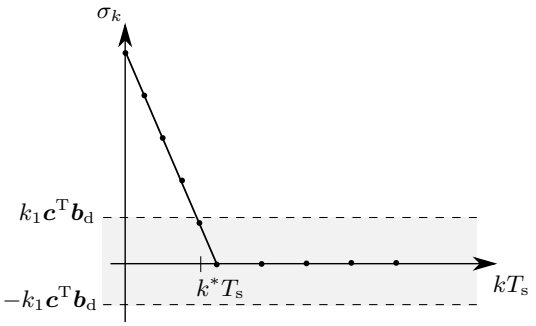

Figure 1.8: Graphical interpretation of the implicit numerical scheme applied to a first-order sliding mode controller.

where it is assumed that $\boldsymbol{c}^{\mathrm{T}} \boldsymbol{b}_{\mathrm{d}} \neq 0$, leads to the actual design problem of a robust controller for the compensated dynamics

$$\sigma_{k+1} = \sigma_k - k_1 \boldsymbol{c}^{\mathrm{T}} \boldsymbol{b}_{\mathrm{d}} u_{\mathrm{s},k} + \boldsymbol{c}^{\mathrm{T}} \boldsymbol{b}_{\mathrm{d}} d_k. \tag{1.16}$$

Now, instead of applying the explicit Euler discretized FOSM controller, which for (1.16) reads as

$$u_{\mathrm{s},k} = \operatorname{sign}(\sigma_k),$$

an implicit scheme is exploited. As the perturbation d_k is unknown, the unperturbed virtual system

$$\begin{cases} \tilde{\sigma}_{k+1} & = \sigma_k - k_1 \boldsymbol{c}^{\mathrm{T}} \boldsymbol{b}_{\mathrm{d}} u_{\mathrm{s},k} \\ u_{\mathrm{s},k} & \in \operatorname{sign}(\tilde{\sigma}_{k+1}) \end{cases} \tag{1.17}$$

is introduced together with the implicit controller. The purpose of the virtual system will be discussed in more detail later on. System (1.17) constitutes a set-valued equation which is solved by a projection

$$u_{\mathrm{s},k} = \operatorname{proj}\left([-1,\, 1]; \frac{\sigma_k}{k_1 \boldsymbol{c}^{\mathrm{T}} \boldsymbol{b}_{\mathrm{d}}} \right)$$

where the projection is

$$\operatorname{proj}\left([-1,\, 1]; \frac{\sigma_k}{k_1 \boldsymbol{c}^{\mathrm{T}} \boldsymbol{b}_{\mathrm{d}}} \right) = \begin{cases} \operatorname{sign}(\sigma_k) & \text{if} \quad |\sigma_k| > k_1 \boldsymbol{c}^{\mathrm{T}} \boldsymbol{b}_{\mathrm{d}} \\ \frac{\sigma_k}{k_1 \boldsymbol{c}^{\mathrm{T}} \boldsymbol{b}_{\mathrm{d}}} & \text{else.} \end{cases} \tag{1.18}$$

A graphical interpretation of this control law is given in Figure 1.8. In the absence of the perturbation, i.e., $(d_k) = (d_0,\, d_1,\, \ldots) = (0,\, 0,\, \ldots)$, and, according to (1.18), $|\sigma_k|$ decreases with the rate $k_1 \boldsymbol{c}^{\mathrm{T}} \boldsymbol{b}_{\mathrm{d}} / T_{\mathrm{s}}$ until it enters the real sliding set $|\sigma_k| \leq k_1 \boldsymbol{c}^{\mathrm{T}} \boldsymbol{b}_{\mathrm{d}}$ at step k^*. Then $u_{\mathrm{s},k} = \sigma_k / (k_1 \boldsymbol{c}^{\mathrm{T}} \boldsymbol{b}_{\mathrm{d}})\ \forall k > k^*$. Whenever $d_k \neq 0$ it is not possible anymore to maintain $\sigma_k = 0$. In the presence of perturbations the sliding variable σ_k will enter the real sliding set $|\sigma_k| \leq k_1 \boldsymbol{c}^{\mathrm{T}} \boldsymbol{b}_{\mathrm{d}}$ within a finite number of steps and $|\sigma_k| \leq k_1 \boldsymbol{c}^{\mathrm{T}} \boldsymbol{b}_{\mathrm{d}}$ is kept for all subsequent time steps. The dynamics eventually reduce to

$$\sigma_{k+1} = \boldsymbol{c}^{\mathrm{T}} \boldsymbol{b}_{\mathrm{d}} d_k, \tag{1.19}$$

hence the implicit discretized FOSM controller provides for the accuracy of the sliding variable

$$|\sigma_k| \leq \boldsymbol{c}^{\mathrm{T}} \boldsymbol{b}_{\mathrm{d}} \bar{d}, \quad \forall k \geq k^*. \tag{1.20}$$

As $\boldsymbol{c}^{\mathrm{T}} \boldsymbol{b}_{\mathrm{d}} = \mathcal{O}(T_{\mathrm{s}})$ it is clear that this scheme also preserves the asymptotic accuracy $\sigma_k = \mathcal{O}(T_{\mathrm{s}})$. Furthermore, it can be concluded form (1.20) that the ultimate precision does not depend on the control gain k_1, i.e., the precision is insensitive to an overestimation of the gain. This is not true in the explicit discretized controller as already in the unperturbed case the oscillation amplitude is proportional to the control gain k_1. Whenever the above relation (1.19) is satisfied, $\tilde{\sigma}_k \equiv 0$. Shifting (1.19) by one step and computing the difference one gets

$$\frac{(\sigma_{k+1} - \sigma_k)}{\boldsymbol{c}^{\mathrm{T}} \boldsymbol{b}_{\mathrm{d}}} = d_k - d_{k-1}.$$

Replacing $(\sigma_{k+1} - \sigma_k)/(\boldsymbol{c}^{\mathrm{T}} \boldsymbol{b}_{\mathrm{d}})$ from recursion (1.16) yields

$$d_k - k_1 u_{\mathrm{s},k} = d_k - d_{k-1}.$$

If the underlying continuous time signal $d(t)$ is Lipschitz continuous with Lipschitz constant L then

$$|d_k - k_1 u_{\mathrm{s},k}| \leq T_{\mathrm{s}} L. \tag{1.21}$$

Whenever $\tilde{\sigma}_k \equiv 0$, the scaled control signal $k_1 u_{\mathrm{s},k}$ tracks the perturbation d_k and the tracking error (1.21) is proportional to the sampling time T_{s}.

The introduction of the auxiliary variable $\tilde{\sigma}_k$ provides for a definition of the sliding motion in discrete-time systems which is closer to the sliding mode concept in continuous-time systems when compared to the concept of quasi sliding mode. The concept of quasi sliding mode requires that the sliding variable σ_k at some time instant k^* crosses the sliding surface and then crosses it in each subsequent step with a non increasing amplitude of oscillation (see [37] for a formal definition of the concept). Taking into account (1.19), a sliding motion in a discrete-time environment may be understood as a motion satisfying $\tilde{\sigma}_k \equiv 0$ for all $k > k^*$.

Figure 1.9 shows results of a simulation which illustrates the major differences between the implicit and the explicit discretized FOSM controller. The plant parameters are

$$\boldsymbol{A} = \begin{bmatrix} 0 & 1 \\ -1 & -2 \end{bmatrix}, \quad \boldsymbol{b} = \begin{bmatrix} 0 \\ 1 \end{bmatrix}, \quad \boldsymbol{c}^{\mathrm{T}} = \begin{bmatrix} 1 & 1 \end{bmatrix}, \quad d(t) = 1.8 \sin(4t).$$

The sampling time is set to $T_{\mathrm{s}} = 0.01$ s and the control gain $k_1 = 2$. The results presented in the plots on the left hand side are obtained by the implicit discretization, the plots on the right hand side result from the explicit discretized controller, respectively. In the upper left plot one can see that eventually $\tilde{\sigma}_k \equiv 0$ and the trajectory σ_k satisfies (1.20). The lower plots show the control signals u_k given in (1.15) and the negative perturbation d_k over time. The implicit discretized controller tracks the perturbation whereas the explicit discretized control law exhibits the high frequency switching. The high frequency switching part of the control signal contains information about the perturbation. The perturbation might be observed by low-pass filtering the signal $k_1 u_{\mathrm{s},k}$, see [1].

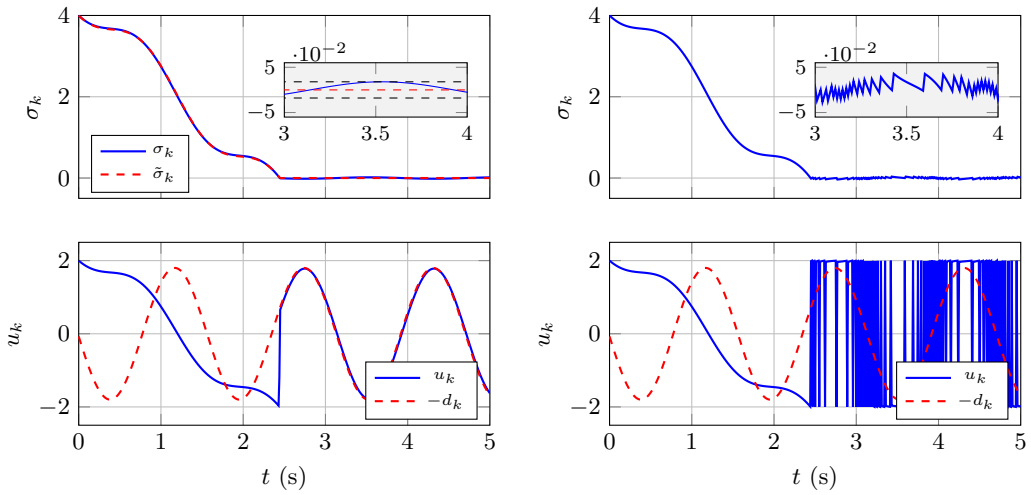

Figure 1.9: Comparison of an implicit discretized and an explicit discretized first-order sliding mode controller. The implicit controller avoids the discretization chattering effect. After some transients the control signal tracks the perturbation. When applying the explicit discretized controller, the control signal exhibits high frequency switching. The switching signal contains information about the perturbation which, in general, can be extracted using a low-pass filter.

From this example it is clear that the discretization process of the continuous-time controller plays a crucial role as it has a significant impact on the closed-loop system performance. A carefully chosen discretization scheme is capable to significantly reduce discretization chattering effects while preserving desired properties like the robustness and asymptotic accuracies known from the forward Euler discretized algorithm.

1.2 Literature Review

Improper discrete-time implementation of sliding mode based control laws as well as the presence of parasitic dynamics contributes to the chattering phenomenon that mainly deteriorates the control performance related to the steady-state accuracy of the controlled variable. In the last decades, much research effort has been spent on this issue. As already mentioned in the introduction, chattering sources are grouped into two categories: the discretization chattering and the control chattering which embodies the effects designated to model imperfections. The numerous root causes of the discretization chattering render the analysis a challenging task. Therefore, the analysis is usually restricted to one particular category. Besides contributions which deal with the analysis of chattering, there are many publications which focus on the development of methods mitigating such negative effects and therewith increase the closed-loop systems performance.

Many sliding mode control systems can be analyzed via a relay control structure. Effects arising in continuous-time relay feedback control systems have been extensively studied in nonlinear control theory, see, e.g., [38, 39] and the references provided therein. In general, for the analysis of the control chattering effects frequency domain techniques such as the

describing function method [2] and the LPRS approach [9, 40] have proven to be effective tools. In particular, the chattering in continuous-time systems controlled by second-order sliding mode algorithms has been analyzed extensively in the literature. The generalized suboptimal controller has been studied in [41]; the twisting controller and the STA have been addressed in [42, 43]. For an analysis via the LPRS method see [44, 9]. The authors in [45] characterized the chattering in terms of stability margins which can be seen as a sort of robustness metrics to parasitic dynamics. In e.g. [46] a numerical approach has been chosen to derive the DF for higher-order sliding mode controllers. The chattering effects in systems controlled by the FOSM controller, the twisting controller, super-twisting controller or the continuous-twisting controller have been studied and compared to each other in [16]. Based on the actuator time constant the authors give a recommendation when to use a continuous or a discontinuous controller. Besides the analysis, the frequency domain techniques facilitate the systematic design of compensating elements in order to adjust the frequency of the chattering effect [47, 48, 49].

Discretization chattering effects in SMC systems are mainly studied in the context of the unperturbed Euler discretized closed-loop system by exploiting time domain techniques. The effects have been studied extensively for the first-order SM controller see, e.g., [50, 32, 33, 51]. The 2-sliding controllers such as the twisting algorithm and STA have been analyzed in [52] and [35] respectively. In those works, the dynamics of the sliding variable under forward Euler discretization are investigated and steady state bounds of the sliding variable are provided. It turns out, that especially for systems controlled by HOSM algorithms, finding exact solutions of periodic points by e.g. computing the fixed points of periodic maps becomes numerically very expensive (even in the unperturbed case). However, an approach allowing to analyze both, the control chattering effects as well as the discretization effects, at once is not yet available from literature and therefore represents an open and active research field.

Increasing the steady-state accuracy in systems controlled by sliding mode algorithms by means of the reduction of the chattering amplitude represents another interesting research field. The approaches mainly rely on enhancing first-order SMC by disturbance estimation schemes, providing estimates of the equivalent control. Incorporating the estimated values in the control law allows to decrease the discontinuous control gain and, thus, reduce the chattering effects [53, 54, 55, 56, 57]. The approach may be extended by some adaptation or learning as suggested in [58, 59, 60, 61]. With the introduction of HOSM algorithms, the number of publication dealing with this approach dropped significantly. In many cases, the HOSM controllers allow to alleviate the chattering effects and also achieve improved asymptotic accuracy in the presence of sampling and measurement noises when compared to the FOSM.

Recently an implicit discretization scheme has been published for the conventional FOSM controller, the twisting controller and a nested SMC, see [36, 62, 17, 63]. An implicit version of the STA been introduced in [64], which deals with the observer, and [65] which is devoted to the controller. Compared to the explicit discretization the implicit approach renders the origin a finite-time Lyapunov stable equilibrium, i.e., in the unperturbed case, the variable to be controlled is steered to zero exactly. In the presence of perturbations, the trajectories preserve the standard accuracies of the $r-$sliding mode. Besides the removal of the control chattering effects, an attractive feature of the implicit scheme is that the obtained precision is not deteriorated by an overestimation of the control gains. This feature is essential in real-world applications, as bounds on the perturbations are almost never known exactly and an overestimation of the gains is therefore almost unavoidable. The discretization of discontinuous

finite-time and fixed-time stable systems, in general, has been addressed recently in [66].

1.3 Aims and Contribution of this Work

The aim of the PhD-thesis is twofold: Firstly, to develop new mathematical tools for the analysis of chattering effects in sampled-data sliding mode control systems caused by both, the discrete-time realization as well as the limitation of the switching frequency by parasitic dynamics. Secondly, to develop new discretization schemes for continuous-time HOSM algorithms that entirely remove the discretization chattering effects.

In view of the first aim, the extension of the describing function analysis to sampled-data systems is applied to analyze chattering effects in linear plants controlled by a second-order sliding mode algorithm. Then, the LPRS approach, that gives an exact analysis of periodic motion in continuous-time relay feedback systems, is extended to the sampled-data system. Formulas for computing the LPRS of the sampled-data system are derived. Within this framework, an approach that allows predicting the basin of attraction of periodic modes is proposed. Simulation examples, as well as the application to a real system, confirm the theoretical findings. The results have been published in [P3] and [P5].

Then, a novel discretization scheme for the STA is derived. The resulting discrete-time variants of the STA exhibit a number of advantages when compared to the state-of-the-art discrete-time version of the STA, which relies on the forward Euler discretization. The advantages are complete removal of the discretization chattering, the hyper-exponential speed of convergence whenever the perturbation vanishes and straight forward implementation in a discrete-time environment (explicit recursions), to name a few. The key is the pseudo-linear system representation of the STA. Based on the point-wise eigenvalues of the dynamic matrix of this pseudo-linear system representation, discrete-time equivalent controllers are constructed by mapping the point-wise eigenvalues from the continuous-time domain to the discrete-time domain. This way, several novel discrete-time versions of the STA, that either significantly reduce or even entirely remove the discretization chattering effects, are presented. Stability and robustness properties of the closed-loop system are investigated. The approach is extended to a family of homogeneous arbitrary-order differentiators, including the sliding mode based robust exact differentiator as well as the high-gain observer. The unique system representation permits to redesign the structure of the family of homogeneous differentiators when exploited as state and unknown input observer. The proposed differentiator/observer structure is inspired by the current estimator, well-known from linear systems theory. Based on the obtained results, a framework, that allows constructing problem specific arbitrary-order homogeneous controllers, including quasi-continuous sliding mode controllers, that can be easily discretized and implemented, is developed. The results have been published in the papers [P6, P7, P8, P9].

Throughout the thesis, practical applicability of selected algorithms is demonstrated with laboratory applications and, in particular, the hydraulic system presented in [P4].

The main contributions of this work are summarized in the following:

- Application of the sampled describing function analysis for the prediction of chattering characteristics in a linear plant controlled by a second-order sliding mode algorithm. Simulation examples as well as a real world application are presented.

- Extension of the LPRS approach to sampled-data systems. Formulas are derived and a tutorial example is given. An approach that allows to predict the basin of attraction of periodic modes is given.
- Development of an entirely new discretization scheme applicable to certain sliding mode algorithms. In particular:
  - A novel discretization scheme is derived based on a pseudo-linear system representation of the STA. Four new discrete-time variants of the STA are proposed.
  - The results are extended to a family of homogeneous differentiators including the sliding mode based arbitrary-order robust exact differentiator and the high-gain observer.
  - A study comparing the new discrete-time variants of the sliding mode based differentiators to the state of the art discrete-time homogeneous differentiator and other real time differentiators such as simple linear filters, the algebraic differentiator and the high-gain observer is conducted.
  - Redesign of the proposed discrete-time homogeneous differentiators based on a current estimator structure for state and unknown input estimation.
- Novel continuous-time higher-order sliding mode algorithms, that can be easily discretized using the developed framework are constructed by exploiting the notion of homogeneous eigenvalues.
- Application of the proposed differentiators as a state and unknown input observer in a position controller for a hydraulic cylinder subject to unknown external load forces.

Parts of this work have been published in the following papers:

List of Publications:

[P1] S. Koch, M. Reichhartinger and M. Horn. On Discretization of Sliding Mode Based Control Algorithms. In *Steirisches Seminar über Regelungstechnik und Prozessautomatisierung*, 2016, 132–152.

[P2] S. Koch, M. Reichhartinger, M. Horn, and L. Fridman. Discrete implementation of sliding mode controllers satisfying accuracy level specifications. In *14th IEEE VSS*, 2016, 154–159.

[P3] S. Koch, M. Reichhartinger, M. Horn, and L. Fridman. Sampled describing function analysis of second-order sliding modes. In *55th IEEE CDC*, 2016, 7318–7324.

[P4] S. Koch and M. Reichhartinger. Observer-based sliding mode control of hydraulic cylinders in the presence of unknown load forces.. In *e&i - Elektrotechnik und Informationstechnik*, 2016, 133(6), 253–260.

[P5] S. Koch and M. Horn. Frequency Domain Analysis of Sampled Variable Structure Systems. In *56th IEEE CDC*, 2017, 6664–6670.

[P6] S. Koch and M. Reichhartinger. Discrete-Time Equivalent Homogeneous Differentiators. In *15th IEEE VSS*, 2018, 354–359.

[P7] M. Reichhartinger, S. Koch, H. Niederwieser and S.K. Spurgeon. The Robust Exact Differentiator Toolbox: Improved Discrete-Time Realization. In *15th IEEE VSS*, 2018, 1–6.

[P8] S. Koch and M. Reichhartinger Discrete-Time Equivalents of the Super-Twisting Algorithm . In *Automatica* vol. 55, no. 9, 2019.

[P9] S. Koch, M. Reichhartinger, M. Horn, and L. Fridman. Discrete-Time Implementation of Homogeneous Differentiators. In *IEEE Transactions on Automatic Control.*, vol. 65, no. 2, 2020.

[P10] S. Koch, M. Reichhartinger and M. Horn On the Discretization of the Super-Twisting Algorithm. In *submitted to: 58th IEEE CDC*, 2019.

1.4 Thesis Outline

The thesis is essentially grouped into three chapters. A brief overview of the main sections of each chapter and its content is given in the following Figures. The first chapter therein is devoted to the analysis of chattering effects caused by both, the discrete-time realization of the controller as wells parasitic dynamics like actuator and/or sensor dynamics. For this purpose, the describing function (DF) analysis is applied to the sampled-data nonlinear unity feedback system. The theoretical background of the "Sampled Describing Function" approach is revisited and a tutorial example demonstrating the effectiveness of the proposed method is presented. Then, the Locus of perturbed relay system (LPRS) approach is extended to the sampled-data system.

Chapter 3 is devoted to the reduction and elimination of the discretization chattering effects. An entirely new approach for the discretization of the STA is developed. The ideas are extended to a family of homogeneous differentiators including the sliding mode arbitrary-order differentiator. The performance is compared to the state of the art discrete-time version of the differentiator in real world applications and to other real-time differentiators in simulation examples.

Chapter 4 lays the foundation for the development of a framework that allows designing problem specific nonlinear robust continuous-time controllers that can be discretized, implemented and tuned in a straightforward way. Therefore, the notion of homogeneous systems, homogeneous eigenvalues, and homogeneous eigenvectors is introduced. A family of arbitrary-order homogeneous nonlinear state feedback controllers is constructed by means of a homogeneous eigenvalue assignment. Discrete-time equivalent controllers are obtained by applying results from the previous chapters.

The last chapter summarizes and concludes the work. Open problems are addressed and a possible direction for future research is given.

Chapter 2

is devoted to the development of tools for the analysis of chattering effects caused by both, the discrete-time realization of the controller and parasitic dynamics.

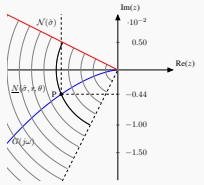

Describing Function Method

The so-called "Sampled Describing Function" approach is applied to study chattering effects in systems controlled by sliding mode algorithms realized in a discrete-time environment. The approach is revisited and applied to the twisting algorithm.

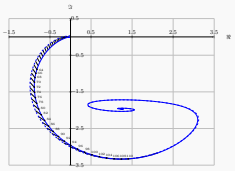

Locus of Perturbed Relay System for Sampled-Data Systems

The LPRS method is extended in order to provide for an analysis of sampled-data systems. The LPRS formulas are derived for the sampled-data system and a tutorial example is given.

Chapter 3

is dedicated to the development of novel discretization schemes that allow to reduce or even entirely avoid the discretization chattering effects.

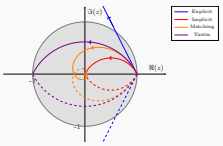

Discrete-Time Equivalent Super-Twisting Algorithm

Three entirely new discrete-time versions of the STA are constructed. A pseudo-linear representation of the closed-loop system allows computing point-wise eigenvalues. Discrete-time equivalent controllers are constructed by mapping the point-wise eigenvalues to the discrete-time domain.

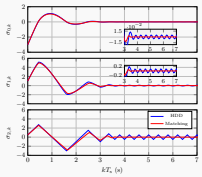

Arbitrary-Order Robust Exact Differentiator

The approach developed in the previous Section is extended to the arbitrary-order robust exact differentiator and a family of homogeneous differentiators.

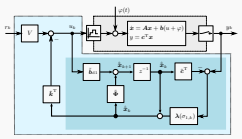

Output Feedback and Higher-Order Sliding Mode Based Current Estimator

The proposed discrete-time differentiators are exploited in an output-feedback controller. Exploiting the pseudo-linear representation, the structure of the homogeneous differentiator is modified as a current estimator.

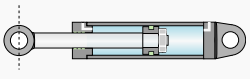

Application - Hydraulic Test Bed

The developed output feedback control structure is applied to control the movement of a hydraulic cylinder piston rod which is subject to unknown external forces.

Chapter 4

deals with the design of homogeneous controllers by means of homogeneous eigenvalue assignment.

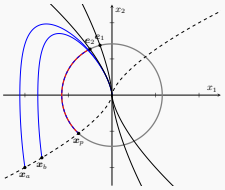

Homogeneous Eigenvalues

The concept of homogenuous eigenvalues and eigenvectors is revisited and examples that illustrate the concept in the context of sliding mode control are provided.

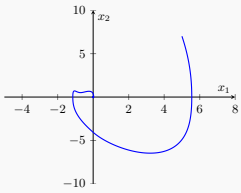

Controller Design

A family of homogeneous state feedback controllers is derived based on the notion of homogeneous eigenvalue analysis and a framework for the design of robust controllers for perturbed linear time-invariant systems is proposed. A real-world application demonstrates the applicability of the proposed controllers.

2 Chattering Analysis in Sampled-Data Systems

Contents

Frequency domain techniques such as the describing function (DF) method and locus of perturbed relay systems (LPRS) have proven to be effective tools to predict the chattering effects in systems regulated by sliding mode controllers [67, 42]. The chattering effects are usually characterized by the amplitude and frequency of the self-sustaining oscillations in the system's output. Moreover, these methods can be used to systematically design compensating elements which are included in the feedback loop such that the amplitude and frequency of the oscillation can be adjusted [47, 48, 49] and, therefore, specify the so-called performance margins. These margins are introduced as the closed-loop system's tolerance to self-sustaining oscillations with a certain amplitude and frequency [68].

The focus of this chapter is on characterizing periodic motions caused by both, the sampling process and parasitic dynamics, in a simple and efficient fashion. The DF analysis is applied to the linear time invariant (LTI) sampled-data system controlled by a static nonlinear, possibly discontinuous, output feedback controller. The proposed approach, the so-called "Sampled Describing Function" (SDF) turns out to be well connected to its corresponding continuous-time counterpart. For some limit cycle modes with a particular frequency the equation of harmonic balance can be solved explicitly based on the knowledge of the DF for the continuous-time configuration.

Then the LPRS method is extended in order to provide for an analysis of sampled-data systems. The LPRS method is, similar to the DF method, a frequency domain technique. The

particular advantage of the approach is, that it yields better accuracy and provides for an analysis of the self sustaining oscillations as well as the input-output properties, see [40]. A formula for the computation of the LPRS for the sampled-data system is derived and stability properties of limit cycles and the basin of attraction of periodic solutions in the sampled-data system are discussed. A tutorial example demonstrates the effectiveness of the approach.

The results discussed in this Chapter have partially been published in [P3] and [P5].

2.1 Describing Function Method for Sampled-Data Systems

For most sliding mode algorithms its describing function is available in literature [69]. A framework, that allows to construct the describing functions of modern HOSM algorithms, e.g. the continuous-twisting algorithm (CTA), in a simple way, has been proposed in literature recently, see [16]. A numerical method for computing the Describing Functions of HOSM control algorithms is presented in [46]. However, as will be seen in the following, the discrete-time realization of the controller will render the analysis more complex. In the sequel, the analysis is restricted to static controllers, dynamic controllers are not considered.

2.1.1 Problem Setting

Consider the plant dynamics described by a continuous-time LTI system represented as

$$\begin{aligned} \frac{\mathrm{d}\boldsymbol{x}}{\mathrm{d}t} &= \boldsymbol{A}\boldsymbol{x} + \boldsymbol{b}\bar{u}, \\ \sigma &= \boldsymbol{c}^{\mathrm{T}}\boldsymbol{x} \end{aligned} \tag{2.1}$$

where $\boldsymbol{x}(t) \in \mathbb{R}^n$ is the state vector, $\bar{u}(t) \in \mathbb{R}$ is a scalar control and the scalar variable $\sigma(t) \in \mathbb{R}$ is regarded as the system output, or can be treated also as sliding variable; $\boldsymbol{A}$, $\boldsymbol{b}$ and $\boldsymbol{c}$ are possibly unknown matrices and vectors of appropriate dimensions. The relative degree of system (2.1), i.e., the smallest integer ρ for which $\boldsymbol{c}^{\mathrm{T}}\boldsymbol{A}^{\rho-1}\boldsymbol{b} \neq 0$ is assumed to be known and constant. The transfer function representation of (2.1) is

$$G(s) = \frac{\mathscr{L}\{\sigma(t), s\}}{\mathscr{L}\{\bar{u}(t), s\}} = \boldsymbol{c}^{\mathrm{T}}(s\boldsymbol{I} - \boldsymbol{A})^{-1}\boldsymbol{b}.$$

The control goal is to drive the output σ to zero within finite time and keep $\sigma \equiv 0$ afterwards. If only the relative degree ρ is known, such a problem might be considered as black-box control problem. It is well-known, see, e.g., [30], that under the assumptions

$$k_{\mathrm{m}} \leq \boldsymbol{c}^{\mathrm{T}}\boldsymbol{A}^{\rho-1}\boldsymbol{b} \leq k_{\mathrm{M}}, \quad |\boldsymbol{c}^{\mathrm{T}}\boldsymbol{A}^{\rho}\boldsymbol{x}| \leq L,$$

with some a priori known bounds k_{m}, k_{M}, $L > 0$ any SM controller of order ρ is capable of solving the stated problem. It drives the output and its subsequent $\rho-1$ derivatives theoretically exactly to zero within finite time. However, as already mentioned in the introduction, any mismatch where the relative degree ρ exceeds the sliding order, as well as the sampling process will lead to undesired oscillations and therefore, any practical implementation of the controller in a real world system will destroy the ideal sliding mode at $\sigma = 0$.

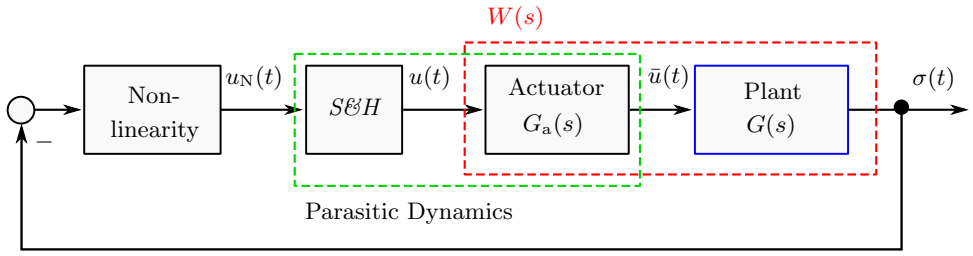

Figure 2.1: Nonlinear sampled-data unity feedback configuration with actuator dynamics.

The control loop depicted in Figure 2.1 forms the basis for the chattering analysis. It is composed of the plant dynamics $G(s)$ regulated by some nonlinear static feedback controller, denoted as "Nonlinearity", and additional stable actuator dynamics $G_{\mathrm{a}}(s)$ which are assumed to be neglected during the controller design. Furthermore, the controller is assumed to be realized in a discrete-time environment. Note that in the case of a static control law, Figure 2.1 represents an equivalent structure of the sampled-data system, i.e., the sampling and hold processes are merged to a single sample and hold element, (see, e.g., [70]). It is worth to mention, that for a static single valued nonlinearity the order of the nonlinear element and the zero-order hold element is interchangeable [71].

Under the assumption that $W(s) = G_{\mathrm{a}}(s)G(s)$ has low pass characteristics and in the absence of the sample and hold block, the chattering amplitude and frequency of the output $\sigma(t)$ can be predicted via the classical DF technique, see, e.g., [2]. However, the sample and the hold device introduce additional dynamics in the feedback loop which may lead to inaccurate prediction or wrong conclusions when neglected in the analysis. The goal of the following section is to incorporate these elements into the framework of chattering analysis via the DF method and consequently provide for an improved prediction of the chattering characteristics.

2.1.2 Sampled Describing Function Analysis

Two types of DFs for sampled-data systems are studied in literature [71]. The first one, often referred to as "Sampled Describing Function", aims to derive a DF characterizing the nonlinear part, the sampler and the hold element. In the second approach only the nonlinearity is approximated by the DF and the remaining parts in the control loop are discretized accordingly. This approach is called "z-Transform Describing Function" [72]. In this work the "Sampled Describing Function" approach is applied. The results presented in the following subsection are mainly based on [71, 73, 69, 74].

Method of Sampled Describing Function Revisited

As mentioned above, the goal is to derive a DF which captures the transfer properties from the negative system output $\sigma(t)$ to the actuator input $u(t)$, i.e., the goal is to derive a DF for the nonlinearity, the sampler and the hold element. The considered configuaration is depicted in detail in Figure 2.2. The input to the nonlinearity is the negative system output $\sigma(t)$. The output of the nonlinearity, which is the input to the sampler is denoted by $u_{\mathrm{N}}(t)$. The output

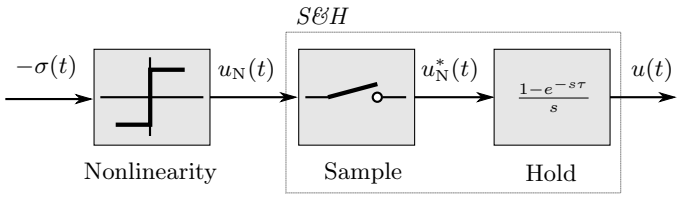

Figure 2.2: Nonlinearity with sampler and hold element. A describing function characterizing the overall series connection of all three elements is derived.

of the sampler is a train of impulses denoted by $u^*_{\mathrm{N}}(t)$. The control signal is assumed to be reconstructed from $u^*_{\mathrm{N}}(t)$ by a ZOH element.

It is assumed that $\sigma(t)$ is a periodic signal represented as

$$-\sigma(t) = A\cos(\omega_1 t + \theta) \tag{2.2}$$

where $\omega_1 = 2\pi/T_1$ is the chattering frequency and θ is the phase relation of the sampling, see Figure 2.3. The value of θ is a priori unknown and is a characteristic of the oscillations. Its value cannot exceed an angle of $T_{\mathrm{s}}\omega_1$. Thus, the inequality

$$0 \leq \theta < T_{\mathrm{s}}\omega_1$$

has to hold. The constant A is the amplitude of the input signal, i.e., the chattering amplitude of $\sigma(t)$. Equivalent to the classical DF approach, the following derivation of the SDF is based on the assumption that the linear part of the control loop, denoted by $W(s)$, has low pass characteristics, i.e.,

$$|W(j\omega)| \gg |W(nj\omega)|, \quad n = 2, 3, \ldots$$

and that the poles of $W(s)$ are located in the left half-plane with the exception of a maximum of one pole at the imaginary axis. Furthermore, it is assumed that a single static and symmetric nonlinearity is present in the control loop.

In order to derive the SDF, all signals shown in Figure 2.2 are represented by their Fourier series. The Fourier series representation of the output $u_{\mathrm{N}}(t)$ of the nonlinearity in exponential form is given by

$$u_{\mathrm{N}}(t) = \sum_{v=-\infty}^{\infty} C_v e^{jv\omega_1 t} \tag{2.3}$$

Figure 2.3: Phase relation of the sampling.

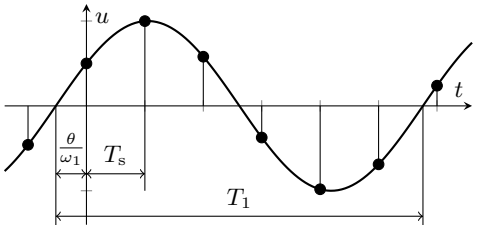

where C_v denotes the complex Fourier coefficient. Note that due to the symmetry of the nonlinearity, the coefficient C_0 is equal to zero. The continuous-time signal $u_{\mathrm{N}}(t)$ and the output of the sampler $u_{\mathrm{N}}^*(t)$ are related by

$$u_{\mathrm{N}}^*(t) = u_{\mathrm{N}}(t)\delta_{T_{\mathrm{s}}}(t) \tag{2.4}$$

where $\delta_{T_{\mathrm{s}}}(t)$ represents a train of unit impulses (see, e.g., [70, 75]) described by

$$\delta_{T_{\mathrm{s}}}(t) = \sum_{k=-\infty}^{\infty} \delta(t - kT_{\mathrm{s}}), \tag{2.5}$$

where $\delta(t)$ is the unit impulse at time instant $t = 0$ s. The Fourier series representation of (2.5), note that $\delta_{T_{\mathrm{s}}}(t)$ is a periodic signal, is

$$\delta_{T_{\mathrm{s}}}(t) = \sum_{k=-\infty}^{\infty} F_k e^{jk\omega_{\mathrm{s}}t}, \quad \text{with} \quad F_k = \frac{1}{T_{\mathrm{s}}} \int_0^{T_{\mathrm{s}}} \delta_{T_{\mathrm{s}}}(t)\mathrm{e}^{-jk\omega_{\mathrm{s}}t}\,\mathrm{d}t, \tag{2.6}$$

where the sampling frequency $\omega_{\mathrm{s}} = 2\pi/T_{\mathrm{s}}$. Since

$$\int_0^{T_{\mathrm{s}}} \delta_{T_{\mathrm{s}}}(t)\mathrm{e}^{-jk\omega_{\mathrm{s}}t}\,\mathrm{d}t = 1,$$

see, e.g., [70], the series expansion (2.6) simplifies to

$$\delta_{T_{\mathrm{s}}}(t) = \frac{1}{T_{\mathrm{s}}} \sum_{k=-\infty}^{\infty} e^{jk\omega_{\mathrm{s}}t}. \tag{2.7}$$

Exploiting the series representation of the output of the nonlinearity given in (2.3) as well as the series representation of $\delta_{T_{\mathrm{s}}}(t)$ given in (2.7), in (2.4), yields the sampler output

$$\begin{aligned} u_{\mathrm{N}}^*(t) &= u_{\mathrm{N}}(t)\frac{1}{T_{\mathrm{s}}} \sum_{k=-\infty}^{\infty} e^{jk\omega_{\mathrm{s}}t} = \frac{1}{T_{\mathrm{s}}} \sum_{k=-\infty}^{\infty} u_{\mathrm{N}}(t)e^{jk\omega_{\mathrm{s}}t} = \frac{1}{T_{\mathrm{s}}} \sum_{k=-\infty}^{\infty} u_{\mathrm{N}}(t)e^{-jk\omega_{\mathrm{s}}t} = \\ &= \frac{1}{T_{\mathrm{s}}} \sum_{k=-\infty}^{\infty} \sum_{v=-\infty}^{\infty} C_v e^{j(v\omega_1 - k\omega_{\mathrm{s}})t}. \end{aligned} \tag{2.8}$$

As can be seen from above representation, if the sampler input is a sinusoidal signal with the frequency ω_1, the output signal $u_{\mathrm{N}}^*(t)$ contains the frequency ω_1 plus additional components with the frequencies $\omega_1 \pm k\omega_{\mathrm{s}}$. That means that additional signals are generated by the sampling process. By introducing the frequency

$$\omega_{v,k} = v\omega_1 - k\omega_{\mathrm{s}},$$

the signal $u_{\mathrm{N}}^*(t)$ in (2.8) can be written as

$$u_{\mathrm{N}}^*(t) = \frac{1}{T_{\mathrm{s}}} \sum_{k=-\infty}^{\infty} \sum_{v=-\infty}^{\infty} C_v e^{j\omega_{v,k}t}. \tag{2.9}$$

The signal $u_{\mathrm{N}}^*(t)$ is the input to the zero order holder. The transfer function of the ZOH element is

$$G_{\mathrm{h}}(s) = \frac{1 - e^{-sT_{\mathrm{s}}}}{s},$$

see, e.g., [31]. The frequency response of the ZOH element is obtained by evaluating $G_{\mathrm{h}}(s)$ along $s = j\omega$. With $T_{\mathrm{s}} = 2\pi/\omega_{\mathrm{s}}$ one gets

$$G_{\mathrm{h}}(j\omega) = \frac{1 - e^{-j\omega\frac{2\pi}{\omega_{\mathrm{s}}}}}{j\omega}.$$

Making use of the trigonometric identity $1 - e^{-jx} = 2je^{-j\frac{x}{2}}\sin(x/2)$, the frequency response of the ZOH element is written as

$$G_{\mathrm{h}}(j\omega) = \frac{2}{\omega}\sin\left(\pi\frac{\omega}{\omega_s}\right)e^{-j\pi\frac{\omega}{\omega_s}} = \frac{2\pi}{\omega_{\mathrm{s}}}\mathrm{sinc}\left(\pi\frac{\omega}{\omega_s}\right)e^{-j\pi\frac{\omega}{\omega_s}},$$

where $\mathrm{sinc}(x) = \sin(x)/x$. The frequency response characteristics of the hold element are

$$|G_{\mathrm{h}}(j\omega)| = \frac{2\pi}{\omega_{\mathrm{s}}}\mathrm{sinc}\left(\pi\frac{\omega}{\omega_s}\right), \quad \angle G_{\mathrm{h}}(j\omega) = -\pi\frac{\omega}{\omega_s}. \tag{2.10}$$

Since the input to the hold element is a periodic signal of frequencies $\omega_{v,k}$ also its output is periodic but with a different amplitude and a phase shift. Thus, by using (2.9) and the frequency response characteristics (2.10), the actuating signal $u(t)$ is given by

$$\begin{aligned} u(t) = &\sum_{k=-\infty}^{\infty}\sum_{v=-\infty}^{\infty} C_v\mathrm{sinc}\left(\omega_{v,k}\frac{T_{\mathrm{s}}}{2}\right)e^{j\left(t-\frac{T_{\mathrm{s}}}{2}\right)\omega_{v,k}} = \\ =&2\sum_{k=-\infty}^{\infty}\sum_{v=0}^{\infty}|C_v|\mathrm{sinc}\left(\omega_{v,k}\frac{T_{\mathrm{s}}}{2}\right)\cos\left(\omega_{v,k}t - \omega_{v,k}\frac{T_{\mathrm{s}}}{2} + \angle C_v\right). \end{aligned} \tag{2.11}$$

The latter representation is derived by exploiting the combined trigonometric form of the Fourier series, see [76], i.e.,

$$u_{\mathrm{N}}(t) = \sum_{v=-\infty}^{\infty} C_v e^{jv\omega_1 t} = C_0 + 2\sum_{v=1}^{\infty}|C_v|\cos\left(v\omega_1 t + \angle C_v\right)$$

where $C_0 = 0$ and the trigonometric identity

$$\cos(v\omega_1 t + \angle C_v)\cos(k\omega_s t) = \frac{1}{2}\left[\cos(v\omega_1 t - \omega_s t + \angle C_v) + \cos(v\omega_1 t - \omega_s t + \angle C_v)\right].$$

Note that, so far no approximations have been made. In the next step, the fundamental component, i.e., the portion of the signal with frequency ω_1, is extracted from the input signal (2.11). This component is obtained by considering only the part of the signal for which $\omega_{v,k} = \pm\omega_1$ holds, i.e.,

$$v\omega_1 - k\omega_{\mathrm{s}} = -\omega_1 \quad \text{and} \quad v\omega_1 - k\omega_{\mathrm{s}} = \omega_1. \tag{2.12}$$

Dividing the equations given in (2.12) by ω_1 one obtains

$$v = \frac{\omega_\mathrm{s}}{\omega_1}k + 1 \quad \text{and} \quad v = \frac{\omega_\mathrm{s}}{\omega_1}k - 1. \tag{2.13}$$

With the frequency ratio

$$q = T_1/T_\mathrm{s} = \omega_\mathrm{s}/\omega_1,$$

and taking into account (2.12) and (2.13) the fundamental component of the actuating signal (2.11), in the following denoted by u_1, is computed as

$$u_1(t) = 2\mathrm{sinc}\left(\frac{\pi}{q}\right)\sum_{k=0}^{\infty}\left[|C_{qk+1}|\cos\left(\omega_1 t - \frac{\pi}{q} + \angle C_{qk+1}\right) + \right. \tag{2.14}$$
$$\left. + |C_{qk-1}|\cos\left(\omega_1 t - \frac{\pi}{q} - \angle C_{qk-1}\right)\right].$$

Note that the frequency ratio q denotes the ratio of the period of the sampled limit cycle to the sampling time. Obviously, $q \geq 2$ has to hold. Furthermore, the indices of the Fourier coefficients in (2.14) can only take integer values larger or equal to zero. For all other values, the coefficients are zero.

The DF of a nonlinear element is defined as the ratio of the phasor representation of the fundamental component of the output, here $u_1(t)$ given in (2.14), and the input to the nonlinearity which is $-\sigma(t)$ given in (2.2). In view of this, the DF of the nonlinearity, the sampler and the ZOH element takes the form

$$\mathcal{B}(A,q,\theta) = \frac{2}{A}\mathrm{sinc}\left(\frac{\pi}{q}\right)e^{-j\left(\theta+\frac{\pi}{q}\right)}\sum_{k=0}^{\infty}\left[|C_{qk+1}|e^{j\angle C_{qk+1}} + |C_{qk-1}|e^{-j\angle C_{qk-1}}\right].$$

Exploiting $C_{-v} = \bar{C}_v = |C_v|e^{-j\angle C_v}$, where $\bar{C}_v$ denotes the conjugate complex of C_v, provides for the representation

$$\mathcal{B}(A,q,\theta) = \frac{2}{A}\mathrm{sinc}\left(\frac{\pi}{q}\right)e^{-j\left(\theta+\frac{\pi}{q}\right)}\sum_{k=0}^{\infty}\left[C_{qk+1} + \bar{C}_{qk-1}\right]. \tag{2.15}$$

As already mentioned above, for the validity of (2.15) the indices $qk \pm 1$ can only be larger or equal to zero. Furthermore, the index can only take integer values, i.e., kq must be an integer value. Therefore, for rational values $q = \frac{Q}{R}$ where Q, $R \in \mathbb{Z}^+$ and coprime, only every R^{th} element can appear in the sum ($k = iR$). Hence $kq = iQ$ and, therefore, it is sufficient to evaluate the sum for $q = Q$.

For the numerical evaluation of (2.15), Ackermann proposed in [71] the following from of the SDF:

$$\mathcal{N}(A,q,\theta) = \frac{2}{Aq}\mathrm{sinc}\left(\frac{\pi}{q}\right)e^{-j\left(\frac{\pi}{q}+\theta\right)}\sum_{m=0}^{q-1}u_\mathrm{N}(mT_\mathrm{s})e^{-jm\frac{2\pi}{q}}.$$

In literature, see [73, 71] the DF is usually rewritten as

$$\mathcal{N}(A,q,\theta) = \operatorname{sinc}\left(\frac{\pi}{q}\right) e^{-j\left(\frac{\pi}{q}+\theta\right)} S_q \tag{2.16}$$

with

$$S_q = \begin{cases} \frac{C_1}{A} & \text{for } q \text{ irrational} \\ \frac{2}{AQ} \sum_{m=0}^{Q-1} u_{\mathrm{N}}(mT_{\mathrm{s}}) e^{-jm\frac{2\pi}{Q}} & \text{otherwise.} \end{cases} \tag{2.17}$$

Similar to the classical DF approach for continuous-time systems, oscillations in the closed-loop system and its characteristics such as its amplitude and frequency can be predicted using the equation of harmonic balance.

Equation of Harmonic Balance

In the continuous-time configuration the equation of harmonic balance is a complex equation of two unknowns whereas the equation of harmonic balance for the sampled-data system

$$W(j\omega_1)\mathcal{N}(A,q,\theta) = -1$$

yields a complex equation of four unknowns: A, ω_1, q, and θ. The problem may be solved in a similar way as for the continuous-time configuration, i.e., determining graphically the solutions of

$$W(j\omega_1) = -\frac{1}{\mathcal{N}(A,q,\theta)}.$$

In contrast to the continuous-time case the dependency on θ causes the locus to be a curve instead of a single point. Furthermore the dependency on the frequency ratio q leads to a family of nonlinear curves, i.e., for each amplitude and frequency ratio q, a curve with θ as parameter is obtained. Thus, the Nyquist curve and the negative reciprocal SDF are plotted in three dimensional space. Each intersection point in the complex plane must additionally satisfy the relation

$$q = \frac{2\pi}{\omega T_{\mathrm{s}}}.$$

The magnitude of the Fourier coefficients decrease with growing v. It is therefore sufficient to consider only a finite number of coefficients. Furthermore, if the nonlinearity is odd only coefficients with odd-numbered index appear. In a particular problem setting the set of frequency ratios may be reduced by considering the following two remarks:

Remark 1. Limit cycles predicted by the DF and belonging to a rational q can only exist if the linear part possesses a resonance frequency at $\omega = Q\omega_1$ [73].

Remark 2. In integrating plants, i.e., plants having a pole at zero, limit cycles belonging to an odd frequency ratio q can only appear if the input sequence to the linear part is unbiased [69]. For instance, consider $q = 3$, the input sequence $(u_k) = (1, 0, -1)$ is unbiased while e.g. the sequence $(u_k) = (1, 0, 0)$ is biased.

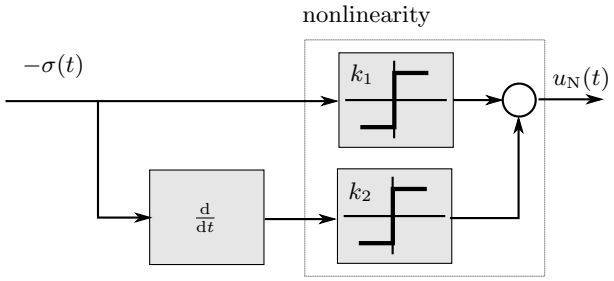

Figure 2.4: Block diagram of twisting algorithm

2.1.3 Sampled Describing Function of the Twisting Algorithm

Consider the sampled-data unity feedback configuration depicted in Figure 2.1 with the particular nonlinearity

$$u_{\mathrm{N}} = -k_1 \mathrm{sign}\,(\sigma(t)) - k_2 \mathrm{sign}\,(\dot{\sigma}(t)), \tag{2.18}$$

i.e., the twisting algorithm is applied as a controller. It is composed of two relays. The control parameters k_1, k_2 are positive constants. A block diagram of the twisting algorithm (2.18) is given in Figure 2.4. Note that (2.18) is an odd function, i.e., $\mathrm{sign}\,(-\sigma) = -\mathrm{sign}\,(\sigma)$.

The DF of the twisting algorithm, e.g. derived in [42] and given in the previous Chapter 1 in (1.11) is independent of the oscillation frequency. The graphical representation of the negative reciprocal DF in the complex plane yields a straight line. Its slope depends solely on the control parameters. For k_1, $k_2 > 0$ the line is located entirely in the second quadrant of the complex plane. Hence a periodic motion occurs only if the relative degree of $W(s)$ satisfies $\rho > 2$.

In the following application of the SDF to the twisting algorithm the input signal is approximated by

$$-\sigma(t) = A\cos(\omega_1 t + \theta) \tag{2.19}$$

and $W(s)$ is strictly proper. Furthermore, the time derivative of the output is assumed to be available e.g. from measurements or a real time differentiator. In order to derive the SDF it is necessary to evaluate the control signal $u_{\mathrm{N}}(mT_{\mathrm{s}})$, $m = 0, \ldots, q-1$. It is derived by substituting $-\sigma(t)$ from (2.19) and its time derivative

$$-\dot{\sigma}(t) = -\omega_1 A \sin(\omega_1 t + \theta)$$

into (2.18). Note that the control signal does not depend on the amplitude of the input signal.

Representing (2.17) in Cartesian coordinates and defining the real constants

$$
\begin{aligned}
a_{1,Q} &:= \sum_{m=0}^{Q-1} \operatorname{sign}\left(\cos\left(\frac{2\pi}{q}m+\theta\right)\right)\cos\left(-\frac{2\pi}{q}m\right),\\
a_{2,Q} &:= \sum_{m=0}^{Q-1} \operatorname{sign}\left(-\sin\left(\frac{2\pi}{q}m+\theta\right)\right)\sin\left(-\frac{2\pi}{q}m\right),\\
b_{1,Q} &:= \sum_{m=0}^{Q-1} \operatorname{sign}\left(\cos\left(\frac{2\pi}{q}m+\theta\right)\right)\sin\left(-\frac{2\pi}{q}m\right),\\
b_{2,Q} &:= \sum_{m=0}^{Q-1} \operatorname{sign}\left(-\sin\left(\frac{2\pi}{q}m+\theta\right)\right)\cos\left(-\frac{2\pi}{q}m\right)
\end{aligned}
$$

the SDF of the twisting algorithm can be rewritten as

$$
S_q = \begin{cases} \frac{C_1}{A} & q \,\text{irrational} \\ \frac{2}{AR}\left(k_1(a_{1,Q}+jb_{1,Q})+k_2(b_{2,Q}+ja_{2,Q})\right). & q=\frac{Q}{R}. \end{cases} \tag{2.21}
$$

The following proposition provides a relation of the sampled DF to its continuous-time counterpart for the special case when the ratio q is an integer multiple of four.

Proposition 1.1: SDF of the Twisting Algorithm

Consider the SDF (2.16) evaluated for the twisting algorithm (2.18). Suppose that $q = 4p$, $p \in \mathbb{Z}^+$ and $\theta \neq 0$ then the SDF is equivalent to

$$
\mathcal{N}(A,q,\theta) = N(A)e^{-j\theta}, \quad 0 \leq \theta < \frac{2\pi}{q}.
$$

Proof. Setting $q = Q$ the relation $a_{1,Q} = a_{2,Q} = a$ with the constant value

$$
a := \sum_{m=0}^{q-1}\left|\cos\left(-\tfrac{2\pi}{q}m\right)\right| = \sum_{m=0}^{q-1}\left|\sin\left(-\tfrac{2\pi}{q}m\right)\right|
$$

holds. Furthermore $b_{1,q} = 2$ and $b_{2,q} = -2$. From (2.21) one gets

$$
S_q = \frac{2}{AR}\left[k_1(a+2j)+k_2(-2+ja)\right].
$$

Denoting $\alpha := \cos(\pi q)$ and $\beta := \sin(\pi q)$ it can be shown that $a\beta = \cos(\pi q) - \cos(\pi q + \pi) = 2\cos(\pi q) = 2\alpha$. The SDF (2.16) becomes

$$
\mathcal{N} = \frac{4}{\pi A}(k_1+jk_2)(\alpha+j\beta)e^{-j\left(\frac{\pi}{q}+\theta\right)}.
$$

The relation $(\alpha+j\beta)e^{-j\left(\frac{\pi}{q}+\theta\right)} = e^{-j\theta}$ completes the proof. □

If the assumptions in Proposition 1.1 hold, it is possible to explicitly calculate the amplitude and phase relation of the limit cycle from

$$e^{-j\theta}W(j\omega_1) = -\frac{1}{N(A)}$$

i.e., by adding a frequency dependent time delay θ to the linear part, yielding

$$\omega_1 = \frac{2\pi}{T_\mathrm{s} q} \tag{2.22a}$$

$$A = \frac{4|W(j\omega_1)|}{\pi}\sqrt{k_1^2 + k_2^2} \tag{2.22b}$$

$$\theta = \angle W(j\omega_1) + \arctan\left(k_2/k_1\right). \tag{2.22c}$$

It is noteworthy, that the sampling process introduces a phase lag and therewith also decreases the practical phase margin [68]. From Theorem 1.1 it becomes evident that for certain frequency ratios it is possible to replace the sample and hold element in Figure 2.2 by a simple time delay. The value of the time delay can be obtained from (2.22c).

2.1.4 Simulation Example and Application to a Laboratory Setup

The application of the SDF approach is demonstrated in a simulation example as well as in a real world application. For this purpose the plant described by the state space model

$$\begin{aligned}\frac{\mathrm{d}\boldsymbol{x}}{\mathrm{d}t} &= \begin{bmatrix}0 & 1\\ 0 & -27\end{bmatrix}\boldsymbol{x} + \begin{bmatrix}0\\1\end{bmatrix}u\\ y &= \begin{bmatrix}48 & 0\end{bmatrix}\boldsymbol{x}\end{aligned} \tag{2.23}$$

is considered. It is a simplified model of a rotating mass driven by a DC motor via a gear box. The state variables $\boldsymbol{x} = \begin{bmatrix}x_1 & x_2\end{bmatrix}^\mathrm{T}$ correspond to the angular position and the angular velocity of the rotating mass, respectively. The control input u is the voltage supplied to the DC motor. The dynamics of the motor as well as friction effects are neglected in the model. The twisting algorithm with parameters $k_1 = 3$, $k_2 = 1.5$ is applied. The initial conditions are $\boldsymbol{x}_0 = \begin{bmatrix}0.2 & -14.4\end{bmatrix}^\mathrm{T}$ and the sampling time is $T_\mathrm{s} = 0.025$ s. The transfer function representation of (2.23) is

$$W(s) = \frac{\mathscr{L}\{y(t), s\}}{\mathscr{L}\{u(t), s\}} = \frac{48}{s(s+27)}.$$

The negative reciprocal SDF of the twisting, obtained by (2.21), is evaluated for the frequency ratios proposed in [71], that are $q = \{2, 5/2, 8/3, 3, 10/3, 4, 5, 6, 8, 10, 12\}$ and plotted together with the plants Nyquist curve in the ($\Re$-$\Im$-q) space in Figure 2.5.

It can be seen from Figure 2.5, that the largest possible frequency ratio is $q = 4$. For $q > 4$ the loci do not intersect and consequently, limit cycles satisfying $q > 4$ are unlikely to appear in the closed-loop system. Taking into account Remark 1, one can further reduce the set of frequency ratios to $q = \{2, 3, 4\}$. According to Remark 2 the cycle belonging to $q = 3$ can only exist if the input sequence is unbiased. Note that the control signal in the twisting algorithm is composed of two parts. In case of an sinusoidal error signal $\sigma(t)$ the two components are

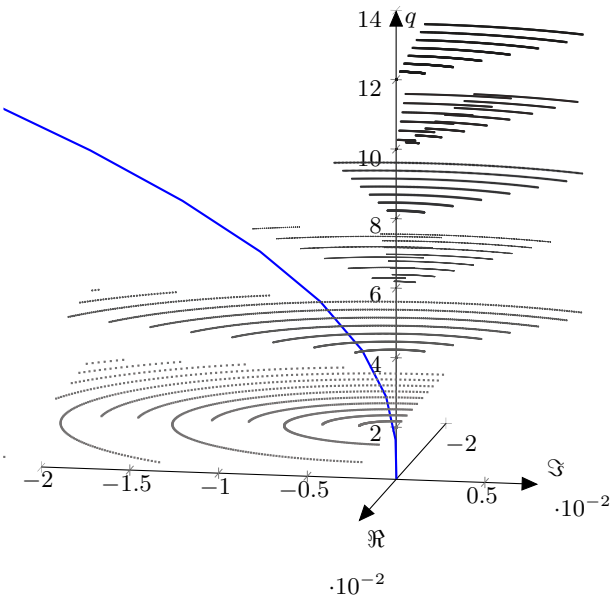

Figure 2.5: Plot of the SDF of the twisting algorithm with parameters $k_1 = 3$, $k_2 = 1.5$ and $T_\mathrm{s} = 0.025$ s together with the Nyquist plot of the plant $W(s)$.

orthogonal. Hence it is *not* possible to generate an unbiased input sequence whenever $q = 3$. Eventually only limit cycles belonging to $q = \{2, 4\}$ need to be analyzed. As an example the negative reciprocal SDF for $q = 4$ is sketched together with the Nyquist curve of the linear part in Figure 2.6. The upper plot provides a side-view of Figure 2.5, i.e., the $(\Re - q)$ plane. In the lower figure the loci are plotted in the complex plane. The gray shaded area illustrate the negative reciprocal SDF evaluated for particular amplitude values. The red line depicts the negative reciprocal DF of the continuous-time configuration, whereas the black dashed line is the same line rotated by $2\pi/q$. In order to obtain the amplitude and phase relation of the limit cycle the intersection point P is transferred from the upper plot to the lower one. Note that, according to Proposition 1.1, the amplitude and phase can also be explicitly calculated by (2.22) yielding $A = 0.048$ and $\theta = 49.8°$. Furthermore, Figure 2.5 reveals that in the absence of the sampling and hold element, i.e., in the continuous-time configuration, there is no intersection of the loci $1/N(A)$ with the Nyquist curve of $W(s)$. Hence, the DF does not predict any oscillation. The following simulation demonstrates that conclusions drawn from an analysis of the continuous-time configuration are not valid for the sampled-data system.

A simulation result is shown in Figure 2.7. The angle of the platform, shown in the upper figure, enters the limit cycle with frequency $\omega_1 = \frac{2\pi}{4T_\mathrm{s}}$ and an amplitude close to $A = 0.048$. The angular velocity exhibits a cycle with the same frequency and amplitude $\omega_1 A = 2.95$. The blue curve represents simulated values, whereas the red curve shows the predicted values. For the mode $q = 2$ one obtains $A = 0.017$ and $\omega_1 A = 2.13$. Figure 2.8a and 2.8b present the data obtained from the real world experiment. In the setup at hand the position as well as the velocity are available from measurements. It can be seen, that both predicted limit cycles

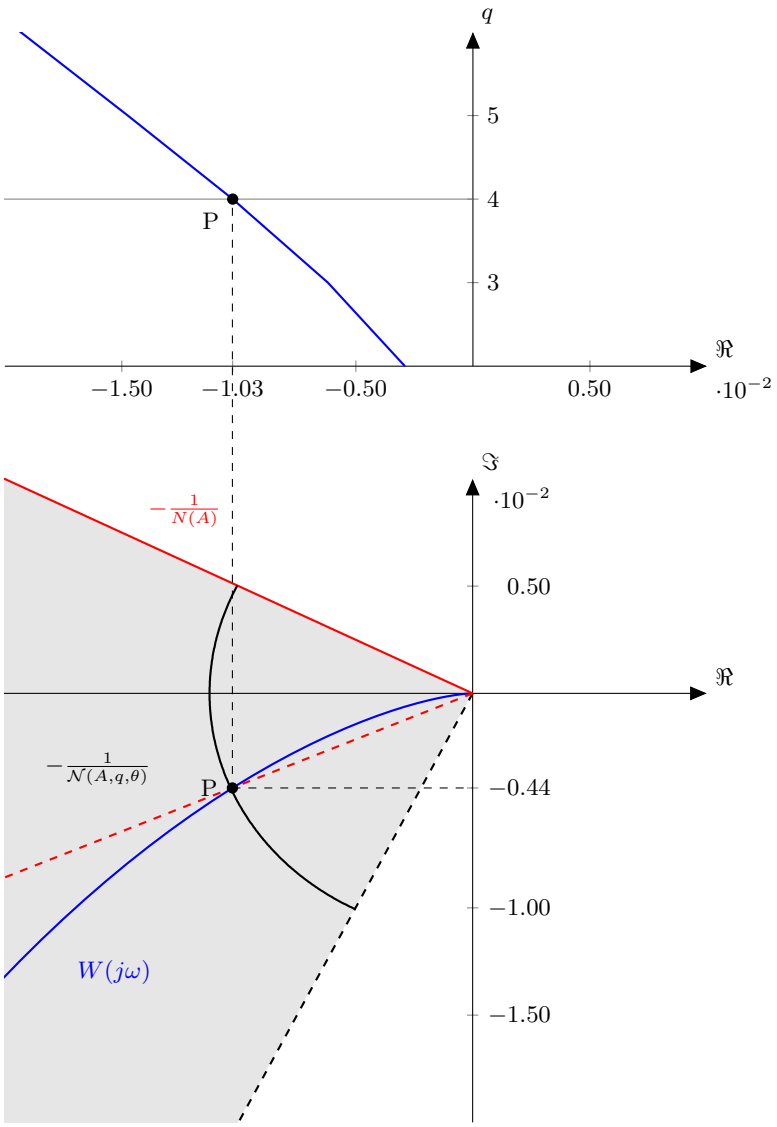

Figure 2.6: SDF of the twisting algorithm for the frequency ratio $q = 4$

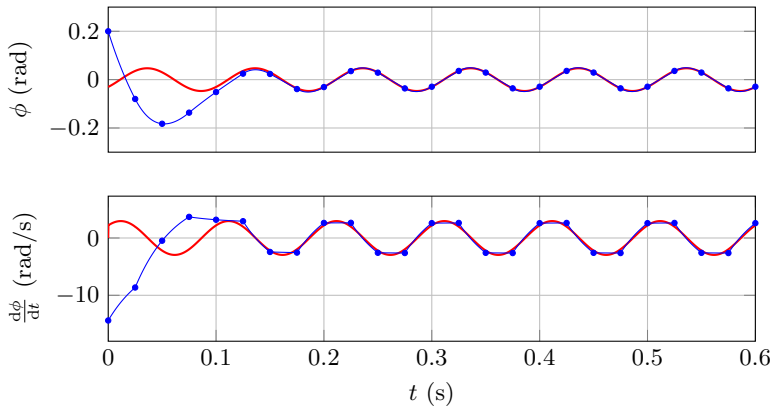

Figure 2.7: Simulated (—) vs. predicted (—) evolution of the closed-loop system response showing the limit cycle mode with $\omega_1 = \frac{2\pi}{4T_s}$.

($q = 2$ and $q = 4$) occur and predicted values agree nicely with the measured ones.

So far the analysis was restricted to the identification of limit cycles. However, the existence of such a cycle does not provide any information about its stability properties. A procedure allowing to determine the stability is discussed in detail in [69]. The analysis is based on transforming the perturbed system to a linear one consisting of q samplers in parallel with corresponding gains K_i. The gains K_i depend on the slope of the nonlinearity. For the particular case of a relay nonlinearity it is verified that $K_i = 0$ and the closed-loop is open on the linear system. The stability properties are therefore purely given by the linear part $L(s) = W(s)G_\mathrm{h}(s)$. For the present example $L(s)$ is unstable. This is reflected by the fact that a perturbation $p(t)$ at the control input may transfer the limit cycle to a neighboring cycle with the same characteristics except an different offset. This stability property may be called "indifferently-stable" [77]. A simulation illustrating this behavior is shown in Figure 2.9. It can be seen, that the cycle is unbiased until $t = 1$ s. The perturbation added to the control input changes the offset but not the characteristics of the mode. The pulse at $t = 1.5$ s forces the cycle to change the period and therewith also the amplitude. The same effects can also be observed in the real system. The measured data obtained from the experiment are shown in Figure 2.10. Note that in the real system the switch from one cylce to another happens naturally. It is not triggered by any externally generated disturbance.

2.2 Locus of Perturbed Relay System Approach for Sampled-Data Systems

The SDF analysis relies on the low-pass characteristic of $W(s)$ (filtering hypothesis), i.e., only the fundamental component of the output of the nonlinearity is considered for analysis. On the other hand, for some simple nonlinearities, the filtering hypothesis and the associated simplifications during the derivation might be dropped. In this regard, the analysis provides for exact values of the oscillation. This approach has essentially been implemented by the LPRS method for the continuous-time nonlinear unity feedback system with the hysteresis relay as a nonlinear element. In addition to the analysis of the self-excited oscillations it additionally

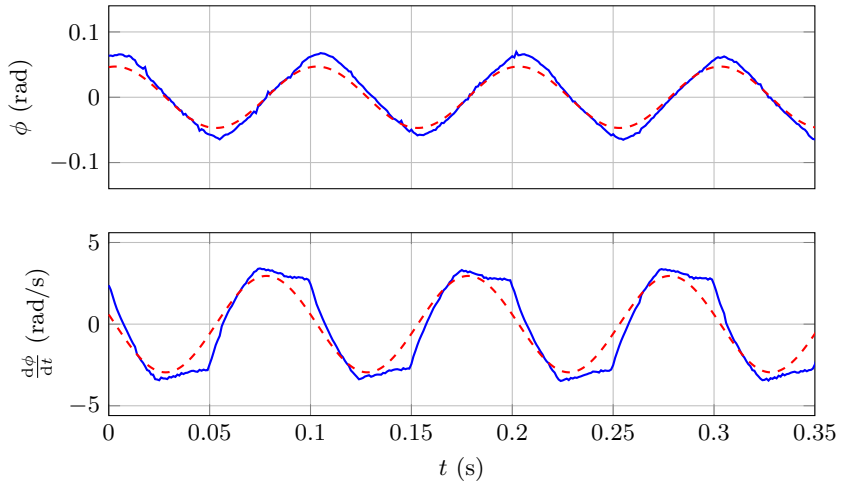

(a) Measured (—) vs. predicted (– –) evolution of the angle and angular velocity. The angle enters a limit cycle with $\omega_1 = \frac{2\pi}{4T_\mathrm{s}}$. The predicted values are $A = 0.048$ and $\omega_1 A = 2.95$.

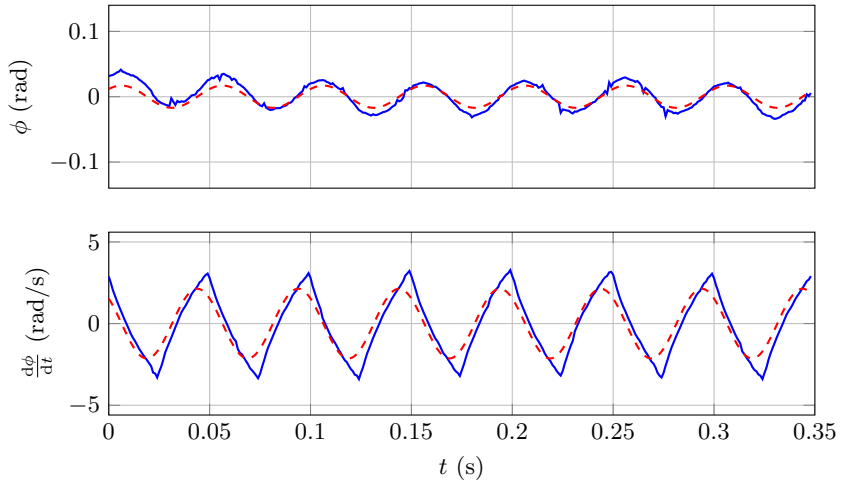

(b) Measured (—) vs. predicted (– –) evolution of the angle and angular velocity. The angle enters a limit cycle with $\omega_1 = \frac{2\pi}{2T_\mathrm{s}}$. The predicted values are $A = 0.017$ and $\omega_1 A = 2.13$.

Figure 2.8: Camparision of the chattering characteristics predicted by the SDF to the measured system response.

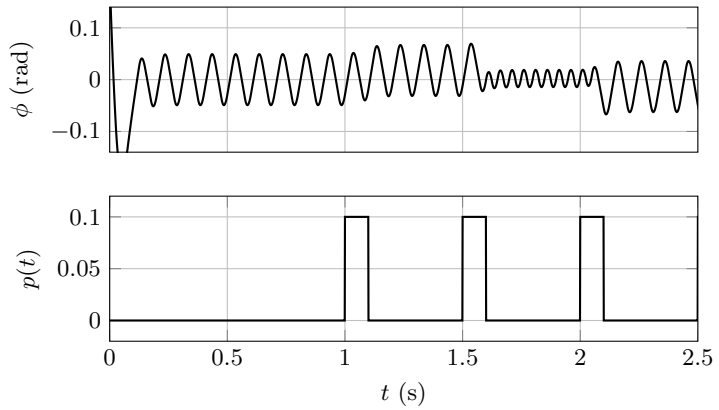

Figure 2.9: Simulation of perturbed system showing the "indifferent-stable" limit cycle with $q = 4$ and $q = 2$

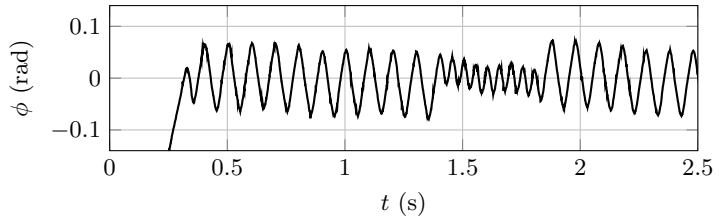

Figure 2.10: Measured system output showing the "indifferent-stable" limit cycle with $q = 4$ and $q = 2$

allows analyzing the system response to an external input. In the following, the LPRS approach is extended to the sampled-data configuration.

2.2.1 Problem Formulation

Consider a nonlinear unity feedback loop consisting of a symmetric hysteresis relay and a linear plant. The dynamics of the linear part are expressed in terms of an LTI state space model of order n. The closed-loop system is given by

$$\Sigma_{\mathrm{c}} \begin{cases} \frac{\mathrm{d}\boldsymbol{x}}{\mathrm{d}t} &= \boldsymbol{A}\boldsymbol{x} + \boldsymbol{b}u, \\ y &= \boldsymbol{c}^{\mathrm{T}}\boldsymbol{x}, \\ u &= g(\sigma), \\ \sigma &= f - y, \end{cases}$$

where $\boldsymbol{x} \in \mathbb{R}^n$ is the state vector and u is a scalar control, the scalar variable y is regarded as the systems output and $\boldsymbol{A}$, $\boldsymbol{b}$ and $\boldsymbol{c}$ are matrices and vectors of appropriate dimensions. The reference signal is denoted by $f(t)$ and $\sigma(t)$ is the error signal. The static control $g(\sigma)$ is a hysteresis relay characterized by the output level c and the width of the hysteresis $2b$. Throughout the subsequent derivations, the transfer function of the plant, which is given by

$$W(s) = \boldsymbol{c}^{\mathrm{T}}(s\boldsymbol{I} - \boldsymbol{A})^{-1}\boldsymbol{b}$$

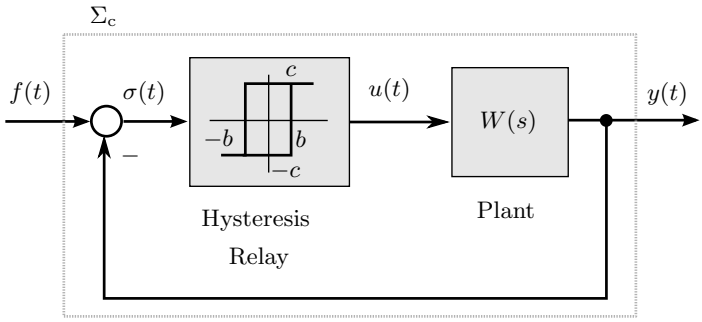

Figure 2.11: Block diagram of the relay servo system Σ_c.

is used. The relative degree $\rho \geq 1$ of $W(s)$ is a known constant. In accordance with [9], the closed-loop system Σ_c is called a relay servo system. A block diagram of Σ_c is provided in Figure 2.11.

The LPRS method provides an analysis of the self-excited periodic motions and the input-output properties. The reference signal $f(t)$ is assumed to be slow in comparison to the self-excited oscillation so that it can be assumed constant over the period of the self-excited motion. The self-excited motion is termed the *fast* motion, whereas the forced motion is considered as the *slow* motion. In the presence of a constant infinitesimal reference signal $f(t) = \bar{f} \to 0$ each signal consists of a constant and a periodic component, i.e.,

$$\begin{aligned} \sigma(t) &= \bar{\sigma} + \sigma_p(t), \\ u(t) &= \bar{u} + u_p(t), \\ y(t) &= \bar{y} + y_p(t). \end{aligned}$$

The constant term is the average of the signal over one period. The LPRS is defined as the complex valued function

$$J(\omega) = -\frac{1}{2} \lim_{\bar{f} \to 0} \frac{\bar{\sigma}}{\bar{u}} + j \frac{\pi}{4c} \lim_{\bar{f} \to 0} y(t)|_{t=0},$$

see [40]. The problem of finding periodic solutions of the closed-loop system Σ_c is solved by determining the intersection point of the locus $J(\omega)$ with the straight line parallel to the real axis with imaginary part $-\pi b/4c$. The method provides the exact oscillation frequency Ω and a constant equivalent gain for the hysteresis denoted by k_n in order to analyze the forced motion. The frequency and the gain are computed via

$$\Im\{J(\Omega)\} = -\frac{\pi b}{4c}, \quad k_n = -\frac{1}{2\Re\{J(\Omega)\}}.$$

Several formulas have been derived for the explicit computation of the LPRS in literature [9]. The following one relies on the transfer function representation of the plant dynamics:

$$J(\omega) = \sum_{\nu=1}^{\infty} (-1)^{\nu+1} \Re\{W(\nu\omega)\} + j \sum_{\nu=1}^{\infty} \frac{1}{2\nu - 1} \Im\{W((2\nu - 1)\omega)\}.$$

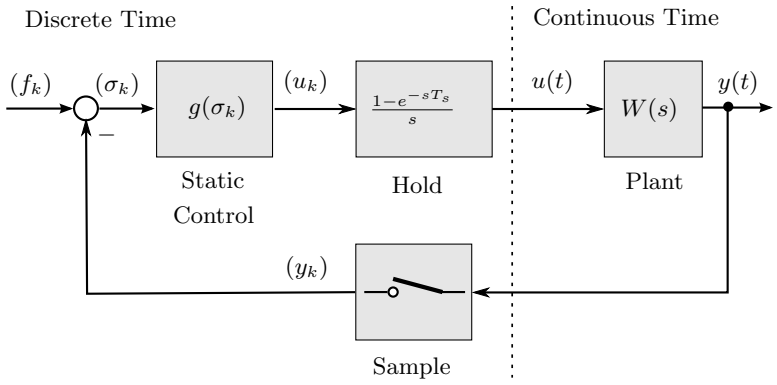

Figure 2.12: Block diagram of the sampled-data relay servo system.

Similar to the frequency response of a linear system, the LPRS is a characteristic function of the linear part only. In the following Section 2.2.2, a formula for the computation of the LPRS of a linear plant under sampling and ZOH is derived.

2.2.2 Locus of Perturbed Relay System - Sampled-Data System

The block diagram depicted in Figure 2.12 forms the basis for the following analysis. The static control law g is assumed to be realized in a digital environment. The input to the controller is the sequence $\sigma_k = f_k - y_k, \quad k = 0, 1, 2, \ldots$, where (f_k) represents a given reference sequence. The output sequence (y_k) is obtained by sampling the continuous-time signal $y(t)$ with constant sampling time T_s, i.e., $y_k = y(kT_\mathrm{s})$. The continuous-time signal $u(t)$ is reconstructed from the controller output (u_k) by a ZOH circuit, hence $u(t) = u_k$, $kT_\mathrm{s} \leq t < (k+1)T_\mathrm{s}$. In this regard, the dynamics of the continuous-time system under sampling and hold is captured by the discrete-time dynamical system

$$\begin{aligned} \boldsymbol{x}_{k+1} &= \boldsymbol{A}_\mathrm{d}\boldsymbol{x}_k + \boldsymbol{b}_\mathrm{d}u_k, \\ y_k &= \boldsymbol{c}^\mathrm{T}\boldsymbol{x}_k. \end{aligned}$$

The dynamic matrix and the input vector of the discrete-time system are given by the well-known relations

$$\boldsymbol{A}_\mathrm{d} = \boldsymbol{\Phi}(T_\mathrm{s}) = e^{\boldsymbol{A}T_\mathrm{s}}, \quad \boldsymbol{b}_\mathrm{d} = \int_0^{T_\mathrm{s}} e^{\boldsymbol{A}s}\boldsymbol{b}\,\mathrm{d}s.$$

The discrete transfer function is computed as

$$H(z) = (1 - z^{-1})\mathscr{Z}\left\{\frac{1}{s}W(s)\right\},$$

where the operator $\mathscr{Z}\left\{\frac{1}{s}W(s)\right\}$ combines the following steps: inverse Laplace transformation of $\frac{1}{s}W(s)$; then sampling of the continuous-time signal and, eventually, z-transformation of

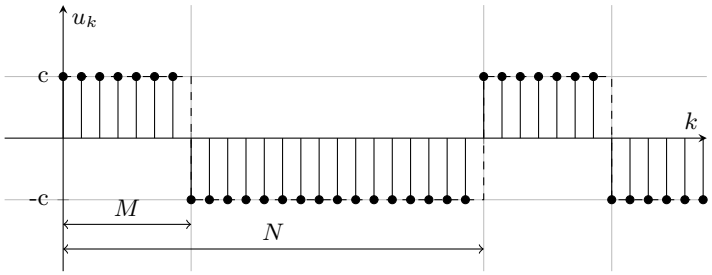

Figure 2.13: Periodic input sequence.

the resulting sequence. The output sequence of the hysteresis relay is given by the expression

$$u_k = \begin{cases} +c & \text{if} \quad \sigma_k \geq b \vee (\sigma_k > -b \wedge u_{k-1} = c) \\ -c & \text{if} \quad \sigma_k \leq -b \vee (\sigma_k < b \wedge u_{k-1} = -c). \end{cases}$$

The reference sequence is assumed to be an infinitesimal constant, i.e., $f_k \equiv \bar{f} \to 0$. If the output sequence (y_k) and its underlying continuous-time signal $y(t)$ exhibits a periodic motion, also the input sequence to $W(s)$ will be periodic. A periodic motion in the input signal is called a mode, whereas a periodic motion in the output is called a limit cycle. Whenever the system trajectory enters an unimodal limit cycle, i.e., it switches twice per period, the input sequence is described by a periodic square wave sequence as depicted in Figure 2.13. The pulse durations MT_s and $(N-M)T_\mathrm{s}$ with $N, M \in \mathbb{Z}^+$ and $N > M \geq 1$ are of unequal length. One period of such a mode is described by

$$u_k = \begin{cases} c & \text{if} \quad 0 \leq k \leq M-1, \\ -c & \text{else.} \end{cases} \tag{2.24}$$

In order to derive the LPRS for the sampled-data system, the periodic input sequence (u_k) is represented by its discrete-time Fourier series

$$u_k = \sum_{\nu=0}^{N-1} C_\nu e^{j\nu\omega_0 k}, \quad \omega_0 = \frac{2\pi}{N}, \tag{2.25}$$

with the complex Fourier coefficients

$$C_\nu = \frac{1}{N} \sum_{k=0}^{N-1} u_k e^{-j\nu\omega_0 k}.$$

Considering the input sequence (2.24), the Fourier coefficients can be given in the closed form as

$$C_\nu = \frac{2c}{N} \begin{cases} \frac{\sin\left(\frac{\nu\omega_0 M}{2}\right)}{\sin\left(\frac{\nu\omega_0}{2}\right)} e^{-j\nu\omega_0 \frac{M-1}{2}} & \text{if} \quad \nu \neq 0,\ N,\ 2N,\ \ldots \\ M - \frac{N}{2} & \text{otherwise.} \end{cases} \tag{2.26}$$

Substituting (2.26) into (2.25) yields the input sequence

$$u_k = \bar{u} + \frac{2c}{N} \sum_{\nu=1}^{N-1} \frac{\sin\left(\frac{\nu\omega_0 M}{2}\right)}{\sin\left(\frac{\nu\omega_0}{2}\right)} e^{j\nu\omega_0 r_k}, \tag{2.27}$$

with

$$r_k = k - \frac{M-1}{2}.$$

The sequence is composed of the constant term

$$\bar{u} = \frac{2c}{N}\left(M - \frac{N}{2}\right) \tag{2.28}$$

and a finite sum of harmonic signals with amplitude $\frac{2c}{N}\sin\left(\frac{\nu\omega_0 M}{2}\right)/\sin\left(\frac{\nu\omega_0}{2}\right)$, frequency $\nu\omega_0$ and phase $\nu\omega_0(M-1)/2$. Therefore, the sampled output of the linear plant $H(z)$, as a response to the input signal (2.27), also is a sum of harmonic signals with same frequency as the input signal but with different amplitude and phase, i.e.,

$$y_k = \bar{y} + \frac{2c}{N} \sum_{\nu=1}^{N-1} \frac{\sin\left(\frac{\nu\omega_0 M}{2}\right)}{\sin\left(\frac{\nu\omega_0}{2}\right)} A_\nu e^{j(\nu\omega_0 r_k + \varphi_\nu)}$$

where

$$A_\nu = \left|H(z)\big|_{z=e^{j\nu\omega_0}}\right|,$$
$$\varphi_\nu = \angle H(z)\big|_{z=e^{j\nu\omega_0}}.$$

Since for a real signal $C_{-\nu} = \bar{C}_\nu$, where $\bar{C}_\nu$ denotes the conjugate complex, it is possible to combine the terms $C_\nu e^{-j\nu\omega_0 k} + C_\nu e^{j\nu\omega_0 k}$ into $2|C_\nu|\cos(\nu\omega_0 k + \angle C_\nu)$. Hence,

$$y_k = \bar{y} + \frac{4c}{N} \sum_{\nu=1}^{\left\lfloor \frac{N}{2} \right\rfloor} \frac{\sin\left(\frac{\nu\omega_0 M}{2}\right)}{\sin\left(\frac{\nu\omega_0}{2}\right)} A_\nu \cos\left(\nu\omega_0 r_k + \varphi_\nu\right) - \frac{2c}{N}\Gamma_k. \tag{2.30}$$

with

$$\Gamma_k = \begin{cases} (-1)^k H\left(-1\right) & \text{if } N \text{ is even and } M \text{ is odd} \\ 0 & \text{else} \end{cases}$$

and $\lfloor\cdot\rfloor$ denotes the floor function, i.e.,

$$\left\lfloor \frac{N}{2} \right\rfloor = \begin{cases} \frac{N}{2} & \text{if } N \text{ is even} \\ \frac{N-1}{2} & \text{else.} \end{cases}$$

The constant component in the output is given by $\bar{y} = \bar{u}\,|H(1)|$. The trigonometric identity $\cos(x_1 + x_2) = \cos(x_1)\cos(x_2) - \sin(x_1)\sin(x_2)$ and a transition to Cartesian coordinates

$$\Re\left\{H(z)\big|_{z=e^{j\nu\omega_0}}\right\} = A_\nu \cos\left(\varphi_\nu\right),$$
$$\Im\left\{H(z)\big|_{z=e^{j\nu\omega_0}}\right\} = A_\nu \sin\left(\varphi_\nu\right)$$

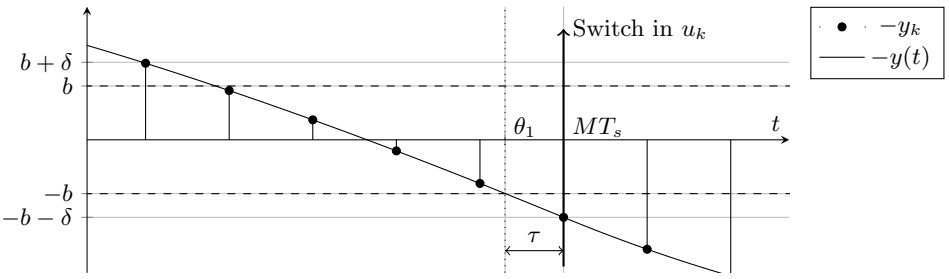

Figure 2.14: Conditions for a switch in the continuous-time configuration and in the sampled-data system.

provides for the alternative representation of (2.30) as

$$y_k = \bar{y} + \frac{4c}{N} \sum_{\nu=1}^{\lfloor \frac{N}{2} \rfloor} \frac{\sin\left(\frac{\nu\omega_0 M}{2}\right)}{\sin\left(\frac{\nu\omega_0}{2}\right)} \Big\{ \cos(\nu\omega_0 r_k) \Re\{H(e^{j\nu\omega_0})\} - \\ - \sin(\nu\omega_0 r_k) \Im\{H(e^{j\nu\omega_0})\} \Big\} - \frac{2c}{N}\Gamma_k. \tag{2.32}$$

When faced with the continuous-time case the conditions for a switch in the relay can be found from inspection of the error signal σ, which needs to take the hysteresis value

$$\bar{f} - y(0) = b, \tag{2.33a}$$
$$\bar{f} - y(\tilde{t}^*) = -b, \tag{2.33b}$$

where it is assumed that the relay switches at $t = 0$ from the negative to the positive value and back to the negative value at time instant $t = \tilde{t}^*$, see [9]. In case of a sampled output signal the above equations (2.33) do not hold in general. In order to find the conditions for a switch in the sampled-data system consider Figure 2.14 where $(f_k) = (0)$. The dots represent the negative output sequence (y_k), the solid black line is the underlying continuous-time signal, i.e., $-y(t)$. The continuous-time trajectory crosses the surface $\boldsymbol{c}^{\mathrm{T}}\boldsymbol{x} = -b$ at $t = \theta_1$, however, the output sequence (y_k) can only trigger a switch at time instants which are integer multiples of the sampling time. Hence, the switch in the sampled-data system appears at the time instant $MT_\mathrm{s} \geq \theta_1$, i.e., if the output sequence crosses the surface $\boldsymbol{c}^{\mathrm{T}}\boldsymbol{x} = -(b+\delta)$. In this regard the surfaces $\boldsymbol{c}^{\mathrm{T}}\boldsymbol{x} = \pm b$ are called the *decision surfaces* and $\boldsymbol{c}^{\mathrm{T}}\boldsymbol{x} = \pm(b+\delta)$ are the *switching surfaces*. The conditions for a switch in the sampled-data system therefore take the form

$$\bar{f} - y_0 = b + \delta, \tag{2.34a}$$
$$\bar{f} - y_M = -b - \delta. \tag{2.34b}$$

The values of the output sequence at the switching instances are obtained from (2.32) by setting $k = 0$ and $k = M$, respectively, i.e.,

$$y_0 = \bar{y} + \frac{4c}{N} \sum_{\nu=1}^{\lfloor \frac{N}{2} \rfloor} \frac{\sin\left(\frac{\nu\omega_0 M}{2}\right)}{\sin\left(\frac{\nu\omega_0}{2}\right)} \Big\{ \cos(-\nu\omega_0 r_0) \Re\{H(e^{j\nu\omega_0})\} + \\ + \sin(-\nu\omega_0 r_0) \Im\{H(e^{j\nu\omega_0})\Big\} - \frac{2c}{N}\Gamma_0 \tag{2.35}$$

and

$$y_M = \bar{y} + \frac{4c}{N} \sum_{\nu=1}^{\lfloor \frac{N}{2} \rfloor} \frac{\sin\left(\frac{\nu\omega_0 M}{2}\right)}{\sin\left(\frac{\nu\omega_0}{2}\right)} \Big\{ \cos\left(\nu\omega_0 r_M\right) \Re\{H(e^{j\nu\omega_0})\} - \\ - \sin\left(\nu\omega_0 r_M\right) \Im\{H(e^{j\nu\omega_0})\} \Big\} - \frac{2c}{N}\Gamma_M. \tag{2.36}$$

Considering the formulas for the closed-loop system in (2.34) the relation

$$y_M - y_0 = 2(b + \delta)$$

holds. The switching in the sampled-data system appears in general with a time-delay τ compared to the time instant θ_1, where $\tau \in [0, T_\mathrm{s})$. Thus, there exists a phase relation of the sampling, denoted by τ^*, such that $\delta = 0$. It is possible to rewrite the conditions for a switching as

$$y(MT_\mathrm{s} - \tau^*) - y(0 - \tau^*) = 2b. \tag{2.37}$$

The phase relation τ^* is characteristic for the limit cycle to be determined and is incorporated into the linear part of the control loop. Therefore, an additional phase shift is added to the frequency response of the linear plant by introducing

$$\tilde{H}(\nu\omega_0, \tau) = A_\nu e^{j\left(\varphi_\nu - \nu\omega_0 \frac{\tau}{T_\mathrm{s}}\right)}. \tag{2.38}$$

Considering (2.38) and substituting (2.35) together with (2.36) into (2.37) and, furthermore, taking into account that $\Gamma_M = -\Gamma_0$, one obtains

$$b = \frac{2c}{N} \sum_{\nu=1}^{\lfloor \frac{N}{2} \rfloor} \left[-\left(1 - \cos(\nu\omega_0 M)\right) \mathcal{W}_I(\nu\omega_0, \tau) \right] + \frac{2c}{N}\Gamma_0, \tag{2.39}$$

where for the sake of a compact representation

$$\mathcal{W}_I(\nu\omega_0, \tau) := \Re\{\tilde{H}(\nu\omega_0, \tau)\} + \frac{\Im\{\tilde{H}(\nu\omega_0, \tau)\}}{\tan\left(\nu\frac{\omega_0}{2}\right)}$$

has been introduced. Taking into account (2.39) and provided that N is even, it follows from the definition of the LPRS

$$\Im\{J\} = -\frac{\pi}{2N} \sum_{\nu=1}^{\frac{N}{2}} \left[\left((-1)^\nu - 1\right) \mathcal{W}_I(\nu\omega_0, \tau) \right] + \frac{\pi}{4N} \left((-1)^{\frac{N}{2}} - 1 \right) H(-1). \tag{2.40}$$

The real part of the LPRS contains information about the equivalent gain k_n. The definition of the real part of the LPRS is transformed into

$$\Re\{J(\omega)\} = \frac{1}{2} \lim_{\gamma \to \frac{1}{2}} \frac{\bar{y}}{\bar{u}}, \quad \gamma = \frac{M}{N}. \tag{2.41}$$

Using (2.35) together with (2.36) in (2.33), the constant part in the output signal, for $\bar{f} \to 0$, yields

$$\bar{y} = -\frac{2c}{N} \sum_{\nu=1}^{\lfloor \frac{N}{2} \rfloor} \sin(\nu\omega_0 M) \mathcal{W}_R(\nu\omega_0, \tau), \tag{2.42}$$

with

$$\mathcal{W}_R(\nu\omega_0, \tau) := -\frac{\Re\{\tilde{H}(\nu\omega_0, \tau)\}}{\tan\left(\nu\frac{\omega_0}{2}\right)} + \Im\{\tilde{H}(\nu\omega_0, \tau)\}.$$

Calculating the limit (2.41) with (2.28) and (2.42) gives

$$\Re\{J(\omega)\} = \frac{\pi}{N} \sum_{\nu=1}^{\frac{N}{2}} \nu(-1)^\nu \mathcal{W}_R(\nu\omega_0, \tau). \tag{2.43}$$

Finally putting together (2.43) with the imaginary part (2.40), the LPRS for the linear plant under sampling and ZOH eventually takes the form

$$J = \frac{\pi}{N} \sum_{\nu=1}^{\frac{N}{2}} \nu(-1)^\nu \mathcal{W}_R(\nu\omega_0, \tau) - j\frac{\pi}{2N} \sum_{\nu=1}^{\frac{N}{2}} ((-1)^\nu - 1)\mathcal{W}_I(\nu\omega_0, \tau) + \tag{2.44}$$
$$+ j\frac{\pi}{4N}\left((-1)^{\frac{N}{2}} - 1\right) H(-1).$$

In contrast to the continuous-time LPRS the locus in (2.44) is not only a function of the frequency but also of the phase relation τ. Thus, one obtains for each frequency $\omega = \omega_0/T_\mathrm{s}$ a curve parametrized by τ. Similar to the frequency response of a linear system, which describes the steady state response of the system due to a harmonic input signal, the LPRS can be interpreted as the response of a linear system to a periodic square wave signal. Hence, in order to represent the LPRS graphically, one might also exploit similar strategies as used in linear systems theory. Prominent tools are the Nyquist and the Bode plot. Commonly the LPRS is plotted in the complex plane equivalent to the Nyquist plot. An example of this graphical representation is provided in Fig 2.15. The LPRS is evaluated for $N = 2l$ where l is a positive integer. The envelopes are the LPRS for the continuous-time system and the continuous-time system with an additional time delay corresponding to the sampling time T_s, i.e., system Σ_c with $\sigma = \bar{f} - y(t - T_\mathrm{s})$. The time delayed system is denoted by $\Sigma_{\mathrm{c},T_\mathrm{s}}$

An intersection of the LPRS with the straight line parallel to the real axis with imaginary part $-\pi b/(4c)$ provides a necessary condition for the existence of a symmetric unimodal limit cycle in the sampled-data system. Under the assumption that the dynamic matrix $\boldsymbol{A}$ is regular, the initial state vector for the identified limit cycles are given by

$$\boldsymbol{\xi}_N = \left(\boldsymbol{I} + \boldsymbol{A}_\mathrm{d}^{\frac{N}{2}}\right)^{-1} \boldsymbol{A}^{-1} \left(\boldsymbol{A}_\mathrm{d}^{\frac{N}{2}} - \boldsymbol{I}\right) \boldsymbol{b}c. \tag{2.45}$$

Additionally, the stability properties of each periodic solution needs to be investigated.

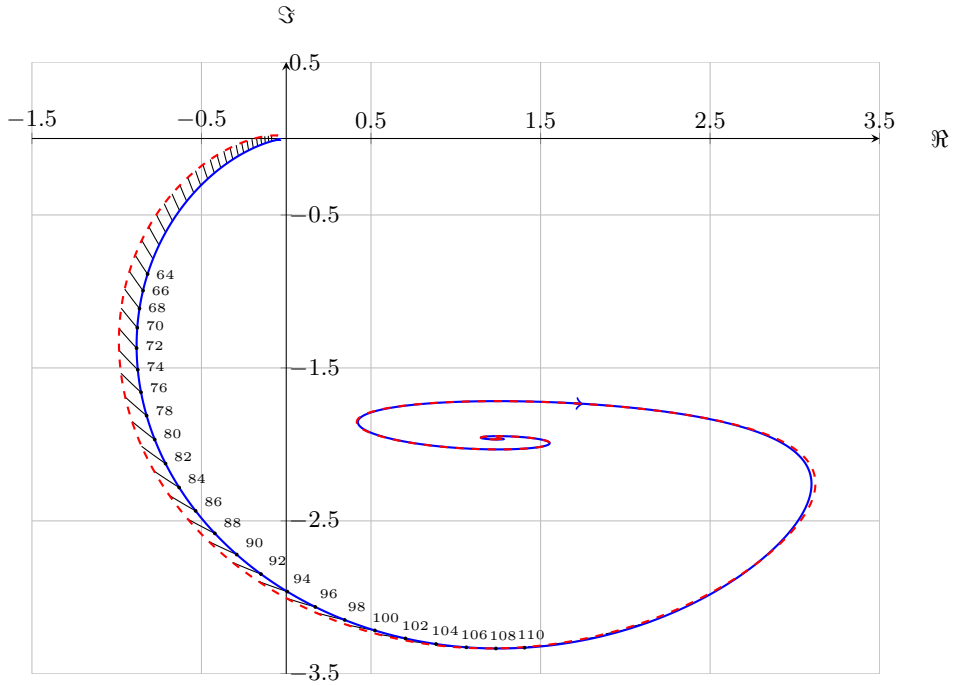

Figure 2.15: LPRS for a second order system under sampling and ZOH (——) evaluated for certain frequency ratios N. The envelopes are the LPRS for the continuous-time system (——) and the continuous-time system with an additional time delay T_s (- - -) respectively.

2.2.3 Stability and Basin of Attraction of Limit Cycles

In continuous-time relay systems the asymptotic orbital stability of a periodic solution is usually concluded from the eigenvalues of the Jacobian of the Poincaré map

$$\boldsymbol{U}(t^*) = \left(\frac{\boldsymbol{v}\boldsymbol{c}^\mathrm{T}}{\boldsymbol{c}^\mathrm{T}\boldsymbol{v}}\right) e^{\boldsymbol{A}t^*}$$

where $\boldsymbol{v} = -\boldsymbol{A}\boldsymbol{x}^* - \boldsymbol{b}$ and $2t^*$ is the period of the limit cycle with initial condition $\boldsymbol{x}^*$. The limit cycle is asymptotically orbital stable if and only if all eigenvalues of $\boldsymbol{U}(t^*)$ are located inside the unit circle [78].

In the sampled-data system the actual existence of a limit cycle depends on the initial conditions. Due to the fact that a switching can only take place at integer multiples of T_s, a small perturbation $\boldsymbol{\Delta} \in \mathbb{R}^n$ to the initial conditions $\boldsymbol{x}(0) = \boldsymbol{\xi}_N$ of the reference solution $\tilde{\boldsymbol{x}}(t)$ does not necessarily alter the input signal $u(t)$. This situation is depicted in Figure 2.16. The reference solution $\tilde{y}(t) = \boldsymbol{c}^\mathrm{T}\tilde{\boldsymbol{x}}(t)$ crosses the decision surface at $t = \tilde{\theta}_1^*$. Suppose that the perturbed solution $y(t) = \boldsymbol{c}^\mathrm{T}\boldsymbol{x}(t)$ crosses the decision surface at $t = \theta_1^*$. If both solutions cross the decision surface within the same sampling interval, i.e., $\theta_1^*, \tilde{\theta}_1^* \in \left(\left(\frac{N}{2} - 1\right), \frac{N}{2}\right] T_\mathrm{s}$ the switching will take place at the same sampling instant $\frac{N}{2}$. If this holds for all subsequent switchings the input signal will remain unchanged.

Let $\boldsymbol{\Phi}_{\frac{N}{2}} = \boldsymbol{\Phi}\left(\frac{N}{2}T_\mathrm{s}\right)$ and $\boldsymbol{\Phi}_{\frac{N}{2}-1} = \boldsymbol{\Phi}\left(\left(\frac{N}{2} - 1\right)T_\mathrm{s}\right)$. Furthermore let $\tilde{\boldsymbol{\xi}}_N$ denote the state of

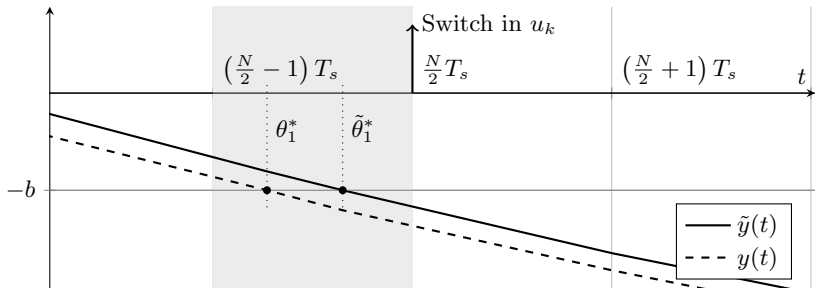

Figure 2.16: Switching triggered by the reference solution and a perturbed solution. If both solutions cross the decision surface $\boldsymbol{c}^{\mathrm{T}}\boldsymbol{x} = \pm b$ in the same sampling interval the switch takes place at the same time instant $t = \frac{N}{2}T_{\mathrm{s}}$.

the periodic solution one sampling step ahead of $\boldsymbol{\xi}_N$, i.e.,

$$\tilde{\boldsymbol{\xi}}_N = e^{-\boldsymbol{A}T_{\mathrm{s}}}\left(\boldsymbol{\xi}_N - \boldsymbol{b}_{\mathrm{d}}c\right)$$

and define

$$\begin{aligned} \boldsymbol{p}_1^{\mathrm{T}} &:= \boldsymbol{c}^{\mathrm{T}}\boldsymbol{\Phi}_{\frac{N}{2}}, & d_1 &:= b - \boldsymbol{c}^{\mathrm{T}}\boldsymbol{\xi}_N, \\ \boldsymbol{p}_2^{\mathrm{T}} &:= \boldsymbol{c}^{\mathrm{T}}\boldsymbol{\Phi}_{\frac{N}{2}-1}, & d_2 &:= b - \boldsymbol{c}^{\mathrm{T}}\tilde{\boldsymbol{\xi}}_N. \end{aligned}$$

If the perturbation lies within the set $\boldsymbol{\Delta} \in \mathcal{D} = \mathcal{D}_U \cap \mathcal{D}_L \cap \mathcal{D}_I$, where

$$\begin{aligned} \mathcal{D}_U &= \left\{ \boldsymbol{\Delta} \in \mathbb{R}^n \,:\, \inf_i \left((-1)^{i+1} \boldsymbol{p}_1^{\mathrm{T}} \boldsymbol{\Phi}_{\frac{N}{2}}^i \boldsymbol{\Delta} - d_1 \right) \geq 0 \right\}, \\ \mathcal{D}_L &= \left\{ \boldsymbol{\Delta} \in \mathbb{R}^n \,:\, \sup_i \left((-1)^{i+1} \boldsymbol{p}_2^{\mathrm{T}} \boldsymbol{\Phi}_{\frac{N}{2}}^i \boldsymbol{\Delta} - d_2 \right) < 0 \right\} \end{aligned}$$

and

$$\mathcal{D}_I = \begin{cases} \left\{ \boldsymbol{\Delta} \in \mathbb{R}^n \,:\, \boldsymbol{c}^{\mathrm{T}}(\boldsymbol{\xi}_N + \boldsymbol{\Delta}) \geq b \right\}, & \text{if } u_{-1} = c \\ \left\{ \boldsymbol{\Delta} \in \mathbb{R}^n \,:\, \boldsymbol{c}^{\mathrm{T}}(\boldsymbol{\xi}_N + \boldsymbol{\Delta}) > -b \right\}, & \text{if } u_{-1} = -c \end{cases}$$

with $i = 0, 1, 2, \ldots$, the perturbed solution will cross the decision surfaces within the intervals $t \in \left(\left(\frac{N}{2}-1\right), \frac{N}{2}\right](i+1)T_{\mathrm{s}}$ and consequently the input sequence of the perturbed system remains the same as for the unperturbed system. This leads to the following:

Theorem 2.1: Admissible Perturbations

Assume that a symmetric unimodal limit cycle with period NT_{s} exists and $\boldsymbol{A}$ is a Hurwitz Matrix. Then all solutions starting from $\boldsymbol{x}(0) = \boldsymbol{\xi}_N + \boldsymbol{\Delta}$ with $\boldsymbol{\Delta} \in \mathcal{D}$ will asymptotically converge to the reference solution.

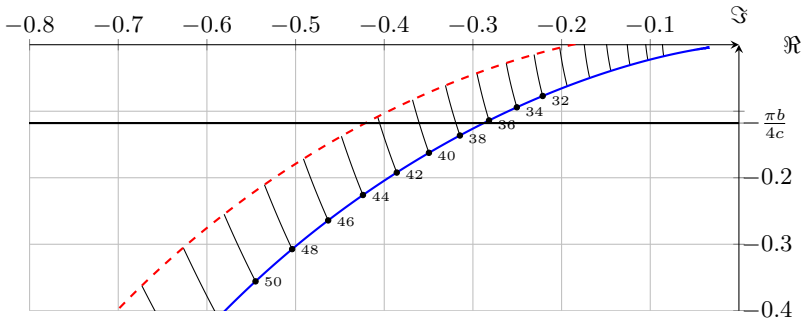

Figure 2.17: LPRS for the example system. The loci of the sampled-data system show three intersections whereas in the continuous-time system Σ_c only one intersection is possible.

Proof. The proof follows directly from the additivity property, i.e., $\lim_{t\to\infty}(\tilde{\boldsymbol{x}}(t) - \boldsymbol{x}(t)) = \lim_{t\to\infty} e^{\boldsymbol{A}t}\boldsymbol{\Delta}$. □

A local prediction of the basin of attraction for a specific limit cycle is obtained from the polytopes defined by the system of inequalities

$$(-1)^i \boldsymbol{p}_1^{\mathrm{T}} \boldsymbol{\Phi}_{\frac{N}{2}}^i \boldsymbol{\Delta} + d_1 \quad \leq 0, \tag{2.46a}$$

$$(-1)^{i+1} \boldsymbol{p}_2^{\mathrm{T}} \boldsymbol{\Phi}_{\frac{N}{2}}^i \boldsymbol{\Delta} - d_2 < 0, \tag{2.46b}$$

$$\begin{cases} \boldsymbol{c}^{\mathrm{T}}(\boldsymbol{\xi}_N + \boldsymbol{\Delta}) \geq b, & \text{if } u_{-1} = c \\ \boldsymbol{c}^{\mathrm{T}}(\boldsymbol{\xi}_N + \boldsymbol{\Delta}) > -b, & \text{if } u_{-1} = -c. \end{cases} \tag{2.46c}$$

The problem is equivalent to finding the output admissible set of a discrete-time dynamical system. Under certain conditions, the underlying continuous-time system must satisfy see [79], this set may be determined by a finite number of linear inequalities given by $i = 0, 1, 2 \ldots \bar{i}$. An estimate of $\bar{i}$ can be found by applying techniques outlined in [79].

2.2.4 Tutorial Example

The system under investigation is given by the state space representation

$$\begin{aligned} \frac{\mathrm{d}\boldsymbol{x}}{\mathrm{d}t} &= \begin{bmatrix} 0 & 1 \\ -0.4 & -0.5 \end{bmatrix} \boldsymbol{x} + \begin{bmatrix} 0 \\ 1 \end{bmatrix} u, \\ y &= \begin{bmatrix} 1 & 0 \end{bmatrix} \boldsymbol{x}, \end{aligned} \tag{2.47}$$

with the hysteresis relay characteristics $b = 1.5$ and $c = 10$. The sampling time is selected as $T_s = 0.1$ s. The LPRS of system (2.47) under sampling and ZOH is plotted in the complex plane in Figure 2.17 for $N = 32, 34, \ldots, 50$. In contrast to the continuous-time configuration, the loci of the sampled-data system shows three intersections $N = \{38, 40, 42\}$. The initial conditions, obtained by (2.45) are provided together with the equivalent gains and the phase relations τ^* in Table 2.1. The trajectories obtained with these initial states and $(f_k) = (0)$ are shown in the phase plane plot in Figure 2.18. Additionally the limit cycle found in the

N	$\boldsymbol{\xi}_N^{\mathrm{T}}$	τ^* (s)	k_{n}
38	[1.74 9.82]	0.024	1.57
40	[2.07 10.36]	0.056	1.39
42	[2.45 10.89]	0.088	1.23

Table 2.1: Limit cycles identified with the LPRS method for the example system.

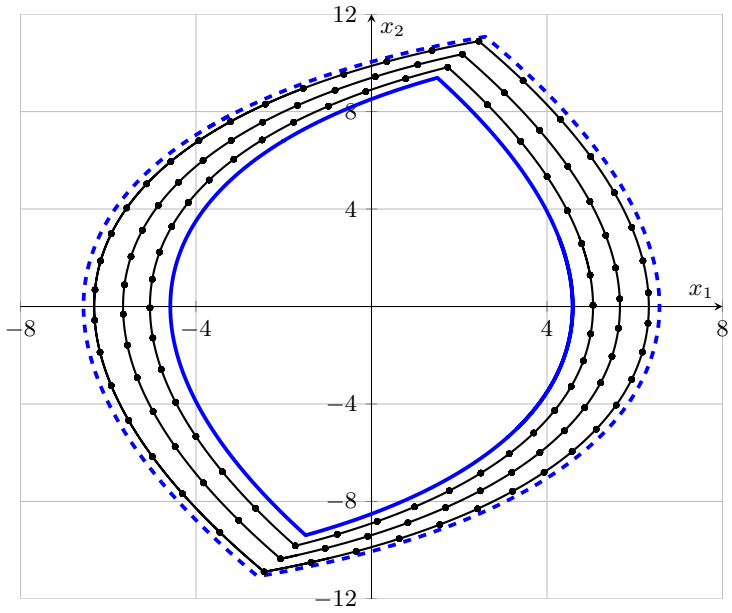

Figure 2.18: Limit cycles indicated by the LPRS in the sampled-data system (——) with frequency ratios $N = \{38, 40, 42\}$ plotted together with the limit cycles observed in the continuous-time system (——) and the continuous-time system with an additional time delay T_{s} (- - -).

continuous-time configuration Σ_{c} and in the time delayed configuration $\Sigma_{\mathrm{c},T_{\mathrm{s}}}$ is plotted. For this example, the limit cycle present in $\Sigma_{\mathrm{c},T_{\mathrm{s}}}$ defines a globally attractive and positively invariant set for the sampled-data system. Hence, if one is only interested in an estimate of the maximum chattering amplitude, it is sufficient to elaborate on system $\Sigma_{\mathrm{c},T_{\mathrm{s}}}$ rather than considering the system under sampling and hold. On the other hand, the set defined by the interior of the limit cycle present in Σ_{c} is a repelling set for the system under sampling and hold. Thus, the discrete implementation of the controller deteriorates the control performance by increasing the chattering amplitude.

The *fast* autonomous motion is recovered by replacing the sampling and hold element with a time delay of τ^* seconds. The *slow* forced motion is analyzed by replacing the hysteresis element with the equivalent gain k_{n}. The LPRS method yields one particular equivalent gain for each intersection point, i.e., for each limit cycle. It is therefore difficult to predict globally to which limit cycle the trajectory will converge. Especially in case of a time-varying input signal, the fast motion is subject to permanent perturbations and the trajectory will not settle to one particular limit cycle. Thus, the choice of the equivalent gain for the analysis of the

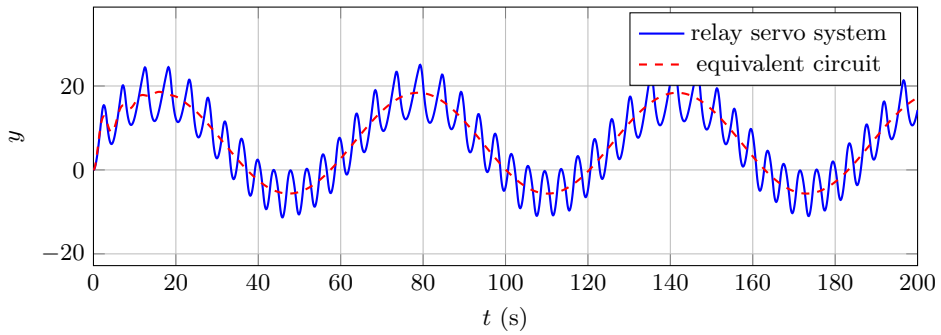

Figure 2.19: Output of the relay servo system and the equivalent circuit due to a sinusoidal reference signal.

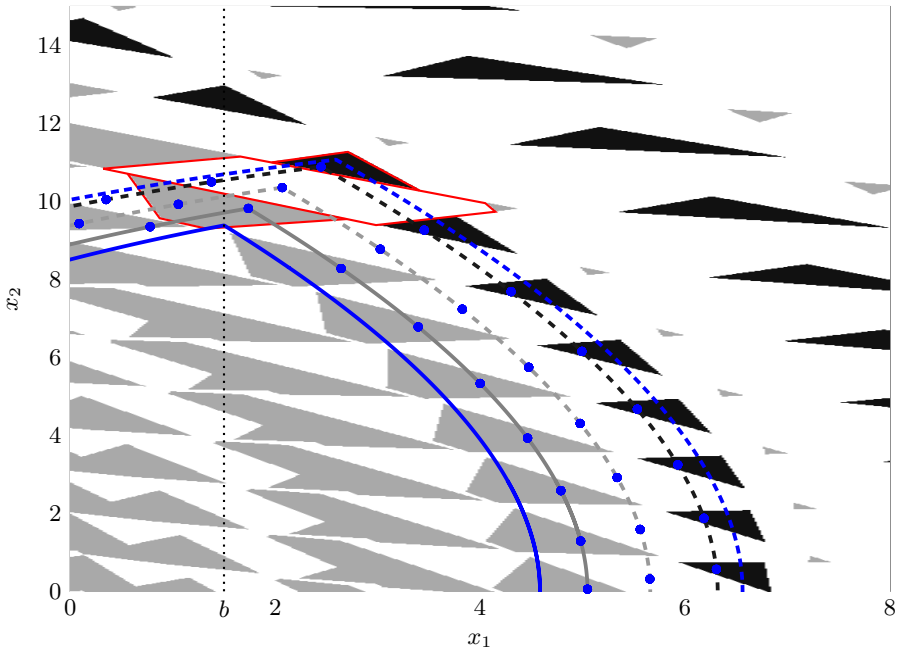

Figure 2.20: Basins of attraction of limit cycles in the sampled-data system.

slow forced motion is not obvious. A possible remedy is to take the average of all determined equivalent gains. A comparison of the output of the relay servo system and the output of the equivalent circuit with $k_\mathrm{n} = 1.39$ due to the reference signal $f_k = 2 + 15\sin(0.01k)$ is given in Figure 2.19.

The basins of attraction of limit cycles are depicted for the first quadrant of the phase plane in Figure 2.20. The results have been obtained by numerical simulations with $u_{-1} = -c$ and $(f_k) = (0)$. For initial conditions chosen from the black colored set the solution is attracted to the black dashed limit cycle ($N = 42$). Starting in the gray colored set the solution settles into the cycle plotted as a gray solid line ($N = 38$) and for all other initial conditions the solution approaches the gray dashed limit cycle ($N = 40$). It can be seen, that the basin of attraction in the sampled-data system is possibly a disconnected set and is much smaller for

some limit cycles than for others. Exploiting the results in [79] one obtains $\bar{i} = 2$. Thus the basin of attraction for the example system can be predicted by the inequalities (2.46) with $i = 0, 1, 2$. The red polygons defined by this system of inequalities are depicted for each of the three limit cycles in Figure 2.20.

2.3 Summary & Concluding Remarks

The describing function method has been used to characterize periodic motions in sampled-data systems controlled by a second-order sliding mode algorithm. In particular the so-called sampled describing function has been applied to a feedback loop including the twisting algorithm. The connection to its continuous time counterpart was shown. It was illustrated that the sampling process reduces the practical phase margin and leads to self sustained oscillations which do not occur in the continuous time configuration. For some limit cycle modes it is possible to replace the sample and hold element by a particular time delay which is obtained from the SDF analysis. In this case further analysis of the system is significantly simplified. The approach has been illustrated in a tutorial example and its efficiency was demonstrated in a real world application.

Then, the locus of perturbed relay system approach has been extended to the sampled-data configuration. The methodology provides an exact frequency domain analysis of the sampled-data relay servo system. A formula that allows to compute the LPRS, based on the transfer function representation of the plant dynamics, has been derived. For the sampled-data system the LPRS results in a family of curves. Existence conditions have been derived for limit cycles indicated by the LPRS method. It was shown, that the basins of attraction for limit cycles, which are possibly disconnected sets, can locally be predicted by a system of linear inequalities. The effectiveness of the approach has been demonstrated in a simulation example.

3 Discretization of Sliding Mode Algorithms

Contents

The previous chapter was devoted to the analysis of chattering effects in relay feedback systems. Accurate prediction of the characteristics of self-excited periodic motions is of importance when e.g. the control accuracy is of major significance. Furthermore, the discussed frequency domain techniques permit designing compensating elements that mitigate the chattering effects, i.e., elements that allow to adjust the frequency and amplitude of the resulting oscillations. On the other hand, in the sampled-data system the chattering characteristics will also depend on the applied discretization scheme. This becomes evident when comparing the implicit discretization of the FOSM controller to its explicit discretized version. Roughly speaking, the implicit discretized FOSM controller can be represented by a saturation function whilst its explicit discretization is represented by a relay. The describing functions of these two elements are fundamentally different, see, e.g., [69]. Hence, the chattering characteristics (amplitude and frequency of the oscillation) will also differ. The implicit scheme entirely removes the discretization chattering effects. Discretization schemes, that remove the discretization chattering are also highly desirable for HOSM algorithms.

In this Chapter, an entirely new discretization scheme, which is applicable to a number of HOSM algorithms, is presented. The approach relies on the representation of the closed-loop system in a pseudo-linear form. This representation has been exploited in [80] to systematically generate parameter settings for the arbitrary-order sliding mode differentiator and facilitate simple adaptation of the gains. Before presenting the main results, an introductory example is given. The pseudo-linear system representation of the STA is discussed and, in terms of structure, compared to the high-gain observer (HGO). The HGO, although a linear algorithm, exhibits a very similar structure as the STA.

3.1 Motivational Example: The High-Gain Observer

Consider the perturbed double integrator system written in state space representation

$$\begin{aligned} \frac{\mathrm{d}\boldsymbol{x}}{\mathrm{d}t} &= \boldsymbol{A}\boldsymbol{x} + \boldsymbol{b}(u+\varphi), \\ y &= \boldsymbol{c}^{\mathrm{T}}\boldsymbol{x} \end{aligned} \tag{3.1}$$

where

$$\boldsymbol{A} = \begin{bmatrix} 0 & 1 \\ 0 & 0 \end{bmatrix}, \quad \boldsymbol{b} = \begin{bmatrix} 0 \\ 1 \end{bmatrix}, \quad \boldsymbol{c} = \begin{bmatrix} 1 \\ 0 \end{bmatrix},$$

$\boldsymbol{x} = \begin{bmatrix} x_1 & x_2 \end{bmatrix}^{\mathrm{T}}$, $x_1, x_2 \in \mathbb{R}$ are the system states, $u \in \mathbb{R}$ is the control input and $y \in \mathbb{R}$ is the system output. The variable $\varphi(t) \in \mathbb{R}$ represents a bounded external disturbance. One might exploit a linear state observer of the form

$$\frac{\mathrm{d}\hat{\boldsymbol{x}}}{\mathrm{d}t} = \boldsymbol{A}\hat{\boldsymbol{x}} + \boldsymbol{b}u + \boldsymbol{l}(y - \hat{x}_1)$$

with the estimated state vector $\hat{\boldsymbol{x}} = \begin{bmatrix} \hat{x}_1 & \hat{x}_2 \end{bmatrix}^{\mathrm{T}}$ and observer gains $\boldsymbol{l} = \begin{bmatrix} l_1 & l_2 \end{bmatrix}^{\mathrm{T}}$, to implement a state feedback control law. The variable $\hat{x}_1$ represents the estimate of the state variable x_1,

$\hat{x}_2$ is the estimate of x_2. Let the estimation errors be defined as $e_1 := x_1 - \hat{x}_1$, $e_2 := x_2 - \hat{x}_2$. Then the estimation error dynamics take the form

$$\frac{\mathrm{d}\boldsymbol{e}}{\mathrm{d}t} = (\boldsymbol{A} - \boldsymbol{l}\boldsymbol{c}^{\mathrm{T}})\boldsymbol{e} + \boldsymbol{b}\varphi \tag{3.2}$$

where $\boldsymbol{e} := \begin{bmatrix} e_1 & e_2 \end{bmatrix}^{\mathrm{T}}$. In the absence of the disturbance term φ the error dynamics converge to zero asymptotically for arbitrary initial errors, iff the gains l_1, l_2 are chosen s.t. the eigenvalues of the dynamic matrix $\boldsymbol{A} - \boldsymbol{l}\boldsymbol{c}^{\mathrm{T}}$ in (3.2) have negative real parts. In the case of a HGO, see [81] ,the gains are chosen as

$$l_1 = \frac{k_1}{\varepsilon}, \quad l_2 = \frac{k_2}{\varepsilon^2}, \tag{3.3}$$

where $\varepsilon \in \mathbb{R}^+$. Introducing the change of coordinates

$$w_1 = \frac{e_1}{\varepsilon}, \quad w_2 = e_2$$

and using (3.3) leads to the singularly perturbed system

$$\varepsilon \frac{\mathrm{d}\boldsymbol{w}}{\mathrm{d}t} = \tilde{\boldsymbol{A}}\boldsymbol{w} + \varepsilon \boldsymbol{b}\varphi, \tag{3.4}$$

where

$$\tilde{\boldsymbol{A}} = \begin{bmatrix} -k_1 & 1 \\ -k_2 & 0 \end{bmatrix}, \quad \boldsymbol{w} = \begin{bmatrix} w_1 \\ w_2 \end{bmatrix}.$$

From the above representation (3.4), it follows that decreasing the scaling ε reduces the impact of the perturbation φ on the system states. The state variables w_1, w_2 evolve in an $1/\varepsilon$ faster time scale compared to the states e_1, e_2, see [82]. The eigenvalues s_1, s_2 of the matrix $1/\varepsilon\tilde{\boldsymbol{A}}$ are the roots p_1, p_2 of the characteristic polynomial

$$s^2 + k_1 s + k_2,$$

i.e., the eigenvalues of $\tilde{\boldsymbol{A}}$ scaled by $1/\varepsilon$

$$s_1 = \frac{1}{\varepsilon} p_1, \quad s_2 = \frac{1}{\varepsilon} p_2.$$

Obviously, the variable $\varepsilon > 0$ does not affect the stability of the estimation error dynamics. The autonomous time scaled system

$$\frac{\mathrm{d}\boldsymbol{w}}{\mathrm{d}t} = \frac{1}{\varepsilon}\tilde{\boldsymbol{A}}\boldsymbol{w} \tag{3.5}$$

is rewritten as

$$\frac{\mathrm{d}\boldsymbol{w}}{\mathrm{d}\theta} = \tilde{\boldsymbol{A}}\boldsymbol{w}, \tag{3.6}$$

with the new scaled time variable θ satisfying $\theta = t/\varepsilon$. Systems (3.5) and (3.6) have the same trajectories in the phase space $\boldsymbol{w}$. Hence, in case $\varphi(t) \equiv 0$, it is sufficient to investigate the stability property of the nominal system (3.6) in order to conclude stability of system (3.5). As the trajectories in the phase space $\boldsymbol{e} = \begin{bmatrix} e_1 & e_2 \end{bmatrix}^{\mathrm{T}}$ remain unaffected by the time scaling, the quadratic form

$$V = \boldsymbol{w}^{\mathrm{T}} \boldsymbol{P} \boldsymbol{w}$$

where $\boldsymbol{P} \in \mathbb{R}^{2\times 2}$ satisfies the Lyapunov equation,

$$\tilde{\boldsymbol{A}}^{\mathrm{T}} \boldsymbol{P} + \boldsymbol{P} \tilde{\boldsymbol{A}} = -\boldsymbol{Q}, \quad \boldsymbol{Q} = \boldsymbol{Q}^{\mathrm{T}} \succ 0,$$

also is a Lyapunov function for system (3.5). This holds independently on the choice of $\varepsilon > 0$.

In the case of the high-gain observer the scaling variable ε is a positive constant. On the other, hand if one introduces the state dependent scaling

$$\varepsilon = \sqrt{|e_1|},$$

the closed-loop system takes the form

$$\frac{\mathrm{d}}{\mathrm{d}t} \begin{bmatrix} e_1 \\ e_2 \end{bmatrix} = \begin{bmatrix} -\frac{k_1}{\sqrt{|e_1|}} & 1 \\ -\frac{k_2}{|e_1|} & 0 \end{bmatrix} \begin{bmatrix} e_1 \\ e_2 \end{bmatrix} + \begin{bmatrix} 0 \\ 1 \end{bmatrix} \varphi, \tag{3.7}$$

or in a more usual notation

$$\begin{aligned} \dot{e}_1 &= -k_1 |e_1|^{\frac{1}{2}} \operatorname{sign}(e_1) + e_2, \\ \dot{e}_2 &= -k_2 \operatorname{sign}(e_1) + \varphi, \end{aligned}$$

which is the STA. The STA reveals a very similar structure as the HGO. In case of the STA, the nominal eigenvalues are scaled by a positive state dependent function, i.e.,

$$s_1 = \frac{1}{\sqrt{|e_1|}} p_1, \quad s_2 = \frac{1}{\sqrt{|e_1|}} p_2.$$

For the discretization of the continuous-time linear observer a variety of methods are available, see, e.g., [31]. On the other hand, when dealing with linear systems it is common to design the observer directly in the discrete-time domain. The basis for this design usually forms the discretized model of (3.1). Besides other methods, such a discrete-time model may be obtained by applying the ZOH method, i.e.,

$$\boldsymbol{x}_{k+1} = \boldsymbol{\Phi}(T_{\mathrm{s}}) \boldsymbol{x}_k + \boldsymbol{b}_{\mathrm{d}} (u_k + \varphi_k)$$

where

$$\boldsymbol{x}_k = \begin{bmatrix} x_{1,k} & x_{2,k} \end{bmatrix}^{\mathrm{T}}, \quad \boldsymbol{\Phi}(T_{\mathrm{s}}) = e^{\boldsymbol{A} T_{\mathrm{s}}}, \quad \boldsymbol{b}_{\mathrm{d}} = \int_0^{T_{\mathrm{s}}} \boldsymbol{\Phi}(s) \boldsymbol{b} \, \mathrm{d}s,$$

and T_s represents the constant sampling time, the index $k \in \mathbb{N}$ denotes the time instant $t = kT_\mathrm{s}$. In case of a piecewise constant input u and disturbance φ this method yields an exact discretization of the continuous time system (3.1). The direct discrete-time observer design is conceptual equivalent to the continuous-time design. However, in general, it is not possible to have an exact discretization of a nonlinear system as it is in most cases not possible to calculate the solution of the continuous-time system which can then be discretized. For some nonlinear systems, however, it could succeed.

3.2 An Attempt at Exact Discretization

The representation of sliding mode algorithms in pseudo-linear form, as has been seen in the previous Section for the STA, serves as a basis for the development of new discretization schemes. Before presenting the approach, some recently published results, such as the implicit discretization of the FOSM controller, see [36, 83], are discussed in this context.

3.2.1 Conventional First-Order Sliding Mode

Consider the closed-loop system imposed by a FOSM controller

$$\frac{\mathrm{d}x}{\mathrm{d}t} = -k_1 \mathrm{sign}\,(x) + \varphi, \quad x(0) = x_0, \tag{3.8}$$

where k_1 is a positive constant and $\varphi(t)$ represents a bounded time dependent, possibly discontinuous perturbation. System (3.8) may be considered as the dynamics of a closed-loop control system or the error dynamics of an observer. If $k_1 > \sup_t |\varphi(t)|$ holds, the closed-loop system exhibits a first-order sliding mode at $x = 0$. For the purpose of analysis the perturbation $\varphi(t)$ is dropped for now. Then an alternative representation of the system is obtained by rewriting the sign function to

$$\mathrm{sign}\,(a) = \frac{a}{|a|}, \quad \text{for} \quad a \neq 0,$$

which yields the pseudo-linear form of (3.8) given by

$$\frac{\mathrm{d}x}{\mathrm{d}t} = -k_1 \frac{x}{|x|},$$

which can be rewritten as

$$|x| \frac{\mathrm{d}x}{\mathrm{d}t} = -k_1 x. \tag{3.9}$$

Again, differential equation (3.9) constitutes a time scaled system, where the time scaling is given by $|x|$. Introducing the new time variable θ, i.e.,

$$|x| \frac{\mathrm{d}x}{\mathrm{d}t} = \frac{\mathrm{d}x}{\mathrm{d}\theta},$$

allows to rewrite system (3.9) in the new time scale

$$\frac{\mathrm{d}x}{\mathrm{d}\theta} = -k_1 x. \tag{3.10}$$

The ansatz

$$x(\theta) = e^{-k_1\theta(t)} x_0 \tag{3.11}$$

satisfies (3.10) for almost all t. Using (3.11) and (3.9) one has for the new time variable

$$\frac{\mathrm{d}\theta}{\mathrm{d}t} = \frac{1}{|x(\theta(t))|}, \quad \theta(0) = 0.$$

Separation of variables and integration gives

$$t = \int_0^{\theta(t)} |x(s)| \,\mathrm{d}s = |x_0| \int_0^{\theta(t)} e^{-k_1 s} \,\mathrm{d}s, \tag{3.12}$$

and solving for $\theta(t)$ yields

$$\theta(t) = \begin{cases} -\frac{1}{k_1} \ln\left(1 - \frac{k_1 t}{|x_0|}\right), & \text{if} \quad \frac{k_1 t}{|x_0|} < 1 \\ \infty, & \text{else.} \end{cases} \tag{3.13}$$

It is well-known, that (3.8) converges in finite time. As a side product of this analysis, one obtains the convergence time T^* of (3.8) (assuming $\varphi(t) \equiv 0$), by integration of (3.12) from zero to infinity. This computation results in

$$T^* = |x_0| \int_0^{\infty} e^{-k_1 s} \,\mathrm{d}s = \frac{|x_0|}{k_1}.$$

Due to the fact that the solution of the unperturbed system (3.8) can be explicitly calculated, it is possible to obtain an exact discrete-time model of (3.8) by discretization of the solution (3.11), i.e.,

$$x_{k+1} = e^{-k_1\theta(T_\mathrm{s})} x_k \tag{3.14}$$

where according to (3.13)

$$\theta(T_\mathrm{s}) = \begin{cases} -\frac{1}{k_1} \ln\left(1 - \frac{k_1 T_\mathrm{s}}{|x_k|}\right), & \text{if} \quad 1 > \frac{k_1 T_\mathrm{s}}{|x_k|} \\ \infty, & \text{else.} \end{cases} \tag{3.15}$$

Substituting (3.15) into (3.14) gives the recursion

$$x_{k+1} = x_k - T_\mathrm{s} k_1 \begin{cases} \operatorname{sign}(x_k), & \text{if} \quad |x_k| > T_\mathrm{s} k_1 \\ \frac{x_k}{T_\mathrm{s} k_1}, & \text{else.} \end{cases} \tag{3.16}$$

It is observed, that this discretization approach naturally introduces a boundary layer, i.e., compared to the explicit discretization

$$x_{k+1} = x_k - T_\mathrm{s} k_1 \mathrm{sign}\,(x_k),$$

the sign function is replaced by a saturation function, that means the discrete-time system (3.16) is written in terms of the saturation function as

$$x_{k+1} = x_k - T_\mathrm{s} k_1 \mathrm{sat}\left(\frac{x_k}{T_\mathrm{s} k_1}\right), \quad \mathrm{sat}\left(\frac{x}{\varsigma}\right) := \begin{cases} \mathrm{sign}\,(x) & \text{if} \quad |x| > \varsigma \\ \frac{x}{\varsigma} & \text{else.} \end{cases}$$

The boundary layer size $\varsigma = T_\mathrm{s} k_1$ results directly from the discretization. Note that recursion (3.16) coincides with the implicit discretization of the conventional FOSM controller proposed by [36] and briefly discussed in Section 1.1.3. From this analysis, it can be concluded that in the unperturbed case the implicit scheme yields an exact discretization of (3.8). The sliding variable x_k is driven to zero in a finite number of steps. Hence, the discretization chattering does not appear. In some sense, the implicit scheme aims to preserve the set-valuedness of the sign function, i.e., as in the continuous-time counterpart it allows the sign function to take values from the interval $[-1,\, 1]$. In the unperturbed case, and under the assumption that the perturbation is unknown, it is not anymore possible to steer the sliding variable to zero exactly.

In the next Section, it is investigated, whether an equivalent result can be obtained for the STA by applying the same ideas.

3.2.2 Super-Twisting Algorithm

Reconsider the closed-loop super-twisting dynamics

$$\begin{aligned} \dot{x}_1 &= -k_1 |x_1|^{\frac{1}{2}} \mathrm{sign}\,(x_1) + x_2, \\ \dot{x}_2 &= -k_2 \mathrm{sign}\,(x_1) + \Delta, \end{aligned} \tag{3.17}$$

where the perturbation satisfies $\sup_t |\Delta(t)| \leq L$. It has been shown in e.g. [84, 28, 85, 86], that a proper choice of the gains k_1, k_2 ensures finite time stability of the origin despite the disturbance $\Delta(t)$, i.e., the closed-loop system exhibits a second-order sliding mode at $x_1 = x_2 = 0$. In the unperturbed case, i.e., $L = 0$, the origin is finite time stable iff the gains k_1, k_2 are positive, see, e.g., [84].

The authors of [84] propose the change of coordinates

$$\boldsymbol{w} = \begin{bmatrix} w_1 \\ w_2 \end{bmatrix} = \boldsymbol{t}(\boldsymbol{x}) = \begin{bmatrix} |x_1|^{1/2} \mathrm{sign}\,(x_1) \\ x_2 \end{bmatrix} \tag{3.18}$$

which allows to formally rewrite system (3.17) in the new coordinates w_1 and w_2 as

$$|w_1| \frac{\mathrm{d}\boldsymbol{w}}{\mathrm{d}t} = \boldsymbol{A}\boldsymbol{w} \tag{3.19}$$

with the constant matrix

$$\boldsymbol{A} = \begin{bmatrix} -\frac{1}{2} k_1 & \frac{1}{2} \\ -k_2 & 0 \end{bmatrix}. \tag{3.20}$$

For the purpose of analysis the perturbation has been dropped. Due to this particular coordinate transformation, the closed-loop dynamics are represented as a time scaled linear time-invariant (LTI) system where $|w_1| = \sqrt{|x_1|}$ represents the time scaling. Introducing the new time variable θ, satisfying

$$\frac{\mathrm{d}\theta}{\mathrm{d}t} = \frac{1}{|w_1(\theta(t))|}, \quad \theta(0) = 0, \tag{3.21}$$

allows to rewrite the closed-loop system (3.19) as

$$\frac{\mathrm{d}\boldsymbol{w}}{\mathrm{d}\theta} = \boldsymbol{A}\boldsymbol{w}. \tag{3.22}$$

The solution of the LTI system (3.22) is given by

$$\boldsymbol{w}(\theta(t)) = e^{\boldsymbol{A}\theta(t)}\boldsymbol{w}(0), \tag{3.23}$$

where $e^{\boldsymbol{A}\theta(t)}$ denotes the matrix exponential function. The original state variables are obtained from the inverse transformation of (3.18) given by

$$\boldsymbol{t}^{-1}(\boldsymbol{w}) = \begin{bmatrix} |w_1|^2 \mathrm{sign}(w_1) \\ w_2 \end{bmatrix}.$$

A discrete-time model of the STA is now obtained through discretization of solution (3.23) as

$$\boldsymbol{w}(\theta_k) = e^{\boldsymbol{A}(\theta_k)}\boldsymbol{w}(0), \quad k \geq 0 \tag{3.24}$$

with $\theta_k := \theta(kT_\mathrm{s})$. This yields the recursion

$$\boldsymbol{w}_{k+1} = \boldsymbol{A}_\mathrm{d}^{\frac{\Delta\theta_{k+1}}{T_\mathrm{s}}}\boldsymbol{w}_k, \tag{3.25}$$

where $\boldsymbol{A}_\mathrm{d} = e^{\boldsymbol{A}T_\mathrm{s}}$ and $\Delta\theta_{k+1} = \theta_{k+1} - \theta_k$. A relation of the new time variable $\Delta\theta_{k+1}$ and time t, more precisely sampling time T_s, is obtained by discretization of (3.21). The most obvious way to discretize this differential equation is the application of the forward Euler scheme which yields

$$\frac{\theta_{k+1} - \theta_k}{T_\mathrm{s}} = \frac{\Delta\theta_{k+1}}{T_\mathrm{s}} = \frac{1}{|w_{1,k}|}.$$

Substituting the expression

$$\Delta\theta_{k+1} = \frac{T_\mathrm{s}}{|w_{1,k}|},$$

into (3.25) eventually gives

$$\boldsymbol{w}_{k+1} = \boldsymbol{A}_\mathrm{d}^{\frac{1}{|w_{1,k}|}}\boldsymbol{w}_k. \tag{3.26}$$

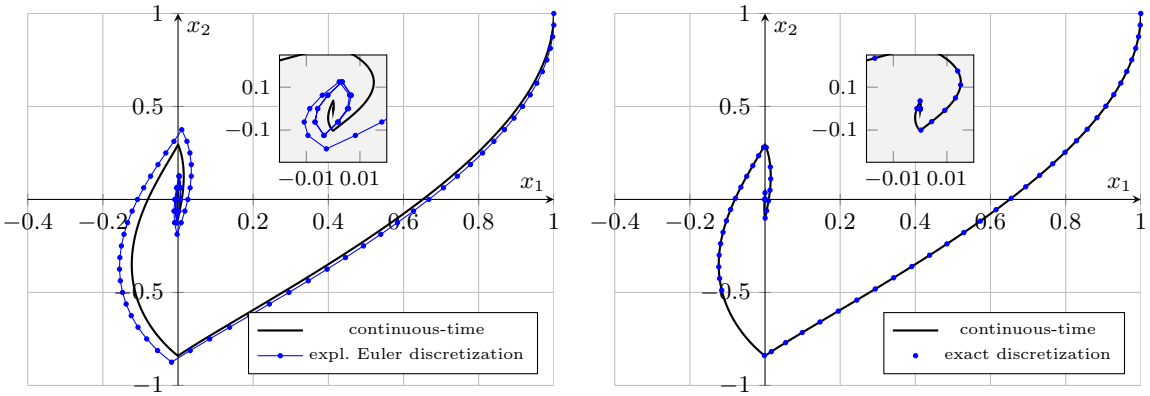

Figure 3.1: Comparison of the trajectory of the continuous-time STA to the discrete-time model (3.26) and the explicit Euler discretized STA. Parameters are $k_1 = 1$, $k_2 = 1.25$ and the discretization step size $T_\mathrm{s} = 0.05$ s

Equivalent to the continuous-time system the exponent $1/|w_{1,k}|$ plays the role of the time-scaling (more precisely a scaling of the sampling time T_s) in the discrete-time system (3.26). The exponent $\Delta\theta_{k+1}/T_\mathrm{s}$ does *not* affect the trajectories in the phase plane. Therefore, the recursion (3.24) represents an *exact* discretization in the sense that at any sampling step its solutions coincide with the solutions of the continuous-time system in the phase plane. In this regard, the quadratic form

$$V_k = \boldsymbol{w}_k^\mathrm{T} \boldsymbol{P} \boldsymbol{w}_k$$

where $\boldsymbol{P} = \boldsymbol{P}^\mathrm{T} \in \mathbb{R}^{2\times 2}$ satisfies the continuous-time Lyapunov equation,

$$\boldsymbol{A}^\mathrm{T}\boldsymbol{P} + \boldsymbol{P}\boldsymbol{A} = -\boldsymbol{Q}, \quad \boldsymbol{Q} = \boldsymbol{Q}^\mathrm{T} \succ 0,$$

also is a Lyapunov function for the discrete-time system (3.25) for all $\Delta\theta_{k+1} > 0$ and consequently also for the discrete-time system (3.26). In this respect, periodic solutions, as they appear in the explicit Euler discretized STA cannot appear in (3.24), i.e., the discretization chattering is avoided.

A comparison of the trajectory of the continuous-time STA to the discrete-time model (3.26) and the explicit Euler discretized STA is shown in Figure 3.1. In case of the forward Euler discretized STA the trajectory eventually enters a limit cycle, whilst in case of the discrete-time system (3.26), which was obtained from the analytic solution of the continuous-time STA, converges to the origin.

The dynamic matrix of the continuous-time system (3.19) given in (3.20) has eigenvalues

$$p_{1,2} = -\frac{1}{4}\left(k_1 \pm \sqrt{k_1^2 - 8k_2}\right).$$

The time scaling $\frac{1}{|w_1|}$ imposes a scaling of the eigenvalues and the matrix $\frac{1}{|w_1|}\boldsymbol{A}$ thus has eigenvalues

$$s_i = \frac{1}{|w_1|} p_i, \quad i = 1, 2 \tag{3.27}$$

which can be easily seen by comparing the determinants

$$\det\left(s_i\boldsymbol{I}-\frac{1}{|w_1|}\boldsymbol{A}\right)=\det(\underbrace{s_i|w_1|}_{p_i}\boldsymbol{I}-\boldsymbol{A}).$$

The eigenvalues λ_i of the matrix $\boldsymbol{A}_\mathrm{d}$ are given by

$$\lambda_i = e^{T_\mathrm{s}p_i} \tag{3.28}$$

By definition of matrix functions for diagonalizable matrices one has

$$\boldsymbol{A}_\mathrm{d}=\boldsymbol{U}\boldsymbol{\Lambda}^{\frac{1}{|w_{1,k}|}}\boldsymbol{U}^{-1}, \tag{3.29}$$

with $\boldsymbol{U}=\begin{bmatrix}\boldsymbol{u}_1 & \boldsymbol{u}_2\end{bmatrix}$ where $\boldsymbol{u}_1$, $\boldsymbol{u}_2$ are the eigenvectors of $\boldsymbol{A}$ and

$$\boldsymbol{\Lambda}=\begin{bmatrix}\lambda_1 & 0\\ 0 & \lambda_2\end{bmatrix}.$$

Hence, $\boldsymbol{A}_\mathrm{d}^{\frac{1}{|w_{1,k}|}}$ has eigenvalues

$$z_{i,k}=\lambda_i^{\frac{1}{|w_{1,k}|}}. \tag{3.30}$$

The following relation of the eigenvalues of the time scaled continuous-time system and the discrete-time system (3.26) is established from (3.27), (3.28) and (3.30):

$$z_{i,k}=\lambda_i^{\frac{1}{|w_{1,k}|}}=e^{\frac{p_iT_\mathrm{s}}{|w_{1,k}|}}=e^{s_{i,k}T_\mathrm{s}}. \tag{3.31}$$

The result is in particular interesting, as it is common in linear systems theory to generate discrete-time equivalents of continuous-time algorithms by transformations of the eigenvalues from the continuous-time to the discrete-time domain. The mapping

$$z_i=e^{s_iT_\mathrm{s}},$$

which in literature often is referred to as eigenvalue matching, is one possible method. However, there are several mappings in literature available, see, e.g., [31]. Relation (3.31) is illustrated graphically in Figure 3.2. In the continuous-time situation the absolute value of the eigenvalues s_i given in (3.27) tends to infinity as w_1 tends to zero. The nominal eigenvalues p_i are mapped to the discrete-time domain by (3.28) and as the state variable w_1, or in the original coordinates x_1, tends to zero the eigenvalues are transferred along a certain locus to the origin of the complex plain. The locus lies entirely inside the unit disk. Exploiting (3.29) allows to rewrite (3.26) into

$$\boldsymbol{w}_{k+1}=\boldsymbol{U}\begin{bmatrix}e^{\frac{p_1T_\mathrm{s}}{|w_{1,k}|}} & 0\\ 0 & e^{\frac{p_2T_\mathrm{s}}{|w_{1,k}|}}\end{bmatrix}\boldsymbol{U}^{-1}\boldsymbol{w}_k, \tag{3.32}$$

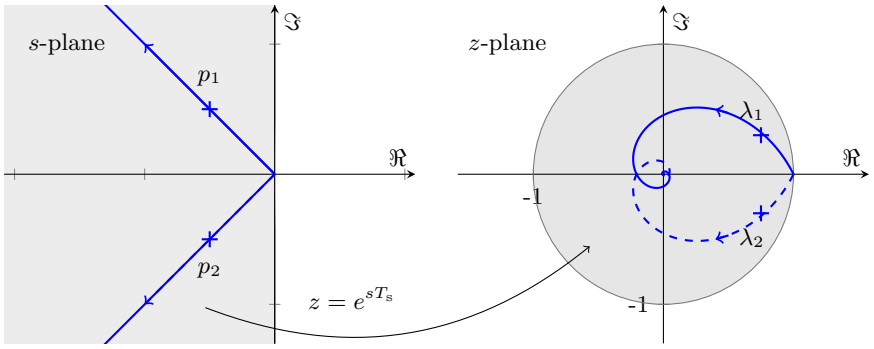

Figure 3.2: Scaling and mapping of eigenvalues.

and as $w_{1,k} \to 0$ the dynamical system (3.32) approaches the dead beat system

$$w_{1,k+1} = w_{2,k+1} = 0.$$

Based on these insights, a systematic approach for the discretization of sliding mode algorithms is established. The basic idea is to design the discrete-time system such that the pseudo-linear representation of the closed-loop system is characterized by a certain eigenvalue structure. These eigenvalues are obtained from mappings of the eigenvalues of the corresponding continuous-time system representation to the discrete-time domain, as e.g. the matching approach in (3.31).

3.3 Discrete-Time Equivalent Super-Twisting Algorithm

In this section, entirely new discrete-time versions of the STA are constructed. Three new discrete-time versions of the STA including also an implicit discretized STA are constructed. The discrete-time controllers are shown to fulfill certain criteria, such as convergence of the trajectories with hyper-exponential speed in case of vanishing perturbations. The discretization schemes have the following advantages/properties:

- in the unperturbed case the closed-loop trajectories converge to the origin, hence oscillations of the system states caused by the discrete-time implementation of the controller are avoided
- the controllers are insensitive to an overestimation of the gains, i.e., the chattering is not amplified by an increase of the control gains
- the standard asymptotic accuracies known for the second order sliding mode are preserved
- the controllers are straightforward to implement as the explicit Euler discretized STA.

Major parts of this Section have been published in [P8].

3.3.1 Problem Formulation and Revision of the Forward Euler Discretized Super-Twisting Algorithm

The dynamics of the system to be controlled are assumed to be given by the perturbed integrator

$$\begin{aligned} \dot{x}_1 &= u + \varphi, \\ \dot{\varphi} &= \Delta(t), \end{aligned} \tag{3.33}$$

with $\Delta(t) \in \mathbb{R}$ satisfying $\sup_t |\Delta(t)| \leq L$. The application of the super-twisting control law

$$\begin{aligned} u &= -k_1 |x_1|^{\frac{1}{2}} \operatorname{sign}(x_1) + \nu, \\ \dot{\nu} &= -k_2 \operatorname{sign}(x_1), \end{aligned} \tag{3.34}$$

to the plant (3.33) yields the closed-loop dynamics

$$\begin{aligned} \dot{x}_1 &= -k_1 |x_1|^{\frac{1}{2}} \operatorname{sign}(x_1) + x_2, \\ \dot{x}_2 &= -k_2 \operatorname{sign}(x_1) + \Delta, \end{aligned} \tag{3.35}$$

where $x_2 := \nu + \varphi$. It is noted, that a proper choice of the controller gains k_1 and k_2 ensures a second-order sliding mode at $x_1 = x_2 = 0$ without requiring information on the perturbation Δ or the state variable x_2. Due to the unknown disturbance $\Delta(t)$, the state variable x_2 is in general not available. Under sampling of x_1 with constant sampling time $T_\mathrm{s} \in \mathbb{R}_{>0}$ and the reconstruction of the control sequence (u_k) by a ZOH element, the state variables of (3.33) at the time instant $(k+1)T_\mathrm{s}$ are computed as

$$\begin{aligned} x_{1,k+1} &= x_{1,k} + T_\mathrm{s}(u_k + \varphi_k) + \frac{T_\mathrm{s}^2}{2} \Delta(\xi_{1,k}), \\ \varphi_{k+1} &= \varphi_k + T_\mathrm{s} \Delta(\xi_{2,k}), \end{aligned} \tag{3.36}$$

where $u_k := u(kT_\mathrm{s})$, $x_{1,k} := x_1(kT_\mathrm{s})$ and $\varphi_k := \varphi(kT_\mathrm{s})$ with $k = 0, 1, 2, \ldots$ and the time $\xi_{i,k} \in (kT_\mathrm{s}, (k+1)T_\mathrm{s})$ with $i = 1, 2$. In terms of the control law (3.34), a discrete-time version is usually obtained by applying the explicit Euler method, yielding

$$\begin{aligned} u_k &= -k_1 |x_{1,k}|^{\frac{1}{2}} \operatorname{sign}(x_{1,k}) + \nu_k, \\ \nu_{k+1} &= \nu_k - k_2 T_\mathrm{s} \operatorname{sign}(x_{1,k}) \end{aligned} \tag{3.37}$$

where the sign function is commonly implemented as

$$\operatorname{sign}(y) = \begin{cases} 1, & y > 0, \\ 0, & y = 0, \\ -1, & y < 0. \end{cases}$$

With $x_{2,k} := \nu_k + \varphi_k$ the dynamics of the closed-loop system is written as

$$\begin{aligned} x_{1,k+1} &= x_{1,k} + T_\mathrm{s} \left(x_{2,k} - k_1 |x_{1,k}|^{\frac{1}{2}} \operatorname{sign}(x_{1,k}) \right) + \frac{T_\mathrm{s}^2}{2} \Delta(\xi_{1,k}), \\ x_{2,k+1} &= x_{2,k} - k_2 T_\mathrm{s} \operatorname{sign}(x_{1,k}) + T_\mathrm{s} \Delta(\xi_{2,k}). \end{aligned} \tag{3.38}$$

With $\Delta(\xi_{1,k}) \equiv 0$ and $\xi_{2,k} = kT_\mathrm{s}$ system (3.38) represents an explicit Euler discretized version of the continuous-time system (3.35). Although (3.38) does not exhibit the above mentioned second-order sliding mode, it is known to offer several remarkable properties. The system features practical stability, i.e., after a finite number of steps the trajectory is confined to a *small* neighborhood of the origin, the so-called real sliding set. The discretized STA is invariant with respect to the parameter/coordinate transformation

$$(T_\mathrm{s}, x_{1,k},\, x_{2,k}\,) \mapsto \left(\kappa T_\mathrm{s}, \kappa^2 x_{1,k}, \kappa x_{2,k}\,\right), \quad \kappa > 0. \tag{3.39}$$

This scaling property essentially ensures that the discrete-time system preserves the asymptotic accuracies of the continuous-time system, see e.g. [87]. In this regard, the real sliding set $\mathcal{R}$ is specified by

$$\mathcal{R} = \left\{x_1,\, x_2 \in \mathbb{R} : |x_1| \leq \mu_1 T_\mathrm{s}^2,\, |x_2| \leq \mu_2 T_\mathrm{s}\right\}, \tag{3.40}$$

where μ_1, μ_2 are positive constants. This means, the controller provides for the accuracy level $x_1 = \mathcal{O}(T_\mathrm{s}^2)$ and $x_2 = \mathcal{O}(T_\mathrm{s})$. The proportionality constants μ_1, μ_2 do not only depend on the perturbation but also on the choice of the control parameters k_1, k_2. As already mentioned in the introductory section, the discrete-time system (3.38) is known to exhibit spurious oscillations after an initial transient time response. These oscillations deteriorate the control performance since the variable x_1, which often is regarded as the tracking error, will not vanish - even in the case $L = 0$. Motivated by the knowledge of the behavior of the continuous-time system this may lead to a retuning of the controller gains. However, it is known, that increasing the controller gains further diminishes the tracking performance by an increased amplitude of the resulting oscillations. This is a direct consequence of the following

Proposition 3.1

Consider the undisturbed system (3.38), i.e., $\Delta \equiv 0$. The choice $k_1,\, k_2 > 0$ ensures the convergence of the trajectory to a real sliding set $\mathcal{R}$. However, every trajectory entering the set $\mathcal{B}_\rho \backslash \{\mathbf{0}\}$, where

$$\mathcal{B}_\rho = \left\{\boldsymbol{x} \in \mathbb{R}^2 : \|\boldsymbol{x}\|_2 \leq \sqrt{2}\min\left(k_2 T_\mathrm{s}(\sqrt{2}-1),\, \frac{(T_\mathrm{s}k_2)^2}{2}\right)\right\},$$

will leave $\mathcal{B}_\rho$.

Proof. Let $V_k(\boldsymbol{x}_k) = |x_{1,k}| + x_{2,k}^2$, with $\boldsymbol{x}_k = \begin{bmatrix} x_{1,k} & x_{2,k} \end{bmatrix}^\mathrm{T}$. Computing the difference $\Delta V_k = V_{k+1} - V_k$ yields

$$\begin{aligned}\Delta V_k(\boldsymbol{x}_k) = -|x_{1,k}| + |x_{1,k} + T_\mathrm{s}x_{2,k} - T_\mathrm{s}k_1|x_{1,k}|^{\frac{1}{2}}\mathrm{sign}\,(x_{1,k})| \\ + k_2 T_\mathrm{s}\mathrm{sign}\,(x_{1,k})\left(k_2 T_\mathrm{s}\mathrm{sign}\,(x_{1,k}) - 2x_{2,k}\right).\end{aligned}$$

Hence

$$\begin{aligned}\Delta V_k(\boldsymbol{x}_k) &\geq -|x_{1,k}| - 2k_2 T_\mathrm{s} x_{2,k}\mathrm{sign}\,(x_{1,k}) + \left(k_2 T_\mathrm{s}\mathrm{sign}\,(x_{1,k})\right)^2 \\ &\geq c\left(|x_{1,k}| + x_{2,k}^2\right) \quad \forall\, \boldsymbol{x}_k \in \mathcal{U}\backslash\{\mathbf{0}\},\, c > 0\end{aligned}$$

$$\mathcal{U} = \left\{ \boldsymbol{x}_k \in \mathbb{R}^2 : \, (1+c)\,|x_{1,k}| + c x_{2,k}^2 + 2k_2 T_\mathrm{s} x_{2,k} \mathrm{sign}\,(x_{1,k}) < T_\mathrm{s}^2 k_2^2 \right\}$$

and

$$\Delta V_k(\mathbf{0}) = 0.$$

Hence, all conditions of Lyapunov's first instability theorem for discrete-time systems, see e.g. [88], are satisfied. It is concluded that the origin of the closed-loop system (3.38) is unstable and $\mathcal{B}_\rho \subset \mathcal{U}$ completes the proof. □

Remark 3. From Proposition 3.1 it can be concluded, that increasing the parameter k_2 or the sampling time T_s will increase the radius of the ball $\mathcal{B}_\rho$ and consequently increases the chattering amplitude due to an increase of the constants μ_1, μ_2.

In the presence of noisy measurements of the output, i.e., $\tilde{x}_1(t) = x_1(t) + \eta(t)$, where the noise $\eta(t)$ satisfies $\sup_t |\eta(t)| < \epsilon$ with $\epsilon > 0$, the asymptotic accuracies $x_1 = \mathcal{O}(\epsilon)$ and $x_2 = \mathcal{O}(\epsilon^{1/2})$ are achieved. In fact, the asymptotic accuracies w.r.t. sampling and noise hold for all homogeneous 2-sliding controllers, see [2].

Another Representation of the Closed-Loop System

In order to derive new discrete-time versions of the STA the close-loop system (3.35) is rewritten in a pseudo-linear system representation (also known as *Rosenbrock* form) as proposed in [80]. Therefore the signum function is written as

$$\mathrm{sign}(y) = \frac{y}{|y|}, \quad y \neq 0$$

which allows to write system (3.35) as

$$\frac{\mathrm{d}\boldsymbol{x}}{\mathrm{d}t} = \boldsymbol{M}(x_1)\boldsymbol{x} + \boldsymbol{e}_2 \Delta(t) \tag{3.41}$$

with $\boldsymbol{x} := \begin{bmatrix} x_1 & x_2 \end{bmatrix}^\mathrm{T}$, $\boldsymbol{e}_2 = \begin{bmatrix} 0 & 1 \end{bmatrix}^\mathrm{T}$ and $\boldsymbol{M} : \mathbb{R} \to \mathbb{R}^{2\times 2}$ where

$$\boldsymbol{M}(x_1) = \begin{bmatrix} -k_1 |x_1|^{-\frac{1}{2}} & 1 \\ -k_2 |x_1|^{-1} & 0 \end{bmatrix}.$$

Note that this is the same form as (3.7) used in the introductory example. Due to dependency on x_1 only, $\boldsymbol{M}(x_1)$ in (3.41) is a unique pseudo linear representation of the closed-loop system which is not true for a general pseudo linear system, see e.g. [89]. For example, consider a pseudo linear system given by

$$\frac{\mathrm{d}\boldsymbol{x}}{\mathrm{d}t} = \boldsymbol{M}(\boldsymbol{x})\boldsymbol{x}, \quad \boldsymbol{x} \in \mathbb{R}^n, n > 1.$$

Then, $\boldsymbol{M}(\boldsymbol{x})\boldsymbol{x} = (\boldsymbol{M}(\boldsymbol{x}) + \boldsymbol{E}(\boldsymbol{x}))\,\boldsymbol{x}$ with $\boldsymbol{E}(\boldsymbol{x})\boldsymbol{x} = \mathbf{0}$, i.e., the representation is not unique. However, taking into account that the system is of the specific form (3.41) i.e., $\boldsymbol{M}(x_1)$ depends only on the first state variable, $\boldsymbol{M}(x_1)\boldsymbol{x} = (\boldsymbol{M}(x_1) + \boldsymbol{E}(x_1))\,\boldsymbol{x}$ only holds if $\boldsymbol{E}(x_1)$ is the zero matrix. Therefore the considered representation is unique.

The characteristic polynomial of $\boldsymbol{M}(x_1)$ (almost everywhere) is given by

$$w(s) = s^2 + k_1|x_1|^{-\frac{1}{2}}s + k_2|x_1|^{-1}$$

and the roots of $w(s) = 0$ are given by

$$s_1(x_1) = |x_1|^{-\frac{1}{2}}p_1 \quad \text{and} \quad s_2(x_1) = |x_1|^{-\frac{1}{2}}p_2, \tag{3.42}$$

with $p_1, p_2 \in \mathbb{C}$, and by Vieta's formula

$$k_2 = p_1 p_2 \quad \text{and} \quad k_1 = -(p_1 + p_2), \tag{3.43}$$

a mapping between the parameters of system (3.35) and the free parameters p_1 and p_2 is established. For any value of $x_1 \neq 0$ the eigenvalues s_1, $s_2 \in \mathbb{C}$ of $\boldsymbol{M}(x_1)$ are given in equation (3.42). By inspecting (3.42) it is obvious that the factor $|x_1|^{-1/2}$ plays the role of the time scaling. For the sake of completeness, the eigenvectors of the matrix $\boldsymbol{M}(x_1)$ are calculated which result in

$$\boldsymbol{v}_1^{\mathrm{T}}(x_1) = \left[-\sqrt{|x_1|}\tfrac{1}{p_2} \quad 1\right], \quad \boldsymbol{v}_2^{\mathrm{T}}(x_1) = \left[-\sqrt{|x_1|}\tfrac{1}{p_1} \quad 1\right]. \tag{3.44}$$

Also the eigenvectors $\boldsymbol{v}_1 : \mathbb{R} \to \mathbb{R}^2$ and $\boldsymbol{v}_2 : \mathbb{R} \to \mathbb{R}^2$ depend on the state variable x_1.

Before presenting novel discrete-time realizations the classical Euler discretization scheme is revisited in terms of the *Rosenbrock* form. Note that system (3.38) also may be obtained by computing

$$\boldsymbol{x}_{k+1} = [\boldsymbol{I} + T_{\mathrm{s}}\boldsymbol{M}(x_{1,k})]\,\boldsymbol{x}_k + T_{\mathrm{s}}\boldsymbol{h}_k \tag{3.45}$$

with $\boldsymbol{x}_k = \begin{bmatrix} x_{1,k} & x_{2,k} \end{bmatrix}^{\mathrm{T}}$, $\boldsymbol{h}_k = \begin{bmatrix} \frac{T_{\mathrm{s}}}{2}\Delta(\xi_{1,k}) & \Delta(\xi_{2,k}) \end{bmatrix}^{\mathrm{T}}$ and $\boldsymbol{I}$ denotes the 2×2 identity matrix. The dynamic matrix therefore reads as

$$[\boldsymbol{I} + T_{\mathrm{s}}\boldsymbol{M}(x_{1,k})] = \begin{bmatrix} 1 - T_{\mathrm{s}}k_1|x_1|^{-\frac{1}{2}} & T_{\mathrm{s}} \\ -T_{\mathrm{s}}k_2|x_1|^{-1} & 1 \end{bmatrix}. \tag{3.46}$$

The eigenvalues $z_i \in \mathbb{C}$ of the matrix $\boldsymbol{I} + T_{\mathrm{s}}\boldsymbol{M}(x_{1,k})$ are located at

$$z_i(T_{\mathrm{s}}, x_{1,k}) = 1 + T_{\mathrm{s}}s_i(x_{1,k}) \quad \text{for} \quad x_{1,k} \neq 0 \tag{3.47}$$

and $\forall T_{\mathrm{s}} \in \mathbb{R}_{>0}$

$$\lim_{x_{1,k} \to 0} |z_i(T_{\mathrm{s}}, x_{1,k})| = \infty.$$

The eigenvectors of the discrete-time system are the same as the eigenvectors of the continuous-time system that are given in (3.44).

Framework for the Design of the Discrete-Time Controllers

The discretization of the STA will now be achieved by mapping the eigenvalues of the continuous-time STA to the discrete-time domain. This is a well-known strategy when dealing with the discrete-time realization of linear time-invariant systems, see e.g. [31]. In order to exploit this approach also for the nonlinear STA, the STA control law is cast into a more general framework. This framework will allow to generate a family of controllers including not only novel discrete-time realizations of the discontinuous STA but also e.g. linear state feedback controllers and nonlinear continuous discrete-time controllers. The design of the algorithms relies on the plant dynamics (3.36), rewritten as

$$\begin{bmatrix} x_{1,k+1} \\ \varphi_{k+1} \end{bmatrix} = \begin{bmatrix} 1 & T_\mathrm{s} \\ 0 & 1 \end{bmatrix} \begin{bmatrix} x_{1,k} \\ \varphi_k \end{bmatrix} + \begin{bmatrix} T_\mathrm{s} \\ 0 \end{bmatrix} u_k + \begin{bmatrix} \frac{T_\mathrm{s}^2}{2} \Delta(\xi_{1,k}) \\ T_\mathrm{s} \Delta(\xi_{2,k}) \end{bmatrix}. \tag{3.48}$$

Note that, due to the fact that φ_k represents an unknown disturbance, only the state variable $x_{1,k}$ is available for the design of the control law, i.e., $u_k = u_k(x_{1,k})$. The general control law

$$\begin{aligned} u_k &= \frac{1}{T_\mathrm{s}} \left[-x_{1,k} + \tilde{u}_{1,k}(T_\mathrm{s}, x_{1,k}) x_{1,k} \right] + \nu_k, \\ \nu_{k+1} &= \nu_k + \tilde{u}_{2,k}(T_\mathrm{s}, x_{1,k}) x_{1,k}, \end{aligned} \tag{3.49}$$

is proposed. Substituting (3.49) into the plant dynamics (3.48) yields the closed-loop dynamics

$$\boldsymbol{x}_{k+1} = \boldsymbol{M}_\mathrm{d}(x_{1,k}) \boldsymbol{x}_k + T_\mathrm{s} \boldsymbol{h}_k, \tag{3.50}$$

with

$$\boldsymbol{M}_\mathrm{d}(x_{1,k}) := \begin{bmatrix} \tilde{u}_{1,k}(T_\mathrm{s}, x_{1,k}) & T_\mathrm{s} \\ \tilde{u}_{2,k}(T_\mathrm{s}, x_{1,k}) & 1 \end{bmatrix}. \tag{3.51}$$

By comparing (3.46) to (3.51), one can observe that the forward Euler discretized STA is obtained from the general control law representation (3.49) with

$$\begin{aligned} \tilde{u}_{1,k}(x_{1,k}) &= 1 - T_\mathrm{s} k_1 |x_1|^{-\frac{1}{2}}, \\ \tilde{u}_{2,k}(x_{1,k}) &= -T_\mathrm{s} k_2 |x_1|^{-1}. \end{aligned}$$

For the general case, the functions $\tilde{u}_{1,k}(T_\mathrm{s}, x_{1,k})$ and $\tilde{u}_{2,k}(T_\mathrm{s}, x_{1,k})$ are now designed by means of an eigenvalue assignment, i.e., the goal is to assign the eigenvalues of $\boldsymbol{M}_\mathrm{d}(x_{1,k})$. The characteristic polynomial computed by $\det(z\boldsymbol{I} - \boldsymbol{M}_\mathrm{d}) = 0$ with $z(T_\mathrm{s}, x_{1,k}) \in \mathbb{C}$ yields

$$z^2 - (\tilde{u}_{1,k} + 1) z + \tilde{u}_{1,k} - T_\mathrm{s} \tilde{u}_{2,k}. \tag{3.52}$$

By specifying a desired characteristic polynomial

$$z^2 - (q_1 + q_2) z + q_1 q_2, \tag{3.53}$$

where $q_i : \mathbb{R}_{>0} \times \mathbb{R} \to \mathbb{C}$ are real or a pair of conjugate complex eigenvalues, and comparing (3.52) to (3.53) yields

$$\tilde{u}_{1,k}(T_\mathrm{s}, x_{1,k}) = q_1(T_\mathrm{s}, x_{1,k}) + q_2(T_\mathrm{s}, x_{1,k}) - 1, \tag{3.54a}$$

$$\tilde{u}_{2,k}(T_\mathrm{s}, x_{1,k}) = \frac{1}{T_\mathrm{s}} \left[q_1(T_\mathrm{s}, x_{1,k}) + q_2(T_\mathrm{s}, x_{1,k}) - 1 - q_1(T_\mathrm{s}, x_{1,k}) q_2(T_\mathrm{s}, x_{1,k}) \right]. \tag{3.54b}$$

Substituting (3.54a) and (3.54b) into (3.51) gives

$$\boldsymbol{M}_{\mathrm{d}} = \left[\begin{array}{c|c} q_1 + q_2 - 1 & T_{\mathrm{s}} \\ \hline \frac{1}{T_{\mathrm{s}}}\left[q_1 + q_2 - 1 - q_1 q_2\right] & 1 \end{array}\right]. \tag{3.55}$$

The eigenvalues of $\boldsymbol{M}_{\mathrm{d}}$ are located at $z_i = q_i$. Note that the explicit Euler discretized STA dynamics is recovered from the general system representation (3.50) by assigning the eigenvalues z_i of $\boldsymbol{M}_{\mathrm{d}}$ as given in (3.47), i.e., selecting

$$q_1 = 1 + T_{\mathrm{s}} s_1(x_{1,k}) \quad \text{and} \quad q_2 = 1 + T_{\mathrm{s}} s_2(x_{1,k}). \tag{3.56}$$

Lemma 3.1

For $x_{1,k} \neq 0$, control law (3.49) with (3.54a), (3.54b) and eigenvalue assignment (3.56) with the continuous-time eigenvalues (3.42) and parameters (3.43) is identical to the forward Euler discretized STA given in (3.37). The resulting closed-loop system (3.50) is identical to system (3.45).

Proof. The proof is by substituting (3.42), (3.56) and (3.54a), (3.54b) into (3.49). Taking into account (3.43) then confirms that (3.49) is identical to the Euler discretized STA (3.37). As (3.48) constitutes only a different representation of (3.36), also the resulting closed-loop systems (3.50) and (3.45) are identical, i.e., $\boldsymbol{M}_{\mathrm{d}}(x_{1,k}) = \boldsymbol{I} + T_{\mathrm{s}}\boldsymbol{M}(x_{1,k})$. □

The closed-loop dynamics (3.50) with (3.55) is characterized by the eigenvalues $q_1(T_{\mathrm{s}}, x_{1,k})$ and $q_2(T_{\mathrm{s}}, x_{1,k})$. Obviously, by specifying these eigenvalues it is possible to generate, in addition to the forward Euler discretized STA, a number of control laws from (3.49). For instance, selecting a *constant* pair of real or conjugate complex eigenvalues $q_1(T_{\mathrm{s}}, x_{1,k}) = Q_1$, $q_2(T_{\mathrm{s}}, x_{1,k}) = Q_2$, $Q_1, Q_2 \in \mathbb{C}$ yields a linear state feedback controller. The choice $Q_1 = 0$, $Q_2 = 0$ gives a deadbeat controller, i.e., in the unperturbed case the output $x_{1,k}$ and the controller state ν_k is steered to zero exactly within two sampling steps. This choice coincides with the definition of a higher-order sliding mode controller for discrete-time systems given in [90].

Exploiting this general controller structure and taking specific functions q_i into account allows to formulate more advanced control laws. The controller design is therefore reduced to the construction of functions q_i providing for a desired behavior of the closed-loop system. Suitable functions may be generated in a straightforward way by mapping the eigenvalues from the continuous-time domain to the discrete-time domain, i.e., designing mappings of the form

$$q_i = f(T_{\mathrm{s}}, s_i(x_{1,k})). \tag{3.57}$$

Definition 3.1

The closed-loop system (3.50) with dynamic matrix (3.55) and functions $q_1(T_{\mathrm{s}}, x_{1,k})$ and $q_2(T_{\mathrm{s}}, x_{1,k})$ designed by specific mappings (3.57) with the continuous-time eigenvalues s_1, s_2 given in (3.42), is referred to as $\boldsymbol{\Sigma}_{\mathrm{d}}$.

The control laws presented in this paper are supposed to satisfy the following criteria:

C1 the controller (3.49) requires only information on $x_{1,k}$
C2 in any compact set not including points $x_{1,k} = 0$ the solutions of the discrete-time system $\mathbf{\Sigma}_\mathrm{d}$ approximate the solutions of system (3.35)
C3 in the unperturbed case the origin of $\mathbf{\Sigma}_\mathrm{d}$ is asymptotically stable
C4 $\mathbf{\Sigma}_\mathrm{d}$ is invariant w.r.t. (3.39)
C5 the convergence of the trajectories of $\mathbf{\Sigma}_\mathrm{d}$ to zero is with hyper-exponential speed

In case criterion C4 holds and assuming that all solutions of the discrete-time system $\mathbf{\Sigma}_\mathrm{d}$ are ultimately bounded then the asymptotic steady-state accuracies $|x_1| \leq \mu_1 T_\mathrm{s}^2$ and $|x_2| \leq \mu_2 T_\mathrm{s}$ with some positive constants μ_1 and μ_2 are achieved. Hence, $\mathbf{\Sigma}_\mathrm{d}$ exhibits a real sliding motion which is characterized by (3.40). In order to verify criterion C4 for $\mathbf{\Sigma}_\mathrm{d}$ it is sufficient to check the following invariance property:

Lemma 3.2

If the eigenvalues are invariant w.r.t.

$$z_i(\kappa T_\mathrm{s}, \kappa^2 x_{1,k}) = z_i(T_\mathrm{s}, x_{1,k}), \quad i = 1, 2 \tag{3.58}$$

$\forall \kappa > 0$, then $\mathbf{\Sigma}_\mathrm{d}$ is invariant w.r.t. (3.39).

Proof. The proof is by inspection of (3.55). □

Novel discrete-time realizations of the STA are now obtained by constructing functions of the form (3.57). These transformations between the continuous-time eigenvalues and the discrete-time eigenvalues are inspired by transformations known from linear systems theory, see e.g. [91, 31]. Substituting the specified discrete-time eigenvalues into the control law (3.54a), (3.54b) yields

$$\begin{aligned} u_k &= \frac{1}{T_\mathrm{s}} \left[(q_1 + q_2 - 2) x_{1,k} \right] + \nu_k, \\ \nu_{k+1} &= \nu_k + \frac{1}{T_\mathrm{s}} \left[q_1 + q_2 - 1 - q_1 q_2 \right] x_{1,k}, \end{aligned} \tag{3.59}$$

or

$$\begin{aligned} u_k &= -k_1 \psi_1 + \nu_k, \\ \nu_{k+1} &= \nu_k - T_\mathrm{s} k_2 \psi_2, \end{aligned} \tag{3.60}$$

with the scaled nonlinear functions

$$\begin{aligned} \psi_1 &= -\frac{1}{T_\mathrm{s} k_1} \left[q_1 + q_2 - 2 \right] x_{1,k}, \\ \psi_2 &= -\frac{1}{T_\mathrm{s}^2 k_2} \left[q_1 + q_2 - 1 - q_1 q_2 \right] x_{1,k}. \end{aligned}$$

As already mentioned above, the forward Euler discretized STA is obtained by selecting

$$q_i(T_\mathrm{s}, x_{1,k}) = \begin{cases} 1 + T_\mathrm{s} s_i(x_1) & x_1 \neq 0 \\ 0 & x_1 = 0 \end{cases}, \quad i = 1, 2$$

and substituting the discrete-time eigenvalues into the general control law (3.59). Different mappings will result in different discrete-time versions of the STA.

3.3.2 Matching Approach

The so-called *matching* approach, which is characterized by the mapping

$$q_i(T_\mathrm{s}, x_{1,k}) = \begin{cases} e^{T_\mathrm{s} s_i(x_{1,k})} & x_{1,k} \neq 0 \\ 0 & x_{1,k} = 0 \end{cases}, \quad i = 1, 2 \tag{3.62}$$

is applied to obtain another discrete-time version of the STA. The particular choice of the mapping (3.62) ensures that continuous-time eigenvalues lying in the left half of the complex plane are mapped inside the unit circle in the complex plane. Consequently $\sup_{x_{1,k}} |q_i(T_\mathrm{s}, x_{1,k})| < 1$ iff $\Re\{p_1\}, \Re\{p_2\} < 0$. The control law then is given by (3.60) with the nonlinear functions

$$\begin{aligned} \psi_1 &= -\frac{1}{k_1 T_\mathrm{s}} \left(e^{\frac{p_1 T_\mathrm{s}}{\sqrt{|x_{1,k}|}}} + e^{\frac{p_2 T_\mathrm{s}}{\sqrt{|x_{1,k}|}}} - 2 \right) x_{1,k}, \\ \psi_2 &= \frac{1}{k_2 T_\mathrm{s}^2} \left(e^{\frac{p_1 T_\mathrm{s}}{\sqrt{|x_{1,k}|}}} - 1 \right) \left(e^{\frac{p_2 T_\mathrm{s}}{\sqrt{|x_{1,k}|}}} - 1 \right) x_{1,k}. \end{aligned} \tag{3.63a}$$

The resulting closed-loop system $\boldsymbol{\Sigma}_\mathrm{d}$ is written as

$$\boldsymbol{x}_{k+1} = \begin{bmatrix} \left(e^{\frac{p_1 T_\mathrm{s}}{\sqrt{|x_{1,k}|}}} + e^{\frac{p_2 T_\mathrm{s}}{\sqrt{|x_{1,k}|}}} - 1 \right) & T_\mathrm{s} \\ \frac{1}{T_\mathrm{s}} \left(e^{\frac{p_1 T_\mathrm{s}}{\sqrt{|x_{1,k}|}}} + e^{\frac{p_2 T_\mathrm{s}}{\sqrt{|x_{1,k}|}}} - e^{\frac{(p_1+p_2) T_\mathrm{s}}{\sqrt{|x_{1,k}|}}} - 1 \right) & 1 \end{bmatrix} \boldsymbol{x}_k + T_\mathrm{s} \boldsymbol{h}_k, \tag{3.64}$$

It is remarkable that for the parameter choice $\Re\{p_1\}$, $\Re\{p_2\} < 0$ the above given functions ψ_1, ψ_2 yield approximations of the signed square root function and the signum function, respectively, as can be seen in Figure 3.3 for some sampling time T_s and the popular parameter choice $k_1 = 1.5$, $k_2 = 1.1$. Furthermore, the functions are smooth on $\mathbb{R}$ which is not the case when applying the forward Euler scheme. The result is in particular interesting as in the case of the FOSM the implicit scheme obviates the discretization chattering effects by a continuous approximation of the signum function. In the SISO case, the signum function is replaced by the saturation function where the boundary layer width results directly from the discretization. Several continuous approximations of relay type discontinuous-controllers have been proposed in the literature, see e.g. [92, 93, 2] to counteract the chattering effects. However, the approximations usually add new parameters in the controller which are not present in the continuous-time controller and consequently the tuning of the controllers is made

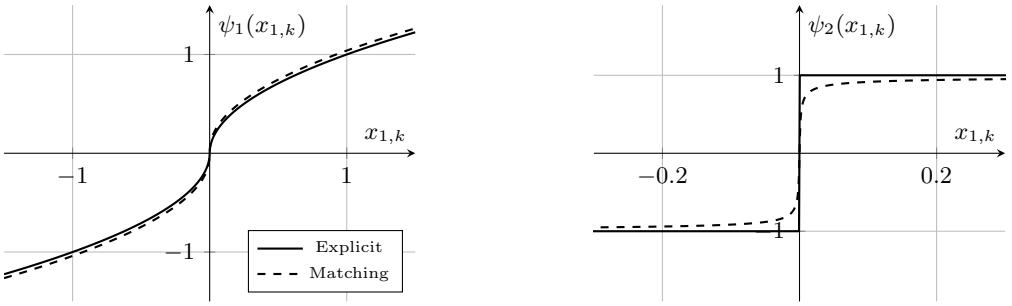

Figure 3.3: Similar as in the case of the implicit discretization of the FOSM controller, the proposed discretization scheme for the STA yields a smooth approximation of the sign function and the signed square root function, respectively.

more difficult. Although these approximations are very intuitive for the first-order system, the complexity increases with the sliding order. On the other hand, the proposed discretization scheme naturally yields such an approximation and no additional parameters are introduced in the controller.

Exploiting the series representation

$$e^{\frac{\alpha}{\sqrt{|x_{1,k}|}}} = \sum_{k=0}^{\infty} \frac{(\alpha)^k |x|^{-k/2}}{k!} = 1 + \frac{\alpha}{\sqrt{|x_{1,k}|}} + \frac{\alpha^2}{2!|x_{1,k}|} + \frac{\alpha^3}{3!|x_{1,k}|^{\frac{3}{2}}} + \dots \tag{3.65}$$

it is easy to show that, in any compact set not including points $x_{1,k} = 0$

$$\lim_{T_\mathrm{s}\to 0} \frac{1}{T_\mathrm{s} p_i} \left(e^{\frac{p_i T_\mathrm{s}}{\sqrt{|x_{1,k}|}}} - 1 \right) x_{1,k} = \frac{x_{1,k}}{\sqrt{|x_{1,k}|}} = |x_{1,k}|^{\frac{1}{2}} \mathrm{sign}\,(x_{1,k}),$$

and consequently

$$\lim_{T_\mathrm{s}\to 0} \psi_1 = \lim_{T_\mathrm{s}\to 0} -\frac{1}{k_1 T_\mathrm{s}} \left(e^{\frac{p_1 T_\mathrm{s}}{\sqrt{|x_{1,k}|}}} + e^{\frac{p_2 T_\mathrm{s}}{\sqrt{|x_{1,k}|}}} - 2 \right) x_{1,k} = |x_{1,k}|^{\frac{1}{2}} \mathrm{sign}\,(x_{1,k})$$

$$\lim_{T_\mathrm{s}\to 0} \psi_2 = \lim_{T_\mathrm{s}\to 0} \frac{1}{k_2 T_\mathrm{s}^2} \left(e^{\frac{p_1 T_\mathrm{s}}{\sqrt{|x_{1,k}|}}} - 1 \right) \left(e^{\frac{p_2 T_\mathrm{s}}{\sqrt{|x_{1,k}|}}} - 1 \right) x_{1,k} = \mathrm{sign}\,(x_{1,k}).$$

Hence, computing

$$\lim_{T_\mathrm{s}\to 0} \frac{1}{T_\mathrm{s}} \left(\boldsymbol{x}_{k+1} - \boldsymbol{x}_k \right) = \lim_{T_\mathrm{s}\to 0} \frac{1}{T_\mathrm{s}} \left(\boldsymbol{M}_\mathrm{d}(x_{1,k}) \boldsymbol{x}_k + T_\mathrm{s} \boldsymbol{h}_k - \boldsymbol{x}_k \right)$$

with (3.55) and (3.62) and for any $x_{1,k} \neq 0$ yields

$$\lim_{T_\mathrm{s}\to 0} \frac{1}{T_\mathrm{s}} \left(\boldsymbol{x}_{k+1} - \boldsymbol{x}_k \right) = \begin{bmatrix} -k_1 |x_{1,k}|^{\frac{1}{2}} \mathrm{sign}\,(x_{1,k}) + x_{2,k} \\ -k_2 \mathrm{sign}\,(x_{1,k}) + \Delta(t) \end{bmatrix},$$

which is the continuous-time STA dynamics. As mentioned above, the function ψ_2 given in (3.63a) yields the sign function in the limit $T_\mathrm{s} \to 0$. At a first glance, this function seems, due to

the multiplication with $x_{1,k}$, unbounded. However, by exploiting the series representation (3.65), one has

$$\lim_{x_{1,k}\to\infty} \psi_2 = \lim_{x_{1,k}\to\infty} \frac{1}{k_1 T_\mathrm{s}^2} \left(\frac{p_1 T_\mathrm{s}}{\sqrt{|x_{1,k}|}} + \frac{(p_1 T_\mathrm{s})^2}{2!|x_{1,k}|} + \dots \right) \left(\frac{p_2 T_\mathrm{s}}{\sqrt{|x_{1,k}|}} + \frac{(p_2 T_\mathrm{s})^2}{2!|x_{1,k}|} + \dots \right) x_{1,k} =$$
$$= \frac{1}{k_2 T_\mathrm{s}^2} \lim_{x_{1,k}\to\infty} \left(\frac{p_1 p_2 T_\mathrm{s}^2}{|x_{1,k}|} + \frac{p_1^2 p_2 T_\mathrm{s}^3}{2|x_{1,k}|^{\frac{3}{2}}} + \frac{p_1 p_2^2 T_\mathrm{s}^3}{2|x_{1,k}|^{\frac{3}{2}}} + \frac{(p_1 p_2)^2 T_\mathrm{s}^4}{4|x_{1,k}|^2} + \dots \right) x_{1,k} = 1$$

which demonstrates that ψ_2 indeed is bounded at infinity.

In the following paragraphs the properties of the discretized STA, obtained by the matching approach, are investigated in detail.

The closed-loop system (3.64) is invariant w.r.t. to the parameter/coordinate transformation (3.39). Due to this homogeneity like property, the trajectories of the system with sampling time T_s are bijectively transferred on the system with sampling time κT_s where $\kappa \in \mathbb{R}$, see [87]. That means, the trajectory of the system with sampling time κT_s and initial condition $\kappa^2 x_{1,0}$ and $\kappa x_{2,0}$ is the same as the trajectory of the system with sampling time T_s and initial condition $x_{1,0}$, $x_{2,0}$ scaled by $\begin{bmatrix}\kappa^2 & \kappa\end{bmatrix} \boldsymbol{x}_k$. More general: Let $\boldsymbol{F}(k, T_\mathrm{s}, \boldsymbol{x}_0)$ denote the solution of the discrete-time system $\boldsymbol{x}_{k+1} = \boldsymbol{f}(T_\mathrm{s}, \boldsymbol{x}_k)$, $\boldsymbol{x}_k = \begin{bmatrix} x_{1,k} & \dots & x_{n,k}\end{bmatrix}^\mathrm{T}$. If the r.h.s. satisfies $\boldsymbol{f}(\kappa T_\mathrm{s}, \boldsymbol{K}\boldsymbol{x}_k) = \boldsymbol{K}\boldsymbol{f}(T_\mathrm{s}, \boldsymbol{x}_k)$, where

$$\boldsymbol{K} = \begin{bmatrix} \kappa^n & & \\ & \ddots & \\ & & \kappa \end{bmatrix},$$

then $\boldsymbol{K}\boldsymbol{F}(k, T_\mathrm{s}, \boldsymbol{x}_0)$ is the solution of the system $\boldsymbol{x}_{k+1} = \boldsymbol{f}(\kappa T_\mathrm{s}, \boldsymbol{K}\boldsymbol{x}_k)$. Figure 3.4 illustrates this property for a planar system. Therefore, besides stability of the closed-loop system, the invariance w.r.t. to the scaling

$$(T_\mathrm{s},\, x_{1,k},\, \dots x_{n,k}) \to (\kappa T_\mathrm{s},\, \kappa^n x_{1,k},\, \dots \kappa x_{n,k}) \tag{3.67}$$

is a fundamental ingredient ensuring the asymptotic accuracies known from the n^{th} order sliding mode.

The stability property of the origin $\boldsymbol{x}_k = \boldsymbol{0}$ is examined in the following:

Theorem 3.1

Suppose that $L = 0$ and let $k_1 > 0$, $k_2 > 0$. Then the origin of the closed-loop system (3.64) is asymptotically stable, i.e., every trajectory starting in some ball around the origin with radius $r > 0$ sufficiently small converges to the origin.

Proof. The r.h.s. of the closed-loop system satisfies

$$\boldsymbol{x}_{k+1} = \boldsymbol{M}_\mathrm{d}(x_{1,k})\boldsymbol{x}_k = \boldsymbol{M}_\mathrm{d}(0)\boldsymbol{x}_k + \boldsymbol{n}(x_{1,k}) \tag{3.68}$$

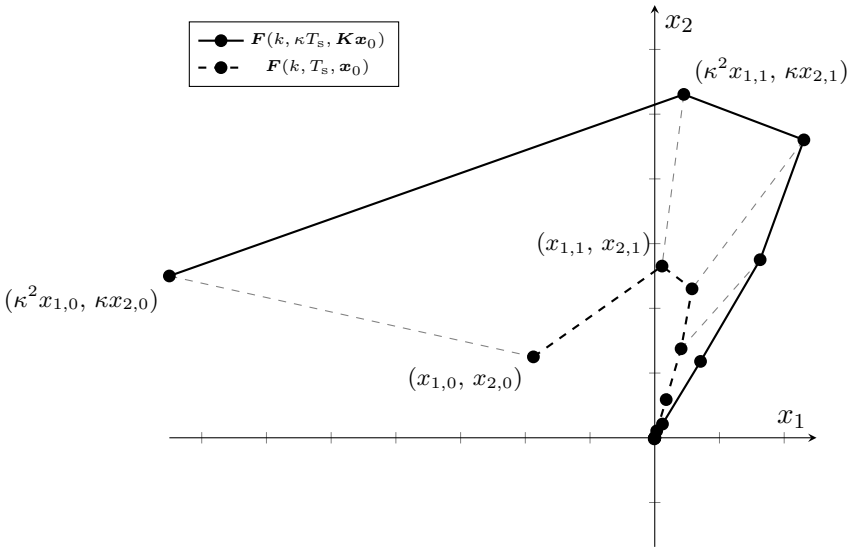

Figure 3.4: Scaling property of the solutions of a discrete-time system satisfying the invariance property (3.67)

where

$$\boldsymbol{n}(x_{1,k}) = \frac{1}{T_\mathrm{s}} \begin{bmatrix} T_\mathrm{s} e^{\frac{p_1 T_\mathrm{s}}{\sqrt{|x_{1,k}|}}} + T_\mathrm{s} e^{\frac{p_2 T_\mathrm{s}}{\sqrt{|x_{1,k}|}}} \\ e^{\frac{p_1 T_\mathrm{s}}{\sqrt{|x_{1,k}|}}} + e^{\frac{p_2 T_\mathrm{s}}{\sqrt{|x_{1,k}|}}} - e^{\frac{(p_1+p_2) T_\mathrm{s}}{\sqrt{|x_{1,k}|}}} \end{bmatrix} x_{1,k}.$$

If the gains $k_1 = -(p_1 + p_2)$, $k_2 = p_1 p_2$ satisfy $k_1, k_2 > 0$ the mapping $\boldsymbol{n} : \mathbb{R}^2 \to \mathbb{R}^2$ is continuous on $\mathbb{R}^2$ and

$$\lim_{\|\boldsymbol{x}\| \to 0} = \frac{\|\boldsymbol{n}(\boldsymbol{x})\|}{\|\boldsymbol{x}\|} = 0. \tag{3.69}$$

The evolution operator $\boldsymbol{M}_\mathrm{d}(0)$ is exponential stable, i.e., $\boldsymbol{M}_\mathrm{d}(0)$ is a Schur matrix. From Lyapunov's indirect method for discrete-time systems, see e.g. [88, 94], it is concluded that the origin of the nonlinear system is exponentially stable. □

Note that Theorem 3.1 provides a local stability result. The vicinity of the origin where the approximate dynamics

$$\boldsymbol{x}_{k+1} = \boldsymbol{M}_\mathrm{d}(0)\boldsymbol{x}_k$$

is valid depends on the sampling time T_s and as $T_\mathrm{s} \to 0$ the vicinity disappears. The continuous-time system obtained in the limit $T_\mathrm{s} \to 0$ cannot be approximated by a linear system in the vicinity of the origin. Near the origin the terms with the smallest homogeneity degree dominate the dynamics. Therefore the linearization has to fail for the continuous-time STA which has negative homogeneity degree, see e.g. [2].

The spectrum of the evolution operator $\boldsymbol{M}_\mathrm{d}(0)$ satisfies $\lambda(\boldsymbol{M}_\mathrm{d}(0)) = \{0,\, 0\}$. The fact, that in the limit the closed-loop system exhibits a dead beat response imposes a stronger convergence

than the exponential convergence known from linear systems (with the exception of a dead beat system, i.e., $q_1 = q_2 = 0$ where the convergence is in a finite number of steps). Hence, criterion C5 is satisfied. The following Lemma is helpful for the proof of this property.

Lemma 3.3

Assume $L = 0$ and $k_1, k_2 > 0$. In the limit $k \to \infty$ the trajectories of the closed-loop system (3.64) approach the origin along the vector

$$\boldsymbol{a}^{\mathrm{T}} = \begin{bmatrix} T_{\mathrm{s}} & 1 \end{bmatrix}.$$

Proof. The absolute value of the angle between the state vector and $\boldsymbol{a}$ at sampling step k is given by

$$|\cos\theta_k| = \frac{|\boldsymbol{a}^{\mathrm{T}}\boldsymbol{x}_k|}{\|\boldsymbol{a}\|\|\boldsymbol{x}_k\|}.$$

The limit is computed as

$$\lim_{k\to\infty} |\cos\theta_k| = \lim_{k\to\infty} |\cos\theta_{k+1}| = \lim_{k\to\infty} \frac{|\boldsymbol{a}^{\mathrm{T}}\boldsymbol{M}_{\mathrm{d}}(0)\boldsymbol{x}_k + \boldsymbol{a}^{\mathrm{T}}\boldsymbol{n}(x_{1,k})|}{\|\boldsymbol{a}\|\|\boldsymbol{M}_{\mathrm{d}}(0)\boldsymbol{x}_k + \boldsymbol{n}(x_{1,k})\|}. \tag{3.70}$$

The matrix $\boldsymbol{M}_{\mathrm{d}}(0)$ is nilpotent and $\boldsymbol{a}$ is Eigenvector of $\boldsymbol{M}_{\mathrm{d}}(0)$, i.e.

$$\boldsymbol{M}_{\mathrm{d}}(0)\boldsymbol{a} = \boldsymbol{0}$$

holds. Thus the recursion (3.68) is rewritten as

$$\boldsymbol{x}_{k+1} = \boldsymbol{M}_{\mathrm{d}}(0)\boldsymbol{x}_k + \boldsymbol{n}(x_{1,k}) = \boldsymbol{a}\left(x_{2,k} - \frac{1}{T_{\mathrm{s}}}x_{1,k}\right) + \boldsymbol{n}(x_{1,k}),$$

and (3.70) takes the form

$$\lim_{k\to\infty} \frac{\|\boldsymbol{a}\||x_{2,k} - \frac{1}{T_{\mathrm{s}}}x_{1,k} + \frac{\boldsymbol{a}^{\mathrm{T}}}{\|\boldsymbol{a}\|^2}\boldsymbol{n}(x_{1,k})|}{\|\boldsymbol{a}(x_{2,k} - \frac{1}{T_{\mathrm{s}}}x_{1,k}) + \boldsymbol{n}(x_{1,k})\|}$$

Using (3.69) one obtains for the limit

$$\lim_{k\to\infty} |\cos\theta_{k+1}| = \left(\lim_{k\to\infty} \frac{\|\boldsymbol{a}(x_{2,k} - \frac{1}{T_{\mathrm{s}}}x_{1,k})\|}{\|\boldsymbol{a}\||x_{2,k} - \frac{1}{T_{\mathrm{s}}}x_{1,k}|}\right)^{-1} = 1$$

and consequently

$$\lim_{k\to\infty} \theta_k = \pi n, \quad n \in \mathbb{Z}.$$

□

Theorem 3.2

Under the assumptions stated in Theorem 3.1, $\boldsymbol{\Sigma}_\mathrm{d}$ with (3.64) converges locally with hyper-exponential speed to the origin.

Proof. Hyper-exponential rate of convergence requires

$$\lim_{k\to\infty} \mu_k = \lim_{k\to\infty} \frac{V_{k+1}}{V_k} = 0.$$

For the pseudo linearized-system (3.68), the quadratic form

$$V_k = \boldsymbol{x}_k^\mathrm{T} \boldsymbol{P} \boldsymbol{x}_k \tag{3.71}$$

with $\boldsymbol{P}$ satisfying the discrete Lyapunov equation

$$\boldsymbol{M}_\mathrm{d}(0)^\mathrm{T} \boldsymbol{P} \boldsymbol{M}_\mathrm{d}(0) - \boldsymbol{P} = -\boldsymbol{I} \tag{3.72}$$

is locally a Lyapunov function. The solution of (3.72)

$$\boldsymbol{P} = \begin{bmatrix} 2 + \frac{1}{T_\mathrm{s}^2} & -\left(\frac{1}{T_\mathrm{s}} + T_\mathrm{s}\right) \\ -\left(\frac{1}{T_\mathrm{s}} + T_\mathrm{s}\right) & 2 + T_\mathrm{s}^2 \end{bmatrix}.$$

has an invariant eigenvalue $\tilde{s}_1 = 1$, $\forall T_\mathrm{s}$. Substituting the closed-loop system $\boldsymbol{\Sigma}_\mathrm{d}$ into (3.71) and exploiting (3.72) one obtains

$$\lim_{k\to\infty} \frac{V_{k+1}}{V_k} = \lim_{k\to\infty} \frac{\boldsymbol{x}_k^\mathrm{T} \left(\boldsymbol{P} - \boldsymbol{I}\right) \boldsymbol{x}_k + f(\boldsymbol{h}(x_{1,k}))}{\boldsymbol{x}_k^\mathrm{T} \boldsymbol{P} \boldsymbol{x}_k}.$$

Furthermore, taking into account the eigenvector equation $\boldsymbol{M}_\mathrm{d}(0)\boldsymbol{a} = 0\boldsymbol{a} = \boldsymbol{0}$ as well as (3.71) gives

$$-\boldsymbol{M}_\mathrm{d}(0)^\mathrm{T} \boldsymbol{P} \boldsymbol{M}_\mathrm{d}(0)\boldsymbol{a} = \left[\boldsymbol{I} - \boldsymbol{P}\right] \boldsymbol{a} = \boldsymbol{0},$$

i.e., the eigenvector $\boldsymbol{a}$ of $\boldsymbol{M}_\mathrm{d}(0)$ also is an eigenvector of $\boldsymbol{P}$ associated with the eigenvalue $\tilde{s}_1 = 1$. Using (3.69) and Lemma 3.3 one gets

$$\lim_{k\to\infty} \frac{V_{k+1}}{V_k} = \lim_{k\to\infty} \left(1 - \frac{\boldsymbol{x_k}^\mathrm{T} \boldsymbol{x_k}}{\boldsymbol{x_k}^\mathrm{T} \boldsymbol{P} \boldsymbol{x_k}^\mathrm{T}}\right) = 1 - \frac{\boldsymbol{a}^\mathrm{T} \boldsymbol{a}}{\boldsymbol{a}^\mathrm{T} \tilde{s}_1 \boldsymbol{a}} = 0$$

which completes the proof. □

Theorem 3.1 provides a local stability result which was obtained by Lyapunov's indirect method. The result is also very helpful when proofing the hyper-exponential rate of convergence. A global stability result, proven by Lyapunov's direct method, is given in the following Theorem:

Theorem 3.3

Suppose that $L = 0$ and let the gains satisfy $p_1 = p_2 = p \in \mathbb{R}$ and $p < 0$. Under these conditions the origin of the closed-loop system (3.64) is globally exponentially stable and

$$V_k = |x_{1,k} - T_\mathrm{s} x_{2,k}| + \frac{1}{2k_2} x_{2,k}^2 \tag{3.73}$$

is a Lyapunov function.

Proof. Let

$$V_k = |x_{1,k} - T_\mathrm{s} x_{2,k}| + a x_{2,k}^2, \quad a \in \mathbb{R}_{>0} \tag{3.74}$$

be the positive definite candidate Lyapunov function. Computing the difference $\Delta V_k = V_{k+1} - V_k$ and substituting the plant dynamics (3.50) with (3.55) and (3.62) yields

$$\begin{aligned}\Delta V_k &= |q^2 x_{1,k}| + a\left(-\frac{1}{T_\mathrm{s}}(q-1)^2 x_{1,k} + x_{2,k}\right)^2 - |x_{1,k} - T_\mathrm{s} x_{2,k}| - a x_{2,k}^2 = \\ &= \left(q^2 \mathrm{sign}\,(x_{1,k}) + \frac{a}{T_\mathrm{s}^2}(q-1)^4 x_{1,k}\right) x_{1,k} - \left(\frac{2a}{T_\mathrm{s}^2}(q-1)^2 x_{1,k}\right) T_\mathrm{s} x_{2,k} - |x_{1,k} - T_\mathrm{s} x_{2,k}|\end{aligned}$$

where $q_1 = q_2 = q$. Introducing the functions

$$f_1(x_{1,k}) = q^2 \mathrm{sign}\,(x_{1,k}) + \frac{a}{T_\mathrm{s}^2}(q-1)^4 x_{1,k}, \tag{3.75a}$$

$$f_2(x_{1,k}) = \frac{2a}{T_\mathrm{s}^2}(q-1)^2 x_{1,k}, \tag{3.75b}$$

provides for

$$\Delta V_k = f_1 x_{1,k} - f_2 T_\mathrm{s} x_{2,k} - |x_{1,k} - T_\mathrm{s} x_{2,k}|.$$

In order to ensure negative definiteness of ΔV_k it needs to be shown that there exists a parameter a, in (3.74) and (3.75), such that the inequality

$$f_1(x_{1,k}) x_{1,k} - f_2(x_{1,k}) T_\mathrm{s} x_{2,k} < |x_{1,k} - T_\mathrm{s} x_{2,k}| \tag{3.76}$$

holds $\forall x_{1,k}, x_{2,k} \in \mathbb{R}$. Note that the functions f_1 and f_2 are odd and $\mathrm{sign}\,(f_1(x_{1,k})) = \mathrm{sign}\,(f_2(x_{1,k})) = \mathrm{sign}\,(x_{1,k})$ which follows from $q \in [0,\, 1)$. Inequality (3.76) is satisfied if

$$|f_1(x_{1,k})| < |f_2(x_{1,k})| < 1, \, \forall\, x_{1,k} \tag{3.77}$$

holds. Exploiting the series representation (3.65), i.e.,

$$q = e^{\frac{pT_\mathrm{s}}{\sqrt{|x_{1,k}|}}} = \sum_{k=0}^{\infty} \frac{(pT_\mathrm{s})^k |x|^{-k/2}}{k!}, \quad x_{1,k} \neq 0 \tag{3.78}$$

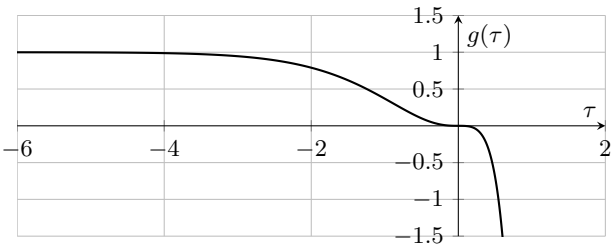

Figure 3.5: Graphical representation of the exponential polynomial on the l.h.s. of the inequality (3.81). The plot reveals that the inequality is satisfied $\forall \tau < 0$.

and taking into account (3.43), it can be shown that

$$\lim_{x_{1,k}\to\infty} f_2(x_{1,k}) = 2ak_2,$$
$$\lim_{x_{1,k}\to\infty} f_1(x_{1,k}) = 1,$$

which restricts the choice of the parameter a in the candidate Lyapunov function (3.74) to

$$a = \frac{1}{2k_2}. \tag{3.80}$$

This is the only possible choice for a because then (3.77) holds with equality in the limit. It remains to show, that with the choice (3.80), the relation $|f_1(x_{1,k})| < |f_2(x_{1,k})|$ is satisfied for all (finite) $x_{1,k}$. Due to symmetry it is sufficient to investigate (3.77) for the case $x_{1,k} \geq 0$ which, after substituting q from (3.62) into the functions f_1 and f_2, leads to

$$e^{\frac{2pT_\mathrm{s}}{\sqrt{|x_{1,k}|}}} \left(2p^2T_\mathrm{s}^2 + \left(e^{\frac{2pT_\mathrm{s}}{\sqrt{|x_{1,k}|}}} - 2 \right)^2 x_{1,k} \right) < x_{1,k} \tag{3.81}$$

Introducing

$$\tau := \frac{pT_\mathrm{s}}{\sqrt{x_{1,k}}}$$

allows to rewrite the inequality (3.81) into

$$g(\tau) := 1 - e^{2\tau} \left(2\tau^2 + (-2 + e^\tau)^2 \right) > 0. \tag{3.82}$$

The function $g(\tau)$ is an exponential polynomial in τ. The problem of determining the zeros of an exponential polynomial is closely related to the problem of determining the zero crossings of the step response of a LTI system. In view of this, the function $g(-\tau)$ is considered as the step response of the asymptotically stable, strictly proper transfer function

$$G(\bar{s}) = \bar{s}\mathscr{L}\{g(-\tau), \bar{s}\} = \frac{12(\bar{s}^2 + 16/3\bar{s} + 8)}{(\bar{s}+2)^3(\bar{s}+3)(\bar{s}+4)}$$

where $\mathscr{L}\{\cdot\}$ denotes the Laplace transform. According to [95], the step response of such a transfer function undergoes a zero crossing if it has at least one positive zero. As the numerator polynomial of $G(\bar{s})$ is a Hurwitz polynomial, there is no zero crossing in the step response of $G(\bar{s})$ and thus, $g(\tau)$ does not change sign. As $G(0) = 1$, $g(\tau)$ is positive for all $\tau < 0$ which confirms that inequality (3.82) holds (see also the plot in Figure 3.5), which completes the proof. □

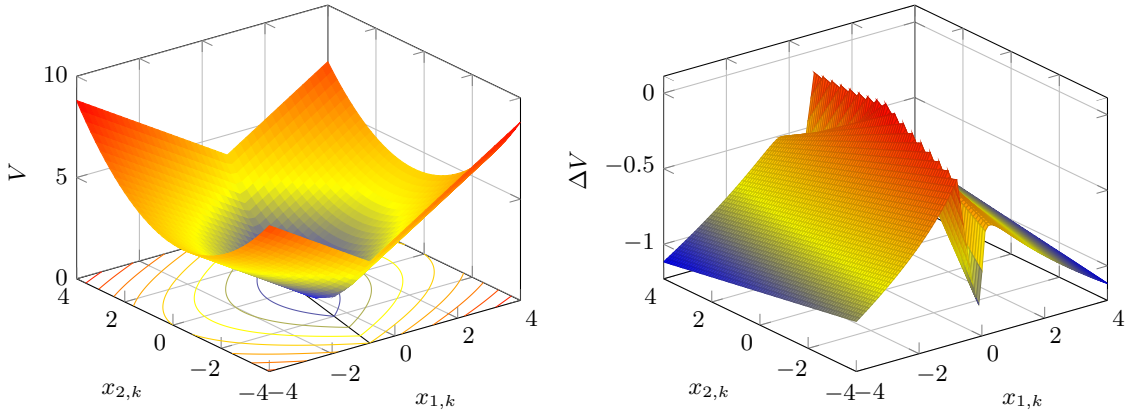

Figure 3.6: Lyapunov function $V_k = |x_{1,k} - T_\mathrm{s} x_{2,k}| + \frac{1}{2k_2} x_{2,k}^2$ for the matched discretized STA and the difference ΔV_k. The parameters are $T_\mathrm{s} = 0.2$, $k_1 = 3$, $k_2 = 2$.

Computing $\lim\limits_{T_\mathrm{s}\to 0} V_k$ of the Lyapunov function (3.73) results in

$$\lim_{T_\mathrm{s}\to 0} V_k = \lim_{T_\mathrm{s}\to 0} |x_{1,k} - T_\mathrm{s} x_{2,k}| + \frac{1}{2k_2} x_{2,k}^2 = |x_1| + \frac{1}{2k_2} x_2^2.$$

The result is in particular interesting as the Lyapunov function of the discrete-time system approaches a weak Lyapunov function of the unperturbed continuous-time STA (3.35) as the sampling time T_s tends to zero. Computing the derivative of

$$V = |x_1| + \frac{1}{2k_2} x_2^2$$

along the trajectories of (3.35) yields

$$\dot{V} = -k_1 \sqrt{|x_1|}.$$

Figure 3.6 shows the Lyapunov function (3.74) together with the difference ΔV_k for the parameters $T_\mathrm{s} = 0.2$, $k_1 = 3$ and $k_2 = 2$.

Remark 4. The choice of two distinct real eigenvalues p_1 and p_2 leads to the inequality

$$\begin{aligned} &1 - e^{2p_1\tau} - e^{2p_2\tau} - 2e^{(p_1+p_2)\tau} - e^{2(p_1+p_2)\tau} + \\ &+ 2e^{(2p_1+p_2)\tau} + 2e^{(p_1+2p_2)\tau} - 2p_1 p_2 \tau^2 e^{(p_1+p_2)\tau} > 0. \end{aligned}$$

For given parameters p_1 and p_2 the global stability of the origin of the unperturbed closed-loop system can be verified graphically from this inequality.

The theoretical findings are studied in a simulation example. The controller parameters are selected as $k_1 = 2$ and $k_2 = 1$ giving $p_1 = p_2 = -1$. The sampling time is set to $T_\mathrm{s} = 0.05$ s. The results obtained from simulating the closed-loop system with initial conditions $\boldsymbol{x}_0 = \begin{bmatrix} -2 & 0.5 \end{bmatrix}^\mathrm{T}$ are plotted in Figure (3.7). The upper left plot shows the trajectories over time, the right plot shows the trajectory in the $x_1 - x_2$ plane. In the zoomed-in view one can recognize that in the

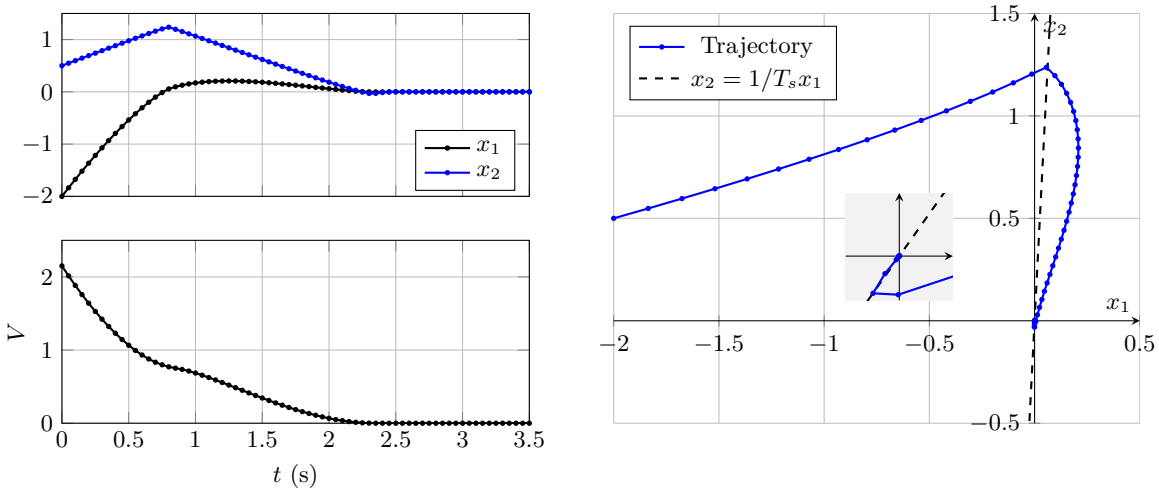

Figure 3.7: Simulation of the closed-loop system. The upper left plot shows the trajectories over time, the lower one is the Lyapunov function evaluated along the trajectory. The plot on the right hand side shows the trajectory in the phase plane.

Figure 3.8: The plot illustrates the hyper-exponential speed of convergence imposed by the matched discretized STA. It is compared to the explicit Euler discretized STA, which provides for practical stability and a linear state feedback controller which gives exponential convergence. The parameters are $p_1 = p_2 = -2$ and $T_s = 0.05$ s.

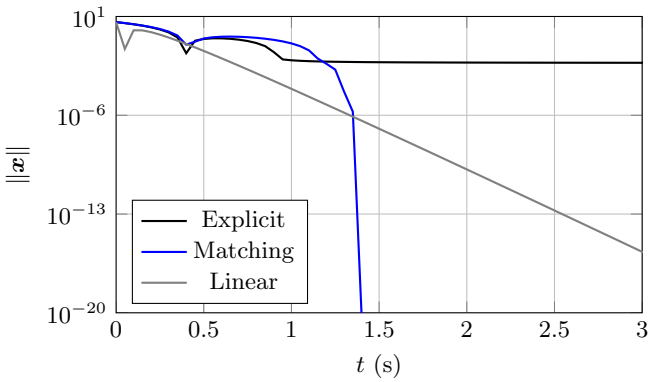

limit $k \to \infty$ the trajectory converges to the origin along the vector $\boldsymbol{a}^{\mathrm{T}} = \begin{bmatrix} T_s & 1 \end{bmatrix}$, i.e., along the line $x_2 = 1/T_s x_1$ as stated in Lemma 3.3. The lower left plot shows the Lyapunov function V_k evaluated along the trajectory. The sequence V_k decreases monotonically in k.

The hyper-exponential rate of convergence can be seen Figure 3.8. The plot compares the norm of the state vector obtained by the matched discretized STA, to the classical forward Euler discretized STA and a linear state feedback controller where $q_1 = q_2 = 0.5$. The parameters of the STA are $p_1 = p_2 = -2$ and $T_s = 0.05$ s. The trajectories are plotted on a logarithmic scale. One can see, that the matched discretized STA imposes a much faster convergence to the origin when compared to the linear state feedback controller. In case of the forward Euler discretized STA the trajectories are ultimately bounded.

Up to here, the analysis was restricted to the unperturbed system. In case of an unknown perturbation it is in general not possible anymore to steer the state variables to exactly zero. However, under the more restrictive assumption that the disturbance $\Delta(t)$ is bounded and Lipschitz continuous it is shown in the following that the discretization scheme ensures

ultimately boundedness for sufficiently small sampling time T_s.

Theorem 3.4

Let the perturbation $\Delta(t)$ be bounded and Lipschitz continuous, i.e., it satisfies $\sup_t |\Delta(t)| \leq L$ and $\sup_t |\dot{\Delta}(t)| \leq \tilde{L}$, and the sampling time T_s sufficiently small. Then there exist gains $k_1 = -(p_1 + p_2)$, $k_2 = p_1 p_2$ with p_1, $p_2 \in \mathbb{R}_{<0}$, positive constants μ_1 and μ_2 and a sampling instant k^* such that the solutions of the closed-loop system $\mathbf{\Sigma}_\mathrm{d}$ with (3.62) satisfy $|x_{1,k}| < \mu_1 T_\mathrm{s}^2$, $|x_{2,k}| < \mu_2 T_\mathrm{s}$, $\forall k > k^*$.

Proof. Consider the general representation of the discretized STA which is given by

$$\begin{aligned} \frac{1}{T_\mathrm{s}}(x_{1,k+1} - x_{1,k}) &= -k_1 \psi_1(x_{1,k}, T_\mathrm{s}) + x_{2,k} + \frac{T_\mathrm{s}}{2}\Delta(\xi_{1,k}), \\ \frac{1}{T_\mathrm{s}}(x_{2,k+1} - x_{2,k}) &= -k_2 \psi_2(x_{1,k}, T_\mathrm{s}) + \Delta(\xi_{2,k}). \end{aligned} \tag{3.83}$$

Adding and subtracting $-k_1|x_{1,k}|^{\frac{1}{2}}\mathrm{sign}\,(x_{1,k})$ and $-k_2\mathrm{sign}\,(x_{1,k})$, respectively on the r.h.s. of the equations allows to rewrite (3.83) into

$$\begin{aligned} \frac{1}{T_\mathrm{s}}(x_{1,k+1} - x_{1,k}) &= -k_1|x_{1,k}|^{\frac{1}{2}}\mathrm{sign}\,(x_{1,k}) + x_{2,k} - k_1\tilde{\psi}_1(x_{1,k}, T_\mathrm{s}), \\ \frac{1}{T_\mathrm{s}}(x_{2,k+1} - x_{2,k}) &= -k_2\mathrm{sign}\,(x_{1,k}) - k_2\tilde{\psi}_2(x_{1,k}, T_\mathrm{s}) + \Delta(\xi_{2,k}), \end{aligned}$$

where

$$\begin{aligned} \tilde{\psi}_1(x_{1,k}, T_\mathrm{s}) &:= \psi_1(x_{1,k}, T_\mathrm{s}) - |x_{1,k}|^{\frac{1}{2}}\mathrm{sign}\,(x_{1,k}) + \frac{T_\mathrm{s}}{2}\Delta(\xi_{1,k}), \\ \tilde{\psi}_2(x_{1,k}, T_\mathrm{s}) &:= \psi_2(x_{1,k}, T_\mathrm{s}) - \mathrm{sign}\,(x_{1,k}), \end{aligned}$$

i.e., the discrete-time system is represented as a forward Euler discretized version of the continuous-time STA plus the (inherent) perturbations $\tilde{\psi}_1(x_{1,k})$, $\tilde{\psi}_2(x_{1,k})$. The discrete-time system (3.83) is obtained by forward Euler discretization of the artificial continuous-time system

$$\begin{aligned} \dot{x}_1 &= -k_1|x_1|^{\frac{1}{2}}\mathrm{sign}\,(x_1) + x_2 - k_1\tilde{\psi}_1(x_1, \tilde{T}_s), \\ \dot{x}_2 &= -k_2\mathrm{sign}\,(x_1) - k_2\tilde{\psi}_2(x_1, \tilde{T}_s) + \Delta(\xi_2) \end{aligned} \tag{3.84}$$

with $T_\mathrm{s} = \tilde{T}_s$ and $\xi_2 \in (t,\, t+\tilde{T}_s)$. In the next step the stability properties of this continuous-time system are investigated. Applying the change of coordinates $\omega_1 = |x_1|^{\frac{1}{2}}\mathrm{sign}\,(x_1)$ and $\omega_2 = x_2$ yields the linear perturbed system

$$\begin{aligned} |x_1|^{\frac{1}{2}}\dot{\omega}_1 &= -\frac{1}{2}k_1\omega_1 + \frac{1}{2}\omega_2 - \frac{1}{2}k_1\tilde{\psi}_1(x_1, \tilde{T}_s) \\ |x_1|^{\frac{1}{2}}\dot{\omega}_2 &= -k_2\omega_1 + |x_1|^{\frac{1}{2}}\left(-k_2\tilde{\psi}_2(x_1, \tilde{T}_s) + \Delta(\xi_2\right) \end{aligned} \tag{3.85}$$

With

$$\boldsymbol{A} = \begin{bmatrix} -\frac{1}{2}k_1 & \frac{1}{2} \\ k_2 & 0 \end{bmatrix}, \quad \tilde{\boldsymbol{\psi}} = \begin{bmatrix} -\frac{1}{2}k_1\tilde{\psi}_1 \\ -k_2|x_1|^{\frac{1}{2}}\tilde{\psi}_2 \end{bmatrix}, \quad \tilde{\Delta}(t,x_1) := |x_1|^{\frac{1}{2}}\Delta(t)$$

and $\boldsymbol{\omega} = \begin{bmatrix} \omega_1 & \omega_2 \end{bmatrix}^{\mathrm{T}}$, (3.85) is rewritten into

$$|x_1|^{\frac{1}{2}}\dot{\boldsymbol{\omega}} = \boldsymbol{A}\boldsymbol{\omega} + \boldsymbol{e}_2\tilde{\Delta}(x_1,t) + \tilde{\boldsymbol{\psi}}(x_1). \tag{3.86}$$

Taking into account the series representation (3.78) allows to rewrite the internal perturbation

$$\begin{aligned}
&-\frac{k_1}{2}\left(\psi_1(x_{1,k},T_\mathrm{s}) - |x_{1,k}|^{\frac{1}{2}}\mathrm{sign}\,(x_{1,k})\right) = \\
&= -\frac{k_1}{2}\left(-\frac{1}{k_1T_\mathrm{s}}\left(e^{\frac{p_1T_\mathrm{s}}{\sqrt{|x_{1,k}|}}} + e^{\frac{p_2T_\mathrm{s}}{\sqrt{|x_{1,k}|}}} - 2\right)x_{1,k} - |x_{1,k}|^{\frac{1}{2}}\mathrm{sign}\,(x_{1,k})\right) = \\
&= \frac{1}{2T_\mathrm{s}}\left(\frac{(p_1+p_2)T_\mathrm{s}}{\sqrt{|x_{1,k}|}} + \frac{(p_1^2+p_2^2)T_\mathrm{s}^2}{2!|x_{1,k}|} + \frac{(p_1^3+p_2^3)T_\mathrm{s}^3}{3!|x_{1,k}|^{\frac{3}{2}}} + \dots\right)x_{1,k} + \frac{k_1}{2}|x_{1,k}|^{\frac{1}{2}}\mathrm{sign}\,(x_{1,k}) = \\
&= \frac{1}{2T_\mathrm{s}}\left(\frac{(p_1^2+p_2^2)T_\mathrm{s}^2}{2!} + \frac{(p_1^3+p_2^3)T_\mathrm{s}^3}{3!|x_{1,k}|^{\frac{1}{2}}} + \dots\right)\mathrm{sign}\,(x_1) = \\
&= \frac{p_1^2T_\mathrm{s}}{2}\left(\frac{1}{2!} + \frac{(s_1(x_{1,k})T_\mathrm{s})}{3!} + \dots\right)\mathrm{sign}\,(x_1) + \frac{p_2^2T_\mathrm{s}}{2}\left(\frac{1}{2!} + \frac{(s_2(x_{1,k})T_\mathrm{s})}{3!} + \dots\right)\mathrm{sign}\,(x_1).
\end{aligned}$$

Multiplication of the individual sums in the expression above by $(s_iT_\mathrm{s})^2$ and adding $1 + s_iT_\mathrm{s}$ yields

$$1 + (s_i(x_{1,k})T_\mathrm{s}) + \frac{(s_i(x_{1,k})T_\mathrm{s})^2}{2!} + \frac{(s_i(x_{1,k})T_\mathrm{s})^3}{3!} + \dots = \sum_{\nu=0}^{\infty}\frac{(s_i(x_{1,k})T_\mathrm{s})^\nu}{\nu!} = e^{s_i(x_{1,k})T_\mathrm{s}}.$$

Hence the expressions simplifiers to

$$\begin{aligned}
&-\frac{1}{2}k_1\left(\psi_1(x_{1,k},T_\mathrm{s}) - |x_{1,k}|^{\frac{1}{2}}\mathrm{sign}\,(x_{1,k})\right) = \\
&= \frac{p_1^2T_\mathrm{s}}{2}\frac{e^{s_1T_\mathrm{s}} - 1 - s_1T_\mathrm{s}}{s_1^2T_\mathrm{s}^2}\mathrm{sign}\,(x_1) + \frac{p_2^2T_\mathrm{s}}{2}\frac{e^{s_2T_\mathrm{s}} - 1 - s_2T_\mathrm{s}}{s_2^2T_\mathrm{s}^2}\mathrm{sign}\,(x_1)
\end{aligned}$$

It can be verified that the remainders satisfy

$$\frac{e^{-|\tau|} - 1 + |\tau|}{|\tau|^2} \le \frac{1}{2}, \quad \forall\tau.$$

Consequently,

$$|\boldsymbol{e}_1^{\mathrm{T}}\tilde{\boldsymbol{\psi}}(x_1)| \le \frac{T_\mathrm{s}}{4}\left(p_1^2 + p_2^2 + 2L\right)$$

holds, By the same argumentations one obtains

$$|\boldsymbol{e}_2^{\mathrm{T}}\tilde{\boldsymbol{\psi}}(x_1)| \leq \frac{T_\mathrm{s}}{2}(p_1+p_2)$$

and consequently, there exists $\delta \in \mathbb{R}$ such that

$$\|\tilde{\boldsymbol{\psi}}(x_1)\|_2 \leq \delta \tag{3.87}$$

holds. The stability of the origin $\boldsymbol{\omega} = \mathbf{0}$ is investigated by means of Lyapunov's direct method. As Lyapunov function candidate, the quadratic form

$$V = \boldsymbol{\omega}^{\mathrm{T}}\boldsymbol{P}\boldsymbol{\omega}$$

is chosen. Its derivative along the trajectories of system (3.86) yields

$$\dot{V} = \boldsymbol{\omega}^{\mathrm{T}}(\boldsymbol{A}^{\mathrm{T}}\boldsymbol{P}+\boldsymbol{P}\boldsymbol{A})\boldsymbol{\omega} + 2\tilde{\Delta}\boldsymbol{e}_2^{\mathrm{T}}\boldsymbol{P}\boldsymbol{\omega} + 2\tilde{\boldsymbol{\psi}}^{\mathrm{T}}\boldsymbol{P}\boldsymbol{\omega},$$

or in matrix representation

$$\dot{V} = \begin{bmatrix}\boldsymbol{\omega}^{\mathrm{T}} & \tilde{\Delta}\end{bmatrix}\begin{bmatrix}\boldsymbol{A}^{\mathrm{T}}\boldsymbol{P}+\boldsymbol{P}\boldsymbol{A} & \boldsymbol{P}\boldsymbol{e}_2 \\ \boldsymbol{e}_2^{\mathrm{T}}\boldsymbol{P} & 0\end{bmatrix}\begin{bmatrix}\boldsymbol{\omega} \\ \tilde{\Delta}\end{bmatrix} + 2\tilde{\boldsymbol{\psi}}^{\mathrm{T}}\boldsymbol{P}\boldsymbol{\omega}. \tag{3.88}$$

The upper bound of the external perturbation$|\Delta(t)| \leq L$ implies $L\omega_1^2 - \Delta^2 \geq 0$ which is written as

$$\begin{bmatrix}\boldsymbol{\omega}^{\mathrm{T}} & \tilde{\Delta}\end{bmatrix}\begin{bmatrix}L^2\boldsymbol{e}_1\boldsymbol{e}_1^{\mathrm{T}} & \mathbf{0}_{2\times 1} \\ 0 & -1\end{bmatrix}\begin{bmatrix}\boldsymbol{\omega} \\ \tilde{\Delta}\end{bmatrix} \geq 0.$$

Combining the above given inequality with (3.88) and furthermore taking into account (3.87) and the inequality

$$\tilde{\boldsymbol{\psi}}^{\mathrm{T}}\boldsymbol{P}\boldsymbol{\omega} \leq \delta\lambda_{\max}(\boldsymbol{P})\|\boldsymbol{\omega}\|_2,$$

eventually gives

$$\begin{aligned}
\dot{V} &\leq \begin{bmatrix}\boldsymbol{\omega}^{\mathrm{T}} & \tilde{\Delta}\end{bmatrix}\begin{bmatrix}\boldsymbol{A}^{\mathrm{T}}\boldsymbol{P}+\boldsymbol{P}\boldsymbol{A}+\frac{L^2}{4}\boldsymbol{e}_1\boldsymbol{e}_1^{\mathrm{T}} & \boldsymbol{P}\boldsymbol{e}_2 \\ \boldsymbol{e}_2^{\mathrm{T}}\boldsymbol{P} & -1\end{bmatrix}\begin{bmatrix}\boldsymbol{\omega} \\ \tilde{\Delta}\end{bmatrix} + \delta\lambda_{\max}(\boldsymbol{P})\|\boldsymbol{\omega}\|_2 \\
&\leq \tilde{\boldsymbol{\omega}}^{\mathrm{T}}\tilde{\boldsymbol{Q}}\tilde{\boldsymbol{\omega}} + \delta\lambda_{\max}(\boldsymbol{P})\|\tilde{\boldsymbol{\omega}}\|_2 \\
&\leq -\lambda_{\min}(\tilde{\boldsymbol{Q}})\|\tilde{\boldsymbol{\omega}}\|_2^2 + \delta\lambda_{\max}(\boldsymbol{P})\|\tilde{\boldsymbol{\omega}}\|_2 \\
&\leq -(1-\theta)\lambda_{\min}(\tilde{\boldsymbol{Q}})\|\tilde{\boldsymbol{\omega}}\|_2^2, \quad \forall\|\tilde{\boldsymbol{\omega}}\|_2 \geq \frac{\delta\lambda_{\max}(\boldsymbol{P})}{\theta\lambda_{\min}(\tilde{\boldsymbol{Q}})}, \quad 0<\theta<1
\end{aligned}$$

which allows to conclude that solutions of the artificial perturbed continuous-time system are uniformly bounded. The artificial continuous-time system (3.84) satisfies a Lipschitz condition, i.e., writing (3.84) as

$$\dot{\boldsymbol{x}} = \boldsymbol{f}(\boldsymbol{x}) + \boldsymbol{\Delta},$$

where $\boldsymbol{\Delta}$ summarizes the external and internal perturbations, one has

$$\|\boldsymbol{f}(\boldsymbol{x}) - \boldsymbol{f}(\boldsymbol{y})\| \leq D\|\boldsymbol{x} - \boldsymbol{y}\|, \quad \forall \boldsymbol{x}, \boldsymbol{y} \in \mathbb{R}^2$$

where $D > 0$ denotes the Lipschitz constant. The second derivative of (3.84) w.r.t. time yields

$$\begin{aligned}
\ddot{x}_1 &= -k_1 \frac{\partial}{\partial x_1} \psi_1(x_{1,k}, T_\mathrm{s}) \dot{x}_1 + \dot{x_2} + \frac{1}{2} T_\mathrm{s} \dot{\Delta}(\xi_1), \\
\ddot{x}_2 &= -k_2 \frac{\partial}{\partial x_1} \psi_2(x_{1,k}, T_\mathrm{s}) \dot{x}_1 + \dot{\Delta}(\xi_2),
\end{aligned}$$

i.e., with $|\dot{\Delta}(t)| < \tilde{L}$ the solution $\boldsymbol{x}(t)$ has a bounded second derivative. Hence, the application of the forward Euler scheme to the artificial continuous-time system, which produces the original discrete-time system (3.83), provides for a local error which is proportional to T_s^2 a global error proportional to T_s, (see e.g. [96]). The asymptotic accuracies follow from the invariance w.r.t. the scaling (3.39). □

A different discrete-time approximation of the STA is obtained by approximating the mapping (3.62). This approach will be called *Bilinear Transformation*.

3.3.3 Bilinear Transformation

An approximation of the mapping (3.62) by a rational function is obtained by the Padé approximation

$$e^{sT_\mathrm{s}} \approx \frac{1 + s\frac{T_\mathrm{s}}{2}}{1 - s\frac{T_\mathrm{s}}{2}}.$$

In a more general sense, the bilinear transformation

$$q_i(T_\mathrm{s}, x_{1,k}) = \begin{cases} \frac{A + s_i(x_{1,k})}{A - s_i(x_{1,k})} & x_{1,k} \neq 0 \\ 0 & x_{1,k} = 0 \end{cases}, \quad i = 1, 2 \tag{3.90}$$

may also be used to transform the STA to the discrete-time domain. In particular when $A = 2/T_\mathrm{s}$, *Tustin's* method is obtained, see [31]. This discrete-time STA obviously satisfies criterion C1. Furthermore it can be verified that criterion C2 holds. Also the invariance property C4 is retained when using this approximation. However, in the limit $x_{1,k} \to 0$ the eigenvalues of the evolution operator are located at $\lambda(\boldsymbol{M}_\mathrm{d}(0)) = \{-1, -1\}$. In the limit $x_{1,k} \to 0$ this discrete-time approximation of the STA does not yield a dead beat controller. Therefore, it is also not possible to apply Lyapunov's indirect method to investigate the stability character of the origin $\boldsymbol{x}_k = \boldsymbol{0}$. A detailed stability analysis of the closed-loop system is omitted in this work.

3.3.4 Implicit Discretization

An implicit[1] discretization of the the closed-loop STA dynamics is obtained by solving

$$\boldsymbol{x}_{k+1} - \boldsymbol{x}_k = T_\mathrm{s}\boldsymbol{M}(x_{1,k})\boldsymbol{x}_{k+1}. \tag{3.91}$$

The recursion yields the explicit solution

$$\boldsymbol{x}_{k+1} = \left[\boldsymbol{I} - T_\mathrm{s}\boldsymbol{M}(x_{1,k})\right]^{-1}\boldsymbol{x_k}.$$

The eigenvalues $z_i(T_\mathrm{s}, x_{1,k})$ of the matrix $\left[\boldsymbol{I} - T_\mathrm{s}\boldsymbol{M}(x_{1,k})\right]^{-1}$ are located at

$$z_i(T_\mathrm{s}, x_{1,k}) = \frac{1}{1 - T_\mathrm{s}s_i(x_{1,k})} \quad \text{for} \quad x_{1,k} \neq 0. \tag{3.92}$$

The corresponding eigenvectors are the same as of the continuous-time system given in (3.44).

Note that a closed-loop system of the form (3.91) is not feasible as it requires information of the state variable $x_{2,k}$ and thus, also of the unknown disturbance. In order to overcome this obstacle, the control law is designed such that the structure of the closed-loop system coincides with $\boldsymbol{\Sigma}_\mathrm{d}$, see Definition 3.1, and the dynamic matrix $\boldsymbol{M}_\mathrm{d}(x_{1,k})$ has eigenvalues located at (3.92). This is achieved by control law (3.49) with q_1, q_2 selected as

$$q_i(T_\mathrm{s}, x_{1,k}) = \begin{cases} \frac{1}{1-T_\mathrm{s}s_i(x_{1,k})} & \text{for} \quad x_{1,k} \neq 0, \\ 0 & \text{for} \quad x_{1,k} = 0. \end{cases} \tag{3.93}$$

With this eigenvalue choice, the eigenvectors of $\boldsymbol{M}_\mathrm{d}(x_{1,k})$ are

$$\boldsymbol{u}_1(x_{1,k})^\mathrm{T} = \begin{bmatrix} T_\mathrm{s} - \sqrt{|x_{1,k}|}\frac{1}{p_2} & 1 \end{bmatrix}, \quad \boldsymbol{u}_2(x_{1,k})^\mathrm{T} = \begin{bmatrix} T_\mathrm{s} - \sqrt{|x_{1,k}|}\frac{1}{p_1} & 1 \end{bmatrix}.$$

The mapping (3.92) turns out to be in particular suitable as not only criterion C1 is satisfied but also C2-C5 as is demonstrated in the following. The injection terms are given by

$$\begin{aligned} \psi_1 &= \frac{x_{1,k}}{(p_1+p_2)T_\mathrm{s}}\left(-2 + \frac{1}{1 - \frac{p_1 T_\mathrm{s}}{\sqrt{|x_{1,k}|}}} + \frac{1}{1 - \frac{p_2 T_\mathrm{s}}{\sqrt{|x_{1,k}|}}}\right), \\ \psi_2 &= \frac{x_{1,k}}{p_1 p_2 T_\mathrm{s}^2 - (p_1+p_2)T_\mathrm{s}\sqrt{|x_{1,k}|} + |x_{1,k}|}. \end{aligned}$$

Computing the limit

$$\lim_{T_\mathrm{s}\to 0}\frac{1}{T_\mathrm{s}}\left(\boldsymbol{x}_{k+1} - \boldsymbol{x}_k\right) = \lim_{T_\mathrm{s}\to 0}\frac{1}{T_\mathrm{s}}\left(\boldsymbol{M}_\mathrm{d}(x_{1,k})\boldsymbol{x}_k + T_\mathrm{s}\boldsymbol{h}_k - \boldsymbol{x}_k\right)$$

[1] Note that (3.91) is *not* an backward Euler discretization of the STA, as the r.h.s. also depends on the current state $\boldsymbol{x}_k$. However the fact, that a recursion of the from

$$\boldsymbol{x}_{k+1} = \boldsymbol{x}_k + T_\mathrm{s}\boldsymbol{\Psi}(\boldsymbol{x}_k, \boldsymbol{x}_{k+1}, T_\mathrm{s}).$$

is solved in each step justifies the term implicit discretization.

with (3.55), (3.93) and for any $x_{1,k} \neq 0$ yields

$$\lim_{T_\mathrm{s}\to 0} \frac{1}{T_\mathrm{s}} \left(\boldsymbol{x}_{k+1} - \boldsymbol{x}_k\right) = \begin{bmatrix} -\lambda_1 |x_{1,k}|^{\frac{1}{2}} \mathrm{sign}\left(x_{1,k}\right) + x_{2,k} \\ -\lambda_2 \mathrm{sign}\left(x_{1,k}\right) + \Delta(t) \end{bmatrix},$$

hence criterion C2 holds. The implicit discretization possesses an interesting behavior, regarding local stability properties when compared to the continuous-time STA. The stability characteristics of the origin $\boldsymbol{x}_k = \boldsymbol{0}$ are stated in the following

Theorem 3.5

Suppose that $L = 0$, T_s is a positive constant and let $k_1 \neq 0$, $k_2 \neq 0$. Then the origin of the discrete-time system $\boldsymbol{\Sigma}_\mathrm{d}$ with (3.93) is asymptotically stable, i.e., every trajectory starting in some ball around the origin with radius $r > 0$ sufficiently small converges to the origin.

Proof. The proof is basically the same as the proof of Theorem (3.1). The r.h.s. of the closed-loop system satisfies

$$\boldsymbol{x}_{k+1} = \boldsymbol{M}_\mathrm{d}(x_{1,k})\boldsymbol{x}_k = \boldsymbol{M}_\mathrm{d}(0)\boldsymbol{x}_k + \boldsymbol{n}(x_{1,k})$$

where in this case

$$\boldsymbol{n}(x_{1,k}) = \begin{bmatrix} \frac{1}{1-\frac{p_1 T_\mathrm{s}}{\sqrt{|x_{1,k}|}}} + \frac{1}{1-\frac{p_2 T_\mathrm{s}}{\sqrt{|x_{1,k}|}}} \\ \frac{-(p_2+p_2)T_\mathrm{s}\sqrt{|x_{1,k}|}+|x_{1,k}|}{T_\mathrm{s}\left(p_1 p_2 T_\mathrm{s}^2 - (p_1+p_2)T_\mathrm{s}\sqrt{|x_{1,k}|}+|x_{1,k}|\right)} \end{bmatrix} x_{1,k}.$$

The mapping $\boldsymbol{n}(x_{1,k}) : \mathbb{R}^2 \to \mathbb{R}^2$ is continuous on a connected set $\Omega \subset \mathbb{R}^2$ containing the origin $\boldsymbol{x} = \boldsymbol{0}$ and

$$\lim_{\|\boldsymbol{x}\|\to 0} = \frac{\|\boldsymbol{n}(\boldsymbol{x})\|}{\|\boldsymbol{x}\|} = 0.$$

If the gains satisfy k_1, $k_2 > 0$ then $\Omega = \mathbb{R}^2$. The evolution operator $\boldsymbol{M}_\mathrm{d}(0)$ is exponential stable, i.e., $\boldsymbol{M}_\mathrm{d}(0)$ is a Schur Matrix. From Lyapunov's indirect method for discrete-time systems, see e.g. [88, 94], it is concluded that the origin of the nonlinear system is exponentially stable. □

The result is in particular interesting because the unperturbed continuous-time closed-loop system is finite time stable if and only if k_1, $k_2 > 0$. Hence, the proposed implicit discretization scheme has a stabilizing effect on the system as the origin is locally asymptotically stable for all possible choices of k_1, $k_2 \neq 0$. The stabilizing property of the implicit scheme is well-known for linear systems. From the mapping (3.92) it is clear that not only eigenvalues lying in the open left half plane are mapped inside the unit circle in the complex plane but also eigenvalues lying in a certain region in the right half plane, see Figure (3.9). Note that contrary to a homogeneous continuous-time system, the local asymptotic stability does not necessarily imply global asymptotic stability.

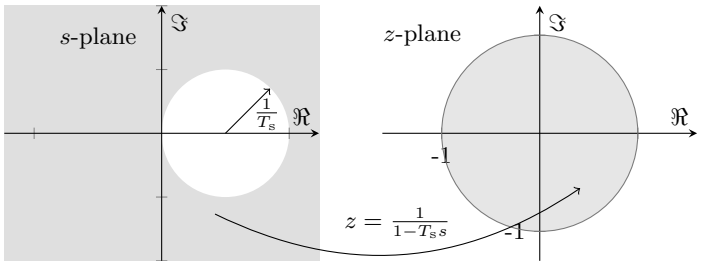

Figure 3.9: Eigenvalue mapping by the implicit scheme.

For the proposed discretization scheme the invariance $\kappa T_\mathrm{s} s(\kappa^2 x_{1,k}) = T_\mathrm{s} s(x_{1,k})$ implies (3.58) and thus confirms criterion C4. Furthermore, as $x_{1,k} \to 0$, the dynamics of the system are governed by the recursion

$$\boldsymbol{x}_{k+1} = \boldsymbol{M}_\mathrm{d}(0)\boldsymbol{x}_k,$$

where

$$\boldsymbol{M}_\mathrm{d}(0) = \begin{bmatrix} -1 & T_\mathrm{s} \\ -1/T_\mathrm{s} & 1 \end{bmatrix}.$$

The spectrum of the evolution operator $\boldsymbol{M}_\mathrm{d}(0)$ satisfies $\sigma(\boldsymbol{M}_\mathrm{d}(0)) = \{0,\, 0\}$. Also here, the fact, that in the limit the closed-loop system exhibits a dead beat response imposes a stronger convergence. Hence, criterion C5 is satisfied.

Theorem 3.6

In the unperturbed case $\boldsymbol{\Sigma}_\mathrm{d}$ with (3.92) converges with hyper-exponential speed to the origin.

Proof. The proof is the same as the proof of Theorem 3.2. □ □

Depending on the chosen discretization scheme the eigenvalues of the discrete-time closed-loop system change by variation of $x_{1,k}$ along a specific locus. The form of the locus will not only depend on the selected discretization scheme but also on the chosen control parameters k_1, k_2. An example of the eigenvalue locus for the classical parameter setting $k_1 = 1.5$, $k_2 = 1.1$ is provided in Figure 3.10. Independent of the chosen discretization scheme and control parameters the eigenvalues originate from $z_1 = z_2 = 1$. When applying the implicit discretization scheme the eigenvalues of $\boldsymbol{M}_\mathrm{d}(x_{1,k})$ are transferred to the origin as $x_{1,k} \to 0$ for all k_1, k_2. When using the matching approach, the eigenvalues are transferred to the origin iff k_1, $k_2 > 0$. As already mentioned above, the eigenvalues are transferred to $z_1 = z_2 = -1$, in case of Tustin's approximation as indicated in (3.90). This holds independent on the choice of k_1, k_2. In the case of the explicit Euler discretization the absolute values of the eigenvalues move towards infinity.

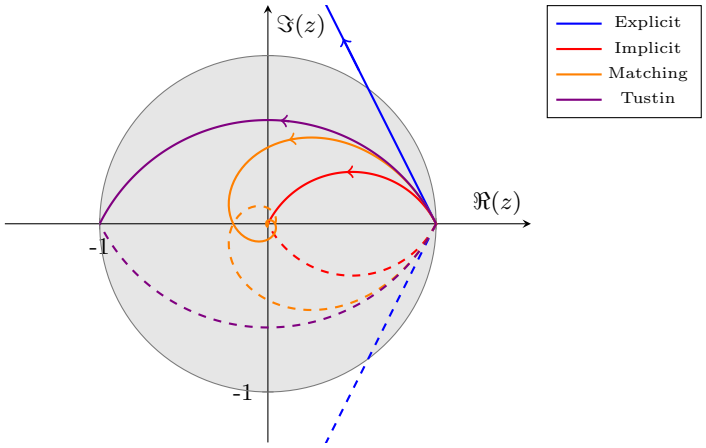

Figure 3.10: Eigenvalue locus for $x_1 \to \infty$. The parameters are $k_1 = 1.5$, $k_2 = 1.1$ and $T_s = 0.05$ s.

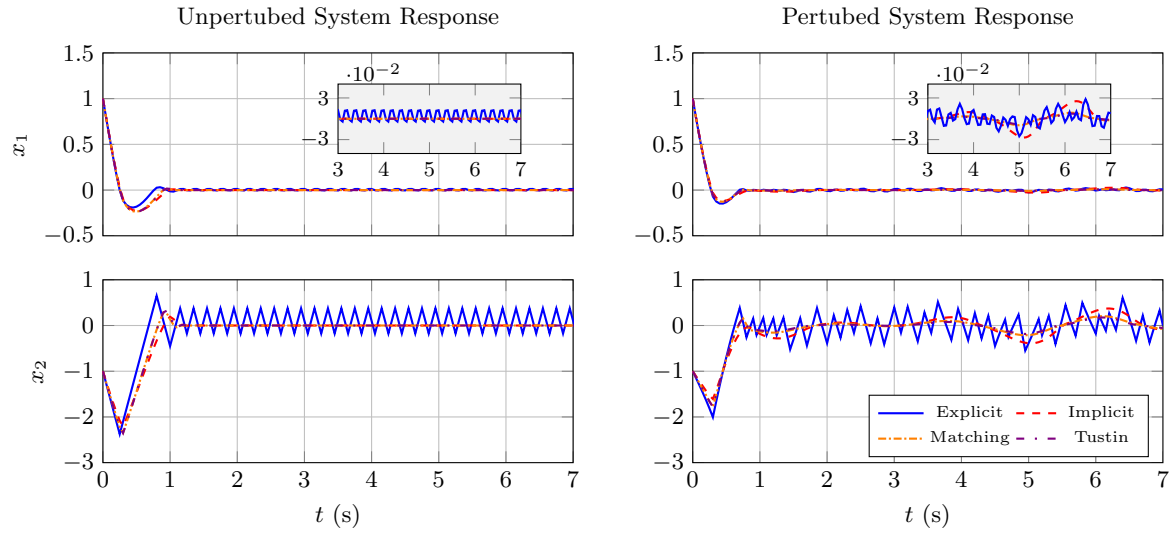

Figure 3.11: Unperturbed and perturbed system responses with the parameters $k_1 = 1.5\sqrt{\Lambda}$, $k_2 = 1.1\Lambda$, $\Lambda = 5$ and $T_s = 0.05$ s.

3.3.5 Simulation Study

In this Section, the performance of the proposed discretization schemes is compared by numerical simulations. The two plots on the left hand side in Figure 3.11 show the unperturbed system response obtained with the classical forward Euler discretized control law and the proposed schemes. In case of the implicit and Matching STA the system state variables x_1 and x_2 are steered to zero exactly, whilst the forward Euler discretized STA evokes the discretization chattering effects. This is also true for the discrete-time STA obtained by using Tustin's approximation, but with much smaller chattering amplitude compared to the forward

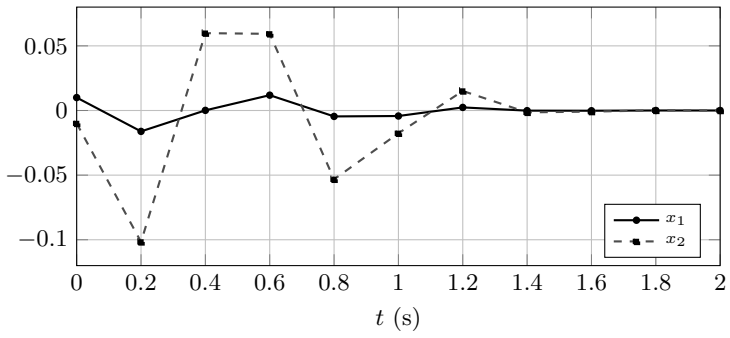

Figure 3.12: Implicit discretization of the STA with the parameter choice $k_1 = -1.5$, $k_2 = 1.1$. The sampling time is $T_\mathrm{s} = 0.2$ s and $L = 0$. With this parameter setting the origin of the continuous-time STA is due to the negative choice of k_1 an unstable equilibrium. The implicit discretization renders the origin exponentially stable.

Euler discretized STA. A simulation of the perturbed system is provided in Figure 3.11 on the right hand side. The perturbation is $\Delta(t) = 1.2\cos(2t) + 0.4\sqrt{10}\cos(\sqrt{10}t)$. All four controllers provide for similar precision. The precision is evaluated using $\limsup_k |x_{1,k}| < \mu_1 T_\mathrm{s}^2$. The value of μ_1 is approximately the same for all four approaches. However, the high frequency switching, present in the forward Euler discretized controller, is eliminated when applying the proposed discretization schemes.

The stabilizing effect of the implicit scheme is demonstrated in Figure 3.12. The control parameters are selected as $k_1 = -1.5$, $k_2 = 1.1$. In the continuous-time configuration the choice $k_1 < 0$ will result in an unstable system response. In contrast, even in this case the implicit discretized STA ensures local asymptotic stability of the origin as stated in Theorem 3.5.

The precision test provided in Figure 3.13 confirms, that all proposed discrete-time versions of the STA provide for the same asymptotic accuracy of the variable to be controlled w.r.t. the sampling time, i.e., $\limsup_k(|x_{1,k}|) \propto T_\mathrm{s}^2$. Results have been obtained by simulating the same perturbed closed-loop system as in the previous simulation. Although the parameter setting is the same for all four controllers, the proportionality constants μ_1, μ_2 are different as can be seen in the plot. In case of the forward Euler scheme the precision is diminished when overestimating the control gains, see Figure 3.14. The gains are selected as $k_1 = 1.5\sqrt{\Lambda}$, $k_2 = 1.1\Lambda$. In the experiment the scaling variable Λ is increased whilst the perturbation as well as the sampling time T_s remain unchanged. When increasing Λ, the precision decreases in the case of the forward Euler scheme as soon as $\Lambda/1.1 > L = 1.2 + 0.4\sqrt{10}$ is satisfied. The asymptotic accuracies with respect to Λ are $\mathcal{O}(\Lambda)$. Contrary, with the proposed schemes the precision is not deteriorated when increasing Λ and the asymptotic accuracy is $\mathcal{O}(1)$. Furthermore the numerical example reveals, that the proposed discretization schemes require larger control gains in order to outperform the forward Euler discretized controller in terms of the achieved precision. For this particular problem setting, the approximation based on Tustin's method provides for the best precision. Note that, near the origin the system dynamics are dominated by the linear part. With very large values $\Lambda \gg L$ this approximation also is valid in the presence of perturbations. This enables to estimate the proportionality constants μ_1 and μ_2. Consider the approximated

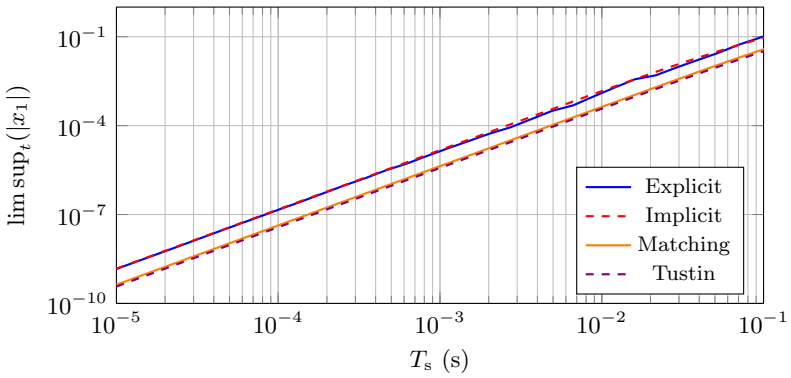

Figure 3.13: Precision test with parameters $k_1 = 1.5\sqrt{\Lambda}$, $k_2 = 1.1\Lambda$, $\Lambda = 5$ showing that all controllers provide for the asymptotic accuracies $\mathcal{O}(T_s^2)$.

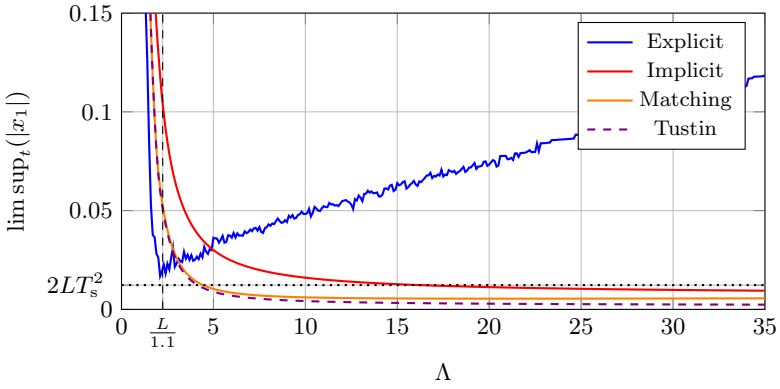

Figure 3.14: Precision w.r.t. an increase of the controllers gains. The parameters are $k_1 = 1.5\sqrt{\Lambda}$, $k_2 = 1.1\Lambda$, $T_s = 0.05$ s.

dynamics with the output $y_k = x_{1,k}$ given by

$$\begin{aligned} \boldsymbol{x}_{k+1} &= \boldsymbol{M}_d(0)\boldsymbol{x}_k + T_s\boldsymbol{h}_k = \begin{bmatrix} -1 & T_s \\ -\frac{1}{T_s} & 1 \end{bmatrix} \boldsymbol{x}_k + \begin{bmatrix} \frac{T_s^2}{2} \\ 0 \end{bmatrix} \Delta(\xi_{1,k}) + \begin{bmatrix} 0 \\ T_s \end{bmatrix} \Delta(\xi_{2,k}) \qquad (3.95) \\ y_k &= \boldsymbol{e}_1^{\mathrm{T}} \boldsymbol{x}_k. \end{aligned}$$

Note that this is a multi-input single-output LTI system and the output y_k is bounded whenever the input is bounded. The peak-gain of the system is given by the 1-norm of the impulse response, see [97], i.e.,

$$\begin{aligned} \|y_k\|_\infty \Big|_{\Delta(\xi_{2,k})\equiv 0} &\leq \sum_{k=0}^{\infty} |\boldsymbol{e}_1^{\mathrm{T}} \boldsymbol{M}_d^k(0)\bar{\boldsymbol{h}}_1| \|\Delta(\xi_{1,k})\|_\infty, \quad \bar{\boldsymbol{h}}_1 = \begin{bmatrix} \frac{T_s^2}{2} & 0 \end{bmatrix}^{\mathrm{T}} \\ \|y_k\|_\infty \Big|_{\Delta(\xi_{1,k})\equiv 0} &\leq \sum_{k=0}^{\infty} |\boldsymbol{e}_1^{\mathrm{T}} \boldsymbol{M}_d^k(0)\bar{\boldsymbol{h}}_2| \|\Delta(\xi_{2,k})\|_\infty, \quad \bar{\boldsymbol{h}}_2 = \begin{bmatrix} 0 & T_s \end{bmatrix}^{\mathrm{T}}. \end{aligned}$$

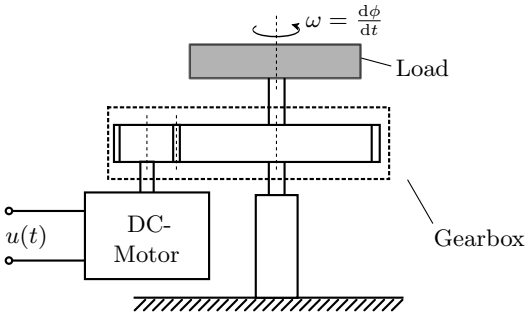

Figure 3.15: Schematic drawing of the revolving platform

Due to linearity, the peak gain for system (3.95) computes as

$$\|x_{1,k}\|_\infty = \|y_k\|_\infty = \|y_k\|_\infty\Big|_{\Delta(\xi_{2,k})\equiv 0} + \|y_k\|_\infty\Big|_{\Delta(\xi_{1,k})\equiv 0}.$$

Taking into account the Lipschitz constant of the perturbation and considering that matrix $\boldsymbol{M}_\mathrm{d}(0)$ is nilpotent, i.e., $\boldsymbol{M}_\mathrm{d}(0)^2 = \boldsymbol{0}$ one obtains for the peak gain

$$\|x_{1,k}\|_\infty \leq 2LT_\mathrm{s}^2. \tag{3.96}$$

Note that this bound does not hold for the original system and (3.96) only is an estimate of the proportionality constant μ_1, i.e., $\mu_1 \approx 2L$. Applying the same approach for the second variable, one obtains

$$\|x_{2,k}\|_\infty \leq \frac{5}{2}LT_\mathrm{s}.$$

i.e., $\mu_2 \approx \frac{5}{2}L$. For the considered example, the estimates yield $\limsup_t(|x_1|) \approx 0.012$ and $\limsup_t(|x_2|) \approx 0.308$. The estimate for the precision of the variable x_1 is depicted as dotted black line in Figure 3.14. In the limit $\Lambda \to \infty$ the proposed algorithms provide for better precision than estimated by this approach. This, however, seems to be due to the fact that the perturbation is a smooth signal. In case of a discontinuous perturbation this might not be true anymore.

3.3.6 Experimental Verification and Comparison

In this section the performance of the implicit and matching discretized control laws are compared to the classical explicit Euler discretized STA in a real world experiment. The schematic drawing of the considered laboratory setup is shown in Figure 3.15. The setup consists of a rotating mass which is connected to a dc-motor via a gear box. The control goal is to make the rotational speed of the load track a given reference profile. A simplified mathematical model describing the plant dynamics is given by

$$T_\mathrm{p}\frac{\mathrm{d}\omega}{\mathrm{d}t} = -\omega + K_\mathrm{p}u,$$

where $\omega \in \mathbb{R}$ is the angular velocity of the rotating mass and $u \in \mathbb{R}$ is the voltage supplied to the dc-motor. The system is operated in a digital control loop with a zero-order-hold reconstruction element. The sequence (ω_k) is obtained by sampling the continuous-time signal $\omega(t)$ with constant sampling time T_s. In this regard the dynamics of the plant are captured by the recursion

$$\omega_{k+1} = a_\mathrm{d}\omega_k + b_\mathrm{d}u_k \tag{3.97}$$

with $a_\mathrm{d} = e^{-T_\mathrm{s}/T_\mathrm{p}}$ and $b_\mathrm{d} = (1-a_\mathrm{d})K_\mathrm{p}$. The control goal is to make (ω_k) track a given reference sequence $(\zeta_{1,k})$. The tracking error is defined as

$$x_{1,k} := \omega_k - \zeta_{1,k}.$$

The reference sequence is generated by the exogenous system

$$\boldsymbol{\zeta}_{k+1} = \begin{bmatrix} 1 & T_\mathrm{s} \\ 0 & 1 \end{bmatrix} \boldsymbol{\zeta}_k + \begin{bmatrix} \frac{T_\mathrm{s}^2}{2} \\ T_\mathrm{s} \end{bmatrix} \ddot{\omega}_{\mathrm{ref},k}$$

with the state vector $\boldsymbol{\zeta}_k^\mathrm{T} = \begin{bmatrix} \zeta_{1,k} & \zeta_{2,k} \end{bmatrix}$. The input sequence to the exosystem is obtained by sampling the continuous-time signal $\ddot{\omega}_{ref}(t)$ which is assumed to be an unknown but bounded signal, i.e., $|\ddot{\omega}_{ref}(t)| < L$. The dynamics of the tracking error are given by

$$x_{1,k+1} = a_\mathrm{d}\omega_k + b_\mathrm{d}u_k - \zeta_{1,k} - T_\mathrm{s}\zeta_{2,k} - \frac{T_\mathrm{s}^2}{2}\ddot{\omega}_{\mathrm{ref},k}.$$

The control signal is designed as

$$\begin{aligned} u_k &= \tfrac{1}{b_\mathrm{d}}\left[(1-a_\mathrm{d})\omega_k - x_{1,k} + \tilde{u}_{1,k} + T_\mathrm{s}\nu_k\right], \\ \nu_{k+1} &= \nu_k + \tilde{u}_{2,k}. \end{aligned} \tag{3.98}$$

Applying control law (3.98) to the plant (3.97), and defining $x_{2,k} := \nu_k - \zeta_{2,k}$ yields

$$\begin{aligned} x_{1,k+1} &= \tilde{u}_{1,k} + T_\mathrm{s}x_{2,k} - \frac{T_\mathrm{s}^2}{2}\ddot{\omega}_{\mathrm{ref},k}, \\ x_{2,k+1} &= \tilde{u}_{2,k} + x_{2,k} - T_\mathrm{s}\ddot{\omega}_{\mathrm{ref},k}, \end{aligned}$$

which coincides with the structure of the closed-loop system (3.50). The plant parameters are $T_\mathrm{p} = 1/27$ and $K_\mathrm{p} = 100$. The experiment is repeated with three different sampling times for each discretization scheme where $T_\mathrm{s} = 10$, 100, 200 ms. For the control parameters the classical setting $k_1 = 1.5\sqrt{\Lambda}$ and $k_2 = 1.1\Lambda$ is used, where Λ is a positive constant gain chosen s.t. $\Lambda > L$. The disturbances are mainly introduced by unknown friction forces and the reference signal. Due to the unknown friction forces the constant L is a priori unknown. Therefore, the controller gain Λ was tuned heuristically. In order to determine a suitable value, the experiment was carried out with the forward Euler discretized STA using the sampling time $T_\mathrm{s} = 1$ ms. Stable tracking error dynamics were obtained for values $\Lambda > 3000$. The parameter was set to $\Lambda = 3500$ for the experimental series.

The obtained results are shown in Figure 3.16. The red dashed line represents the reference

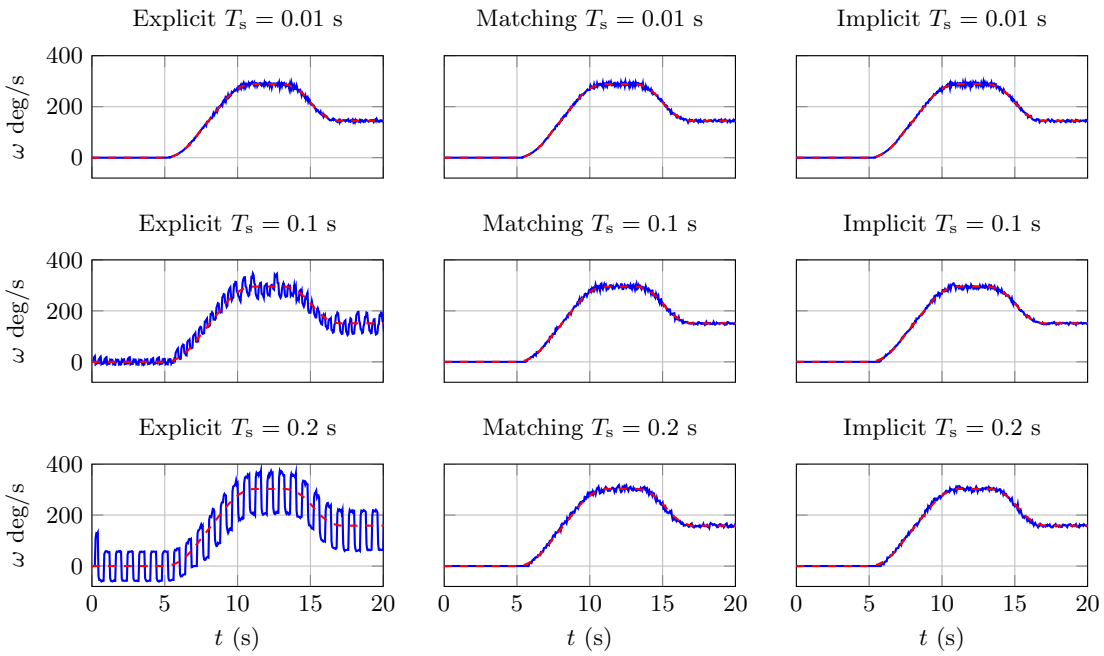

Figure 3.16: Comparison of the tracking performance obtained with the explicit Euler, implicit and matching discretized STA for various sampling times T_s.

trajectory, the blue solid line is the measured rotational speed which was acquired from a tachometer generator. During the first experimental series, with $T_s = 10$ ms, all three discretization schemes reveal almost identical results regarding the tracking performance. As soon as the sampling time is increased by one decade the discretization chattering effects become clearly visible when using the explicit Euler discretized STA. The control loops with the novel discretized STA's are barely affected by this increase of T_s. The advantage of the proposed discretization schemes becomes evident when further increasing the sampling step size to $T_s = 200$ ms. Even during the first 5 seconds, where $\omega_{\text{ref}} = 0$, and no perturbations are present in the control loop, as the friction forces vanish in the origin, the explicit Euler discretized STA causes significant discretization chattering whilst in the other two loops the system is stabilized in the origin. A deterioration of the tracking performance by an increase of the sampling time can hardly be recognized in the loops containing the STA obtained by the proposed discretization schemes.

3.3.7 Robust Exact Differentiator

Up to now the analysis was restricted to the control problem. In the particular case of the trajectory tracking problem, the application of the STA leads to the closed-loop system

$$\begin{aligned} \frac{\mathrm{d}x}{\mathrm{d}t} &= -k_1|x - f(t)|^{\frac{1}{2}}\operatorname{sign}(x - f(t)) + \nu, \\ \frac{\mathrm{d}\nu}{\mathrm{d}t} &= -k_2\operatorname{sign}(x - f(t)). \end{aligned} \tag{3.100}$$

Introducing the variables $x_1 := x - f(t)$, $x_2 := \nu - \dot{f}(t)$ gives

$$\begin{aligned} \frac{\mathrm{d}x_1}{\mathrm{d}t} &= -k_1|x_1|^{\frac{1}{2}}\mathrm{sign}\,(x_1) + x_2, \\ \frac{\mathrm{d}x_2}{\mathrm{d}t} &= -k_2\mathrm{sign}\,(x_1) - \ddot{f}(t). \end{aligned} \tag{3.101}$$

If $\dot{f}(t)$ has a known Lipschitz constant L, i.e., $\ddot{f}(t) \in [-L,\, L]$ then one can find parameters k_1, k_2 s.t.

$$x_1 \equiv 0 \implies x \equiv f(t), \quad x_2 \equiv 0 \implies \nu \equiv \dot{f}(t),$$

almost everywhere holds after finite time, i.e., the state variable x tracks the unknown reference signal and the controller variable ν tracks its first derivative theoretically exact in finite time. Even more, if the signal ν is taken as the output, the STA as given in (3.100) represents a real-time differentiator. Note that the differentiator may also be interpreted as a state estimator, i.e., the problem of designing a real-time differentiator is equivalent to designing a state estimator for the generating system of the signal to be differentiated, i.e.[2],

$$\begin{aligned} \frac{\mathrm{d}x_0}{\mathrm{d}t} &= x_1, \\ \frac{\mathrm{d}x_1}{\mathrm{d}t} &\in [-L,\, L], \\ f(t) &= x_0, \end{aligned} \tag{3.102}$$

Strong observability, see [98] for more details, of the integrating system (3.102) is obvious and the problem is solved by applying the STA

$$\begin{aligned} \frac{\mathrm{d}\hat{x}_0}{\mathrm{d}t} &= k_0|f(t) - \hat{x}_0|^{\frac{1}{2}}\mathrm{sign}\,(f(t) - \hat{x}_0) + \hat{x}_1, \\ \frac{\mathrm{d}\hat{x}_1}{\mathrm{d}t} &= k_1\mathrm{sign}\,(f(t) - \hat{x}_0) + \hat{x}_1. \end{aligned}$$

Defining $\sigma_0 := f(t) - \hat{x}_0$, $\sigma_1 := x_1 - \hat{x}_1$ provides for

$$\begin{aligned} \frac{\mathrm{d}\sigma_0}{\mathrm{d}t} &= -k_0|\sigma_0|^{\frac{1}{2}}\mathrm{sign}\,(\sigma_0) + x_1, \\ \frac{\mathrm{d}\sigma_1}{\mathrm{d}t} &\in -k_1\mathrm{sign}\,(\sigma_1) + [-L,\, L], \end{aligned}$$

which is the same closed-loop system (3.101) as obtained in the tracking problem, and

$$\sigma_0 \equiv 0 \implies \hat{x}_0 \equiv f(t), \quad \sigma_1 \equiv 0 \implies \hat{x}_1 \equiv \dot{f}(t).$$

Therefore, also the developed discrete-time versions of the STA can be utilized as real-time differentiators in almost the same manner. In case of the discrete-time realization of

[2] In case of the differentiator it is common to number the state variables starting with zero. The index i then corresponds to the i^{th} derivative.

the differentiator the signal $f(t)$ is measured at discrete-time steps. Applying Taylor series expansion with Lagrange remainders to $f(t)$ at $(k+1)T_\mathrm{s}$ yields

$$f((k+1)T_\mathrm{s}) = f(kT_\mathrm{s}) + T_\mathrm{s}\dot{f}(kT_\mathrm{s}) + \frac{T_\mathrm{s}^2}{2}\ddot{f}(\xi_k)$$

where $\xi_k \in (kT_\mathrm{s},\, (k+1)T_\mathrm{s})$. With $x_{0,k} := f(kT_\mathrm{s})$, $x_{1,k} := \dot{f}(kT_\mathrm{s})$ one gets

$$\begin{aligned} x_{0,k+1} &\in x_{0,k} + T_\mathrm{s}x_{1,k} + \frac{T_\mathrm{s}^2}{2}[-L,\, L], \\ x_{1,k+1} &\in x_{1,k} + T_\mathrm{s}[-L,\, L]. \end{aligned}$$

The discrete-time algorithm

$$\begin{aligned} \hat{x}_{0,k+1} &= \hat{x}_{0,k} + T_\mathrm{s}k_1\psi_0(x_k - \hat{x}_{0,k}) + T_\mathrm{s}\hat{x}_{1,k} \\ \hat{x}_{1,k+1} &= \hat{x}_{1,k} + T_\mathrm{s}k_2\psi_1(x_k - \hat{x}_{0,k}) \end{aligned}$$

and the definition of the error variables as $\sigma_{i,k} = x_{i,k} - \hat{x}_{i,k}$ leads to the discrete-time dynamical system

$$\begin{aligned} \sigma_{0,k+1} &\in \sigma_{0,k} - T_\mathrm{s}k_1\psi_0(\sigma_{0,k}) + T_\mathrm{s}\sigma_{1,k} + \frac{T_\mathrm{s}^2}{2}[-L,\, L], \\ \sigma_{1,k+1} &\in \sigma_{1,k} - T_\mathrm{s}k_2\psi_1(\sigma_{0,k}) + T_\mathrm{s}[-L,\, L]. \end{aligned}$$

The injection terms are chosen as

$$\begin{aligned} \psi_0(\sigma_{0,k}) &= -\frac{1}{k_1T_\mathrm{s}}\left[q_1(T_\mathrm{s},\sigma_{0,k}) + q_2(T_\mathrm{s},\sigma_{0,k}) - 2\right]\sigma_{0,k} \\ \psi_1(\sigma_{0,k}) &= \frac{1}{k_2T_\mathrm{s}^2}\left[(q_1(T_\mathrm{s},\sigma_{0,k}) - 1)(q_2(T_\mathrm{s},\sigma_{0,k}) - 1)\right]\sigma_{0,k}. \end{aligned}$$

In this regard, the the error dynamics are determined by the choice of $q_1(\sigma_{0,k})$, $q_2(\sigma_{0,k})$. The choice

$$q_i(T_\mathrm{s},\sigma_{0,k}) = 1 + T_\mathrm{s}s_i(\sigma_{0,k}), \quad s_i(\sigma_{0,k}) = \frac{p_i}{\sqrt{|\sigma_{0,k}|}}, \quad i = 1,2$$

gives an explicit Euler discretized version of the continuous-time robust exact differentiator written in (3.101). A specific discrete-time realization of the robust exact differentiator is now obtained by simply selecting one of the eigenvalue mappings introduced in the previous sections. As the discrete-time closed-loop system then is governed by the same dynamics as analyzed in the previous section, stability results are also valid for the differentiator.

In the next Section, the proposed discretization schemes are extended to the arbitrary-order RED. The arbitrary-order RED is a generalization of the first-order differentiator, which is based on the STA, to the arbitrary order. Its structure is very similar to the STA and it might be utilized as a differentiator or as a robust state estimator.

3.4 Arbitrary-Order Robust Exact Differentiator

In this section the differentiation problem is considered as a state estimation problem for the generating system of the signal $f(t)$ to be differentiated, i.e., a chain of integrators subject to an unknowing external input. The input corresponds to the $(n+1)$ th derivative of $f(t)$ and acts in the input channel of the integrator chain. The output is the signal itself, i.e., $y = f(t)$. In general, when facing the problem of reconstructing the state variables of an unperturbed LTI system, i.e.,

$$\begin{aligned} \frac{\mathrm{d}\boldsymbol{x}}{\mathrm{d}t} &= \boldsymbol{A}\boldsymbol{x} + \boldsymbol{b}u, \\ y &= \boldsymbol{c}^{\mathrm{T}}\boldsymbol{x}, \end{aligned}$$

where the pair $(\boldsymbol{A},\, \boldsymbol{c}^{\mathrm{T}})$ is observable, an asymptotic observer like the Luenberger observer, see [99, 100] usually is the first choice. The Luenberger observer

$$\frac{\mathrm{d}\hat{\boldsymbol{x}}}{\mathrm{d}t} = \left(\boldsymbol{A} + \boldsymbol{l}\boldsymbol{c}^{\mathrm{T}}\right)\hat{\boldsymbol{x}} + \boldsymbol{b}u + \boldsymbol{l}y$$

is capable of reconstructing the state variables $\boldsymbol{x}$ asymptotically. In the presence of an bounded unknown disturbance $\Delta(t)$, i.e.,

$$\begin{aligned} \frac{\mathrm{d}\boldsymbol{x}}{\mathrm{d}t} &= \boldsymbol{A}\boldsymbol{x} + \boldsymbol{b}u + \boldsymbol{d}\Delta(t), \\ y &= \boldsymbol{c}^{\mathrm{T}}\boldsymbol{x}, \end{aligned}$$

the Luenberger observer is capable of ensuring input to state stability of the estimation error dynamics, i.e., boundedness of the estimation errors $\boldsymbol{\sigma} = \boldsymbol{x} - \hat{\boldsymbol{x}}$. However, in general, it *cannot* ensure exact reconstruction of the state variables in the presence of the perturbation $\Delta(t)$ in general. On the other hand, as has been seen in the introductory part of this chapter, it is possible to improve the disturbance rejection by increasing the gains of the observer. This is the basic idea behind the high-gain observer. The high-gain observer aims to assign the observer eigenvalues, i.e., the eigenvalues of the matrix $\left(\boldsymbol{A} - \boldsymbol{l}\boldsymbol{c}^{\mathrm{T}}\right)$, to the roots of the characteristic polynomial

$$s^{n+1} + k_0 s^n + \ldots k_{n-1} s + k_n$$

scaled by $1/\varepsilon$, $\varepsilon > 0$. By decreasing the value of ε the dynamics of the observer are made faster and as a consequence the disturbance rejection properties are improved. Therefore, the high-gain observer may also be utilized as a real-time differentiator. In contrast to these asymptotic observers, observers based on sliding mode concepts are capable of ensuring finite-time convergence of the estimation error in the presence of bounded disturbances. When dealing with the problem of real-time differentiation, which is a key issue in control theory, the arbitrary-order robust exact differentiator (RED) proposed in [14] provides a simple and efficient solution. In the absence of noise and given that the n^{th} time-derivative of the signal to be differentiated is Lipschitz continuous with known Lipschitz constant, the RED provides the *exact* n^{th} time-derivative. Besides the RED and the HGO, linear differentiators, like

the Kalman filter, see [101, 102], or the algebraic differentiator, see, e.g., [103], as well as nonlinear continuous differentiators, see [104] might be used to estimate the derivatives of a signal in a real-time environment. Recently, a unified framework for the stability analysis of homogeneous continuous differentiators (linear and nonlinear), as well as the discontinuous RED was proposed by [105]. In the following, the approach proposed by [105], that allows generating families of homogeneous differentiators, is extended to the discrete-time case.

3.4.1 Notation and Preliminaries

Homogeneous continuous-time systems have a number of beneficial properties, e.g. local attractivity implies global stability, asymptotic stability with negative homogeneity implies convergence in finite time, see, e.g., [23, 106] for a more detailed discussion. A vector field $\boldsymbol{f} : \mathbb{R}^n \to \mathbb{R}^n$ with $\boldsymbol{x}^{\mathrm{T}} = \begin{bmatrix} x_1 & x_2 & \dots & x_n \end{bmatrix}$ is called $\boldsymbol{r}$ homogeneous of degree $d \in \mathbb{R}$ if the identity $\boldsymbol{f}(\Lambda_\kappa^r \boldsymbol{x}) = \kappa^d \Lambda_\kappa^r \boldsymbol{f}(\boldsymbol{x})$ holds for all $\kappa > 0$ where the dilation operator is defined as

$$\Lambda_\kappa^{\boldsymbol{r}} \boldsymbol{x} := \begin{bmatrix} \kappa^{r_1} x_1 & \kappa^{r_2} x_2 & \dots & \kappa^{r_n} x_n \end{bmatrix},$$

$\boldsymbol{r} = \begin{bmatrix} r_1 & r_2 & \dots & r_n \end{bmatrix}$ is the vector of weights with the positive weights r_i of the coordinates. Furthermore a system $\dot{\boldsymbol{x}} = \boldsymbol{f}(\boldsymbol{x})$ is called $\boldsymbol{r}$-homogeneous of degree d if the vector field $\boldsymbol{f}(\boldsymbol{x})$ is $\boldsymbol{r}$-homogeneous of degree d.

3.4.2 Continuous-Time Homogeneous Differentiators

Consider now the specific problem of constructing an arbitrary-order real-time differentiator by designing a state observer. The unknown signal $f(t)$ to be differentiated is assumed to be n-times differentiable with the n^{th} derivative having a known Lipschitz constant L. In this regard, $f^{(n)}$ is an absolutely continuous function. Hence, $f^{(n)}(t)$ has a derivative $g(t)$ almost everywhere, and there exists a Lebesgue integrable function $f^{(n+1)}(t) \in [-L,\, L]$ for all $t \geq 0$, such that $f^{(n)}(t) = \int_0^t f^{(n+1)}(\tau)\,\mathrm{d}\tau + f^{(n)}(0)$ for all $t \geq 0$ and $f^{(n+1)} = g(t)$ almost everywhere. Thus, the generator of the signal $f(t)$ is written as

$$\begin{aligned} \frac{\mathrm{d}\boldsymbol{x}}{\mathrm{d}t} &= \boldsymbol{A}\boldsymbol{x} + \boldsymbol{e}_{n+1} f^{(n+1)}, \quad f^{(n+1)} \in [-L,\, L], \\ y &= f = \boldsymbol{e}_1^{\mathrm{T}} \boldsymbol{x}, \end{aligned} \tag{3.105}$$

with state vector $\boldsymbol{x} \in \mathbb{R}^{n+1}$ given by

$$\boldsymbol{x} := \begin{bmatrix} x_0 \\ \vdots \\ x_n \end{bmatrix}, \quad \text{and} \quad \boldsymbol{A} = \left(\begin{array}{c|c} \boldsymbol{0}_{n\times 1} & \boldsymbol{I}_{n\times n} \\ \hline 0 & \boldsymbol{0}_{1\times n} \end{array}\right)$$

where $\boldsymbol{I}_{n\times n}$ denotes the identity matrix of dimension n, and $\boldsymbol{0}_{i\times j}$ denotes the $i \times j$ zero matrix. The vector $\boldsymbol{e}_i$ denotes the i^{th} standard basis vector, i.e., the i-th column of the identity matrix of dimension $n+1$. Note that the exo-system (3.105) is in observable-canonical form, which implies observability of $(\boldsymbol{A},\, \boldsymbol{e}_1^{\mathrm{T}})$. The relative degree of the output y w.r.t. to the unknown

input $f^{(n+1)}$ is equal to $n+1$ which implies strong observability. An observer for (3.105), which represents a differentiator, is

$$\frac{\mathrm{d}\hat{\boldsymbol{x}}}{\mathrm{d}t} = \boldsymbol{A}\hat{\boldsymbol{x}} + \boldsymbol{\psi}(\sigma_0)\sigma_0 \tag{3.106}$$

where the elements of the vector $\hat{\boldsymbol{x}}$ are the estimates of the elements of $\boldsymbol{x}$, the estimation error vector is given by $\boldsymbol{\sigma} := \boldsymbol{x} - \hat{\boldsymbol{x}}$ and $\sigma_0 = \boldsymbol{e}_1^{\mathrm{T}}\boldsymbol{\sigma} = f - \hat{x}_0$. The vector

$$\boldsymbol{\psi}(\sigma_0) = \begin{bmatrix}\psi_0(\sigma_0) & \psi_1(\sigma_0) & \dots & \psi_n(\sigma_0)\end{bmatrix}^{\mathrm{T}}$$

contains the general, possibly nonlinear and discontinuous, output injection terms

$$\psi_i(\sigma_0) = k_i|\sigma_0|^{\frac{r_{i+1}}{r_0}-1}, \quad i = 0 \dots n$$

with the constant gains $k_0, k_1, \dots, k_n \in \mathbb{R}$. Designing the weights according to

$$r_i = r_n - (n-i)d \tag{3.107}$$

where $r_n = 1$ is fixed and $r_{n+1} = r_n + d$ allows to parametrize the homogeneity degree $d \in [-1, 0]$ of the estimation error dynamics formed by the differentiator (3.106) and system (3.105). By selecting d it is possible to obtain either a continuous ($d \in (-1, 0)$) or a discontinuous differentiator. Latter one is obtained by $d = -1$. This recovers the arbitrary-order robust exact differentiator proposed by Levant in [14]:

$$\begin{aligned}\dot{\hat{x}}_j &= k_j\lfloor f - \hat{x}_0\rceil^{\frac{n-j}{n+1}} + \hat{x}_{j+1}, \quad j = 0, \dots, n-1,\\ \dot{\hat{x}}_n &= k_n \mathrm{sign}\,(f - \hat{x}_0).\end{aligned}$$

In the general case, i.e., $d \in [-1, 0]$, the computation of the estimation error dynamics yields the pseudo-linear system

$$\frac{\mathrm{d}\boldsymbol{\sigma}}{\mathrm{d}t} = \boldsymbol{M}(\sigma_0)\boldsymbol{\sigma} + \boldsymbol{e}_{n+1}f^{(n+1)}, \tag{3.108}$$

with $\boldsymbol{M}(\sigma_0) = \boldsymbol{A} - \boldsymbol{\psi}(\sigma_0)\boldsymbol{e}_1^{\mathrm{T}}$ in observable canonical form

$$\boldsymbol{M}(\sigma_0) = \begin{bmatrix} -k_0|\sigma_0|^{\frac{r_1}{r_0}-1} & 1 & 0 & \dots & 0\\ \vdots & \ddots & \ddots & \ddots & \vdots\\ \vdots & \ddots & \ddots & 1 & 0\\ -k_{n-1}|\sigma_0|^{\frac{r_n}{r_0}-1} & \dots & \dots & 0 & 1\\ -k_n|\sigma_0|^{\frac{r_{n+1}}{r_0}-1} & 0 & 0 & 0 & 0\end{bmatrix}.$$

The characteristic polynomial of the matrix $\boldsymbol{M}(\sigma_0)$ is

$$s^{n+1} + k_0|\sigma_0|^{\frac{r_1}{r_0}-1}s^n + \dots + k_{n-1}|\sigma_0|^{\frac{r_n}{r_0}-1}s + k_n|\sigma_0|^{\frac{r_{n+1}}{r_0}-1} = 0, \tag{3.109}$$

or, taking the calculation rule (3.107) for the weights r_i into account, one obtains

$$s^{n+1} + k_0|\sigma_0|^{\frac{d}{1-nd}}s^n + \ldots + k_{n-1}|\sigma_0|^{\frac{nd}{1-nd}}s + k_n|\sigma_0|^{\frac{(1+n)d}{1-nd}} = 0.$$

Multiplying the polynomial by $|\sigma_0|^{-\frac{(1+n)d}{1-nd}}$ yields

$$\begin{gathered}|\sigma_0|^{-\frac{(n+1)d}{1-nd}}s^{n+1} + k_0|\sigma_0|^{-\frac{nd}{1-nd}}s^n + \ldots + k_{n-1}|\sigma_0|^{-\frac{d}{1-nd}}s + k_n = \\ (|\sigma_0|^{-\frac{d}{1-nd}}s)^{n+1} + k_0(|\sigma_0|^{-\frac{d}{1-nd}}s)^n + \ldots + k_{n-1}(|\sigma_0|^{-\frac{d}{1-nd}}s) + k_n,\end{gathered}$$

which reveals that the roots s_i of (3.109) are the roots $p_i \in \mathbb{C}$ of the polynomial

$$p^{n+1} + k_0p^n + \ldots + k_{n-1}p + k_n, \tag{3.110}$$

scaled by the factor $|\sigma_0|^{\frac{d}{1-nd}}$, i.e.

$$s_i = |\sigma_0|^{\frac{d}{1-nd}}p_i = |\sigma_0|^{\frac{r_1}{r_0}-1}p_i. \tag{3.111}$$

Note that the choice $d = 0$ yields a linear (asymptotic) differentiator and the dynamic matrix of the closed-loop system then is given by

$$\boldsymbol{M} = \begin{bmatrix} -k_0 & 1 & 0 & \ldots & 0 \\ \vdots & \ddots & \ddots & \ddots & \vdots \\ \vdots & \ddots & \ddots & 1 & 0 \\ -k_{n-1} & \ldots & \ldots & 0 & 1 \\ -k_n & 0 & 0 & 0 & 0 \end{bmatrix}.$$

From this representation it also is straightforward to construct a high-gain observer by introducing a parameter scaling of the form

$$k_i = \frac{l_i}{\varepsilon^{i+1}}, \quad \varepsilon > 0, \quad i = 0 \ldots n,$$

The characteristic polynomial then is

$$(\varepsilon s)^{n+1} + l_0(\varepsilon s)^n + \ldots + l_{n-1}(\varepsilon s) + l_n.$$

and its roots s_i are the roots $p_i \in \mathbb{C}$ of the polynomial

$$p^{n+1} + l_0p^n + \ldots + l_{n-1}p + l_n$$

scaled by the factor ε^{-1}, i.e.,

$$s_i = \frac{1}{\varepsilon}p_i.$$

As mentioned previously, the choice $d = -1$ in (3.111) results in the arbitrary-order RED. In pseudo-linear system form this differentiator is given by (3.108) with

$$\boldsymbol{M}(\sigma_0) = \begin{bmatrix} -k_0|\sigma_0|^{-\frac{1}{n+1}} & 1 & 0 & \dots & 0 \\ \vdots & \ddots & \ddots & \ddots & \vdots \\ \vdots & \ddots & \ddots & 1 & 0 \\ -k_{n-1}|\sigma_0|^{-\frac{n}{n+1}} & \dots & \dots & 0 & 1 \\ -k_n|\sigma_0|^{-1} & 0 & 0 & 0 & 0 \end{bmatrix}.$$

and the eigenvalues of $\boldsymbol{M}(\sigma_0)$ are

$$s_i = |\sigma_0|^{-\frac{1}{n+1}} p_i.$$

The choice $d \in (-1, 0)$ results in a nonlinear continuous differentiator. Hence, a family of differentiators is obtained with the help of this framework. By selecting the homogeneity d it is possible to generate linear, nonlinear continuous or discontinuous differentiators. In the unperturbed case ($f^{(n+1)} \equiv 0$), i.e., when differentiating polynomials of order less or equal to n, the linear differentiators ensure asymptotic convergence whilst the nonlinear continuous differentiators ensure finite-time convergence. However, in the presence of perturbations, only the sliding mode based differentiator is capable to reconstruct the state variables exactly. The stability properties of the family of differentiators ($d \in [-1, 0]$) have been proven by means of Lyapunov's direct method in [107].

Under the assumption that the signal $f(t)$ is obtained by discrete-time measurements but integration is performed in continuous-time, the differentiator with $d = -1$ provides for the accuracies

$$|x_i - f^{(i)}| = \mathcal{O}\left(T_\mathrm{s}^{n-i+1}\right) \tag{3.112}$$

These asymptotic accuracies are also valid if the sampling time is non-constant. In this case

$$|x_i - f^{(i)}| = \mathcal{O}\left({T_\mathrm{s}^*}^{n-i+1}\right), \quad T_\mathrm{s}^* = \sup(t_{k+1} - t_k)$$

where t_k denotes the time t at the sampling instant k.

A realization of the differentiator in a discrete-time environment requires the discretization of the continuous-time differentiator (3.106). When dealing with discontinuous differentiators the first choice in terms of the discretization scheme often is the application of the forward Euler scheme. However, in case of the arbitrary-order RED, this scheme does not only evoke the discretization chattering phenomenon but also destroys the asymptotic accuracies (3.112). The root cause for this issue is discussed in the next section.

3.4.3 Explicit Euler Discretization of the Differentiator

Application of the forward Euler scheme to the differentiator (3.106) yields

$$\hat{\boldsymbol{x}}_{k+1} = \boldsymbol{A}_\mathrm{d}\hat{\boldsymbol{x}}_k + T_\mathrm{s}\boldsymbol{\psi}(\sigma_{0,k})\sigma_{0,k} \tag{3.113}$$

with $\boldsymbol{A}_\mathrm{d} := \boldsymbol{I} + T_\mathrm{s}\boldsymbol{A}$, $T_\mathrm{s} \in \mathbb{R}_{>0}$ is the constant sampling time and $\sigma_{0,k} = f_k - \hat{x}_{0,k}$, $k = 1, 2, \ldots$, $f_k = f(kT_\mathrm{s})$. In terms of the exo-system (3.105) a discrete-time model is obtained by applying Taylor series expansion with Lagrange's remainders, see [108], which yields the recursion

$$\begin{aligned} \boldsymbol{x}_{k+1} &= \boldsymbol{\Phi}\boldsymbol{x}_k + T_\mathrm{s}\boldsymbol{h}_k, \\ y_k &= f_k \end{aligned} \tag{3.114}$$

where $\boldsymbol{\Phi}(T_\mathrm{s}) = e^{\boldsymbol{A}T_\mathrm{s}}$ denotes the matrix exponential function and

$$\boldsymbol{h}_k = \begin{bmatrix} h_n & \ldots & h_0 \end{bmatrix}^\mathrm{T}, \quad h_i = \frac{T_\mathrm{s}^i}{(i+1)!} f^{(n+1)}(\xi_i),$$

with $\xi_i \in (kT_\mathrm{s},\, (k+1)T_\mathrm{s})$. Computing the error dynamics $\boldsymbol{\sigma}_{k+1} = \boldsymbol{x}_{k+1} - \hat{\boldsymbol{x}}_{k+1}$, taking into account (3.113) and (3.114), gives

$$\boldsymbol{\sigma}_{k+1} = \boldsymbol{\Phi}\boldsymbol{x}_k - \boldsymbol{A}_\mathrm{d}\hat{\boldsymbol{x}}_k - T_\mathrm{s}\boldsymbol{\psi}(\sigma_{0,k})\boldsymbol{e}_1^\mathrm{T}\boldsymbol{\sigma}_k + T_\mathrm{s}\boldsymbol{h}_k. \tag{3.115}$$

Note that matrix $\boldsymbol{A}$ is nilpotent with degree $n+1$, i.e, $\boldsymbol{A}^{n+1} = \boldsymbol{0}$. Therefore, it is possible to represent the state-transition matrix $\boldsymbol{\Phi}(T_\mathrm{s})$ as the finite sum

$$e^{\boldsymbol{A}T_\mathrm{s}} = \boldsymbol{I} + \boldsymbol{A}T_\mathrm{s} + \sum_{k=2}^{n} \frac{\boldsymbol{A}^k T_\mathrm{s}^k}{k!} = \boldsymbol{A}_\mathrm{d} + \boldsymbol{R}.$$

This representation of $\boldsymbol{\Phi}(T_\mathrm{s})$ allows to rewrite the error dynamics (3.115) into

$$\boldsymbol{\sigma}_{k+1} = \left[\boldsymbol{A}_\mathrm{d} - T_\mathrm{s}\boldsymbol{\psi}(\sigma_{0,k})\boldsymbol{e}_1^\mathrm{T}\right]\boldsymbol{\sigma}_k + T_\mathrm{s}\boldsymbol{h}_k + \boldsymbol{R}\boldsymbol{x}_k. \tag{3.116}$$

The dynamic matrix $\left[\boldsymbol{A}_\mathrm{d} - T_\mathrm{s}\boldsymbol{\psi}(\sigma_{0,k})\boldsymbol{e}_1^\mathrm{T}\right]$ of the error dynamics has eigenvalues located at

$$z_i = 1 + T_\mathrm{s}s_i. \tag{3.117}$$

Apart from the vector $\boldsymbol{h}_k$, the dynamical system (3.116) represents an explicit Euler discretized version of the closed-loop dynamics (3.108) additionally driven by the higher-order terms $\boldsymbol{R}\boldsymbol{x}_k$. Recall that in case of the explicit Euler scheme $f_k^{(n+1)}$ acts only in the last channel, whereas in the closed-loop system (3.116) it is spread to all channels by $\boldsymbol{h}_k$. In the absence of the term $\boldsymbol{R}\boldsymbol{x}_k$ and $d \in [-1,\, 0)$, the discrete-time dynamics (3.116) would remain invariant w.r.t. the parameter coordinate change

$$(T_\mathrm{s}, \sigma_{0,k},\, \sigma_{1,k}, \ldots, \sigma_{n,k}) \to \left(\kappa T_\mathrm{s},\, \kappa^{n+1}\sigma_{0,k},\, \kappa^n\sigma_{1,k}, \ldots,\, \kappa\sigma_{n,k}\right) \tag{3.118}$$

and consequently the differentiator would preserve the asymptotic accuracies w.r.t. the sampling time, i.e., in steady state $|\sigma_i| = \mathcal{O}\left(T_\mathrm{s}^{n-i+1}\right)$. It is noteworthy that these terms only appear in differentiators with order $n > 1$. Therefore, e.g. the robust exact differentiator, which is characterized by $n = 1$, $d = -1$, does *not* require any modifications in order to provide for these standard accuracies of the second-order sliding mode. For $d = -1$, the authors in [87] proved, that in the presence of this terms, the accuracies diminish and are proportional to the sampling time T_s, except the tracking error of f which remains proportional to T_s^{n+1}. In order to maintain the asymptotic accuracies w.r.t. to discrete measurements, one has to ensure that

the discrete-time algorithm preserves the scaling property (3.118). In this regard, trajectories of the discrete-time error dynamics with parameter T_s are mapped onto trajectories with sampling time κT_s as illustrated for a planar system in the previous section in Figure 3.4. Therefore, besides stability of the closed-loop system, the invariance w.r.t. to the scaling (3.118) is a the fundamental property ensuring the standard asymptotic accuracies of the estimation errors.

3.4.4 Homogeneous Discrete-Time Differentiator

In order to preserve the invariance property (3.118) for the discrete-time differentiators, the authors in [87] proposed a modification of (3.113) by incorporating additional linear higher-order terms. The proposed differentiator is given by the recursions

$$\begin{aligned}\hat{x}_{j,k+1} &= \hat{x}_{j,k} + T_\mathrm{s} k_j \lfloor f_k - \hat{x}_{0,k} \rceil^{\frac{n-j}{n+1}} + \sum_{l=1}^{n-j} \frac{T_\mathrm{s}^l}{l!} \hat{x}_{l+j,k}, \quad j = 0, \dots, n-1, \\ \hat{x}_{n,k+1} &= \hat{x}_{n,k} + T_\mathrm{s} k_n \mathrm{sign}\,(f_k - \hat{x}_{0,k}).\end{aligned} \tag{3.119}$$

Obviously, the first-order differentiator ($n = 1$) remains unchanged. It corresponds to the forward Euler discretization of the STA given by

$$\begin{aligned}\hat{x}_{0,k+1} &= \hat{x}_{0,k} + T_\mathrm{s} k_0 \lfloor f_k - \hat{x}_{0,k} \rceil^{\frac{1}{2}} + T_\mathrm{s} \hat{x}_{1,k}, \\ \hat{x}_{1,k+1} &= \hat{x}_{1,k} + T_\mathrm{s} k_1 \mathrm{sign}\,(f_k - \hat{x}_{0,k}).\end{aligned}$$

The difference of the proposed scheme to the forward Euler discretized algorithm becomes apparent in the second-order differentiator. The second-order differentiator obtained from (3.119) yields

$$\begin{aligned}\hat{x}_{0,k+1} &= \hat{x}_{0,k} + T_\mathrm{s} k_0 \lfloor f_k - \hat{x}_{0,k} \rceil^{\frac{2}{3}} + T_\mathrm{s} \hat{x}_{1,k} + \frac{T_\mathrm{s}^2}{2} \hat{x}_{2,k}, \\ \hat{x}_{1,k+1} &= \hat{x}_{1,k} + T_\mathrm{s} k_1 \lfloor f_k - \hat{x}_{0,k} \rceil^{\frac{1}{3}} + T_\mathrm{s} \hat{x}_{2,k}, \\ \hat{x}_{2,k+1} &= \hat{x}_{2,k} + T_\mathrm{s} k_2 \mathrm{sign}\,(f_k - \hat{x}_{0,k}).\end{aligned}$$

Compared to the forward Euler discretized algorithm the proposed scheme includes the additional term $\frac{T_\mathrm{s}^2}{2} \hat{x}_{2,k}$ in the first equation. This term is introduced in order to guarantee the scaling property of the closed-loop system. It turns out, that the discrete-time differentiator (3.119) can be represented in the matrix notation by

$$\hat{\boldsymbol{x}}_{k+1} = \boldsymbol{\Phi} \hat{\boldsymbol{x}}_k + T_\mathrm{s} \boldsymbol{\psi}(\sigma_{0,k}) \boldsymbol{e}_1^\mathrm{T} \boldsymbol{\sigma}_k, \tag{3.120}$$

which leads to the estimation error dynamics

$$\boldsymbol{\sigma}_{k+1} = \left[\boldsymbol{\Phi} - T_\mathrm{s} \boldsymbol{\psi}(\sigma_{0,k}) \boldsymbol{e}_1^\mathrm{T} \right] \boldsymbol{\sigma}_k + T_\mathrm{s} \boldsymbol{h}_k. \tag{3.121}$$

The differentiator in (3.120) is termed homogeneous discrete-time differentiator (HDD), see [87]. Compared to the error dynamics obtained with the forward Euler discretized differentiator (3.116), the error dynamics (3.121), which are obtained with the HDD, do *not* dependent on

the plant state variables $\boldsymbol{x}_k$. From the viewpoint of an observer design, the higher-order terms[3] in the HDD are a quite natural thing. Usually, a state observer is composed of two parts, a copy of the known plant dynamics, in this specific case of (3.114), and output injection terms. The output injection terms are commonly designed s.t. the closed-loop dynamics have desired behavior, e.g. assignment of the eigenvalues when dealing with a linear time-invariant system. Obviously, also the HDD in (3.120) follows this structure. In contrast to the forward Euler discretized continuous-time differentiator, the HDD incorporates a copy of the plant dynamics. However, the output injection terms still originate from the forward Euler discretized continuous-time system and are not redesigned according to the discrete-time system (3.114).

The advantage of redesigning the injection terms is discussed in the next section. The redesign is achieved by taking into account the ideas of the previous sections, bearing in mind that the resulting differentiator needs to retain the scaling property (3.118). In a first step, this leads to a discrete-time differentiator that takes not only linear higher-order terms into account (as the HDD does) but also nonlinear higher-order terms.

3.4.5 Generalized Homogeneous Discrete-Time Differentiator

As a motivational example and for the purpose of analysis consider the closed-loop dynamics induced by a second-order HDD without perturbation, i.e., $f^{(3)} \equiv 0$. The dynamics are written in terms of the first forward difference $\sigma'_{i,k} := (\sigma_{i,k+1} - \sigma_{i,k})/T_\mathrm{s}$,

$$\begin{aligned}
\sigma'_{0,k} &= \psi_0(\sigma_{0,k})\sigma_{0,k} + \sigma_{1,k} + \frac{T_\mathrm{s}}{2}\sigma_{2,k},\\
\sigma'_{1,k} &= \psi_1(\sigma_{0,k})\sigma_{0,k} + \sigma_{2,k},\\
\sigma'_{2,k} &= \psi_2(\sigma_{0,k})\sigma_{0,k}.
\end{aligned} \tag{3.122}$$

Introducing the coordinates $\tilde{\sigma}_{0,k} := \sigma_{0,k}$, $\tilde{\sigma}_{1,k} := \sigma_{1,k} + \frac{T_\mathrm{s}}{2}\sigma_{2,k}$ and $\tilde{\sigma}_{2,k} = \sigma_{2,k}$ leads to the following system representation:

$$\begin{aligned}
\tilde{\sigma}'_{0,k} &= \psi_0(\tilde{\sigma}_{0,k})\tilde{\sigma}_{0,k} + \tilde{\sigma}_{1,k},\\
\tilde{\sigma}'_{1,k} &= \psi_1(\tilde{\sigma}_{0,k})\tilde{\sigma}_{0,k} + \tilde{\sigma}_{2,k} + \frac{T_\mathrm{s}}{2}\psi_2\tilde{\sigma}_{0,k},\\
\tilde{\sigma}'_{2,k} &= \psi_2(\tilde{\sigma}_{0,k})\tilde{\sigma}_{0,k}.
\end{aligned} \tag{3.123}$$

In $\tilde{\sigma}_{i,k}$-coordinates, the dynamics (3.123) represent a forward Euler discretized version of the continuous-time differentiator additionally driven by the *switching* term $\frac{T_\mathrm{s}}{2}\psi_2\tilde{\sigma}_{0,k}$. Also in the absence of this term the inequalities $\tilde{\sigma}_{i,k} = \mathcal{O}(T_\mathrm{s}^{n+1-i})$ hold after finite-time transients, (see [109]), implying the same asymptotic accuracies in the original coordinates, i.e., $|\sigma_{i,k}| = \mathcal{O}(T_\mathrm{s}^{n+1-i})$, $i = 0, 1, 2$. The term $\frac{T_\mathrm{s}}{2}\psi_2\tilde{\sigma}_{0,k}$, which is essentially introduced by the linear higher-order term, appears as a relict from the *mixed* discretization and neither contributes to the stability of the closed-loop system (3.123) or (3.122), nor is it required to maintain the asymptotic accuracies. Even more, this additional switching term might lead to unnecessary high oscillation amplitudes whenever the $(n+1)$th derivative vanishes. Adding the corresponding

[3] with respect to the sampling time T_s

nonlinear higher-order term to the differentiator, i.e.,

$$\begin{aligned}
\hat{x}_{0,k+1} &= \hat{x}_{0,k} + T_\mathrm{s}\psi_0(\sigma_{0,k})\sigma_{0,k} + T_\mathrm{s}\hat{x}_{1,k} + \frac{T_\mathrm{s}^2}{2}\hat{x}_{2,k},\\
\hat{x}_{1,k+1} &= \hat{x}_{1,k} + T_\mathrm{s}\psi_1(\sigma_{0,k})\sigma_{0,k} + T_\mathrm{s}\hat{x}_{2,k} - \frac{T_\mathrm{s}}{2}\psi_2(\sigma_{0,k})\sigma_{0,k}\\
\hat{x}_{2,k+1} &= \hat{x}_{2,k} + T_\mathrm{s}\psi_2(\sigma_{0,k})\sigma_{0,k}.
\end{aligned}$$

allows to cancel the term $\frac{T_\mathrm{s}}{2}\psi_2\tilde{\sigma}_{0,k}$ in the closed-loop system, which then is described by

$$\tilde{\boldsymbol{\sigma}}_{k+1} = \left[\boldsymbol{A}_\mathrm{d} - T_\mathrm{s}\boldsymbol{\psi}(\sigma_{0,k})\boldsymbol{e}_1^\mathrm{T}\right]\tilde{\boldsymbol{\sigma}}_k. \tag{3.124}$$

The dynamic matrix in (3.124) has the same eigenvalues as given in (3.117). The original states are obtained by the constant state transformation

$$\boldsymbol{\sigma}_k = \boldsymbol{P}\tilde{\boldsymbol{\sigma}}_k, \quad \boldsymbol{P} = \begin{bmatrix} 1 & 0 & 0 \\ 0 & 1 & -\frac{T_\mathrm{s}}{2} \\ 0 & 0 & 1 \end{bmatrix}.$$

The approach is generalized in the next subsection. The objective is to redesign the injection terms for the arbitrary-order differentiator s.t. the closed-loop system has eigenvalues which are related to the eigenvalues of the continuous-time system by the mapping (3.117).

The modification of the HDD

$$\hat{\boldsymbol{x}}_{k+1} = \boldsymbol{\Phi}\hat{\boldsymbol{x}}_k + T_\mathrm{s}\boldsymbol{P}\boldsymbol{\psi}(\sigma_{0,k})\sigma_{0,k}, \tag{3.125}$$

which will be termed as generalized homogeneous discrete-time differentiator (GHDD), is proposed. Setting $\boldsymbol{P} = \boldsymbol{I}$ recovers the HDD given in (3.120). The matrix $\boldsymbol{P}$ is fixed to the structure

$$\boldsymbol{P} = \left(\begin{array}{c|c} 1 & \boldsymbol{0}_{1\times n} \\ \hline \boldsymbol{0}_{n\times 1} & \tilde{\boldsymbol{P}} \end{array}\right), \quad \tilde{\boldsymbol{P}} = \begin{bmatrix} 1 & \beta_{12}T_\mathrm{s} & \dots & \beta_{1n}T_\mathrm{s}^n \\ & 1 & \dots & \beta_{2n}T_\mathrm{s}^{n-1} \\ & & \ddots & \vdots \\ & & & 1 \end{bmatrix}, \tag{3.126}$$

with constants $\beta \in \mathbb{R}$. The following lemma is helpful in the proof of the main results.

Lemma 4.1

There exists $\boldsymbol{P}$ satisfying structure (3.126) s.t.

$$\boldsymbol{\Phi}\boldsymbol{P} = \boldsymbol{P}\boldsymbol{A}_\mathrm{d}. \tag{3.127}$$

Proof. Matrix $\boldsymbol{A}$ has a repeated eigenvalue $\lambda = 0$ with algebraic multiplicity $n+1$ and the only eigenvector $\boldsymbol{p} = \boldsymbol{e}_1$. As matrices $\boldsymbol{\Phi}$ and $\boldsymbol{A}_\mathrm{d}$ are matrix functions of $\boldsymbol{A}$, both matrices, $\boldsymbol{\Phi}$ and $\boldsymbol{A}_\mathrm{d}$ have the same eigenvector $\boldsymbol{p} = \boldsymbol{e}_1$ associated with the eigenvalue $\tilde{\lambda} = 1$ of algebraic

multiplicity $n+1$. Consequently both matrices also have the same Jordan normal form. Hence the matrices are similar and there is an invertible $(n+1)\times(n+1)$ matrix $\boldsymbol{P}$ s.t.

$$\boldsymbol{\Phi} = \boldsymbol{P}\boldsymbol{A}_{\mathrm{d}}\boldsymbol{P}^{-1}.$$

Furthermore, as $\boldsymbol{\Phi}$ and $\boldsymbol{A}_{\mathrm{d}}$ describe a chain of integrators, the pairs are $\left(\boldsymbol{A}_{\mathrm{d}},\, \boldsymbol{e}_1^{\mathrm{T}}\right)$ and $\left(\boldsymbol{\Phi},\, \boldsymbol{e}_1^{\mathrm{T}}\right)$ are observable. In this regard,

$$\boldsymbol{P} = \boldsymbol{B}_{\Phi}^{-1}\boldsymbol{B}_{A_{\mathrm{d}}}, \tag{3.128}$$

where $\boldsymbol{B}_{\Phi}$ and $\boldsymbol{B}_{A_{\mathrm{d}}}$ denote the observability matrix of $\boldsymbol{A}_{\mathrm{d}}$ and $\boldsymbol{\Phi}$, respectively, given by

$$\boldsymbol{B}_{\Phi} = \begin{bmatrix} \boldsymbol{e}_1^{\mathrm{T}} \\ \boldsymbol{e}_1^{\mathrm{T}}\boldsymbol{\Phi} \\ \boldsymbol{e}_1^{\mathrm{T}}\boldsymbol{\Phi}^2 \\ \vdots \end{bmatrix}, \quad \boldsymbol{B}_{A_{\mathrm{d}}} = \begin{bmatrix} \boldsymbol{e}_1^{\mathrm{T}} \\ \boldsymbol{e}_1^{\mathrm{T}}\boldsymbol{A}_{\mathrm{d}} \\ \boldsymbol{e}_1^{\mathrm{T}}\boldsymbol{A}_{\mathrm{d}}^2 \\ \vdots \end{bmatrix}. \tag{3.129}$$

□

For differentiators of order $n = 1, 2, 3, 4, 5$ matrix $\boldsymbol{P}$, computed according to (3.128), is

$$\begin{pmatrix} \boldsymbol{P}_1 & & & & \\ & \boldsymbol{P}_2 & & & \\ & & \boldsymbol{P}_3 & & \\ & & & \boldsymbol{P}_4 & \\ & & & & \boldsymbol{P}_5 \end{pmatrix} = \left(\begin{array}{cc|c|c|c|c} 1 & 0 & 0 & 0 & 0 & 0 \\ 0 & 1 & -\frac{1}{2}T_{\mathrm{s}} & \frac{1}{3}T_{\mathrm{s}}^2 & -\frac{1}{4}T_{\mathrm{s}}^3 & \frac{T_{\mathrm{s}}^4}{5} \\ \hline 0 & 0 & 1 & -T_{\mathrm{s}} & \frac{11}{12}T_{\mathrm{s}}^2 & -\frac{5}{6}T_{\mathrm{s}}^3 \\ \hline 0 & 0 & 0 & 1 & -\frac{3}{2}T_{\mathrm{s}} & \frac{7}{4}T_{\mathrm{s}}^2 \\ \hline 0 & 0 & 0 & 0 & 1 & -2T_{\mathrm{s}} \\ \hline 0 & 0 & 0 & 0 & 0 & 1 \end{array}\right)$$

Taking into account Lemma 4.1, allows to state

Lemma 4.2

The eigenvalues of $\left[\boldsymbol{\Phi} - T_{\mathrm{s}}\boldsymbol{P}\boldsymbol{\psi}(\sigma_{0,k})\boldsymbol{e}_1^{\mathrm{T}}\right]$, with $\boldsymbol{P}$ satisfying (3.127), are located at $z_i = 1 + T_{\mathrm{s}}s_i(\sigma_{0,k})$ and the closed-loop system obtained with the GHDD, given by

$$\boldsymbol{\sigma}_{k+1} = \left[\boldsymbol{\Phi} - T_{\mathrm{s}}\boldsymbol{P}\boldsymbol{\psi}(\sigma_{0,k})\boldsymbol{e}_1^{\mathrm{T}}\right]\boldsymbol{\sigma}_k + T_{\mathrm{s}}\boldsymbol{h}_k, \tag{3.130}$$

is algebraically equivalent to the system

$$\tilde{\boldsymbol{\sigma}}_{k+1} = \left[\boldsymbol{A}_{\mathrm{d}} - T_{\mathrm{s}}\boldsymbol{\psi}(\tilde{\sigma}_{0,k})\boldsymbol{e}_1^{\mathrm{T}}\right]\tilde{\boldsymbol{\sigma}}_k + T_{\mathrm{s}}\boldsymbol{P}^{-1}\boldsymbol{h}_k, \tag{3.131}$$

that means, the constant invertible linear mapping $\boldsymbol{P}$ maps each trajectory $\tilde{\boldsymbol{\sigma}}_k$ to a trajectory $\boldsymbol{\sigma}_k$, i.e.,

$$\tilde{\boldsymbol{\sigma}}_k = \boldsymbol{P}^{-1}\boldsymbol{\sigma}_k. \tag{3.132}$$

Proof. From the structure of $\boldsymbol{P}$ in (3.126) it follows that $\boldsymbol{e}_1$ is a left eigenvector of $\boldsymbol{P}$ associated with the eigenvalue $\lambda = 1$. Therefore, relation $\boldsymbol{e}_1^{\mathrm{T}}\boldsymbol{P} = \boldsymbol{e}_1^{\mathrm{T}} = \boldsymbol{e}_1^{\mathrm{T}}\boldsymbol{P}^{-1}$ holds and consequently $\tilde{\sigma}_{0,k} = \sigma_{0,k}$ holds. Substituting (3.130) into (3.132) yields (3.131) which confirms the algebraic equivalence. Because of the invariance of eigenvalues under similarity transformation also $\left[\boldsymbol{\Phi} - T_{\mathrm{s}}\boldsymbol{P}\boldsymbol{\psi}(\sigma_{0,k})\boldsymbol{e}_1^{\mathrm{T}}\right]$ has eigenvalues $z_i = 1 + T_{\mathrm{s}}s_i(\sigma_{0,k})$. □

Note that recursion (3.131) represents an forward Euler discretized version of the *artificial* continuous-time system

$$\dot{\tilde{\boldsymbol{\sigma}}} = \left[\boldsymbol{A} - \boldsymbol{\psi}(\tilde{\sigma}_0)\boldsymbol{e}_1^{\mathrm{T}}\right]\tilde{\boldsymbol{\sigma}} + \boldsymbol{P}^{-1}\boldsymbol{h},$$

where

$$\boldsymbol{h} = \left[\begin{array}{c:c:c:c} \frac{T_{\mathrm{s}}^n}{(n+1)!}f^{(n+1)}(\xi_0) & \frac{T_{\mathrm{s}}^{n-1}}{n!}f^{(n+1)}(\xi_1) & \dots & f^{(n+1)}(\xi_n) \end{array}\right]^{\mathrm{T}}$$

with $\xi_i \in (t,\, t+T_{\mathrm{s}})$, $i = 0 \dots n$. Therefore, it is expected that the differentiator (3.125) preserves the asymptotic accuracies of the continuous-time differentiator w.r.t. to discrete-measurements and noise. The result is stated in

Theorem 4.1

Let $d = -1$ and the signal to be differentiated be composed of $f(t) = f_0(t) + \eta$, $\eta \in \epsilon[-1,\, 1]$ denotes the noise and $\sup_t\left(|f_0^{(n+1)}(t)|\right) < L$. Then there exist parameters $\boldsymbol{k} = [k_0, \dots k_n]^{\mathrm{T}}$, $T^* > 0$ and positive constants μ_i s.t. the differentiator (3.130) provides for the asymptotic accuracies $|\sigma_i(t)| \leq \mu_i\rho^{n+1-i}$, $\forall t > T^*$ where $\rho = \max[(\epsilon/L)^{1/(n+1)}, T_{\mathrm{s}}]$.

Proof. The proof is essentially based on the results presented in [87, 110, 111]. The discrete-time error dynamics (3.131) is written in the scaled variables $\tilde{\boldsymbol{\zeta}}_k := \tilde{\boldsymbol{\sigma}}_k/L$ as

$$\tilde{\boldsymbol{\zeta}}_{k+1} \in \tilde{\boldsymbol{\zeta}}_k + T_{\mathrm{s}}\boldsymbol{\Theta}\left(\tilde{\zeta}_{0,k} + \tilde{\epsilon}[-1,1], \tilde{\boldsymbol{\zeta}}_k, \boldsymbol{k}\right) + T_{\mathrm{s}}\boldsymbol{\gamma}(T_{\mathrm{s}}) \tag{3.133}$$

where $\tilde{\epsilon} = \epsilon/L$ and

$$\boldsymbol{\gamma}(T_{\mathrm{s}}) = \begin{bmatrix} \gamma_n\frac{T_{\mathrm{s}}^n}{(n+1)!}[-1,1] \\ \gamma_{n-1}\frac{T_{\mathrm{s}}^{n-1}}{n!}[-1,1] \\ \vdots \\ \gamma_1\frac{T_{\mathrm{s}}}{2}[-1,1] \\ [-1,1] \end{bmatrix}, \quad \gamma_i \in \mathbb{R}.$$

Piecewise linear functions connecting solutions of the recursion (3.133) satisfy the continuous-time differential inclusion

$$\frac{\mathrm{d}\tilde{\boldsymbol{\zeta}}(t)}{\mathrm{d}t} \in \boldsymbol{\Theta}\left(\tilde{\zeta}_0(t - T_{\mathrm{s}}) + \tilde{\epsilon}[-1,1], \tilde{\boldsymbol{\zeta}}(t - T_{\mathrm{s}}), \boldsymbol{k}\right) + \boldsymbol{\gamma}(T_{\mathrm{s}}). \tag{3.134}$$

Solutions of (3.134) also satisfy the larger inclusion

$$\frac{\mathrm{d}\tilde{\boldsymbol{\zeta}}(t)}{\mathrm{d}t} \in \boldsymbol{\Theta}\left(\tilde{\zeta}_0(t-\rho[0,1]) + \rho^{n+1}[-1,1], \tilde{\boldsymbol{\zeta}}(t-\rho[0,1]), \boldsymbol{k}\right) + \boldsymbol{\gamma}(\rho)$$

which allows to conclude the asymptotic accuracies $|\tilde{\sigma}_{i,k}| \leq \tilde{\mu}_i \rho^{n+1-i}$, $\rho = \max[(\epsilon/L)^{1/(n+1)}, T_\mathrm{s}]$ (see [110, 87]). From Lemma 4.2 and taking into account the structure of $\boldsymbol{P}$ it follows $|\sigma_i(t)| \leq \tilde{\mu}_i \rho^{n+1-i} + \sum_{l=i+1}^{n} c_{i,l} \rho^{n+1-l} T_\mathrm{s}^{l-i}$ for some positive constants $c_{i,l}$ which implies the asymptotic accuracies $|\sigma_i(t)| \leq \mu_i \rho^{n+1-i}$. □

By exploiting the pseudo-linear system representation of the arbitrary-order RED, it is possible to obtain an extended version of the HDD which also preserves the asymptotic accuracies known from the continuous-time differentiator subject to discrete-time measurements and noise. The advantage of taking also the nonlinear higher-order terms into account will be demonstrated in a simulation example and by applying the differentiator to a measured signal.

Simulation and Application

The asymptotic accuracies w.r.t. sampling are demonstrated by differentiating the sinusoidal signal $f(t) = f_0(t) = 0.5\cos(T_\mathrm{s}k) + \sin(0.5T_\mathrm{s}k)$. In order to see how the nonlinear higher-order terms affect the performance, a third order differentiator is implemented. The homogeneity degree is set to $d = -1$, hence the HDD and the GHDD are compared. A third order GHDD is obtained from system (3.125) with

$$\boldsymbol{P} = \begin{bmatrix} 1 & 0 & 0 & 0 \\ 0 & 1 & -\frac{T_\mathrm{s}}{2} & \frac{T_\mathrm{s}^2}{3} \\ 0 & 0 & 1 & -T_\mathrm{s} \\ 0 & 0 & 1 & 0 \end{bmatrix}, \quad \boldsymbol{\Phi} = \begin{bmatrix} 1 & T_\mathrm{s} & \frac{T_\mathrm{s}^2}{2} & \frac{T_\mathrm{s}^3}{6} \\ 0 & 1 & T_\mathrm{s} & \frac{T_\mathrm{s}^2}{2} \\ 0 & 0 & 1 & T_\mathrm{s} \\ 0 & 0 & 1 & 0 \end{bmatrix}, \quad \boldsymbol{\psi}(\sigma_{0,k})\sigma_{0,k} = \begin{bmatrix} k_0 \lfloor \sigma_{0,k} \rceil^{\frac{3}{4}} \\ k_1 \lfloor \sigma_{0,k} \rceil^{\frac{1}{2}} \\ k_2 \lfloor \sigma_{0,k} \rceil^{\frac{1}{4}} \\ k_3 \lfloor \sigma_{0,k} \rceil^{0} \end{bmatrix},$$

or by the system

$$\begin{aligned}
\hat{x}_{1,k+1} &= \hat{x}_{1,k} + T_\mathrm{s}\hat{x}_{2,k} + T_\mathrm{s}k_0 \lfloor \sigma_{0,k} \rceil^{\frac{3}{4}} + \frac{T_\mathrm{s}^2}{2}\hat{x}_{3,k} + \frac{T_\mathrm{s}^3}{6}\hat{x}_{4,k}, \\
\hat{x}_{2,k+1} &= \hat{x}_{2,k} + T_\mathrm{s}\hat{x}_{3,k} + T_\mathrm{s}k_1 \lfloor \sigma_{0,k} \rceil^{\frac{1}{2}} + \frac{T_\mathrm{s}^2}{2}\hat{x}_{4,k} - \frac{T_\mathrm{s}^2}{2}k_2 \lfloor \sigma_{0,k} \rceil^{\frac{1}{4}} + \frac{T_\mathrm{s}^3}{3}k_3 \lfloor \sigma_{0,k} \rceil^{0}, \\
\hat{x}_{3,k+1} &= \hat{x}_{3,k} + T_\mathrm{s}\hat{x}_{4,k} + T_\mathrm{s}k_2 \lfloor \sigma_{0,k} \rceil^{\frac{1}{4}} - T_\mathrm{s}^2 k_3 \lfloor \sigma_{0,k} \rceil^{0}, \\
\hat{x}_{4,k+1} &= \hat{x}_{4,k} + T_\mathrm{s}k_3 \lfloor \sigma_{0,k} \rceil^{0}.
\end{aligned}$$

The parameters are set to the same values in both algorithms and are tuned according to the approach proposed in [80], that is

$$k_0 = 4\alpha^{\frac{1}{4}}, \quad k_1 = 6\alpha^{\frac{1}{2}}, \quad k_2 = 4\alpha^{\frac{3}{4}}, \quad k_3 = \alpha,$$

with the choice $\alpha = 2$. The results shown in Figure 3.17 confirm the asymptotic accuracies stated in Theorem 4.1. Up to a certain sampling-time T_s the GHDD provides, in this specific

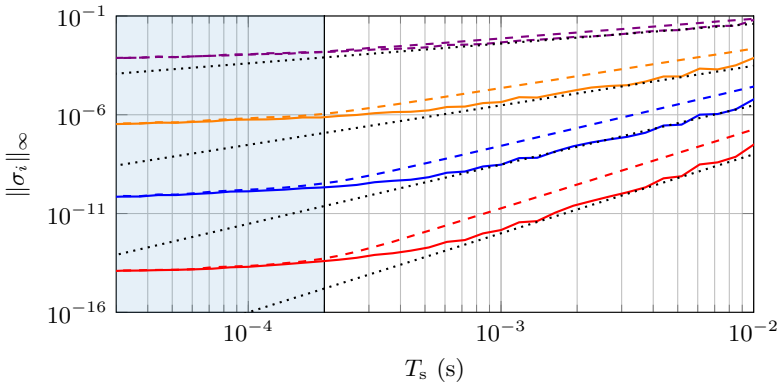

Figure 3.17: Comparison of the asymptotic accuracies w.r.t. *sampling* achieved with the (——) GHDD and HDD (- - -). Estimation errors are colored as (——) σ_0, (——) σ_1, (——) σ_2, (——) σ_3.

example, for better precision, i.e., smaller constants μ_i when compared to the HDD. Due to numerical reasons, which also can be regarded as noise, the asymptotic accuracies are abandoned for small sampling steps, see [110]. In the case of noisy measurements and small sampling times, i.e., $T_s \ll (\epsilon/L)^{1/4}$, the accuracy cannot further be improved by reducing the sampling time. Both algorithms then provide the same precision, see blue shaded area in the plot in Figure 3.17. The accuracies w.r.t. noise are shown in Figure 3.18. The plot shows the steady state error obtained with the GHDD and the HDD. The signal to be differentiated is the same but with additional noise $\eta(t)$. The noise is chosen as $\eta \in \epsilon[-1, 1]$ with $\epsilon = \Upsilon T_s^4 L$ and $\Upsilon \in \mathbb{R}_{>0}$ represents a scaling factor. The plot demonstrates the effect of increasing the noise amplitude while keeping the sampling time $T_s = 5$ ms constant. According to the theoretical results (see Theorem 4.1), the noise effects dominate over the sampling effects for $(\epsilon/L)^{(1/4)} > T_s$ which corresponds to $\Upsilon > 1$ and vice versa for $\Upsilon < 1$. In the plot it can be seen, that in the region $\Upsilon > 1$ (blue shaded area), where the noise effects dominate, both algorithms provide almost the same results. For $\Upsilon < 1$, i.e., where the sampling effects dominate, the GHDD clearly outperforms the HDD in terms of precision.

In the next example, the same differentiators are exploited for real-time differentiation of a measured displacement signal. The parameters are tuned according to the same rule as in the previous example. The experiment is carried out with sampling time $T_s = 1$ ms and $T_s = 5$ ms. The parameter α is tuned heuristically. Selecting $\alpha = 10^4$ provides for suitable performance in the experiment where $T_s = 1$ ms. The results obtained with this setting are provided in Figure 3.19. Herein both differentiators achieve similar results in terms of the estimation quality of the velocity and the acceleration. However, as can be seen in the plots on the right hand side the chattering effects become clearly visible when increasing the sampling time to $T_s = 5$ ms. As expected, the chattering amplitude in the third derivative is similar for both algorithms. However, especially during time periods of vanishing derivatives, the chattering amplitude in the first and also in the second derivative is much smaller when using the GHDD.

The decrease of the oscillation amplitude is achieved by extending the HDD with nonlinear higher-order terms. The reduction of the chattering amplitude during periods of vanishing

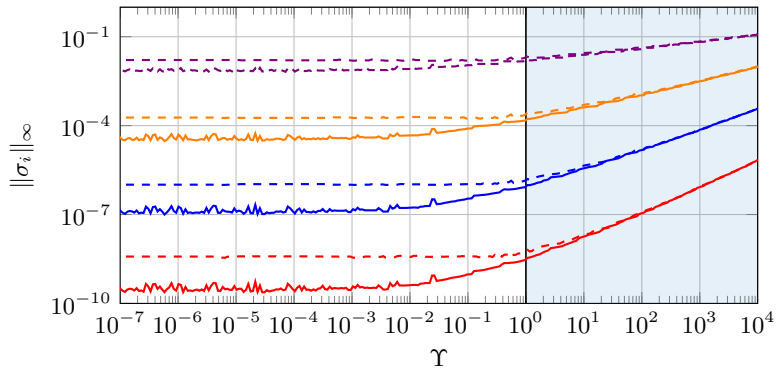

Figure 3.18: Comparison of the asymptotic accuracies w.r.t. to *noise* achieved with the (——) GHDD and HDD (- - -). Estimation errors are colored as (——) σ_0, (——) σ_1, (——) σ_2, (——) σ_3.

derivatives is of advantage when utilizing the differentiator, e.g. for on-line fault detection tasks. In such applications, a fault is usually captured by reconstructing an unknown signal where large transients in the reconstructed signal indicate a fault. Therefore, it might be impossible to detect a fault if the chattering amplitude is very large. In the following section the matching approach, which was used to obtain a discrete-time version of the super-twisting algorithm, will be applied to discretize the differentiator. This approach will allow to further decrease the chattering amplitude, even in the last channel of the differentiator. With this scheme, it will be possible to exactly reconstruct signals with vanishing $(n+1)$ th derivative.

3.4.6 Matching Approach

The differentiator design is again considered as an observer design problem for the discrete-time system (3.114). The more general injection terms are included in the vector

$$\boldsymbol{\lambda}(\sigma_{0,k}) = \begin{bmatrix} \lambda_0(\sigma_{0,k}) & \lambda_1(\sigma_{0,k}) & \dots & \lambda_n(\sigma_{0,k}) \end{bmatrix}^{\mathrm{T}}, \tag{3.135}$$

where $\sigma_{0,k} := x_{0,k} - \hat{x}_{0,k}$. With (3.135) the differentiator is written as

$$\hat{\boldsymbol{x}}_{k+1} = \boldsymbol{\Phi}\hat{\boldsymbol{x}}_k + \boldsymbol{\lambda}(\sigma_{0,k})^{\mathrm{T}}\sigma_{0,k}. \tag{3.136}$$

where $\hat{\boldsymbol{x}}_k = \begin{bmatrix} \hat{x}_{0,k} & \hat{x}_{1,k} & \dots & \hat{x}_{n,k} \end{bmatrix}^{\mathrm{T}}$ denotes the estimate of $\boldsymbol{x}_k$. The estimation error dynamics is given by

$$\boldsymbol{\sigma}_{k+1} = [\boldsymbol{\Phi} - \boldsymbol{\lambda}(\sigma_{0,k})\boldsymbol{e}_1^{\mathrm{T}}]\boldsymbol{\sigma}_k + T_{\mathrm{s}}\boldsymbol{h}_k, \tag{3.137}$$

with the estimation error $\boldsymbol{\sigma}_k := \boldsymbol{x}_k - \hat{\boldsymbol{x}}_k$. In (3.137) the relation $\sigma_{0,k} = \boldsymbol{e}_1^{\mathrm{T}}\boldsymbol{\sigma}_k$ has been used.

The injection vector $\boldsymbol{\lambda}(\sigma_{0,k})$ is now designed by assigning eigenvalues to the matrix $[\boldsymbol{\Phi} - \boldsymbol{\lambda}(\sigma_{0,k})\boldsymbol{e}_1^{\mathrm{T}}]$. The eigenvalue assignment problem is solved via Ackerman's formula

$$\boldsymbol{\lambda}(\sigma_{0,k}) = \chi(\boldsymbol{\Phi}, \sigma_{0,k})\boldsymbol{B}_{\Phi}^{-1}\boldsymbol{e}_{n+1}, \tag{3.138}$$

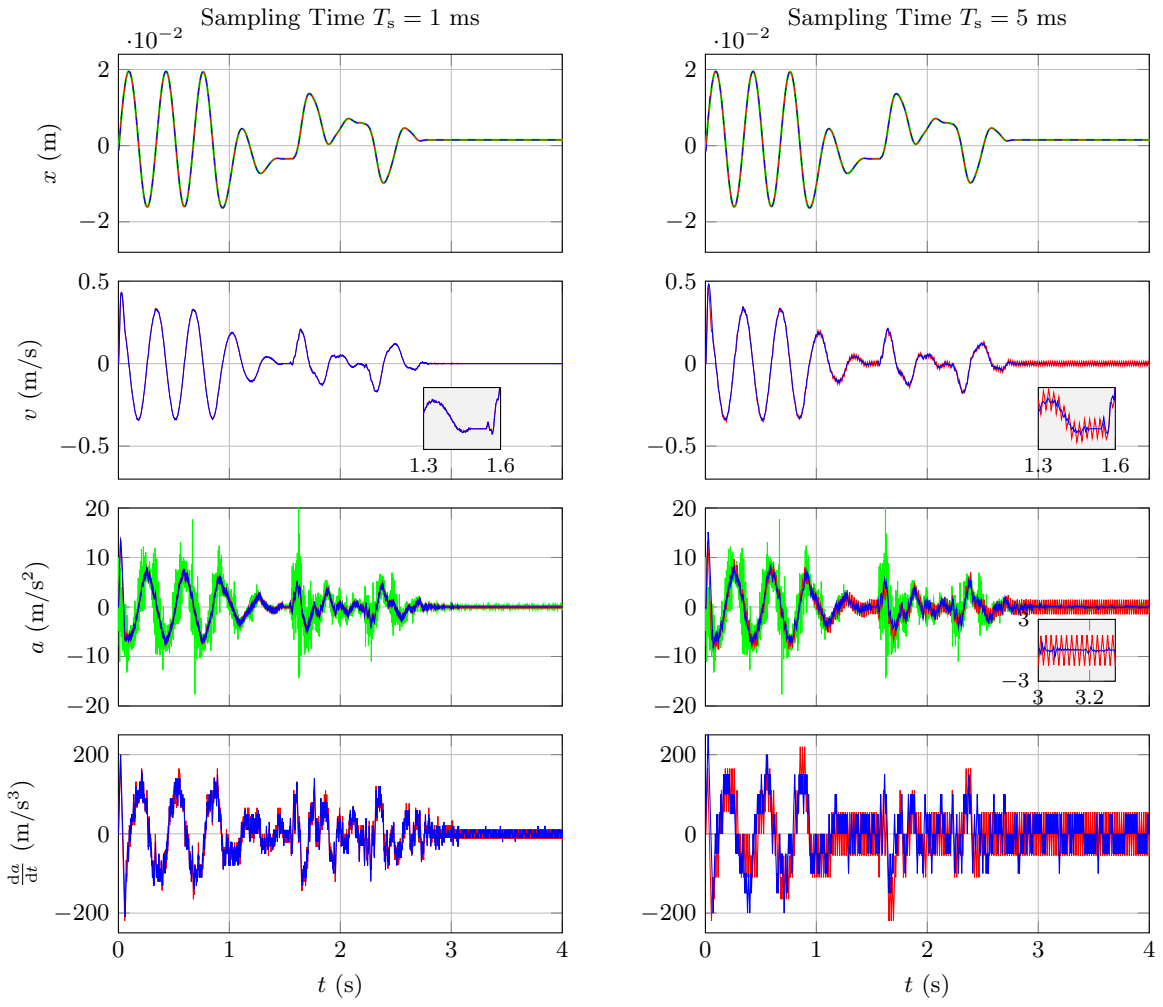

Figure 3.19: Comparison of the HDD and the GHDD by differentiating a displacement signal in a real-time environment. The experiment is carried out with sampling time $T_s = 1$ ms and $T_s = 5$ ms. The coloring is: (——) Measured Signal, (——) HDD, (——) GHDD. With increasing sampling time the chattering effects become clearly visible when using the HDD. The GHDD allows to significantly reduce the oscillation amplitude in the estimated derivatives, except in the last channel.

with $\boldsymbol{B}_\Phi$ being the observability matrix (3.129) and

$$\chi(\boldsymbol{\Phi}, \sigma_{0,k}) = \prod_{i=0}^{n} (\boldsymbol{\Phi} - q_i(T_\mathrm{s}, \sigma_{0,k})\boldsymbol{I}), \tag{3.139}$$

where q_i are the desired eigenvalues of the closed-loop dynamic matrix. The desired characteristic polynomial is denoted by

$$\chi(z, \sigma_{0,k}) = \prod_{i=0}^{n} (z - q_i(T_\mathrm{s}, \sigma_{0,k})) = 0.$$

The differentiator design is therefore reduced to the selection of a set of appropriate closed-loop eigenvalues q_i, $i = 0 \dots n$ in (3.139). As in the case of the STA, appropriate eigenvalues are obtained by a mapping of the eigenvalues of the continuous-time differentiator (3.111) to the discrete-time domain. The GHDD, presented in the previous section, is obtained by selecting the mapping

$$q_i = 1 + T_\mathrm{s} s_i(\sigma_{0,k}). \tag{3.140}$$

Substituting (3.111) into the mapping (3.140) yields

$$q_i = 1 + T_\mathrm{s} p_i |\sigma_{0,k}|^{\frac{r_1}{r_0}-1}. \tag{3.141}$$

The eigenvalues (3.141) are the same eigenvalues as those of the matrix $\boldsymbol{I} + T_\mathrm{s}\left(\boldsymbol{A} - \boldsymbol{\psi}(\sigma_{0,k})\boldsymbol{e}_1^\mathrm{T}\right)$, i.e., this approach is equivalent to the forward Euler discretization of the closed-loop system (3.108). Another possible choice of the mapping is the matching approach, which has been studied in course of the STA. It is given by

$$q_i = e^{T_\mathrm{s} s_i(\sigma_{0,k})}. \tag{3.142}$$

Substituting (3.111) into the mapping (3.142) yields

$$q_i = e^{T_\mathrm{s} p_i |\sigma_0|^{\frac{r_1}{r_0}-1}}. \tag{3.143}$$

The differentiator obtained with eigenvalue assignment (3.143) and $d = -1$ is termed *Matching* HDD.

In the same manner as has already been seen for the STA, in the continuous-time case the absolute value of the the eigenvalues (3.111) approaches infinity as the absolute value of the tracking error σ_0 tends to zero. Similar, when applying the forward Euler scheme to the closed-loop system, the absolute value of the eigenvalues z_i also approach infinity, see the locus plotted in Figure 3.20 for the second order differentiator ($n = 2$). Exploiting the matching approach (3.143), in particular if $\Re(p_i) < 0$ then $\lim_{|\sigma_{0,k}| \to 0} z_i = 0$ holds, see red colored locus in Figure 3.20. Despite these very different behavior in the limit $|\sigma_0| \to 0$ both discrete-time differentiators are a numerical scheme of the original continuous-time differentiator.

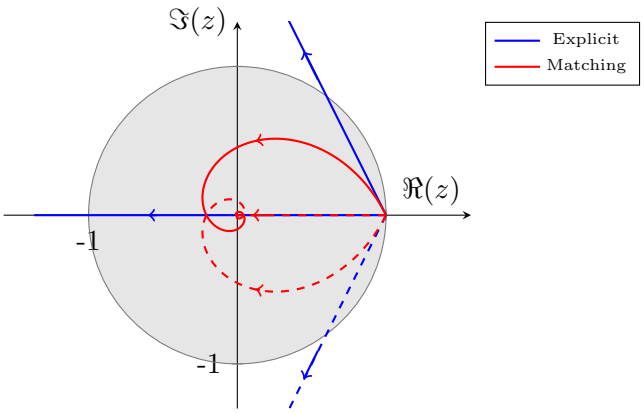

Figure 3.20: Eigenvalue locus for $|\sigma_{0,k}| \to 0$. The parameters are $k_0 = 3$, $k_1 = 7$, $k_2 = 5$ and $T_\mathrm{s} = 0.05$ s.

Proposition 4.1

In every compact set not including $\sigma_{0,k} = 0$, the solutions of the estimation error dynamics (3.137) formed by the discrete-time differentiator obtained from (3.135) and (3.136) with the eigenvalue choice (3.141) or (3.143) approximate the solutions of the error dynamics (3.108) formed by continuous-time differentiator (3.106) as $T_\mathrm{s} \to 0$.

Proof. The limit computes as

$$\lim_{T_\mathrm{s}\to 0} \frac{1}{T_\mathrm{s}}(\boldsymbol{\sigma}_{k+1} - \boldsymbol{\sigma}_k) = \lim_{T_\mathrm{s}\to 0} \left(\frac{1}{T_\mathrm{s}}[\boldsymbol{\Phi} - \boldsymbol{I} - \boldsymbol{\lambda}(\sigma_{0,k})\boldsymbol{e}_1^\mathrm{T}]\boldsymbol{\sigma}_k + \boldsymbol{h}_k \right).$$

As $\lim_{T_\mathrm{s}\to 0} \frac{1}{T_\mathrm{s}}(\boldsymbol{\Phi} - \boldsymbol{I}) = \boldsymbol{A}$ and $\lim_{T_\mathrm{s}\to 0} \boldsymbol{h}_k = \boldsymbol{e}_{n+1} f^{(n+1)}$ holds, it remains to show that

$$\lim_{T_\mathrm{s}\to 0} \frac{1}{T_\mathrm{s}} \boldsymbol{\lambda}(\sigma_{0,k}) \stackrel{!}{=} \boldsymbol{\psi}(\sigma_0), \tag{3.144}$$

or, using (3.138) and rewriting $\boldsymbol{\psi}(\sigma_0)$ in terms of Ackermann's formula, one gets

$$\lim_{T_\mathrm{s}\to 0} \frac{1}{T_\mathrm{s}} \prod_{i=0}^{n} (\boldsymbol{\Phi} - q_i(T_\mathrm{s}, \sigma_{0,k})\boldsymbol{I}) \boldsymbol{B}_\Phi^{-1} \boldsymbol{e}_{n+1} \stackrel{!}{=} \prod_{i=0}^{n} (\boldsymbol{A} - s_i(\sigma_0)\boldsymbol{I}) \boldsymbol{e}_{n+1}. \tag{3.145}$$

The relation

$$\lim_{T_\mathrm{s}\to 0} \frac{1}{T_\mathrm{s}^{n+1}} \prod_{i=0}^{n} (\boldsymbol{\Phi} - q_i(T_\mathrm{s}, \sigma_{0,k})\boldsymbol{I}) = \prod_{i=0}^{n} (\boldsymbol{A} - s_i(\sigma_0)\boldsymbol{I}) \tag{3.146}$$

holds for the choices (3.141) and (3.143). Furthermore, taking into account the structure of $\boldsymbol{\Phi}$, and considering the equation

$$\begin{bmatrix} y_k \\ y_{k+1} \\ \vdots \\ y_{k+n} \end{bmatrix} \stackrel{!}{=} \boldsymbol{e}_{n+1} = \begin{bmatrix} 0 \\ 0 \\ \vdots \\ 1 \end{bmatrix} = \begin{bmatrix} \boldsymbol{e}_1^\mathrm{T} \\ \boldsymbol{e}_1^\mathrm{T}\boldsymbol{\Phi} \\ \vdots \\ \boldsymbol{e}_1^\mathrm{T}\boldsymbol{\Phi}^n \end{bmatrix} \begin{bmatrix} x_{0,k} \\ x_{1,k} \\ \vdots \\ x_{n,k} \end{bmatrix} = \boldsymbol{B}_\Phi \boldsymbol{x}_k, \tag{3.147}$$

it is clear that $\boldsymbol{x} = \boldsymbol{B}_\Phi^{-1}\boldsymbol{e}_{n+1}$ has to satisfy the structure

$$\boldsymbol{B}_\Phi^{-1}\boldsymbol{e}_{n+1} = \begin{bmatrix} 0 & \tilde{\beta}_1 \frac{1}{T_\mathrm{s}} & \tilde{\beta}_2 \frac{1}{T_\mathrm{s}^2} & \dots & \tilde{\beta}_n \frac{1}{T_\mathrm{s}^n} \end{bmatrix}^\mathrm{T}, \quad \beta_i \in \mathbb{R}. \tag{3.148}$$

In view of (3.147) and due to the fact that (3.114) describes an exact discretization of an integrator chain, it is obvious that for the last coefficient $\tilde{\beta}_n = 1$ holds. Thus,

$$\lim_{T_\mathrm{s}\to 0} T_\mathrm{s}^n \boldsymbol{B}_\Phi^{-1}\boldsymbol{e}_{n+1} = \boldsymbol{e}_{n+1}. \tag{3.149}$$

Considering (3.146) and (3.149) in (3.145) confirms (3.144) which completes the proof. □

In the following it is shown, that under certain conditions placed on the eigenvalues, the estimation error dynamics given in (3.137) also preserves this scaling property with respect to (3.118).

Lemma 4.3

If the desired eigenvalues $q_i(T_\mathrm{s},\, \sigma_{0,k})$ satisfy

$$q_i(\kappa T_\mathrm{s},\, \kappa^{n+1}\sigma_{0,k}) = q_i(T_\mathrm{s},\, \sigma_{0,k})$$

$\forall \kappa > 0$, then the error dynamics (3.137) are invariant w.r.t. the scaling (3.118).

Proof. If the relation

$$\boldsymbol{K}^{-1}[\boldsymbol{\Phi}(\kappa T_\mathrm{s}) - \boldsymbol{\lambda}(\kappa T_\mathrm{s}, \kappa^{n+1}\sigma_{0,k})\boldsymbol{e}_1^\mathrm{T}]\boldsymbol{K} \stackrel{!}{=} [\boldsymbol{\Phi}(T_\mathrm{s}) - \boldsymbol{\lambda}(T_\mathrm{s}, \sigma_{0,k})\boldsymbol{e}_1^\mathrm{T}],$$

where

$$\boldsymbol{K} = \begin{bmatrix} \kappa^{n+1} & & & \\ & \kappa^n & & \\ & & \ddots & \\ & & & \kappa \end{bmatrix},$$

holds, the trajectories satisfy the scaling property. Exploiting $\boldsymbol{K}^{-1}\boldsymbol{A}^l\boldsymbol{K}\kappa^l = \boldsymbol{A}^l, l = 0, 1, \dots n+1$ and using the series expansion of $\boldsymbol{\Phi}(T_\mathrm{s})$ it is easy to show that

$$\boldsymbol{K}^{-1}\boldsymbol{\Phi}(\kappa T_\mathrm{s})\boldsymbol{K} = \boldsymbol{\Phi}(T_\mathrm{s}). \tag{3.150}$$

Therefore it is sufficient to check whether the remaining part satisfies the invariance property, i.e.,

$$\boldsymbol{K}^{-1}\boldsymbol{\lambda}(\kappa T_\mathrm{s}, \kappa^{n+1}\sigma_{0,k})\boldsymbol{e}_1^\mathrm{T}\boldsymbol{K} \stackrel{!}{=} \boldsymbol{\lambda}(T_\mathrm{s}, \sigma_{0,k})\boldsymbol{e}_1^\mathrm{T} \tag{3.151}$$

with

$$\boldsymbol{\lambda}(T_\mathrm{s}, \sigma_{0,k}) = \prod_{i=0}^{n}(\boldsymbol{\Phi}(T_\mathrm{s}) - q_i(T_\mathrm{s}, \sigma_{0,k})\boldsymbol{I})\boldsymbol{B}_\Phi^{-1}(T_\mathrm{s})\boldsymbol{e}_{n+1}.$$

From (3.148) one gets

$$\boldsymbol{B}_{\Phi}^{-1}(\kappa T_{\mathrm{s}})\boldsymbol{e}_{n+1}\boldsymbol{e}_1^{\mathrm{T}}\boldsymbol{K} = \boldsymbol{K}\boldsymbol{B}_{\Phi}^{-1}(T_{\mathrm{s}})\boldsymbol{e}_{n+1}\boldsymbol{e}_1^{\mathrm{T}}. \tag{3.152}$$

Under the given assumptions one has

$$\begin{aligned}\boldsymbol{K}^{-1}\prod_{i=0}^{n}(\boldsymbol{\Phi}(\kappa T_{\mathrm{s}}) - q_i(\kappa T_{\mathrm{s}}, \kappa^{n+1}\sigma_{0,k})\boldsymbol{I})\boldsymbol{K} = \boldsymbol{K}^{-1}\prod_{i=0}^{n}(\boldsymbol{\Phi}(\kappa T_{\mathrm{s}}) - q_i(T_{\mathrm{s}}, \sigma_{0,k})\boldsymbol{I})\boldsymbol{K} = \\ \boldsymbol{K}^{-1}\Big[\boldsymbol{\Phi}((n+1)\kappa T_{\mathrm{s}}) + a_n(T_{\mathrm{s}}, \sigma_{0,k})\boldsymbol{\Phi}(n\kappa T_{\mathrm{s}}) + \dots \\ + a_1(T_{\mathrm{s}}, \sigma_{0,k})\boldsymbol{\Phi}(\kappa T_{\mathrm{s}}) + a_0(T_{\mathrm{s}}, \sigma_{0,k})\boldsymbol{I}\Big]\boldsymbol{K},\end{aligned} \tag{3.153}$$

where the coefficients $a_i(T_{\mathrm{s}}, \sigma_{0,k})$ are given by Vieta's formula. Exploiting once more (3.150) in (3.153) yields

$$\boldsymbol{K}^{-1}\prod_{i=0}^{n}(\boldsymbol{\Phi}(\kappa T_{\mathrm{s}}) - q_i(\kappa T_{\mathrm{s}}, \kappa^{n+1}\sigma_{0,k})\boldsymbol{I})\boldsymbol{K} = \prod_{i=0}^{n}(\boldsymbol{\Phi}(T_{\mathrm{s}}) - q_i(T_{\mathrm{s}}, \sigma_{0,k})\boldsymbol{I}). \tag{3.154}$$

Putting together (3.152) and (3.154) gives (3.151) which completes the proof. □

In the following analysis, focus is placed on the Matching HDD. For the differentiator similar results are obtained as for the STA. As stated in the next theorem, this choice allows to avoid the discretization chattering.

Theorem 4.2

Suppose that $d = -1$, $L = 0$ and let the gains k_i be chosen s.t. $\Re(p_i) < 0$, $i = 0, \dots, n$. Under these conditions the origin of the discrete-time error dynamics (3.137), obtained with the differentiator (3.135) with (3.136) and (3.143) is locally asymptotically stable.

Proof. The r.h.s. of the closed-loop system satisfies

$$\boldsymbol{\sigma}_{k+1} = \boldsymbol{M}_{\mathrm{d}}(\sigma_{0,k})\boldsymbol{\sigma}_k = \boldsymbol{M}_{\mathrm{d}}(0)\boldsymbol{\sigma}_k + \boldsymbol{h}(\sigma_{0,k}) \tag{3.155}$$

where $\boldsymbol{M}_{\mathrm{d}}(\sigma_{0,k}) = [\boldsymbol{\Phi} - \boldsymbol{\lambda}(\sigma_{0,k})\boldsymbol{e}_1^{\mathrm{T}}]$. The vector field $\boldsymbol{h}(\sigma_{0,k})$ is continuous and

$$\lim_{\|\sigma_{0,k}\|\to 0} = \frac{\|\boldsymbol{h}(\sigma_{0,k})\|}{\|\sigma_{0,k}\|} = 0 \tag{3.156}$$

holds. The evolution operator $\boldsymbol{M}_{\mathrm{d}}(0)$ is a stable matrix, i.e., $\boldsymbol{M}_{\mathrm{d}}(0)$ is a Schur matrix. From Lyapunov's indirect method for discrete-time systems, see, e.g., [88, 94], it is concluded that the origin of the nonlinear system is asymptotically stable. The quadratic form

$$V_k = \boldsymbol{\sigma}_k^{\mathrm{T}}\boldsymbol{P}\boldsymbol{\sigma}_k, \tag{3.157}$$

with $\boldsymbol{P}$ satisfying the Lyapunov equation

$$\boldsymbol{M}_{\mathrm{d}}(0)^{\mathrm{T}}\boldsymbol{P}\boldsymbol{M}(0)_d - \boldsymbol{P} = -\boldsymbol{I} \tag{3.158}$$

is locally a Lyapunov function for (3.155). □

For $d = -1$ the trajectories converge much faster to the origin compared to the linear differentiator obtained with $d = 0$.

Theorem 4.3

Under the conditions stated in Theorem 4.2, the error variables converge locally with hyper exponential speed to the origin.

The following Lemma is helpful in the Proof of Theorem 4.3.

Lemma 4.4

Under the conditions given in Theorem 4.2, the trajectories approach the origin along the eigenvector $\boldsymbol{a}$ of $\boldsymbol{M}_{\mathrm{d}}(0)$.

Proof. Matrix $\boldsymbol{M}_{\mathrm{d}}(0)$ has $n+1$ eigenvalues $\tilde{z} = 0$ and one corresponding eigenvector $\boldsymbol{a}$ obtained from

$$\boldsymbol{M}_{\mathrm{d}}(0)\boldsymbol{a} = \boldsymbol{0}.$$

Taking into account (3.156) it is evident that an arbitrary small neighborhood of the origin the linear part dominates the dynamics in (3.155), i.e., as $k \to \infty$ the error dynamics are governed by the recursion

$$\boldsymbol{\sigma}_{k+1} = \boldsymbol{M}_{\mathrm{d}}(0)\boldsymbol{\sigma}_k.$$

The matrix $\boldsymbol{M}_{\mathrm{d}}(0)$ is nilpotent with degree $n+1$, i.e.,

$$\boldsymbol{\sigma}_{n+1} = \boldsymbol{M}_{\mathrm{d}}(0)^{n+1}\boldsymbol{\sigma}_0 = \boldsymbol{M}_{\mathrm{d}}(0)\boldsymbol{M}_{\mathrm{d}}(0)^{n}\boldsymbol{\sigma}_0 = \boldsymbol{0}$$

Thus, for $\boldsymbol{\sigma}_n = \boldsymbol{M}_{\mathrm{d}}(0)^{n}\boldsymbol{\sigma}_0 \neq \boldsymbol{0}$ the vector $\boldsymbol{\sigma}_n$ must be an eigenvector of $\boldsymbol{M}_{\mathrm{d}}(0)$, i.e., after n steps the initial state is transferred to $\boldsymbol{\sigma}_n = \alpha\boldsymbol{a}$, $\alpha \in \mathbb{R}$. Therefore, as $k \to \infty$ the trajectories convergence along the eigenvector $\boldsymbol{a}$ to the origin. □

Proof. Hyper-exponential rate of convergence requires

$$V_{k+1} = \mu_k V_k, \quad \lim_{k\to\infty} \mu_k = \lim_{k\to\infty} \frac{V_{k+1}}{V_k} = 0.$$

Substituting the closed-loop system (3.155) into (3.157) allows to write

$$\lim_{k\to\infty} \frac{V_{k+1}}{V_k} = \lim_{k\to\infty} \frac{\boldsymbol{\sigma}_k^{\mathrm{T}} \left(\boldsymbol{M}_{\mathrm{d}}(0)^{\mathrm{T}}\boldsymbol{P}\boldsymbol{M}_{\mathrm{d}}(0)\right)\boldsymbol{\sigma}_k + f(\boldsymbol{h}(\sigma_{0,k}))}{\boldsymbol{\sigma}_k^{\mathrm{T}}\boldsymbol{P}\boldsymbol{\sigma}_k}. \tag{3.159}$$

From the Lyapunov equation (3.158) one obtains

$$\boldsymbol{M}_{\mathrm{d}}(0)^{\mathrm{T}}\boldsymbol{P}\boldsymbol{M}(0)_d\boldsymbol{a} = [\boldsymbol{P} - \boldsymbol{I}]\,\boldsymbol{a} = \boldsymbol{0}, \tag{3.160}$$

i.e., $\boldsymbol{a}$ also is an eigenvector of $\boldsymbol{P}$ associated with the (invariant) eigenvalue $\tilde{s}_1 = 1$, $\forall T_{\mathrm{s}}$. Substituting (3.160) into (3.159) gives

$$\lim_{k\to\infty} \mu_k = \lim_{k\to\infty} \frac{\boldsymbol{\sigma}_k^{\mathrm{T}} \left(\boldsymbol{P} - \boldsymbol{I}\right)\boldsymbol{\sigma}_k + f(\boldsymbol{h}(\sigma_{0,k}))}{\boldsymbol{\sigma}_k^{\mathrm{T}}\boldsymbol{P}\boldsymbol{\sigma}_k}.$$

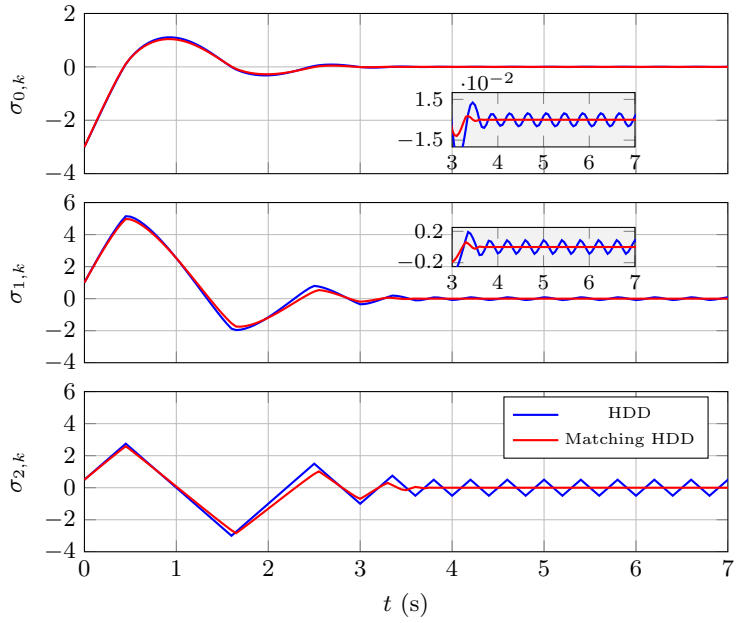

Figure 3.21: Estimation errors for $n = 2$ and $f^{(3)} \equiv 0$. The HDD features practical stability whilst the Matching HDD ensures asymptotic stability of the origin whenever the $(n+1)^{\text{th}}$ derivative vanishes. The parameters are $k_0 = 3$, $k_1 = 7$, $k_2 = 5$ and $T_\text{s} = 0.05$ s.

Using (3.156) and Lemma 4.4 one gets

$$\lim_{k\to\infty} \mu_k = \lim_{k\to\infty} 1 - \frac{\boldsymbol{\sigma}_k^\mathrm{T}\boldsymbol{\sigma}_k}{\boldsymbol{\sigma}_k^\mathrm{T}\boldsymbol{P}\boldsymbol{\sigma}_k^\mathrm{T}} = 1 - \frac{\boldsymbol{a}^\mathrm{T}\boldsymbol{a}}{\boldsymbol{a}^\mathrm{T}\tilde{s}_1\boldsymbol{a}} = 0$$

which completes the proof. □

Note that for the choice $d = 0$ and $L = 0$, i.e., for the linear differentiator, the gain selection $\Re(p_i) < 0$ is necessary and sufficient for global asymptotic stability. In this case, the trajectories converge exponentially to the origin. The mapping (3.143) ensures that the discrete-time error dynamics are globally asymptotically stable iff the corresponding continuous-time algorithm yields globally asymptotically stable error dynamics, see, e.g., [112].

Simulation Study & Experiments

Figure 3.21 compares the trajectories obtained with a second-order ($n = 2$) HDD to the Matching HDD. In this example the same parameter setting k_0, k_1, k_2 is used for the HDD and the Matching HDD and $L = 0$. In case of the HDD the trajectories show the discretization chattering whereas the Matching HDD provides for convergence to the origin. The convergence speed is demonstrated in Figure. 3.22. The plot shows the norm of the error variables over time on a logarithmic scale. The HDD ensures only practical stability, i.e., converges to a neighborhood of the origin. Additionally, the plot shows the results obtained with a linear

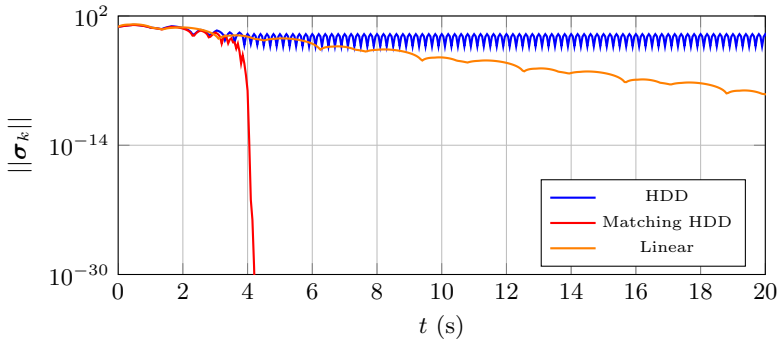

Figure 3.22: Illustration of the convergence rate obtained with the HDD, the Matching HDD and a linear differentiator ($d = 0$) for $f^{(n+1)} \equiv 0$ and $n = 2$. The parameters are $k_0 = 3$, $k_1 = 7$, $k_2 = 5$ and $T_\mathrm{s} = 0.05$ s.

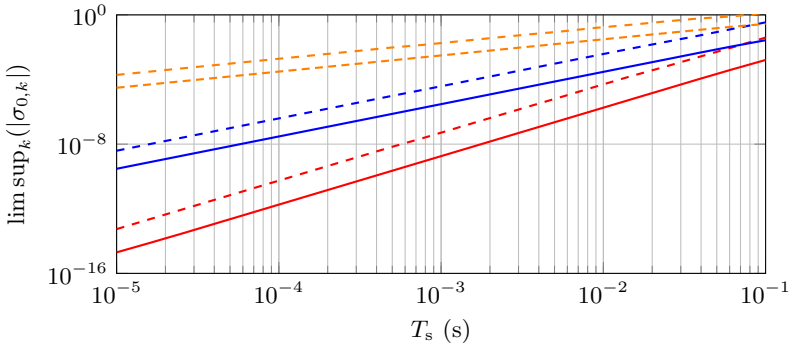

Figure 3.23: Comparison of the asymptotic accuracies for $n = 2$ demonstrating that the (——) Matching HDD offers the same asymptotic accuracies as the (- - -) HDD. The parameters are $k_0 = 3$, $k_1 = 7$, $k_2 = 5$, $T_\mathrm{s} = 0.05$ s and $f^{(3)} = 0.3\sin(2kT_\mathrm{s}) + \cos(\sqrt{10}kT_\mathrm{s})$. Coloring: (——) σ_0, (——) σ_1, (——) σ_2.

differentiator which provides for exponential stability. Compared to that, the Matching HDD provides for much faster convergence to the origin.

For $L > 0$ the Matching HDD provides for the same asymptotic accuracies as the HDD, see Figure 3.23, i.e., the trajectories converge to the real sliding set

$$\mathcal{R} = \{\boldsymbol{\sigma}_k \in \mathbb{R}^3 : |\sigma_{0,k}| \leq \mu_0 T_\mathrm{s}^3, |\sigma_{1,k}| \leq \mu_1 T_\mathrm{s}^2, \ |\sigma_{2,k}| \leq \mu_2 T_\mathrm{s}\},$$

where μ_i are some positive constants. For the specific example the Matching HDD offers better precision than the HDD, i.e., the constants μ_i are smaller.

In the next simulation, given in Figure 3.24, the sampling time T_s is fixed and the gains are subject to the homogeneous scaling $k_0 = \tilde{k}_0\Lambda^{\frac{1}{3}}$, $k_1 = \tilde{k}_1\Lambda^{\frac{2}{3}}$, $k_2 = \tilde{k}_2\Lambda$ with $\Lambda > 0$. As it can be seen, the trajectories start to converge as soon as Λ exceeds a certain value ($\Lambda > L/\tilde{k}_2$). Further increasing Λ in the HDD eventually leads to a deterioration of the precision, whereas the precision is maintained with the Matching HDD when overestimating Λ. From Figure 3.14 it may seem reasonable to increase the scaling $\Lambda \to \infty$ in order to ensure the best possible precision. However, in the presence of noise this approach might be detrimental.

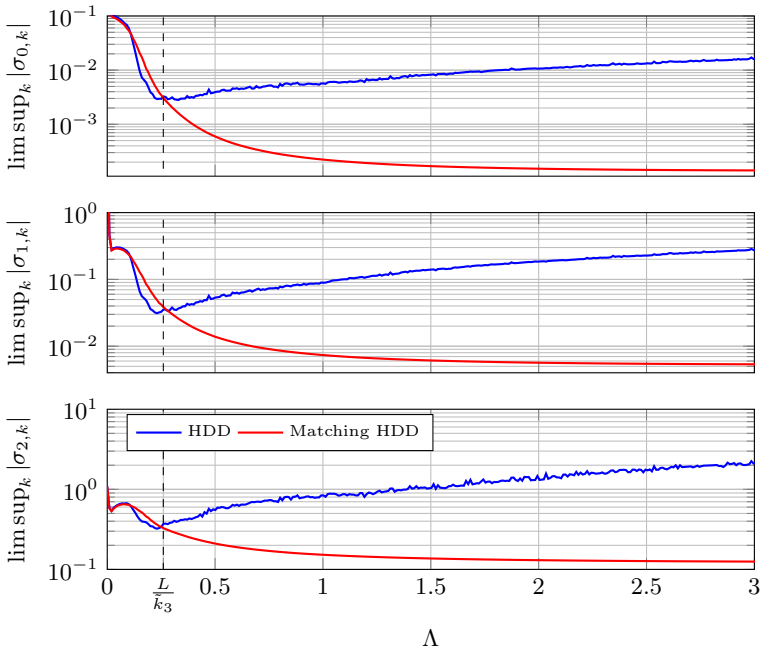

Figure 3.24: Influence of an overestimation of the gains on the precision in the case of $n = 2$. The gains are subject to the homogeneous scaling $k_0 = \tilde{k}_0\Lambda^{\frac{1}{3}}$, $k_1 = \tilde{k}_1\Lambda^{\frac{2}{3}}$, $k_2 = \tilde{k}_2\Lambda$ where $\tilde{k}_0 = 3$, $\tilde{k}_1 = 7$, $\tilde{k}_2 = 5$ and $f^{(3)} = 0.3\sin(2kT_\mathrm{s}) + \cos(\sqrt{10}kT_\mathrm{s})$. The sampling time $T_\mathrm{s} = 0.05$ s.

The Matching HDD is compared to the GHDD by differentiating the same displacement signal as in the previous section when the GHDD has been compared to the HDD. The parameter setting is the same as used in the previous comparison. The results are given in Figure 3.25. Also here the experiment is carried out with two different sampling times ($T_\mathrm{s} = 1$ ms and $T_\mathrm{s} = 5$ ms). For the larger sampling time also the GHDD exhibits significant chattering in the last channel whilst the discretization chattering is avoided by the Matching HDD. This can be seen clearly in time intervals where the $(n+1)$ th derivative vanishes (see $t > 3$ s). There, the Matching HDD ensures convergence to the origin and the tracking error vanishes.

It has been demonstrated, that the proposed differentiator (Matching HDD) preserves the asymptotic accuracies $\limsup_k |\sigma_i| \propto T_\mathrm{s}^{n-i+1}$ and the precision is insensitive to an overestimation of the gains. Local asymptotic stability of the origin has been proven for the unperturbed error dynamics by means of Lyapunov's indirect method. Furthermore, the trajectories converge with hyper exponential speed to the origin whenever the $(n+1)^{\text{th}}$ derivative vanishes. It is noteworthy, that also this discretization scheme is applicable to the family of differentiators including the linear, nonlinear continuous as well as discontinuous differentiators. In the following section the presented discrete-time variants of the arbitrary-order RED are compared with state-of-the-art numerical derivative estimators.

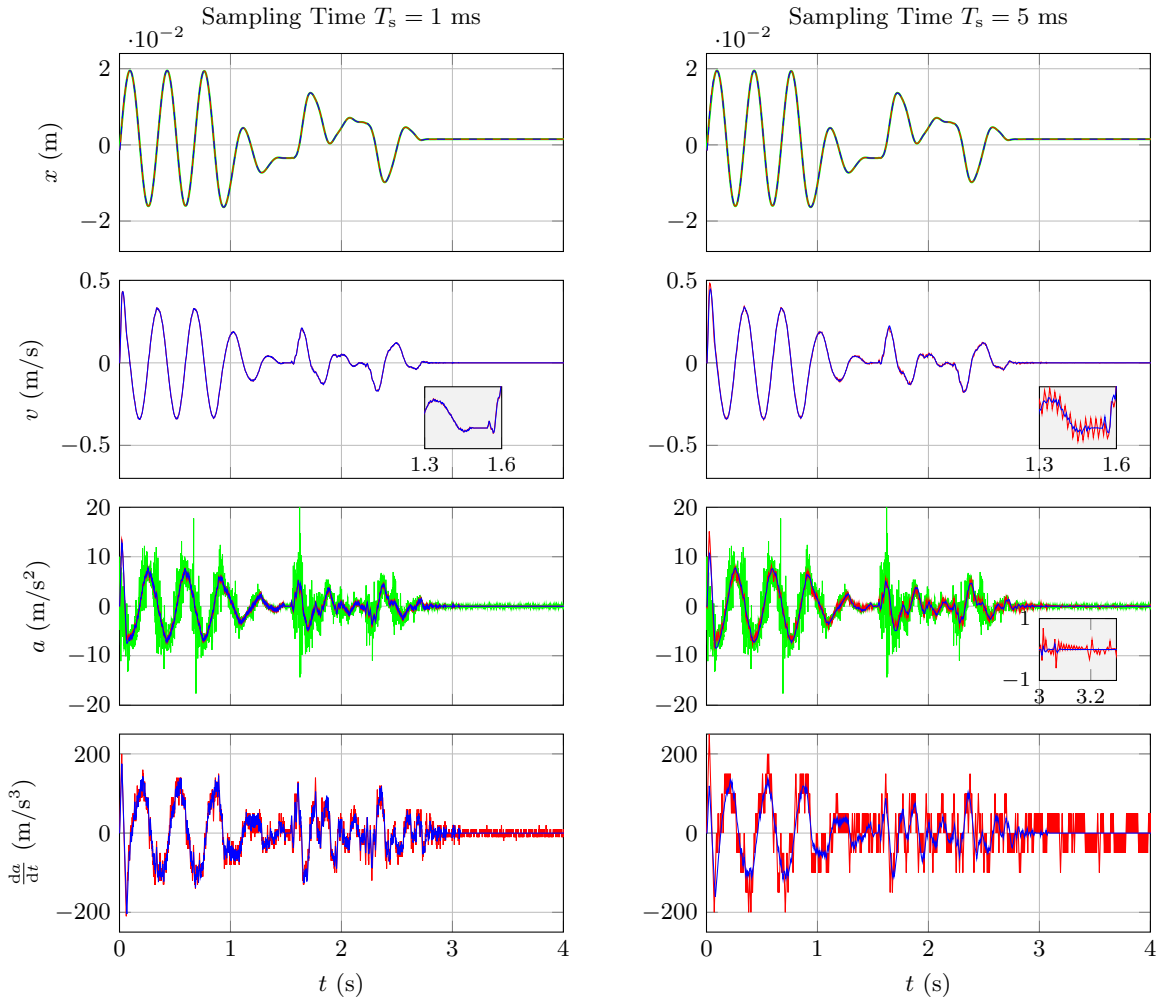

Figure 3.25: Comparison of the Matching HDD and the GHDD by differentiating a displacement signal in a real-time environment. The experiment is carried out with sampling times $T_s = 1$ ms and $T_s = 5$ ms. The coloring is: (—) Measured Signal, (—) GHDD, (—) Matching HDD.

Matlab/Simulink® Differentiator Toolbox

The Matching HDD has been implemented in a new version of the MATLAB/Simulink® robust exact differentiator toolbox originally presented in [113]. The toolbox, which can be used for both numerical simulation studies as well as for real-time experiments, is freely available at `www.reichharting.at`. Following the design of the discrete-time differentiator it is clear that the tuning of the differentiator can be carried out by specifying $n+1$ roots p_i of the polynomial given in equation (3.110). It is of interest to provide a toolbox implementing the proposed differentiation strategy in order to offer an intuitive and straightforward way to integrate the algorithm into existing simulation and real world implementations. To reduce the number of tuning parameters, all roots are selected as $p_i = -c$, where the positive real constant c can be adjusted by the user of the toolbox. This choice of the roots yields the desired closed-loop eigenvalues

$$q_i(T_\mathrm{s}, \sigma_{0,k}) = \mathrm{e}^{-cT_\mathrm{s}|\sigma_{0,k}|^{-\frac{1}{n+1}}}.$$

The choice of repeated roots significantly reduces the computational effort required in implementation. Note that k_n is equal to the product of the specified eigenvalues and therefore $k_n = c^{n+1}$. In the case of a known Lipschitz constant L and considering that $k_n > L$ it is necessary to select $c > L^{\frac{1}{n+1}}$. This is consistent with the strategy adopted in a previous version of the toolbox, where the tuning was also reduced to a single positive real parameter. The differentiator block requires the signal $f(t)$ as the input signal and it provides the estimation error $\sigma_{0,k}$ and the estimates $\hat{\boldsymbol{x}}_k$ as output signals. The parameters T_s and c can be adjusted as parameters of the differentiator block and the desired order n of the differentiator can also be chosen. As in the previous version, the maximum available differentiator order is set to $n = 10$. A code fragment of the implementation of the Matching HDD is shown in Figure 3.26. It is noteworthy, that the Matching HDD is given by explicit recursion; no implicit equations need to be solved. Therefore, the implementation of the differentiator is straightforward. Furthermore, the eigenvalue based approach allows to obtain various realization, such as the GHDD, the Matching HDD or even an implicit version of the robust exact differentiator by changing one single code line in the implementation. In the particular example in Figure 3.26, computing the eigenvalues from line 9 gives a Matching HDD whilst code line 10 yields the GHDD. An implicit version is obtained by selecting the eigenvalues according to (3.93), which is implemented in code line 11.

3.4.7 Comparison to State-of-the-Art Methods

As already mentioned in the introductory part, there are several methods available in literature to estimate the derivative of a measured signal. Basically every state observer might be exploited as a real-time differentiator. Besides the arbitrary-order robust exact differentiator, the algebraic differentiator, the HGO or the Kalman filter are often used as real-time differentiators. Additionally, in real control problems so-called derivative filters are often used. In contrast to the sliding mode based differentiator, these differentiators basically rely on linear algorithms. Therefore, in general this algorithms are not capable to estimate the derivatives exact, even in an ideal scenario, i.e., in the continuous-time domain without noise. However, in practical applications, where noise and discretization effects come into play, these differentiators usually

```
n = 2;                                  % n ... order of the differentiator

% Compute Error
sigma_0=f-xp(1);                        % sigma_0 ... estimation error
if abs(sigma_0) == 0
        z = 0;
else
        s = -c*(abs(sigma_0))^(-1/(n+1));  % current eigenvalue
        z = exp(tau*s);                    % Matching HDD
        %z = 1+s*tau;                      % GHDD
        %z = 1/(1-(s*tau));                % Implicit discretization
end
% Second Order Differentiator
lambda = ...
[(3 - 3*z)*abs(sigma_0)
(((z - 1)/tau*abs(sigma_0)^(1/2))^2*(z + 5))*tau/2
-((z - 1)/tau*abs(sigma_0)^(1/3))^3*tau];
% Compute Estimates
xp = Phi*xp + lambda*sign(sigma_0);
```

Figure 3.26: Code fragment of the Matching HDD of order $n = 2$ implemented in the MATLAB/Simulink® robust exact differentiator toolbox.

work well and are often, due to chattering effects, preferred over sliding mode based differentiation. In the following, some selected state-of-the-art differentiators are compared to the proposed discrete-time versions of the arbitrary-order RED in simulation. The test signal is generated by the dynamical system

$$\dot{x}_1 = x_2, \quad \dot{x}_2 = x_3, \quad \dot{x}_3 = f(\boldsymbol{x}), \quad y = x_1 + \eta(t) \tag{3.161}$$

where $\boldsymbol{x} = \begin{bmatrix} x_1 & x_2 & x_3 \end{bmatrix}^{\mathrm{T}}$ and

$$\begin{aligned} f(\boldsymbol{x}) &= \alpha(\boldsymbol{x}) g_{\mathrm{s}}(\boldsymbol{x}) + (1 - \alpha(\boldsymbol{x})) g_{\mathrm{u}}(\boldsymbol{x}), \\ \alpha(\boldsymbol{x}) &= 2 \frac{\boldsymbol{x}^{\mathrm{T}} \boldsymbol{x}}{1 + \boldsymbol{x}^{\mathrm{T}} \boldsymbol{x}}, \\ g_{\mathrm{s}}(\boldsymbol{x}) &= -54 x_1 - 36 x_2 - 9 x_3, \\ g_{\mathrm{u}}(\boldsymbol{x}) &= 54 x_1 - 36 x_2 + 9 x_3. \end{aligned}$$

The task is to estimate the state variable x_3 by two times differentiating the sampled noisy output $y_k = y(kT_{\mathrm{s}})$. The variable $\eta(t)$ denotes uniform distributed noise from $\eta(t) \in \epsilon[-1, 1]$. System (3.161) was also utilized in the works [114, 112] to test real-time differentiators. In this experiment the sampling time is set to $T_{\mathrm{s}} = 1$ ms. A second-order HDD, GHDD and a Matching HDD are compared to the HGO, the algebraic differentiator and a classical derivative filter. The second-order HDD and the GHDD are obtained from the general representation (3.136) where the estimation error $\sigma_{0,k} := y_k - \boldsymbol{e}_1^{\mathrm{T}} \hat{\boldsymbol{x}}_k$. Choosing the gains in the same way as in the toolbox implementation, i.e., $p_1 = p_2 = p_3 = -c$, $c \in \mathbb{R}$ yields the injection terms

$$\boldsymbol{\lambda}(\sigma_{0,k}) = \begin{bmatrix} 3 - 3q \\ \frac{1}{2T_{\mathrm{s}}}(q-1)(q^2 + 4q - 5) \\ -\frac{1}{T_{\mathrm{s}}^2}(q-1)^3 \end{bmatrix}, \quad \text{and} \quad \boldsymbol{\Phi} = \begin{bmatrix} 1 & T_{\mathrm{s}} & \frac{T_{\mathrm{s}}^2}{2} \\ 0 & 1 & T_{\mathrm{s}} \\ 0 & 0 & 1 \end{bmatrix}.$$

The choice

$$q = 1 - T_{\mathrm{s}} c |\sigma_{0,k}|^{-\frac{1}{3}}$$

gives the GHDD, whilst choosing

$$q = e^{-T_{\mathrm{s}} c |\sigma_{0,k}|^{-\frac{1}{3}}}$$

yields the Matching HDD. Furthermore, with this framework one can obtain a discrete-time version of the HGO in a straightforward way by simply setting

$$q_i = e^{-T_{\mathrm{s}} \frac{c}{\varepsilon}}, \quad \varepsilon > 0. \tag{3.162}$$

With this choice the injection terms do not depend on the estimation error $\sigma_{0,k}$ anymore and the differentiator takes the form

$$\hat{\boldsymbol{x}}_{k+1} = \left(\boldsymbol{\Phi} - \boldsymbol{\lambda} \boldsymbol{e}_1^{\mathrm{T}} \right) \hat{\boldsymbol{x}}_k + \boldsymbol{\lambda} y_k, \tag{3.163}$$

i.e., it is a LTI system driven by the system output y_k. For the realization of the algebraic differentiator in MATAB/SIMULINK environment the toolbox presented in [115] is used. The second-order derivative filter is obtained by a series connection of a discrete-time differentiator and a low pass filter. Its transfer function is given by

$$H(z) = \frac{\hat{x}_3(z)}{y(z)} = \frac{(z-1)^2}{(T_{\mathrm{s}} z)^2} \frac{(1-p_{\mathrm{z}})^2}{(z-p_{\mathrm{z}})^2} \tag{3.164}$$

where $p_{\mathrm{z}} \in \mathbb{R}$, $|p_{\mathrm{z}}| < 1$ is a tuning parameter.

The tuning of each of the six discrete-time differentiators, the HDD, GHDD, Matching HDD, HGO, algebraic differentiator and the linear differentiation filter is essentially reduced to the selection of one single parameter. In the discrete-time versions of the second-order RED the choice of three repeated roots $p_i = -c$ reduces the tuning to the selection of the parameter c. For the HGO it is convenient to set $c = 1$ in (3.162) which reduces the tuning to the selection of the scaling parameter ε. In case of the algebraic differentiator one has to select the window length, denoted by T, and the order of the Taylor series expansion. It is set to its minimal values, which if interested in the second derivative, equals $N = 2$. The linear filter is tuned by selecting the pole p_{z} of the low pass filter.

It is noteworthy, that the discrete-time realization of the algebraic differentiator constitutes a non-recursive filter, i.e., it has finite impulse response, see, e.g., [103] for more details, unlike the linear differentiation filter (3.164) which is a recursive filter and therefore has an infinite impulse response. The transfer function representation of the HGO (3.163) with $c = 1$ is given by

$$H(z) = \frac{\hat{x}_3(z)}{y(z)} = \frac{(z-1)^3 (e^{-T_{\mathrm{s}} \frac{1}{\varepsilon}} - 1)^2}{T_{\mathrm{s}}^2 (z - e^{-T_{\mathrm{s}} \frac{1}{\varepsilon}})^3},$$

i.e., it also is a LTI system with infinite impulse response.

The test signal for comparing the performance of these six differentiators is generated by simulating system (3.161) with initial conditions $\boldsymbol{x}_0 = \begin{bmatrix} -0.5 & 1 & 3 \end{bmatrix}^{\mathrm{T}}$. The amplitude of the

noise is set to $\epsilon = 1 \cdot 10^{-3}$. The simulation time is set to $T_{\text{sim}} = 10$ s. The mean absolute error (MAE) between the estimated variable $\hat{x}_3$ and the real state variable x_3 serves as criterion for the comparison of the differentiators. The transient phase is excluded by taking only values from $t > 2$ s into account. The MAE is computed by

$$MAE = \frac{1}{N} \sum_{i=0}^{N} |\hat{x}_{3,k} - x_{3,k}|,$$

where N denotes the length of the sequence.

The parameter c in the HDD, GHDD and the Matching HDD is set to $c = 3$ which is slightly greater than the Lipschitz constant of x_3. The Lipschitz constant of x_3 is found by inspection in the simulation. The other differentiators are tuned by minimizing the MAE with the help of MATLAB's nonlinear programming solver *fminsearch*. The results are given in Table 3.1. Simulation results are provided in Figure 3.27, the computed MAE is also found in Table 3.1.

	Tuning Parameter	MAE
HDD	$c = 3$	0.2563
GHDD	$c = 3$	0.2586
Matching HDD	$c = 3$	0.2580
HGO	$\varepsilon = 0.022$	0.2016
Algebraic Differentiator	$T = 0.125$	0.1978
Linear Filter	$p_z = 0.983$	0.3287

Table 3.1: Tuning parameters used for the comparison of the differentiators. The parameter minimizes the mean absolute error when differentiating the test signal.

According to this numbers the algebraic differentiator gives the best results, followed by the high-gain observer. In spite of the different discretization methods the results obtained with the three arbitrary-order RED's are very close to each other. Worst results were achieved with the linear derivative filter.

In the following, the effect of scaling the amplitude by $\epsilon = 1 \cdot 10^{-3}\Upsilon$ is demonstrated. Figure 3.28 gives an idea about the performance of the differentiators when the noise amplitude increases but the algorithms are *not* retuned accordingly. In this simulation the scaling factor is chosen as $\Upsilon = 4$. Figure 3.29 shows the MAE over the scaling factor Υ. For small deviations of the noise amplitude from its nominal values the algebraic differentiator and the high-gain observer still outperform the discrete-time version of the second-order RED. However, if the noise amplitude decreases, the precision obtained with algebraic differentiator, the high-gain observer and the differentiation filter has a horizontal asymptote. The precision further increases with the discrete-time version of the second-order RED as long as the effects due to noise dominate the effects caused by sampling. The algebraic differentiator, the HGO and the differentiation filter, which are essentially linear differentiators, would require a retuning, e.g. increasing the gain in the HGO in order to increase the tracking precision. Such an retuning is unnecessary when applying the second-order RED. In case of increasing noise amplitude the precision diminishes much faster in case of the algebraic differentiator, the HGO and the differentiation filter when compared to the RED.

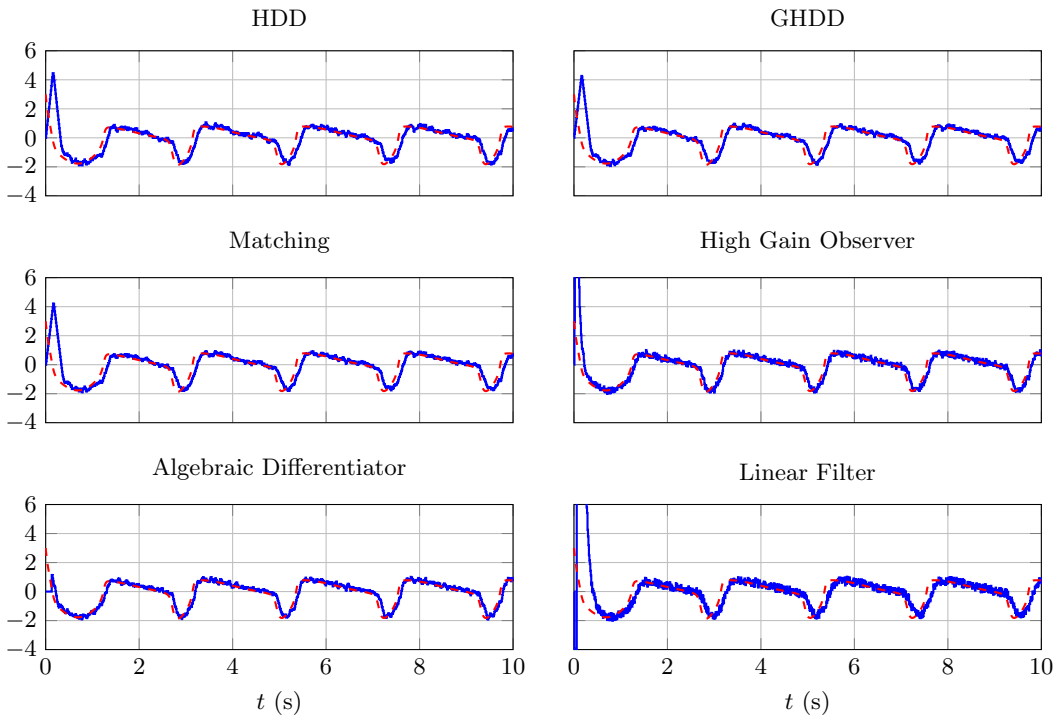

Figure 3.27: Comparison of the differentiators for the nominal noise amplitude.

In the next Section the proposed differentiators are exploited in an output feedback framework. For this purpose the structure of the differentiators is modified to yield a current estimator.

3.5 Output Feedback and Higher-Order Sliding Mode Based Current Estimator

Consider the continuous-time single-input single-output LTI system

$$\begin{aligned} \frac{\mathrm{d}\boldsymbol{x}}{\mathrm{d}t} &= \boldsymbol{A}\boldsymbol{x} + \boldsymbol{b}(u+\varphi), \\ y &= \boldsymbol{c}^{\mathrm{T}}\boldsymbol{x}, \end{aligned} \tag{3.165}$$

with state vector $\boldsymbol{x} \in \mathbb{R}^n$ which is supposed to be regulated by a controller implemented in a discrete-time environment. The output $y(t)$ is sampled with sampling period T_s and the plant input $u(t)$ is reconstructed from the controller output u_k by a ZOH element. The plant itself is assumed to be a chain of n integrators subject to the matched Lipschitz continuous perturbation $\varphi(t) \in \mathbb{R}$, i.e.,

$$\boldsymbol{A} = \begin{bmatrix} \boldsymbol{0}_{(n-1)\times 1} & \boldsymbol{I}_{(n-1)\times(n-1)} \\ 0 & \boldsymbol{0}_{1\times(n-1)} \end{bmatrix}, \quad \boldsymbol{b} = \boldsymbol{e}_n, \quad \boldsymbol{c} = \boldsymbol{e}_1,$$

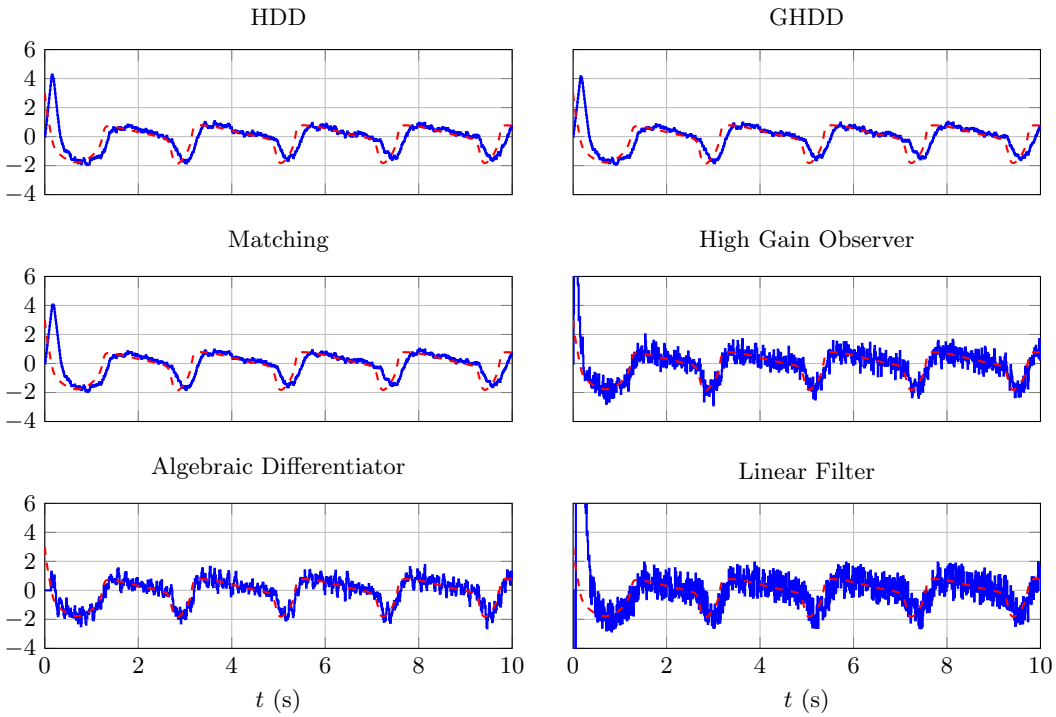

Figure 3.28: Comparison of the differentiators for increased noise amplitude. The differentiators are *not* retuned and the parameters remain the same as in the previous example.

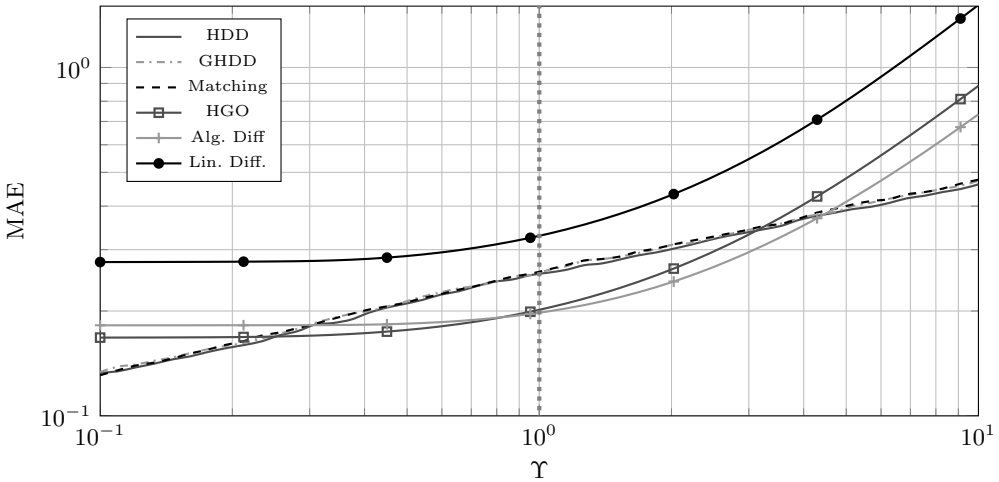

Figure 3.29: Robustness of real-time differentiators against a scaling of the noise amplitude. The case $\Upsilon = 1$ resorts to the nominal scenario for which the tuning has been carried out.

where $\boldsymbol{I}_{(n-1)\times(n-1)}$ denotes the identity matrix of dimension $n-1$ vector $\boldsymbol{e}_i$ denotes the i^{th} standard basis vector. The controller is designed directly in the discrete-time domain. Neglecting the inter-sample effects during the controller design, i.e., it is assumed that the perturbation also enters the plant via the ZOH element, the plant dynamics are described by the discrete-time dynamical model

$$\begin{aligned} \boldsymbol{x}_{k+1} &= \boldsymbol{A}_{\mathrm{d}}\boldsymbol{x}_k + \boldsymbol{b}_{\mathrm{d}}(u_k + \varphi_k), \\ y_k &= \boldsymbol{c}^{\mathrm{T}}\boldsymbol{x}_k, \end{aligned}$$

where $\boldsymbol{A}_{\mathrm{d}} = e^{\boldsymbol{A}T_{\mathrm{s}}}$ and $\boldsymbol{b}_{\mathrm{d}} = \begin{bmatrix} \frac{T_{\mathrm{s}}^n}{n!} & \dots & \frac{T_{\mathrm{s}}^2}{2} & T_{\mathrm{s}} \end{bmatrix}^{\mathrm{T}}$. The task is to make the output y_k take the constant reference value r_∞ in steady state despite the perturbation φ_k. If the perturbation $\varphi_k \equiv 0$, the task is easily solved by a discrete-time state feedback controller

$$u_k = -\boldsymbol{k}^{\mathrm{T}}\boldsymbol{x}_k + Vr_\infty, \quad \boldsymbol{k}^{\mathrm{T}} = \begin{bmatrix} k_1 & \dots & k_n \end{bmatrix}, \tag{3.166}$$

where the constant real values $k_1 \dots k_n$ are designed s.t. the matrix $\boldsymbol{A}_{\mathrm{dcl}} := \boldsymbol{A}_{\mathrm{d}} - \boldsymbol{b}_{\mathrm{d}}\boldsymbol{k}^{\mathrm{T}}$ is Schur and the gain V is chosen[4] s.t. the output tracks a constant reference input, i.e.,

$$V = -\frac{1}{\boldsymbol{e}_1^{\mathrm{T}}(\boldsymbol{A}_{\mathrm{dcl}} - \boldsymbol{I})^{-1}\boldsymbol{b}_{\mathrm{d}}}.$$

However, assuming only the output y_k measurable it is required to replace the measured state vector $\boldsymbol{x}_k$ in (3.166) by and estimate $\hat{\boldsymbol{x}}_k$. Furthermore, in order to render the closed-loop dynamics robust against the perturbation φ_k, an estimated value of the perturbation is incorporated into the control law, i.e.,

$$u_k = -\boldsymbol{k}^{\mathrm{T}}\hat{\boldsymbol{x}}_k - \hat{\varphi}_k + Vr_\infty \tag{3.167}$$

The vector $\hat{\boldsymbol{x}}_k$ includes the estimated state variables and $\hat{\varphi}_k$ represents an estimate of the perturbation. For the realization of the controller an estimate of the state vector, as well as an estimate of the perturbation $\hat{\varphi}_k$, is obtained from an observer. In order to achieve the simultaneous estimation of the state variables and the perturbation, the augmented system

$$\begin{aligned} \frac{\mathrm{d}\boldsymbol{x}_{\mathrm{a}}}{\mathrm{d}t} &= \boldsymbol{A}_{\mathrm{a}}\boldsymbol{x}_{\mathrm{a}} + \boldsymbol{b}_{\mathrm{a}}u + \boldsymbol{d}_{\mathrm{a}}\Delta, \\ y &= \boldsymbol{c}_{\mathrm{a}}^{\mathrm{T}}\boldsymbol{x}_{\mathrm{a}} \end{aligned} \tag{3.168}$$

with

$$\boldsymbol{x}_{\mathrm{a}} = \begin{bmatrix} \boldsymbol{x} \\ \varphi \end{bmatrix}, \quad \boldsymbol{A}_{\mathrm{a}} = \begin{bmatrix} \boldsymbol{A} & \boldsymbol{e}_n \\ \boldsymbol{0}_{1\times n} & 0 \end{bmatrix}, \quad \boldsymbol{b}_{\mathrm{a}} = \begin{bmatrix} \boldsymbol{b} \\ 0 \end{bmatrix}, \quad \boldsymbol{d}_{\mathrm{a}} = \begin{bmatrix} \boldsymbol{0}_{n\times 1} \\ 1 \end{bmatrix}, \quad \boldsymbol{c}_{\mathrm{a}}^{\mathrm{T}} = \begin{bmatrix} \boldsymbol{c}^{\mathrm{T}} & 0 \end{bmatrix}$$

and $\Delta(t) := \dot{\varphi}(t)$, $\sup_t |\Delta(t)| \leq L$ is considered. A discrete-time version of the augmented system, which serves as basis for the observer design, then is obtained via ZOH discretization of the augmented continuous-time system

$$\begin{aligned} \boldsymbol{x}_{\mathrm{a},k+1} &= \boldsymbol{A}_{\mathrm{ad}}\boldsymbol{x}_{\mathrm{a},k} + \boldsymbol{b}_{\mathrm{ad}}u_k + \boldsymbol{d}_{\mathrm{ad}}\Delta_k, \\ y_k &= \boldsymbol{c}_{\mathrm{a}}^{\mathrm{T}}\boldsymbol{x}_{\mathrm{a},k}, \end{aligned}$$

[4] It is assumed that the feedback is designed s.t. the closed-loop system is asymptotically stable which ensures that $[\boldsymbol{I} - (\boldsymbol{A}_{\mathrm{d}} - \boldsymbol{b}_{\mathrm{d}}\boldsymbol{k}^{\mathrm{T}})]$ is regular.

with

$$\left[\begin{array}{cc:c} \boldsymbol{A}_{\mathrm{ad}} & \boldsymbol{b}_{\mathrm{ad}} & \boldsymbol{d}_{\mathrm{ad}} \\ \boldsymbol{0}_{2\times(n+1)} & \boldsymbol{I}_{2\times 2} & \end{array}\right] = e^{\left[\begin{array}{cc:c} \boldsymbol{A}_{\mathrm{a}} & \boldsymbol{b}_{\mathrm{a}} & \boldsymbol{d}_{\mathrm{a}} \\ & \boldsymbol{0}_{2\times(n+3)} & \end{array}\right]T_{\mathrm{s}}}.$$

An observer of the form

$$\hat{\boldsymbol{x}}_{\mathrm{a},k+1} = \boldsymbol{A}_{\mathrm{ad}}\hat{\boldsymbol{x}}_{\mathrm{a},k} + \boldsymbol{b}_{\mathrm{ad}}u_k + \boldsymbol{\lambda}(\sigma_{1,k})\sigma_{1,k}, \tag{3.169}$$

with $\sigma_{1,k} := y_k - \boldsymbol{c}_{\mathrm{a}}^{\mathrm{T}}\hat{\boldsymbol{x}}_{\mathrm{a},k}$ might be used to estimate the augmented state vector $\boldsymbol{x}_{\mathrm{a},k}$. Note that the general observer representation (3.169) also includes the previously discussed discrete-time versions of the arbitrary-order RED. The control law (3.167) written in terms of the estimated augmented state vector $\hat{\boldsymbol{x}}_{\mathrm{a},k}$ is

$$u_k = -\boldsymbol{k}_{\mathrm{a}}^{\mathrm{T}}\hat{\boldsymbol{x}}_{\mathrm{a},k} + Vr_\infty \tag{3.170}$$

with $\boldsymbol{k}_{\mathrm{a}}^{\mathrm{T}} = \begin{bmatrix}\boldsymbol{k}^{\mathrm{T}} & 1\end{bmatrix}$. The observer (3.169) leads to the estimation error dynamics

$$\boldsymbol{\sigma}_{k+1} = [\boldsymbol{A}_{\mathrm{ad}} - \boldsymbol{\lambda}(\sigma_{1,k})\boldsymbol{c}_{\mathrm{a}}^{\mathrm{T}}]\boldsymbol{\sigma}_k + \boldsymbol{d}_{\mathrm{ad}}\Delta_k,$$

with the estimation error $\boldsymbol{\sigma}_k = \boldsymbol{x}_{\mathrm{a},k} - \hat{\boldsymbol{x}}_{\mathrm{a},k}$.

If the observer gains are chosen constant, i.e., $\boldsymbol{\lambda}(\sigma_{0,k}) = \boldsymbol{\lambda}$ then (3.169) gives a Luenberger observer. Due to the reason that the observer is constructed for the augmented system it is capable to reconstruct the state variables asymptotically in the presence of a constant perturbation ($\Delta_k \equiv 0$). The continuous-time counterpart often is referred to as PI observer in literature.

In general, an observer of the structure presented in (3.169) is called prediction estimator (see, e.g., [31]) which is due to the reason that it predicts at the current step k the state vector $\boldsymbol{x}_{\mathrm{a},k+1}$ taking into account the measured output y_k. Therefore, the control law, which is given in (3.170), does not rely on the most recent measurement as its computation is based on the estimate $\hat{\boldsymbol{x}}_{\mathrm{a},k}$, i.e., it relies on the measurement y_{k-1}. When dealing with linear estimators, an alternative estimator, that takes the most recent measurement into account, is the so-called *current* estimator (see, e.g., [31]). Due to representation of the estimator (3.169) as a pseudo-linear system, it is reasonable to extend this approach also to the discrete-time versions of the arbitrary-order robust exact differentiator. A current estimator is obtained by customizing the predictor (3.169) to

$$\bar{\boldsymbol{x}}_{\mathrm{a},k} = \hat{\boldsymbol{x}}_{\mathrm{a},k} + \boldsymbol{\lambda}_{\mathrm{c}}(\sigma_{1,k})\sigma_{1,k} \tag{3.171}$$

and $\hat{\boldsymbol{x}}_{\mathrm{a},k}$ represents the predicted value

$$\hat{\boldsymbol{x}}_{\mathrm{a},k} = \boldsymbol{A}_{\mathrm{ad}}\bar{\boldsymbol{x}}_{\mathrm{a},k-1} + \boldsymbol{b}_{\mathrm{ad}}u_{k-1}. \tag{3.172}$$

A block diagram of this estimator which is composed of equation (3.171) and (3.172) is provided in Figure 3.30. Note that also the Kalman filter relies on the current estimator structure [116]. Substituting (3.171) into (3.172) and shifting one time step yields

$$\hat{\boldsymbol{x}}_{\mathrm{a},k+1} = \boldsymbol{A}_{\mathrm{ad}}\hat{\boldsymbol{x}}_{\mathrm{a},k} + \boldsymbol{b}_{\mathrm{ad}}u_k + \boldsymbol{A}_{\mathrm{ad}}\boldsymbol{\lambda}_{\mathrm{c}}(\sigma_{1,k})\sigma_{1,k}. \tag{3.173}$$

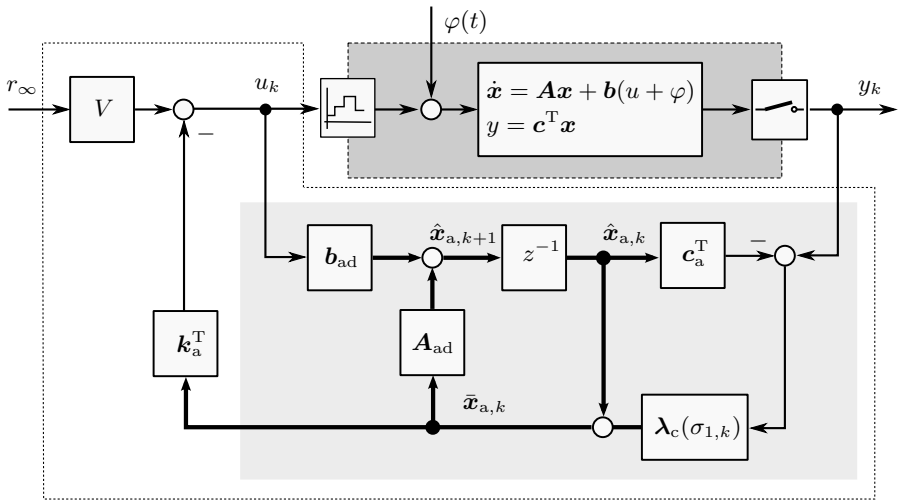

Figure 3.30: Block diagram of the current estimator. The injection terms are allowed to be nonlinear in the estimation error $\sigma_{1,k}$. Therefore it also includes the discrete-time versions of the arbitrary-order RED.

When comparing the estimator dynamics (3.173) to the predictor (3.169) it is apparent that the current estimator is obtained from the prediction estimator by setting

$$\boldsymbol{\lambda}(\sigma_{1,k}) = \boldsymbol{A}_{\mathrm{ad}}\boldsymbol{\lambda}_{\mathrm{c}}(\sigma_{1,k}).$$

Hence, the estimates $\hat{\boldsymbol{x}}_{\mathrm{a},k}$ represents the same quantity in both estimators (3.169) and (3.173), (see also [116, 31]). In view of this, the estimation error dynamics take the form

$$\boldsymbol{\sigma}_{k+1} = [\boldsymbol{A}_{\mathrm{ad}} - \boldsymbol{A}_{\mathrm{ad}}\boldsymbol{\lambda}_{\mathrm{c}}(\sigma_{1,k})\boldsymbol{c}_{\mathrm{a}}^{\mathrm{T}}]\boldsymbol{\sigma}_k + \boldsymbol{d}_{\mathrm{ad}}\Delta_k.$$

In the linear case, the gains are chosen s.t. the matrix $[\boldsymbol{A}_{\mathrm{ad}} - \boldsymbol{A}_{\mathrm{ad}}\boldsymbol{\lambda}_{\mathrm{c}}\boldsymbol{c}_{\mathrm{a}}^{\mathrm{T}}]$ has eigenvalues located in the open unit disk in the complex plane. Under the assumption that $\boldsymbol{A}_{\mathrm{ad}}$ is regular, this goal is achieved e.g. by designing $\boldsymbol{\lambda}_{\mathrm{c}} = \boldsymbol{A}_{\mathrm{ad}}^{-1}\boldsymbol{\lambda}$ where $\boldsymbol{\lambda}$ is designed s.t. the matrix $[\boldsymbol{A}_{\mathrm{ad}} - \boldsymbol{\lambda}\boldsymbol{c}_{\mathrm{a}}^{\mathrm{T}}]$ has desired eigenvalues. When dealing with a nonlinear estimator the situation is, in general, much more complex because placing the eigenvalues inside the unit circle does not necessarily imply asymptotic stability.

One particular nonlinear estimator is obtained by designing the gains s.t. the estimator corresponds to the generalized homogeneous discrete-time differentiator. This estimator is obtained by setting

$$\boldsymbol{\lambda} = T_{\mathrm{s}}\boldsymbol{P}\boldsymbol{\psi}(\sigma_{1,k})\sigma_{1,k} \implies \boldsymbol{\lambda}_c = T_{\mathrm{s}}\boldsymbol{A}_{\mathrm{ad}}^{-1}\boldsymbol{P}\boldsymbol{\psi}(\sigma_{1,k})\sigma_{1,k}$$

which yields the closed-loop dynamics

$$\boldsymbol{\sigma}_{k+1} = [\boldsymbol{A}_{\mathrm{ad}} - T_{\mathrm{s}}\boldsymbol{P}\boldsymbol{\psi}(\sigma_{1,k})\boldsymbol{c}_{\mathrm{a}}^{\mathrm{T}}]\boldsymbol{\sigma}_k + \boldsymbol{d}_{\mathrm{ad}}\Delta_k.$$

Remark 5. Apparently, these closed-loop dynamics are exactly the same as analyzed in Section 3.4.5. Hence, it is evident that all results regarding the closed-loop stability as well as results concerning the estimation precision w.r.t. sampling and noise remain valid for the predicted states $\hat{\boldsymbol{x}}_{\mathrm{a},k}$.

It is noteworthy, that this approach is not only limited to the GHDD but also applies to e.g. the Matching HDD. In fact, setting $\boldsymbol{P} = \boldsymbol{I}$ it is possible to construct a current estimator based on the HDD.

For the implementation of the output feedback controller the current estimate $\bar{\boldsymbol{x}}_{\mathrm{a},k}$ is used. The control law eventually is

$$u_k = -\boldsymbol{k}_{\mathrm{a}}^{\mathrm{T}} \bar{\boldsymbol{x}}_{\mathrm{a},k} + V r_\infty.$$

The discussion concerning the stability addressed the predicted estimate $\hat{\boldsymbol{x}}_{\mathrm{a},k}$. However, since the current estimate $\bar{\boldsymbol{x}}_{\mathrm{a},k}$ represents only another output of the same dynamical system, all stability results are valid for this estimate. This becomes evident by inspecting the block diagram of the current estimator drawn in Figure 3.30 where both quantities, $\hat{\boldsymbol{x}}_{\mathrm{a},k}$ and $\bar{\boldsymbol{x}}_{\mathrm{a},k}$, appear.

Simulation Example

Consider the undamped harmonic oscillator with a disturbance acting at the input channel, given by

$$\begin{aligned} \frac{\mathrm{d}\boldsymbol{x}}{\mathrm{d}t} &= \begin{bmatrix} 0 & 1 \\ -a_0 & 0 \end{bmatrix} \boldsymbol{x} + \begin{bmatrix} 0 \\ 1 \end{bmatrix} (u + \varphi(t)) \\ y &= \begin{bmatrix} 1 & 0 \end{bmatrix}, \quad \text{with } a_0 > 0. \end{aligned}$$

The angular frequency of the oscillator equals $\omega_0 = \sqrt{a_0}$ rad/s. The task is to make the position x_1 track a constant reference signal r_∞ under the assumption that the coefficient a_0 as well as the external disturbance $\varphi(t)$ is unknown. The controller is intended to be implemented in a discrete-time environment with sampling time $T_{\mathrm{s}} = 0.2$ s. For the purpose of the controller design, the plant model is rewritten into

$$\frac{\mathrm{d}\boldsymbol{x}}{\mathrm{d}t} = \begin{bmatrix} 0 & 1 \\ 0 & 0 \end{bmatrix} \boldsymbol{x} + \begin{bmatrix} 0 \\ 1 \end{bmatrix} (u + \tilde{\varphi}(t, \boldsymbol{x}))$$

where the $\tilde{\varphi}(t, \boldsymbol{x}) = \varphi(t) + a_0 x_1$. In this way, the considered problem matches the initial problem setting for the current estimator design in (3.165) except that the perturbation depends also on the state variable x_1. Under the assumption that the velocity x_2 is bounded, it is possible to write the system in terms of the augmented state vector $\boldsymbol{x}_{\mathrm{a}} = \begin{bmatrix} x_1 & x_2 & \varphi \end{bmatrix}$ and design a state feedback controller in combination with a current estimator based on a second-order GHDD. The current estimator based on the GHDD is obtained by computing

$$\boldsymbol{\lambda}_{\mathrm{c}} = T_{\mathrm{s}} \boldsymbol{A}_{\mathrm{ad}}^{-1} \boldsymbol{P} \boldsymbol{\psi}(\sigma_{1,k}) \sigma_{1,k} = T_{\mathrm{s}} \begin{bmatrix} 1 & -T_{\mathrm{s}} & T_{\mathrm{s}}^2 \\ 0 & 1 & -3T_{\mathrm{s}}/2 \\ 0 & 0 & 1 \end{bmatrix} \begin{bmatrix} \lambda_0 \lfloor \sigma_{1,k} \rceil^{\frac{2}{3}} \\ \lambda_1 \lfloor \sigma_{1,k} \rceil^{\frac{1}{3}} \\ \lambda_2 \lfloor \sigma_{1,k} \rceil^{0} \end{bmatrix}.$$

where $\lambda_i \in \mathbb{R}$ denote the observer gains. Compared to that, the GHDD is obtained with

$$\boldsymbol{\lambda} = T_{\mathrm{s}} \boldsymbol{P} \boldsymbol{\psi}(\sigma_{1,k}) \sigma_{1,k} = T_{\mathrm{s}} \begin{bmatrix} 1 & 0 & 0 \\ 0 & 1 & -T_{\mathrm{s}}/2 \\ 0 & 0 & 1 \end{bmatrix} \begin{bmatrix} \lambda_0 \lfloor \sigma_{1,k} \rceil^{\frac{2}{3}} \\ \lambda_1 \lfloor \sigma_{1,k} \rceil^{\frac{1}{3}} \\ \lambda_2 \lfloor \sigma_{1,k} \rceil^{0} \end{bmatrix}.$$

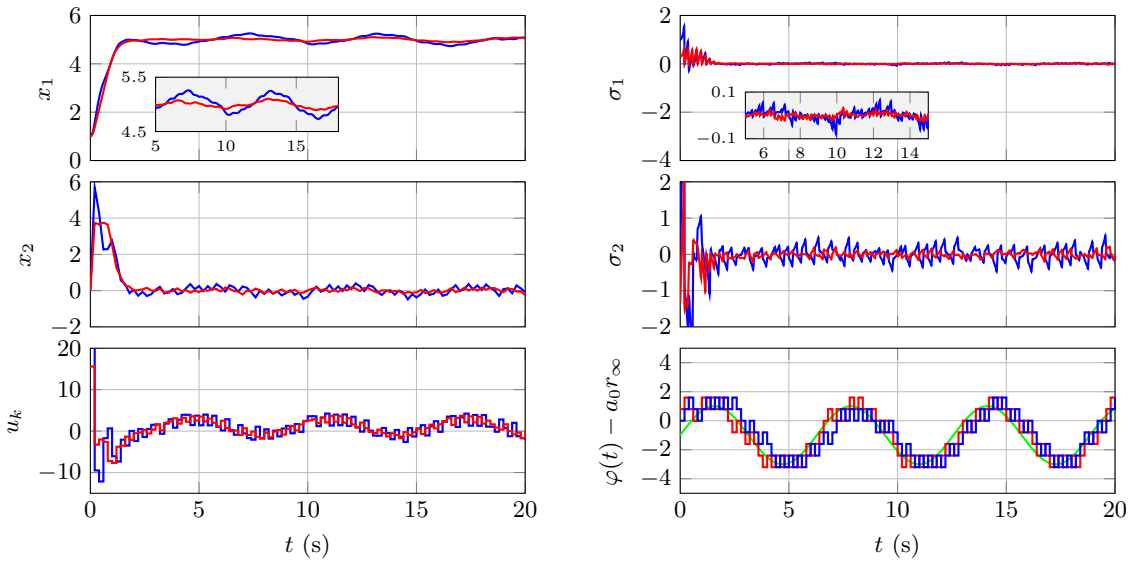

Figure 3.31: Performance evaluation of an output feedback controller based on the current estimator (——) and a prediction estimator (——). Both estimators are constructed based on the generalized homogeneous differentiator. The estimated perturbation is compared to the quantity $\varphi(t) + a_0 r$ (——), which corresponds to the perturbation whenever $x_1 \equiv r$.

Recall that the GHDD aims to place the eigenvalues of the closed-loop system to

$$z_i = 1 + T_\mathrm{s} s_i = 1 + T_\mathrm{s} |\sigma_{1,k}|^{-\frac{1}{n+1}} p_i.$$

A simulation example which compares the two estimators is presented in Figure 3.31. The disturbance is selected as $\varphi(t) = 2\sin(t) + 2$ and $a_0 = 1$. The parameters of the estimator are selected as $p_0 = p_1 = -2$, and $p_2 = -1$, hence $\lambda_0 = 5$, $\lambda_1 = 10$ and $\lambda_2 = 4$. The state feedback controller is designed so that the eigenvalues of the closed-loop dynamic matrix $\boldsymbol{A}_\mathrm{dcl}$ are located at $z_1 = z_2 = e^{-3T_\mathrm{s}}$. The reference value is set to $r_\infty = 5$.

The first two plots on the left show the state variables x_1 and x_2. The blue colored trajectories correspond to the prediction estimator whilst the red colored ones are obtained with the current estimator. Apparently, the output feedback controller based on the current estimator allows for more tight control of the state variables. Also the estimation of the state variables appears to be more precise when compared to the control loop based on the prediction estimator (see upper two plots on the r.h.s.). The reason for the improved performance is found in the last plot on the right hand side. Therein, the disturbance minus the set-point, i.e., $\varphi(t) - a_0 r_\infty$, is plotted. It can be seen, that the estimated perturbation provided by the current estimator is approximately one step ahead of the estimate provided by the prediction estimator, hence it is more close to the real perturbation.

3.6 Application - Hydraulic Test Bed

The proposed output feedback control structure is applied to control the position of the piston rod of a hydraulic differential cylinder. Hydraulic actuators offer a very high power-to-weight-ratio, modular design, high precision, and durability. Typically they are used in industrial applications which demand high forces or torques (e.g. in heavy equipment like earth moving or forestry machines). Currently, there is a strong trend towards fully or at least partially automating such working machines. Automation requires advanced low-level control strategies allowing precise control of the hydraulic actuators. However, uncertainties like unknown load forces, external disturbances and changing operating conditions render the control design a rather challenging task.

The synthesis of position control systems of hydraulic cylinders usually is divided into two steps. The first step aims to design a controller for the non-linear valve system which, in most cases, relies on an exact linearization of the valve dynamics. Typically the valve dynamics are well-known and the parameters, which remain constant during operation, are mostly available in data-sheets. In the second step, an outer loop controller is designed for the moving piston. This mechanical subsystem is subject to external forces and possibly time-varying plant parameters e.g., due to changing masses of the load. Therefore, usually a robust control strategy is essential.

Hence, such a system represents an ideal platform to test the presented discretized sliding mode algorithms in a realistic use case. The work presented in [P4] forms the basis for the following study. Therein, a cascaded control structure was designed for the reference trajectory tracking of the piston rod of the hydraulic differential cylinder subject to an unknown load force. The proposed control law is implemented on the test bench which is equipped with industrial hydraulic components. It consists of two coupled hydraulic cylinders. One of these cylinders is regarded as the operating cylinder whilst the other one is used to apply certain load profiles (disturbances). For evaluation purposes, a force sensor which provides real-time measurements of the external load force is installed at the test rig. The controller for the operating cylinder is composed of an inner loop, which aims to linearize the valve dynamics and an outer loop, which essentially is a linear state feedback controller for reference trajectory tracking. A third-order sliding mode differentiator is implemented to estimate unmeasured state variables and the external load force. The latter one is used to compensate the load force in the outer piston position control loop. The inner and outer control loop requires full state information, hence, the information of the observer is provided to both loops.

The mechanical subsystem essentially is of the same structure as the system considered in the example discussed in Section 3.5. Hence; the proposed discrete-time versions of the RED are applicable. In the following analysis the nominal controller remains as suggested in [P4]. The reader is referred to this work for a detailed discussion about the controller design. In the following Section, only a brief overview of the modelling approach is given before discussing the estimator design.

3.6.1 System Model

A schematic diagram of a hydraulic differential cylinder is depicted in Figure 3.32. A typical feature of a differential cylinder is, that the effective piston cross sections have different area.

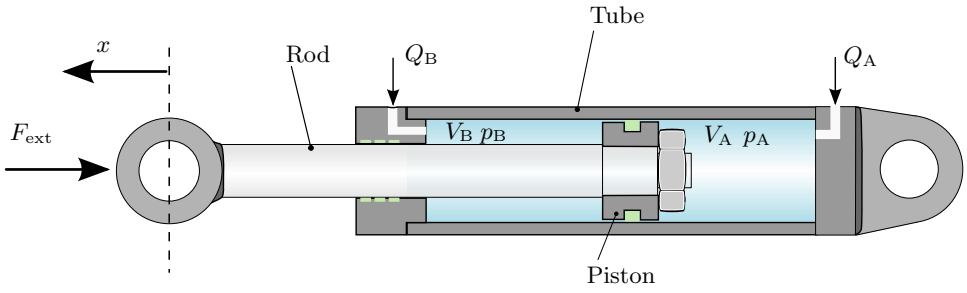

Figure 3.32: Schematic representation of the differential hydraulic cylinder.

Due to this characteristic, depending on the direction, the cylinder moves at two different velocities at a constant flow rate Q_A and Q_B. The control goal is to make the position of the piston rod x track a certain reference profile despite the unknown load force F_{ext}. The flows Q_A and Q_B are regulated by a servo valve. A hydraulic pump supplies the valve with a substantially constant pressure which is assumed to be independent on the external load force. The pressure and the volume in each chamber is denoted by p_A, p_B and V_A, V_B, respectively.

A mathematical model describing the dynamics of the piston movement is derived by applying Newton's second law of motion, yielding

$$m\ddot{x} = F_h - F_r - F_{ext}, \tag{3.174}$$

where the parameter m denotes the total moving mass, i.e., the piston mass plus the mass of the hydraulic medium, F_r represents the friction force. The hydraulic force is given by

$$F_h = (p_A - \alpha p_B)A \tag{3.175}$$

where the parameter A is the so-called piston ring surface and α represents the ratio between the piston rod cross section and the piston ring surface. It is assumed that the valve is controlled and that the closed-loop dynamics is described by an integrator, i.e.,

$$\dot{F}_h = u.$$

where u is considered as the system's input.

3.6.2 Nominal Controller

The control input is selected as

$$u = k_0(F_{h,d} - F_h),$$

where $F_{h,d}$ denotes the desired piston force and k_0 is a positive constant. Hence, an inner force control loop with closed-loop dynamics

$$\frac{1}{k_0}\dot{F}_h + F_h = F_{h,d}.$$

is established. The choice $k_0 > 0$ ensures that the hydraulic force F_h asymptotically tracks constant desired forces $F_\mathrm{h,d}$. The authors in [117, 118] suggest to choose the desired piston force as

$$F_\mathrm{h,d} = m\ddot{x}_\mathrm{d} - k_\mathrm{v}(\dot{x} - \dot{x}_\mathrm{d}) - k_\mathrm{p}(x - x_\mathrm{d}) + F_\mathrm{ext} + F_\mathrm{r},$$

which, eventually yields an outer feedback loop for reference trajectory tracking of the piston position, velocity and acceleration. By defining $e := x - x_\mathrm{d}$ and making use of the dynamic equation of the piston movement given in (3.174), one gets the differential equation

$$m\ddot{e} + k_\mathrm{v}\dot{e} + k_\mathrm{p}e = F_\mathrm{h} - F_\mathrm{h,d} = -\frac{1}{k_0}\dot{F}_\mathrm{h}$$

describing the position error dynamics. Selecting the parameters k_v and k_p strictly positive will ensure asymptotic stability of the tracking error. In [117] the authors suggest to choose

$$k_0 = \omega_0, \quad k_v = 2\omega_0 m, \quad k_p = \omega_0^2 m,$$

which ensures the second-order system behavior, described by the transfer function representation

$$G(s) = \frac{\mathscr{L}\{e(t), s\}}{\mathscr{L}\{\dot{F}_\mathrm{h}(t), s\}} = -\frac{V\omega_0^2}{s^2 + 2\zeta\omega_0 s + \omega_0^2},$$

with damping coefficient $\zeta = 1$, cut-off frequency ω_0 and gain $V = 1/(m\omega_0^3)$. Note that this control strategy does not require any knowledge on the piston acceleration. However, implementation of the outer control loop requires knowledge of the external load- and friction force. This information is rarely available from measurements in real world applications and therewith needs to be estimated.

3.6.3 State Observer and Unknown Load Force Estimator

The next design step aims to develop a sliding mode observer that provides both, an estimate of the unmeasured system state, that is the piston velocity $\dot{x}$, and the external load force F_ext. For designing the observer, the second-order system (3.174), that describes the dynamics of the piston, is rewritten as a system of first-order differential equations

$$\begin{aligned} \dot{\boldsymbol{x}} &= \boldsymbol{A}\boldsymbol{x} + \boldsymbol{b}\,(w + \varphi)\,, \\ y &= \boldsymbol{c}^\mathrm{T}\boldsymbol{x}, \end{aligned} \tag{3.176}$$

where the state variables $\boldsymbol{x} = \begin{bmatrix} x_1 & x_2 \end{bmatrix}^\mathrm{T}$ with $x_1 := x$, $x_2 := \dot{x}$ and

$$\boldsymbol{A} = \begin{bmatrix} 0 & 1 \\ 0 & 0 \end{bmatrix}, \quad \boldsymbol{b} = \begin{bmatrix} 0 \\ 1 \end{bmatrix}, \quad \boldsymbol{c}^\mathrm{T} = \begin{bmatrix} 1 & 0 \end{bmatrix}, \quad w = \frac{1}{m}(F_\mathrm{h} - F_\mathrm{r}), \quad \varphi = -\frac{1}{m}F_\mathrm{ext}.$$

The hydraulic force F_h given in (3.175) is available from measurements. The friction force is assumed to be sufficiently well described by the static model

$$F_\mathrm{r} = b_1 \mathrm{sign}(x_2) + b_2 x_2.$$

The parameters b_1 and b_2 have been identified in [P4]. In this regard the quantity w is treated as a *known* input; the external force F_{ext} represents an *unknown* input. Furthermore, under the assumption that the external load force satisfies

$$\sup_t |\dot{F}_{\text{ext}}| \leq L,$$

and by introducing $\Delta := \dot{\varphi}$, it is possible to write the dynamic model (3.176) as

$$\begin{aligned} \frac{\mathrm{d}\boldsymbol{x}_{\text{a}}}{\mathrm{d}t} &= \boldsymbol{A}_{\text{a}}\boldsymbol{x}_{\text{a}} + \boldsymbol{b}_{\text{a}}w + \boldsymbol{d}_{\text{a}}\Delta, \\ y &= \boldsymbol{c}_{\text{a}}^{\text{T}}\boldsymbol{x}_{\text{a}} \end{aligned}$$

with

$$\boldsymbol{x}_{\text{a}} = \begin{bmatrix} \boldsymbol{x} \\ \varphi \end{bmatrix}, \quad \boldsymbol{A}_{\text{a}} = \begin{bmatrix} \boldsymbol{A} & \boldsymbol{b} \\ \boldsymbol{0}_{1\times 2} & 0 \end{bmatrix}, \quad \boldsymbol{b}_{\text{a}} = \begin{bmatrix} \boldsymbol{b} \\ 0 \end{bmatrix}, \quad \boldsymbol{d}_{\text{a}} = \begin{bmatrix} \boldsymbol{0}_{2\times 1} \\ 1 \end{bmatrix}, \quad \boldsymbol{c}_{\text{a}}^{\text{T}} = \begin{bmatrix} \boldsymbol{c}^{\text{T}} & 0 \end{bmatrix}.$$

This augmented system representation exactly matches the structure presented in (3.168). Consequently the discrete-time differentiators presented in Section 3.5 can be utilized as a state and unknown input observer for the hydraulic system in a straightforward manner.

According to (3.171), a second-order differentiator in the current estimator form is

$$\begin{aligned} \bar{x}_{1,k} &= \hat{x}_{1,k} + (1 - q_1q_2q_3)\sigma_{1,k}, \\ \bar{x}_{2,k} &= \hat{x}_{2,k} + \frac{1}{2T_{\text{s}}}[3q_1q_2q_3 - q_1q_2 - q_1q_3 - q_2q_3 - q_1 - q_2 - q_3 + 3]\sigma_{1,k}, \\ \bar{\varphi}_k &= \hat{\varphi}_k - \frac{1}{Ts^2}[(q_1 - 1)(q_2 - 1)(q_3 - 1)]\sigma_{1,k}, \end{aligned}$$

where $\sigma_{1,k} := x_k - \hat{x}_{1,k}$ and $\hat{x}_{i,k}$ represent the predicted value

$$\begin{aligned} \hat{x}_{1,k} &= \bar{x}_{1,k-1} + T_{\text{s}}\bar{x}_{2,k-1} + \frac{T_{\text{s}}^2}{2}\bar{\varphi}_{k-1} + \frac{T_{\text{s}}^2}{2}w_{k-1}, \\ \hat{x}_{2,k} &= \bar{x}_{2,k-1} + T_{\text{s}}\bar{\varphi}_{k-1} + T_{\text{s}}w_{k-1}, \\ \hat{\varphi}_k &= \bar{\varphi}_{k-1}. \end{aligned}$$

The variable $\bar{x}_{2,k}$ is an estimate of the piston velocity x_2 and $\bar{\varphi}_k$ is an estimate of φ. Hence, with knowledge of the parameter m, the estimate $\hat{F}_{\text{ext}}$ of the external load force F_{ext} is given by $\hat{F}_{\text{ext}} = -m\bar{\varphi}_k$. For the implementation of the estimator, the functions q_1, q_2, q_3 have to be chosen in order to yield the desired version of the differentiator. The above given general representation also includes the GHDD as it is applied in the example in Section 3.5. It is obtained by the selection $q_i = 1 + T_{\text{s}}s_i(\sigma_{1,k})$ with $s_i(\sigma_{1,k}) = |\sigma_{1,k}|^{-\frac{1}{3}}p_i$. In the following experiment the differentiator with $q_i = e^{T_{\text{s}}s_i(\sigma_{1,k})}$ is used.

3.6.4 Implementation & Experimental Results

The developed controller is implemented on a programmable logic device (PLC) from company Bernecker & Rainer. The PLC is connected via TCP/IP to a PC and supports automatic

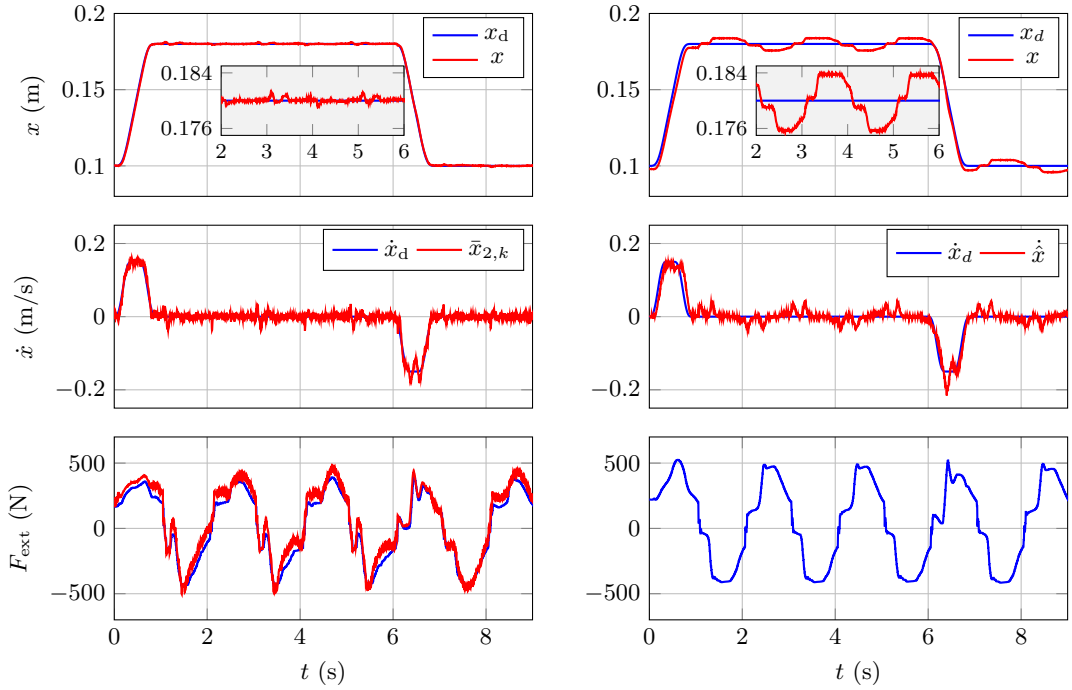

(a) Results of the experiment obtained with the proposed observer-based control concept.

(b) Results achieved *without* disturbance compensation and *without* sliding mode based differentiation.

Figure 3.33: Comparision of the experimental results obtained from the test rig.

code generation from MATLAB/Simulink® environment. The sampling time is set to $T_{\text{s}} = 1$ ms. The parameters for the cascaded control structure are selected as $k_0 = 125$, $k_{\text{p}} = 1.1054 \cdot 10^4$ and $k_{\text{v}} = 175$. The supply pressure is adjusted at 60 bar via a pressure relief valve. The piston position is measured using a linear potentiometer which is attached to the piston rod. The position can be varied from $0 - 0.47$ m. A 300 kg compression/tension load cell is mounted in-between the piston rod of the load and the working cylinder. The parameters of the differentiator are set to $p_i = -5$.

In the experiment, a sinusoidal reference signal is applied to the disturbance cylinder and the operating cylinder is supposed to track a desired reference position, velocity and acceleration. As reference trajectory a sine-squared function is used. The experiment is carried out twice, using the proposed control strategy with and without disturbance compensation. In order to compare the proposed compensation with a strategy not including any of the above mentioned sliding mode based concepts, the piston velocity x_2 is obtained by a linear differentiation filter

$$G_{\text{d}}(s) = \frac{s}{1 + sT_{\text{f}}}. \tag{3.177}$$

Using $s \approx \frac{1-z^{-1}}{T_{\text{s}}}$, the continuous-time transfer function (3.177) becomes

$$H_{\text{d}}(z) = \frac{1 - z^{-1}}{(T_{\text{s}} + T_{\text{f}}) - T_{\text{f}} z^{-1}}, \tag{3.178}$$

which can be implemented on the controller. The positive constant T_f is selected such that an acceptable trade-off between noise attenuation and the phase shift of the signal to be differentiated is achieved. In this context the choice $T_\mathrm{f} = 0.03$ s is made.

The results obtained with the sliding mode based control strategy are shown in Figure 3.33a. Figure 3.33b shows the results achieved not using any disturbance compensation. The blue line in the upper plots illustrate the reference trajectory for the piston position, the red line is the measured position. The initial value is set to 0.1 m, the desired final position is 0.18 m. The plots in the middle show the reference trajectory for the piston velocity and the estimated velocity obtained from the differentiator and from the filter given in equation (3.178). The plots on the bottom show the measured external load force and, in the case of the sliding mode approach, also its estimated value. It can be seen, that without incorporating the estimates of external forces in the control law, the load stiffness[5] is reduced significantly. The robust sliding mode control strategy is capable to significantly improve this stiffness and therewith, achieves superior reference trajectory tracking of the piston position and velocity in the presence of the unknown load forces.

3.7 Summary & Concluding Remarks

In this chapter, entirely new discrete-time variants of the super-twisting algorithm and the arbitrary-order robust exact differentiator have been derived. The proposed approach allows obtaining discrete-time algorithms which remove the discretization chattering effects. The continuous-time algorithm is converted into a discrete-time algorithm by an eigenvalue-based transformation. The resulting controllers/differentiators are given by explicit recursions which render the implementation straightforward. In the unperturbed case, the algorithms provide for a hyper-exponential speed of convergence to the origin. Local stability results have been obtained using Lyapunov's indirect method. For the super-twisting algorithm, global results have been obtained by Lyapunov's direct method. Simulation studies demonstrate that the proposed algorithms are insensitive to an overestimation of the gains, i.e., the precision of the variable to be controlled is not deteriorated when increasing the controller gains. The performance of the obtained controllers is compared to the classical forward Euler discretized STA in simulation examples as well as in a real-world application. Based on this discrete-time versions, the arbitrary-order robust exact differentiator has been incorporated in a current estimator structure and an output-feedback control structure relying on this configuration has been developed. The current estimator based observer takes the most recent measurement into account and thus, depending on the application, may yield improved precision in the estimation and consequently also in the control accuracy. The approach has been applied to control the piston rod movement of a hydraulic cylinder.

[5]The load stiffness is defined as the ability of the cylinder to yield as less as possible under external load forces.

4 Robust Control Systems Design via Homogeneous Eigenvalue Assignment

Contents

Homogeneity has turned out to be a valuable tool for the design of HOSM algorithms. Many sliding mode algorithms, especially modern higher-order algorithms have been designed so that the closed-loop system is a homogeneous one. It is a highly useful and promising tool for the generalization of the sliding mode controller design for arbitrary order systems. In recent years a lot of research effort has been spent on the theory of homogeneous systems.

However, in most cases, the approaches are limited to the continuous-time domain and the discretization process, which eventually has to be carried out in order to implement the controller in some digital environment, is ignored. From the control engineering point of view, a framework that allows both, designing problem specific sliding mode controllers that can then be easily discretized, implemented and tuned is desirable. The approach discussed in this chapter is an attempt to close this gap. The question that arises is whether it is possible to design and also discretize sliding mode controllers by adopting tools from the previous section. The previously analyzed systems have been characterized by the point-wise eigenvalues of the dynamic matrix of the closed-loop system represented in pseudo-linear form. This pseudo-linear representation and the eigenvalue considerations set the basis for the development of more advanced discretization schemes that offer several remarkable advantages when compared to the classical forward Euler discretization. Unfortunately, not all existing sliding mode algorithms

exhibit a unique pseudo-linear representation as e.g. the STA does[1]. It is not entirely clear, how different pseudo-linear representations and their associated eigenvalues, which, after all, are the basis for the discretization, affect the discretization process and eventually the performance of the closed-loop system. On the other hand, if the continuous-time algorithm is designed such that it satisfies a certain structure, then also its discrete-time realization might be straightforward. Homogeneity and the concept of so-called homogeneous eigenvalues set the starting point for this approach.

4.1 Weighted Homogeneity and Homogeneous Systems

The notion of weighted homogeneity, introduced in [119], is a generalization of the classical homogeneity in the following way: Consider the vector field $\boldsymbol{f} : \mathbb{R}^n \to \mathbb{R}^n$, $\boldsymbol{f}(\boldsymbol{x}) = \begin{bmatrix} f_1(\boldsymbol{x}) & \dots & f_n(\boldsymbol{x}) \end{bmatrix}^{\mathrm{T}}$ and associated with this vector field the autonomous system described by the differential equation

$$\dot{\boldsymbol{x}} = \boldsymbol{f}(\boldsymbol{x}). \tag{4.1}$$

The vector field is $\boldsymbol{r}$-homogeneous of degree $d \in \mathbb{R}$ if there exists $d \geq -\min\limits_{1 \leq i \leq n} r_i$ s.t

$$\boldsymbol{f}(\boldsymbol{K}_{\boldsymbol{r}}\boldsymbol{x}) = \kappa^d \boldsymbol{K}_{\boldsymbol{r}} \boldsymbol{f}(\boldsymbol{x})$$

holds $\forall \boldsymbol{x} \in \mathbb{R}^n$, $\forall \kappa > 0$ where the so-called dilation matrix is given by $\boldsymbol{K}_{\boldsymbol{r}} = \operatorname{diag}\{\kappa^{r_i}\}_{i=1}^n$, i.e.,

$$\boldsymbol{K}_{\boldsymbol{r}}\boldsymbol{x} = \begin{bmatrix} \kappa^{r_1} x_1 & \kappa^{r_2} x_2 & \dots & \kappa^{r_n} x_2 \end{bmatrix}^{\mathrm{T}}.$$

The positive constants $r_i > 0$ are summarized in the so-called dilation coefficient vector (also called generalized weight) $\boldsymbol{r} = \begin{bmatrix} r_1 & r_2 & \dots & r_n \end{bmatrix}$. System (4.1) is said to be $\boldsymbol{r}$-homogeneous of degree d if its r.h.s. is $\boldsymbol{r}$-homogeneous of degree d. Homogeneous systems of degree d possess the following scaling property: Consider a dilation of $\boldsymbol{x}$ given by $\boldsymbol{z} = \boldsymbol{K}_{\boldsymbol{r}}\boldsymbol{x}$. Then the derivative of $\boldsymbol{z}$ w.r.t. time yields

$$\dot{\boldsymbol{z}} = \boldsymbol{K}_{\boldsymbol{r}} \boldsymbol{f}(\boldsymbol{x}) = \kappa^{-d} \boldsymbol{f}(\underbrace{\boldsymbol{K}_{\boldsymbol{r}}\boldsymbol{x}}_{\boldsymbol{z}}),$$

and eventually, by multiplying with κ^d, one obtains

$$\frac{1}{\kappa^{-d}} \dot{\boldsymbol{z}} = \frac{\mathrm{d}\boldsymbol{z}}{\mathrm{d}(\kappa^{-d}t)} := \frac{\mathrm{d}\boldsymbol{z}}{\mathrm{d}\theta} = \boldsymbol{f}(\boldsymbol{z}).$$

In this regard system (4.1) is invariant w.r.t. the time-coordinate transformation

$$(t, \boldsymbol{x}) \mapsto (\kappa^{-d}t, \boldsymbol{K}_{\boldsymbol{r}}\boldsymbol{x}) = (\theta, \boldsymbol{z}).$$

[1] The representation is unique as long as the dynamic matrix is allowed to depend only on the first state variable.

Furthermore, let $\vartheta(t, \boldsymbol{x_0})$ denote the solution of (4.1) with initial state $\boldsymbol{x_0} := \boldsymbol{x}(\boldsymbol{0})$. Then a scaling of the initial state is equivalent to a scaling of the trajectory, i.e.,

$$\vartheta(t, \boldsymbol{K_r x_0}) = \boldsymbol{K_r}\vartheta(\kappa^d t, \boldsymbol{x_0}),$$

see [120]. From this scaling property it is possible to derive certain beneficial properties of homogeneous systems, e.g. local attractivity implies global stability, asymptotic stability with negative homogeneity degree implies convergence in finite time, see, e.g., [23, 22, 24] for a more detailed discussion. The concept of weighted homogeneity also applies to differential inclusions. A differential inclusion

$$\dot{\boldsymbol{x}} \in \boldsymbol{F}(\boldsymbol{x}),$$

with $\boldsymbol{F}(\boldsymbol{x}) \subset \mathbb{R}^n$, $\boldsymbol{x} \in \mathbb{R}^n$ is homogeneous of degree $d \in \mathbb{R}$ if the vector-set field is invariant w.r.t.

$$\boldsymbol{F}(\boldsymbol{K_r x}) = \kappa^d \boldsymbol{K_r F}(\boldsymbol{x}).$$

Furthermore, a scalar valued function $f : \mathbb{R}^n \to \mathbb{R}$ is homogeneous of degree $d \in \mathbb{R}$ if

$$f(\boldsymbol{K_r x}) = \kappa^d f(\boldsymbol{x}).$$

Associated with homogeneity is the homogeneous norm[2]

$$\|\boldsymbol{x}\|_{\boldsymbol{r},p} = \left(|x_1|^{\frac{p}{r_1}} + \ldots + |x_1|^{\frac{p}{r_n}}\right)^{\frac{1}{p}},$$

which is a homogeneous function of degree $d = 1$.

4.2 Controller Design via Point-Wise Eigenvalue Assignment

As an illustrative example consider the problem of stabilizing the perturbed integrator

$$\dot{x} = u + \varphi(t), \quad |\dot{\varphi}| \leq L, \tag{4.2}$$

by means of a homogeneous integrating controller, i.e., the control law u is of the general form

$$\begin{aligned} u &= -h_1(x)x + \nu, \\ \dot{\nu} &= -h_{\mathrm{i}}(x)x. \end{aligned} \tag{4.3}$$

The goal is to design the controller signals $h_1 : \mathbb{R} \to \mathbb{R}$ and $h_{\mathrm{i}} : \mathbb{R} \to \mathbb{R}$ s.t. the closed-loop system is a weighted homogeneous system and the state variable x tends to zero in finite time despite the perturbation $\varphi(t)$. Obviously, one possibility to solve this task is to directly apply the STA. Note that the STA satisfies the general structure of the control law given in (4.3). Using the ideas developed in the previous sections, the same result may also be achieved by an

[2] It is not a norm in the classical sense as it is not subadditive.

eigenvalue assignment. Applying the general control law (4.3) to (4.2) yields the closed-loop system

$$\dot{\boldsymbol{x}} = \begin{bmatrix} -h_1(x_1) & 1 \\ -h_\mathrm{i}(x_1) & 0 \end{bmatrix} \boldsymbol{x} + \begin{bmatrix} 0 \\ 1 \end{bmatrix} \Delta,$$

with $\boldsymbol{x} = [x_1\, x_2]^\mathrm{T}$, $x_1 := x$, $x_2 := \nu + \varphi$ and $\Delta := \dot{\varphi}$. The characteristic polynomial of the dynamic matrix of the closed-loop system is

$$s^2 + h_1(x_1)s + h_\mathrm{i}(x_1). \tag{4.4}$$

At this stage it is not clear how the desired characteristic polynomial should be chosen in order to obtain a meaningful controller. However, recalling the results of the previous sections, the eigenvalue choice

$$s_i = |x_1|^{-\frac{1}{2}} p_i,\ i = 1, 2,$$

with $p_i \in \mathbb{C}$ seems reasonable. Thus, the desired characteristic polynomial is:

$$\begin{aligned} &s^2 + k_1|x_1|^{-\frac{1}{2}}s + k_2|x_1|^{-1}, \\ &k_1 := -(p_1 + p_2), \quad k_2 := p_1 p_2. \end{aligned}$$

Comparing the desired characteristic polynomial to (4.4) gives the functions

$$h_1(x_1) = k_1|x_1|^{-\frac{1}{2}}, \quad h_\mathrm{i}(x_1) = k_2|x_1|^{-1}, \tag{4.5}$$

and eventually, substituting (4.5) back into the general control law (4.3), restores the STA

$$\begin{aligned} u &= -k_1 \lfloor x_1 \rceil^{\frac{1}{2}} + \nu, \\ \dot{\nu} &= -k_2 \lfloor x_1 \rceil^0. \end{aligned}$$

It sounds logical and enticing to apply this approach also to higher-order systems, e.g. the perturbed double integrator

$$\dot{\boldsymbol{x}} = \begin{bmatrix} 0 & 1 \\ 0 & 0 \end{bmatrix} \boldsymbol{x} + \begin{bmatrix} 0 \\ 1 \end{bmatrix} (u + \varphi), \quad y = \begin{bmatrix} 1 & 0 \end{bmatrix} \boldsymbol{x}, \quad \boldsymbol{x} = \begin{bmatrix} x_1 & x_2 \end{bmatrix}^\mathrm{T}. \tag{4.6}$$

For the second-order system a general nonlinear integrating state feedback controller is

$$\begin{aligned} u &= -\boldsymbol{h}^\mathrm{T}(\boldsymbol{x})\boldsymbol{x} + \nu = -h_1(\boldsymbol{x})x_1 - h_2(\boldsymbol{x})x_2 + \nu, \\ \dot{\nu} &= -h_\mathrm{i}(\boldsymbol{x})y. \end{aligned} \tag{4.7}$$

One particular control law that satisfies this structure and achieves robust stabilization of the state variables x_1, x_2 is the so-called discontinuous integral (DI) controller, see [121] for more details, given by

$$\begin{aligned} u &= -k_1 \lfloor x_1 \rceil^{\frac{1}{3}} - k_2 \lfloor x_2 \rceil^{\frac{1}{2}} + \nu, \\ \dot{\nu} &= -k_3 \lfloor x_1 \rceil^0, \end{aligned}$$

i.e., $h_1(\boldsymbol{x}) = |x_1|^{-\frac{2}{3}}$, $h_2(\boldsymbol{x}) = |x_2|^{-\frac{1}{2}}$ and $h_\mathrm{i}(\boldsymbol{x}) = |x_1|^{-1}$. The closed-loop system formed by plant (4.6) and the controller (4.7) is

$$\dot{\tilde{\boldsymbol{x}}} = \boldsymbol{M}(\boldsymbol{x})\tilde{\boldsymbol{x}} + \boldsymbol{e}_3\Delta = \begin{bmatrix} 0 & 1 & 0 \\ -h_1(\boldsymbol{x}) & -h_2(\boldsymbol{x}) & 1 \\ -h_\mathrm{i}(\boldsymbol{x}) & 0 & 0 \end{bmatrix} \tilde{\boldsymbol{x}} + \begin{bmatrix} 0 \\ 0 \\ 1 \end{bmatrix} \Delta, \tag{4.8}$$

with the state vector $\tilde{\boldsymbol{x}} := \begin{bmatrix} x_1 & x_2 & x_3 \end{bmatrix}^\mathrm{T}$, $x_3 := \nu + \varphi$. It is noted, that the DI controller leads to a closed-loop system which is homogeneous of degree $d = -1$ with weights $\boldsymbol{r} = \begin{bmatrix} 3 & 2 & 1 \end{bmatrix}$. Now, instead of applying the DI controller one might exploit the same approach as in the previous example to design a nonlinear state feedback controller. Based on the previous example and taking into account the analysis of the arbitrary-order robust exact differentiator, the choice

$$s_i = |x_1|^{-\frac{1}{3}} p_i, \quad i = 1, 2, 3,$$

seems reasonable for the structure of the closed-loop eigenvalues. The corresponding desired characteristic polynomial then is

$$\begin{aligned} &s^3 + k_1|x_1|^{-\frac{1}{3}}s^2 + k_2|x_1|^{-\frac{2}{3}}s + k_3|x_1|^{-1}, \\ &k_1 := -(p_1 + p_2 + p_3), \quad k_2 := p_1p_2 + p_1p_3 + p_2p_3, \quad k_3 := -p_1p_2p_3. \end{aligned}$$

Again, comparing the desired characteristic polynomial to the characteristic polynomial of $\boldsymbol{M}(\boldsymbol{x})$, which is

$$s^3 + h_2(\boldsymbol{x})s^2 + h_1(\boldsymbol{x})s + h_\mathrm{i}(\boldsymbol{x}),$$

yields the nonlinear state feedback controller

$$\begin{aligned} u &= -k_2\lfloor x_1 \rceil^{\frac{1}{3}} - k_1|x_1|^{-\frac{1}{3}}x_2 + \nu, \\ \dot{\nu} &= -k_3\lfloor x_1 \rceil^0. \end{aligned} \tag{4.9}$$

The closed-loop system (4.8) with the control law (4.9) can be verified to be homogeneous of degree $d = -1$ w.r.t. to the weights $\boldsymbol{r} = \begin{bmatrix} 3 & 2 & 1 \end{bmatrix}$. A simulation result with this controller and $\Delta \equiv 0$ is provided in Figure 4.1. At a first glance, the simulation results look convincing. The state variables x_1 and x_2 as well as the controller state $\nu = x_3$ tend to zero. Due to the negative homogeneity degree it is expected that the state variables, supposing that local attractivity of the origin is given, converge in finite time. However, on closer inspection of the control law, it becomes evident, that due to the expression $k_1|x_1|^{-\frac{1}{3}}x_2$, the control signal tends to infinity as the state variable x_1 tends to zero and $x_2 \neq 0$. Such a singular control law is, of course, undesirable in a real system and has to be avoided. Therefore the control law obtained by this eigenvalue choice is not viable. To achieve a closed-loop system with homogeneity degree $d = -1$ and weights $\boldsymbol{r} = \begin{bmatrix} 3 & 2 & 1 \end{bmatrix}$, every element in u has to have degree two. Specifically, this means

$$\deg h_1(\boldsymbol{x}) \stackrel{!}{=} -2, \quad \text{and} \quad \deg h_2(\boldsymbol{x}) \stackrel{!}{=} -1 \tag{4.10}$$

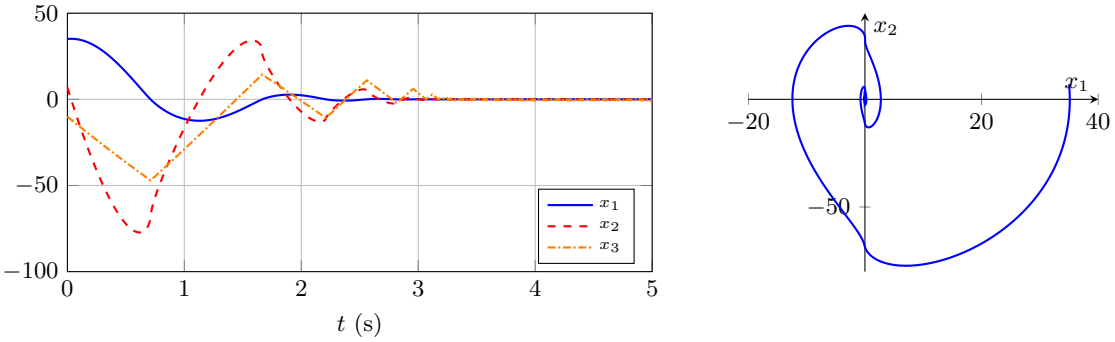

Figure 4.1: Trajectories of the closed-loop system (4.8) with a nonlinear state feedback controller obtained by an eigenvalue assignment.

has to hold. Due to the fact that the state variable x_3 is not available for the design of the controller, rememberer x_3 includes the unknown perturbation, the only two choices for $h_2(\boldsymbol{x})$ which depend on a single state variable and satisfy (4.10) are

$$h_2(\boldsymbol{x}) = |x_1|^{-\frac{1}{3}}, \quad \text{or} \quad h_2(\boldsymbol{x}) = |x_2|^{-\frac{1}{2}}.$$

The latter choice leads to the discontinuous integral controller and obviously is the preferable one as the resulting control signal is continuous. However, the DI controller cannot be obtained by an eigenvalue assignment when restricting the scaling of the eigenvalues to functions of one single state variable.

So far, the analysis was restricted to eigenvalue choices where the eigenvalues depend only on *one* state variable. On the other hand one might choose eigenvalues that depend on all available state variables, i.e., in this example on x_1 and x_2. It is not obvious how the eigenvalues should be chosen in order to yield a meaningful controller. The concept of homogeneous eigenvalues is helpful to answer this question.

4.3 Homogeneous Eigenvalues

Before defining homogeneous eigenvalues of homogeneous systems of the form (4.1) the so-called Euler vector field is introduced: The vector field $\boldsymbol{\nu}(\boldsymbol{x}) : \mathbb{R}^n \to \mathbb{R}^n$ with respect to dilation coefficient $\boldsymbol{r}$ defined by

$$\boldsymbol{\nu}(\boldsymbol{x}) = \begin{bmatrix} r_1 x_1 & \dots & r_n x_n \end{bmatrix}^{\mathrm{T}}.$$

is called an Euler vector field. The Euler vector field is in the normal space of the Euler sphere

$$E_1^{\boldsymbol{r}} = \left\{ \boldsymbol{x} \in \mathbb{R} : \frac{r_1}{2} x_1^2 + \frac{r_2}{2} x_2^2 + \dots \frac{r_n}{2} x_n^2 = 1 \right\}.$$

Definition 3.1: Homogeneous Eigenvalues [122]

Consider a vector field $\boldsymbol{f}(\boldsymbol{x}) : \mathbb{R}^n \to \mathbb{R}^n$ such that $\boldsymbol{f}(\boldsymbol{x})$ is continuous, homogeneous of degree d with respect to dilation coefficient vector $\boldsymbol{r}$ and $\boldsymbol{f}(\boldsymbol{0}) = \boldsymbol{0}$. Then, $\lambda \in \mathbb{R}$ is called a homogeneous eigenvalue if there exist $\lambda \in \mathbb{R}$ and $\boldsymbol{w} \in \mathbb{R}^n$ such that

$$\boldsymbol{f}(\boldsymbol{w}) = \lambda \|\boldsymbol{w}\|_{\boldsymbol{r},2}^d \boldsymbol{\nu}(\boldsymbol{w}). \tag{4.11}$$

Moreover, $\boldsymbol{w}$ is called an homogeneous eigenvector.

For systems of degree $d = 0$ the homogeneous eigenvalue equation (4.11) simplifies to

$$\boldsymbol{f}(\boldsymbol{w}) = \lambda \boldsymbol{\nu}(\boldsymbol{w}). \tag{4.12}$$

For linear systems, i.e., $\boldsymbol{f}(\boldsymbol{x}) = \boldsymbol{A}\boldsymbol{x}$, $\boldsymbol{A} \in \mathbb{R}^{n \times n}$ the eigenequation

$$\boldsymbol{A}\boldsymbol{w} = \lambda \boldsymbol{w}.$$

is recovered.

In order to analyze the homogeneous eigenvectors in more detail, the homogeneous ray $\boldsymbol{\gamma}(\boldsymbol{x}_0)$ is introduced. Homogeneous rays are solutions of the differential equation

$$\frac{\mathrm{d}\boldsymbol{x}}{\mathrm{d}t} = \boldsymbol{\nu}(\boldsymbol{x}). \tag{4.13}$$

The system of differential equations (4.13) is decoupled. Therefore it is easy to see that a homogeneous ray for a fixed $\boldsymbol{x}_0$ is given by

$$\boldsymbol{\gamma}(\boldsymbol{x}_0) = \left\{ \begin{bmatrix} x_{0,1} e^{r_1 t} & x_{0,2} e^{r_2 t} & \dots & x_{0,n} e^{r_n t} \end{bmatrix}^{\mathrm{T}} : t \in \mathbb{R} \right\}$$

see [122]. For a weighted homogeneous system of order $n = 2$ with weights $\boldsymbol{r} = \begin{bmatrix} 2 & 1 \end{bmatrix}$ the homogeneous rays can be obtained by solving the phase differential equation

$$\frac{\mathrm{d}x_2}{\mathrm{d}x_1} = \frac{x_2}{2x_1}, \quad x_2(x_{0,1}) = x_{0,2}$$

which has the solutions in the phase space $(x_1 - x_2)$

$$x_2 = c\sqrt{|x_1|}\mathrm{sign}(x_1), \quad c = \frac{x_{0,2}}{\sqrt{|x_{0,1}|}\mathrm{sign}(x_{0,1})}. \tag{4.14}$$

For points $\boldsymbol{x}_0$ which lie on the Euler sphere

$$x_1^2 + \frac{x_2}{2} = 1,$$

the constant c in (4.14) is given by

$$c = \frac{\sqrt{2(1 - x_{0,1}^2)}}{\sqrt{|x_{0,1}|}\mathrm{sign}(x_{0,1})}, \quad x_{0,1} \in [-1,\, 1].$$

Hence, a homogeneous ray is uniquely determined by one point on the Euler sphere. The definition of the homogeneous ray provides for the following dynamic interpretation of the homogeneous eigenvector: Every trajectory starting on a homogeneous eigenvector at $t = 0$ remains on it for all $t > 0$. Note that this is equivalent to the eigenvector of a linear time-invariant system. This property becomes evident by analyzing the homogeneous eigenvalue equation. For simplicity $d = 0$. The following ansatz is considered

$$\boldsymbol{x}(t) = \boldsymbol{K_r}\boldsymbol{x}_0 = \begin{bmatrix} x_{0,1}e^{\lambda t r_1} \\ x_{0,2}e^{\lambda t r_2} \\ \vdots \\ x_{0,n}e^{\lambda t r_n t} \end{bmatrix}, \tag{4.15}$$

where $\kappa = e^{\lambda t}$. The derivative of (4.15) can be represented by

$$\dot{\boldsymbol{x}} = \lambda \boldsymbol{K_r}\boldsymbol{\nu}(\boldsymbol{x}_0).$$

Taking into account the homogeneous eigenvalue equation (4.12), with the assumption that the initial state lies on a homogeneous eigenvector $\boldsymbol{x}_0 = \boldsymbol{w}$, provides for the simplification

$$\dot{\boldsymbol{x}} = \boldsymbol{K_r}\boldsymbol{f}(\boldsymbol{w}) = \boldsymbol{f}(\boldsymbol{K_r}\boldsymbol{w}) = \boldsymbol{f}(\boldsymbol{x})$$

which confirms that (4.15) satisfies the differential equation and proofs that trajectories starting on an eigenvector remain on it. The fact that every homogeneous system of arbitrary degree can be transformed to a homogeneous system of degree zero by an appropriate time scaling allows to extend this result to homogeneous systems of degree $d \neq 0$.

The STA

$$\frac{\mathrm{d}\boldsymbol{x}}{\mathrm{d}t} = \begin{bmatrix} -k_1|x_1|^{-\frac{1}{2}} & 1 \\ -k_2|x_1|^{-1} & 0 \end{bmatrix} \boldsymbol{x} =: \boldsymbol{M}(\boldsymbol{x})\boldsymbol{x}, \quad \boldsymbol{M} : \mathbb{R}^2 \mapsto \mathbb{R}^{n\times n}$$

which is a homogeneous system of degree $d = -1$ with weights $\boldsymbol{r} = \begin{bmatrix} 2 & 1 \end{bmatrix}$ is considered to illustrate this result. Note that the STA, which has negative homogeneity degree, can be transformed to a system of degree $d = 0$ by an appropriate time scale transformation. Introducing the time scaling

$$\frac{\mathrm{d}\theta}{\mathrm{d}t} = |x_1(t)|^{-\frac{1}{2}}$$

provides for the corresponding degree zero system

$$|x_1|^{\frac{1}{2}}\frac{\mathrm{d}\boldsymbol{x}}{\mathrm{d}t} = \frac{\mathrm{d}\boldsymbol{x}}{\mathrm{d}\theta} = \begin{bmatrix} -k_1 & |x_1|^{\frac{1}{2}} \\ -k_2|x_1|^{-\frac{1}{2}} & 0 \end{bmatrix} \boldsymbol{x} =: \tilde{\boldsymbol{M}}(\boldsymbol{x})\boldsymbol{x}. \tag{4.16}$$

The weights remain $\boldsymbol{r} = \begin{bmatrix} 2 & 1 \end{bmatrix}$. According to (4.11), the homogeneous eigenvalues of the degree 0 system are calculated by solving

$$\left(\boldsymbol{R}^{-1}\tilde{\boldsymbol{M}}(\boldsymbol{w}) - \lambda \boldsymbol{I}\right)\boldsymbol{w} = \boldsymbol{0},$$

where the Euler vector field is written in the form

$$\boldsymbol{\nu}(\boldsymbol{w}) = \boldsymbol{R}\boldsymbol{w}, \quad \boldsymbol{R} = \mathrm{diag}(\boldsymbol{r}).$$

The homogeneous eigenvalues are

$$\lambda_{1,2} = \frac{1}{4}\left(-k_1 \pm \sqrt{{k_1}^2 - 8k_2}\right).$$

The corresponding homogeneous eigenvectors result in

$$\boldsymbol{w}_{1,2} = \left[\frac{\left(k_1 \pm \sqrt{{k_1}^2 - 8k_2}\right)}{4k_2}\sqrt{|x_1|} \quad 1\right]^{\mathrm{T}}. \tag{4.17}$$

Note that the homogeneous eigenvectors are invariant w.r.t. a time-scaling. Comparing the homogeneous ray (4.14) to the eigenvectors of the STA in (4.17), represented as curves in the state space parametrized by x_1, i.e.,

$$x_2 = \frac{4k_2}{\left(k_1 \pm \sqrt{{k_1}^2 - 8k_2}\right)}\sqrt{|x_1|}\mathrm{sign}(x_1),$$

it can be seen that the homogeneous eigenvector is a homogeneous ray with

$$c = \frac{4k_2}{\left(k_1 \pm \sqrt{{k_1}^2 - 8k_2}\right)}.$$

The eigenvector passes through the Euler sphere at

$$x_1 = \frac{1}{4}(-c^2 + \sqrt{16 + c^4}).$$

Recall that the time-scaling does *not* affect the trajectories in the phase space, i.e., the degree zero system (4.16) has the same solutions in the phase space as the original STA. In Figure 4.2 solutions of the STA are plotted in the phase space together with the homogeneous eigenvectors. The parameters are selected as $k_1 = 4$, $k_2 = 1$. It can be seen that trajectories converge to a homogeneous eigenvector as $t \to \infty$ and, furthermore, trajectories starting on a homogeneous eigenvector converge to the origin along the eigenvector. Obviously, to ensure contraction of the mode requires $\lambda < 0$. On the other hand, it follows immediately that for $\lambda > 0$ the homogeneous system is unstable, as a trajectory which starts on a homogeneous eigenvector expands in the direction of the eigenvector, see also [123].

4.4 Controller Design

From the previous discussion it can be concluded that: in case of the existence of real homogeneous eigenvalues and homogeneous eigenvectors, a necessary condition for asymptotic stability of the equilibrium is $\lambda < 0$. In [122] sufficient stability criteria have been derived based on homogeneous eigenvalue analysis. The results are applied in the following section to construct static and dynamic homogeneous state feedback controllers, in particular r-sliding mode controllers, by means of homogeneous eigenvalue assignment. The approach allows to assign the homogeneous eigenvalues with a certain degree of freedom regarding the selection of the homogeneity degree and the weights of the resulting closed-loop system.

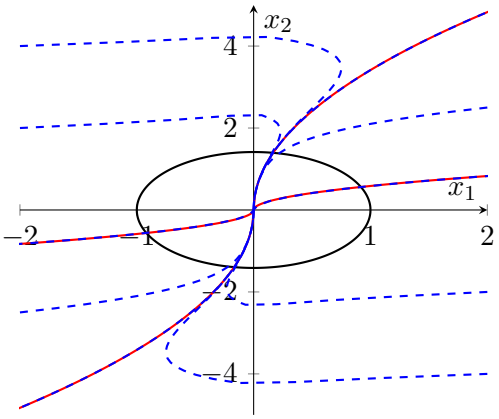

Figure 4.2: Trajectories of the STA (——) and homogeneous eigenvectors (——). A trajectory starting on an homogeneous eigenvector converges to the origin along the eigenvector. (——) Euler sphere.

4.4.1 Second-Order Static State Feedback Controller

Consider the double integrating system exploited in the motivational example

$$\dot{\boldsymbol{x}} = \begin{bmatrix} 0 & 1 \\ 0 & 0 \end{bmatrix} \boldsymbol{x} + \begin{bmatrix} 0 \\ 1 \end{bmatrix} (u + \varphi), \quad y = \begin{bmatrix} 1 & 0 \end{bmatrix} \boldsymbol{x}, \tag{4.18}$$

where φ represents a perturbation which will be specified in more detail later on. The goal is to drive the states to zero within finite time. As a starting point for the controller design the general static state feedback controller

$$u = -\boldsymbol{h}^{\mathrm{T}}(\boldsymbol{x})\boldsymbol{x} = -h_1(\boldsymbol{x})x_1 - h_2(\boldsymbol{x})x_2$$

is applied. The closed-loop system with this controller reads as

$$\dot{\boldsymbol{x}} = \boldsymbol{M}(\boldsymbol{x})\boldsymbol{x} + \boldsymbol{e}_2\varphi = \begin{bmatrix} 0 & 1 \\ -h_1(\boldsymbol{x}) & -h_2(\boldsymbol{x}) \end{bmatrix} \boldsymbol{x} + \begin{bmatrix} 0 \\ 1 \end{bmatrix} \varphi.$$

Besides the stability of the closed-loop system it is claimed that the closed-loop dynamics is a weighted homogeneous system of the degree $d \in [-1, 0)$ and weights $\boldsymbol{r} = \begin{bmatrix} r_1 & r_2 \end{bmatrix}$. In this regard, the homogeneous eigenvalue equation of the unperturbed closed-loop system is given by

$$\left(\boldsymbol{R}^{-1}\boldsymbol{M}(\boldsymbol{w}) - \tilde{\lambda}\boldsymbol{I}\right)\boldsymbol{w} = \boldsymbol{0}, \quad \tilde{\lambda} = \lambda\|\boldsymbol{w}\|_{\boldsymbol{r},2}^{d}.$$

The characteristic equation of $\boldsymbol{R}^{-1}\boldsymbol{M}(\boldsymbol{w})$ is

$$\tilde{\lambda}^2 + \frac{1}{r_2}h_2(\boldsymbol{w})\tilde{\lambda} + \frac{1}{r_1 r_2}h_1(\boldsymbol{w}) = 0$$

or, by substituting $\tilde{\lambda} = \lambda\|\boldsymbol{w}\|_{\boldsymbol{r},2}^{d}$ and multiplying by $\|\boldsymbol{w}\|_{\boldsymbol{r},2}^{-2d}$, one gets

$$\lambda^2 + \frac{1}{r_2}h_2(\boldsymbol{w})\lambda\|\boldsymbol{w}\|_{\boldsymbol{r},2}^{-d} + \frac{1}{r_1 r_2}h_1(\boldsymbol{w})\|\boldsymbol{w}\|_{\boldsymbol{r},2}^{-2d} = 0. \tag{4.19}$$

At this design stage, one has to select suitable functions $h_1 : \mathbb{R}^2 \to \mathbb{R}$ and $h_2 : \mathbb{R}^2 \to \mathbb{R}$. It seems reasonable to choose these functions such that the homogeneous eigenvalues $\lambda_i = p_i$, $i = 1, 2$ with $p_i \in \mathbb{R}$. This is achieved by selecting

$$\begin{aligned} h_1(\boldsymbol{x}) &= k_1 r_1 r_2 \|\boldsymbol{x}\|_{\boldsymbol{r},2}^{2d}, \\ h_2(\boldsymbol{x}) &= k_2 r_2 \|\boldsymbol{x}\|_{\boldsymbol{r},2}^{d}, \end{aligned}$$

where $k_1 := p_1 p_2$ and $k_2 := -(p_1 + p_2)$. This particular choice simplifies the characteristic equation (4.19) to

$$\lambda^2 + k_2 \lambda + k_1 = 0$$

and the roots of the polynomial are located at $\lambda_{1,2} = p_{1,2}$. The control law takes the form

$$u(t) = \psi(\boldsymbol{x}(t)) = -k_1 r_1 r_2 \|\boldsymbol{x}\|_{\boldsymbol{r},2}^{2d} x_1 - k_2 r_2 \|\boldsymbol{x}\|_{\boldsymbol{r},2}^{d} x_2, \quad \|\boldsymbol{x}\|_{\boldsymbol{r},2} = \left(|x_1|^{\frac{2}{r_1}} + |x_2|^{\frac{2}{r_2}} \right)^{\frac{1}{2}}, \tag{4.20}$$

and, eventually, the closed-loop dynamics are

$$\dot{\boldsymbol{x}} = \begin{bmatrix} 0 & 1 \\ -k_1 r_1 r_2 \|\boldsymbol{x}\|_{\boldsymbol{r},2}^{2d} & -k_2 r_2 \|\boldsymbol{x}\|_{\boldsymbol{r},2}^{d} \end{bmatrix} \boldsymbol{x} + \begin{bmatrix} 0 \\ 1 \end{bmatrix} \varphi. \tag{4.21}$$

The homogeneous eigenvectors of the closed-loop system compute to

$$\boldsymbol{w}_1 = \begin{bmatrix} \frac{1}{r_1 p_1} \|\boldsymbol{x}\|_{\boldsymbol{r},2}^{-d} \\ 1 \end{bmatrix}, \quad \boldsymbol{w}_2 = \begin{bmatrix} \frac{1}{r_1 p_2} \|\boldsymbol{x}\|_{\boldsymbol{r},2}^{-d} \\ 1 \end{bmatrix},$$

or as curves in the phase plane described by the implicit equation

$$x_2 - r_1 p_{1,2} \|\boldsymbol{x}\|_{\boldsymbol{r},2}^{d} x_1 = 0.$$

An analysis of the unperturbed closed-loop dynamics regarding the homogeneity properties gives a constraint on the weights r_1, r_2 and the degree d, i.e.,

$$\begin{aligned} \kappa^{r_2} x_2 &\stackrel{!}{=} \kappa^{d+r_1} x_2, \\ -k_1 r_1 r_2 \|\boldsymbol{K}_{\boldsymbol{r}} \boldsymbol{x}\|_{\boldsymbol{r},2}^{2d} \kappa^{r_1} x_1 - k_2 r_2 \|\boldsymbol{K}_{\boldsymbol{r}} \boldsymbol{x}\|_{\boldsymbol{r},2}^{d} \kappa^{r_2} x_2 &\stackrel{!}{=} \kappa^{d+r_2} (-2k_1 \|\boldsymbol{x}\|_{\boldsymbol{r},2}^{2d} x_1 - k_2 \|\boldsymbol{x}\|_{\boldsymbol{r},2}^{d} x_2). \end{aligned}$$

Taking into account that the homogeneous norm is a homogeneous function of degree $d = 1$, i.e.,

$$\|\boldsymbol{K}_{\boldsymbol{r}} \boldsymbol{x}\|_{\boldsymbol{r},2} = \kappa \|\boldsymbol{x}\|_{\boldsymbol{r},2}$$

one gets

$$r_1 \stackrel{!}{=} r_2 - d, \quad r_2 > 0, \quad r_2 - d > 0, \quad d \geq -\min\{r_1, r_2\}.$$

It is noteworthy that the degree and the weights are *not* uniquely determined. One can assign the homogeneity degree d as well as one of the weights r_1 or r_2, or both weights, bearing

in mind that both weights have to be positive. Obviously, this freedom in the choice of the weights and the degree is lost in the presence of a perturbation. In order to account for the perturbation the control signal u has to have the same homogeneity degree as the perturbation term. In particular: in the presence of a non-vanishing bounded perturbation $\varphi \in [-L,\, L]$, the closed-loop system is governed by the differential inclusion

$$\begin{aligned}\dot{x}_1 &= x_2,\\ \dot{x}_2 &\in -k_1 r_1 r_2 \|\boldsymbol{x}\|_{\boldsymbol{r},2}^{2d} x_1 - k_2 r_2 \|\boldsymbol{x}\|_{\boldsymbol{r},2}^{d} x_2 + [-L,\, L]\end{aligned}$$

and the degree of the r.h.s. of the second equation has to be zero, which means that

$$r_1 = -2d, \quad \text{and} \quad r_2 = -d \implies r_1 = 2r_2.$$

With $d = -1$ one obtains the homogeneity weights $r_1 = 2$, $r_2 = 1$ which in literature usually is termed *r-sliding homogeneity*, see [2]. The control signal generated by the controller (4.20) with this particular choice of the degree is continuous everywhere except on $x_1 = x_2 = 0$. However, in contrast to the motivational example, the control signal remains bounded. The upper bound of the control signal is determined by computing the critical points of $u(t) = \psi(\boldsymbol{x}(t))$. The control signal has a critical point provided that

$$\nabla\psi(\boldsymbol{x}^*) = \boldsymbol{0}. \tag{4.22}$$

For the considered control law the partial derivatives are

$$\begin{aligned}\frac{\partial\psi}{\partial x_1} &= \frac{x_2\left((p_1+p_2)x_1 + 4p_1p_2x_2\|\boldsymbol{x}\|_{\boldsymbol{r},2} + (p_1+p_2)x_2^2\mathrm{sign}(x_1)\right)}{2\|\boldsymbol{x}\|_{\boldsymbol{r},2}^5},\\ \frac{\partial\psi}{\partial x_2} &= \frac{-(p_1+p_2)x_2^2|x_1| - x_1\left((p_1+p_2)x_1 + 4p_1p_2\|\boldsymbol{x}\|_{\boldsymbol{r},2}|x_2|\mathrm{sign}(x_2)\right)}{\|\boldsymbol{x}\|_{\boldsymbol{r},2}^5}.\end{aligned}$$

For the r-sliding homogeneous system one obtains that (4.22) holds for all points at the homogeneous ray

$$x_1^* = \frac{\left(-2p_1p_2 - p_2^2 + p_1^2(-1+16p_2^2)\right)}{(p_1+p_2)^2}x_2^{*2} \tag{4.23}$$

as well as for all points on the x_2 axis, i.e.

$$x_2^* = 0.$$

Computing the control signal along the homogeneous ray (4.23), yields

$$\psi(\boldsymbol{x}^*) = \frac{1}{8}\left(-2 - \frac{p_1}{p_2} - \frac{p_2}{p_1} + 16p_1p_2 - \frac{2(p_1+p_2)}{\sqrt{\frac{{p_1}^2{p_2}^2}{(p_1+p_2)^2}}}\right) \tag{4.24}$$

whereas along the x_2 axis

$$\psi(\boldsymbol{x}^*) = 2p_1p_2. \tag{4.25}$$

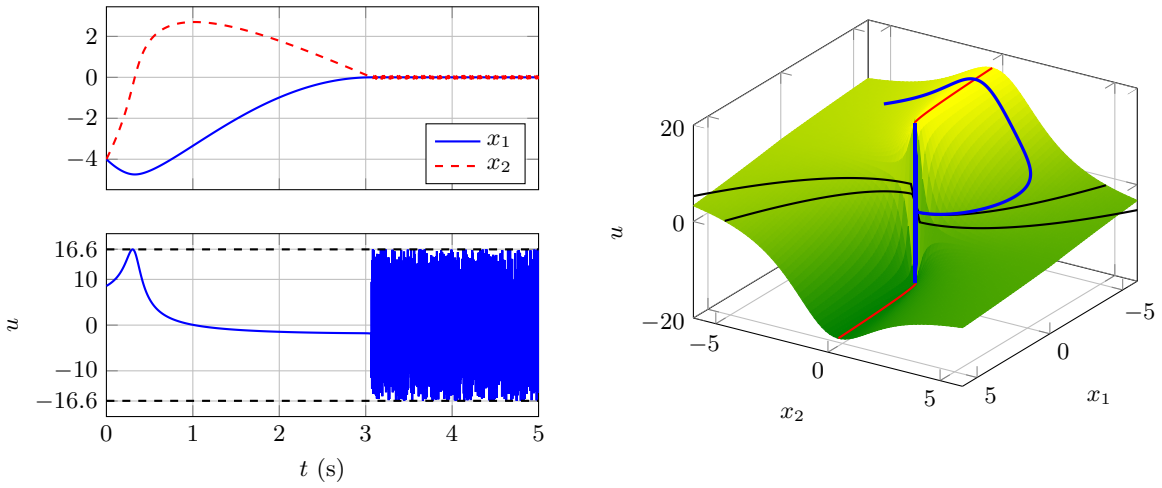

Figure 4.3: Trajectories of the closed-loop system with a nonlinear state feedback controller obtained by an eigenvalue assignment. The control signal is bounded and discontinuous only in the origin. Trajectories converge to the origin along a homogeneous eigenvector.

For the preferred choice p_1, $p_2 < 0$, and from comparing (4.24) to (4.25), it can be concluded that the control signal takes a maximum along the homogeneous ray (4.23). Taking into account symmetry provides for the upper bound of the control signal

$$\sup_t |u| \leq \frac{1}{8}\left(-2 - \frac{p_1}{p_2} - \frac{p_2}{p_1} + 16p_1p_2 - \frac{2(p_1+p_2)}{\sqrt{\frac{{p_1}^2{p_2}^2}{(p_1+p_2)^2}}}\right), \quad p_1,\, p_2 < 0. \tag{4.26}$$

Simulation results of the unperturbed system with the proposed controller are provided in Figure 4.3. The degree is set to $d = -1$ with weights $\boldsymbol{r} = \begin{bmatrix} 2 & 1 \end{bmatrix}$. The controller parameters are $k_1 = 8$ and $k_2 = 6$ i.e., the homogeneous eigenvalues are $\lambda_1 = -2$, $\lambda_2 = -4$. According to (4.26), the bound of the control signal is $\sup_t |u| \leq 16.56$. The upper left plot shows the trajectories over time, the lower plot shows the control signal. As can be seen, the trajectories are driven to the origin by means of a bounded control signal. The plot on the r.h.s. illustrates the control signal over the state plane, i.e., $\psi(\boldsymbol{x})$. Furthermore, the control signal evaluated along the trajectory, i.e., $u(\boldsymbol{x}(t))$is depicted in blue color. The black colored rays are the homogeneous eigenvalues, the red colored one is the ray at which the control signal takes its maximum. One can observe, that the trajectory converges to a homogeneous eigenvector and that the control signal is discontinuous only in the origin.

So far the homogeneity properties, and in particular the concept of homogeneous eigenvalues, have been exploited in order to construct a control law. However, the stability of the closed-loop system has not yet been addressed. For a planar weighted homogeneous and continuous system, a sufficient condition for asymptotic stability is, that homogeneous eigenvalues exist and all homogeneous eigenvalues are negative, see [122] Corollary 2. Hence, in the unperturbed case ($\varphi \equiv 0$) the equilibrium $\boldsymbol{x} = \boldsymbol{0}$ of (4.21) is globally asymptotically stable for all choices $d \in (-1,\, 0)$. Furthermore, due to the negative homogeneity degree, the system states converge

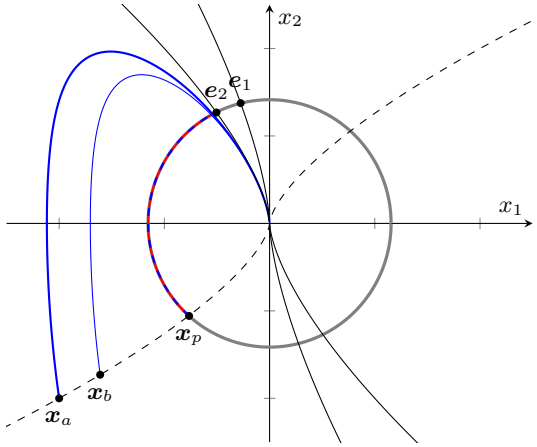

Figure 4.4: Projection of solutions on the Euler sphere versus solution of the projection system. Projection Solutions coincide with a solution of the projection system.

in finite time. The proof is essentially based on the analysis of the projection of solutions onto the Euler sphere. See the blue colored trajectory in Figure 4.4 with initial state $\boldsymbol{x}_a$. Its projection solution is depicted as a blue dashed line. The trajectory of the projection solution with initial state $\boldsymbol{x}_a$ coincides with the projection solution of the trajectory with initial condition $\boldsymbol{x}_b$ where $\boldsymbol{x}_b$ is from the same homogeneous ray as $\boldsymbol{x}_a$. This is true for all trajectories with initial condition lying on the same homogeneous ray. Furthermore, the projection solution coincides with a solution of the projection system

$$\dot{\boldsymbol{x}} = \boldsymbol{f}_0(\boldsymbol{x}) \tag{4.27}$$

where the vector field

$$\boldsymbol{f}_0(\boldsymbol{x}) = \boldsymbol{f}(\boldsymbol{x}) - \frac{\boldsymbol{\nu}^{\mathrm{T}}(\boldsymbol{x})\boldsymbol{f}(\boldsymbol{x})}{\|\boldsymbol{\nu}(\boldsymbol{x})\|^2}\boldsymbol{\nu}(\boldsymbol{x}) \tag{4.28}$$

is in the tangent space of the Euler sphere. Every point on a homogeneous eigenvector is an equilibrium point of the projection system (4.27), i.e., $\boldsymbol{f}_0(\boldsymbol{w}) = \boldsymbol{0}$. This property is verified by substituting the homogeneous eigenvalue equation (4.11) into the r.h.s. of (4.27) which yields

$$\lambda\|\boldsymbol{w}\|_{\boldsymbol{r},2}^d\boldsymbol{\nu}(\boldsymbol{w}) - \frac{\boldsymbol{\nu}^{\mathrm{T}}(\boldsymbol{w})\lambda\|\boldsymbol{w}\|_{\boldsymbol{r},2}^d\boldsymbol{\nu}(\boldsymbol{w})}{\|\boldsymbol{\nu}(\boldsymbol{w})\|^2}\boldsymbol{\nu}(\boldsymbol{w}) = \boldsymbol{0}.$$

Furthermore, it can be verified that there are no further equilibrium points, in the following denoted by $\boldsymbol{x}_e$, other then those on the homogeneous eigenvectors. This property can be seen by setting (4.28) to zero, which yields

$$\boldsymbol{f}(\boldsymbol{x}_e) = \frac{\boldsymbol{\nu}^{\mathrm{T}}(\boldsymbol{x}_e)\boldsymbol{f}(\boldsymbol{x}_e)}{\|\boldsymbol{\nu}(\boldsymbol{x}_e)\|^2}\boldsymbol{\nu}(\boldsymbol{x}_e), \tag{4.29}$$

i.e., $\boldsymbol{f}(\boldsymbol{x}_e)$ and $\boldsymbol{\nu}(\boldsymbol{x}_e)$ are collinear. Comparing (4.29) to the homogeneous eigenvalue equation (4.11) revelas that (4.29) satisfies (4.11) with

$$\lambda = \frac{\boldsymbol{\nu}^{\mathrm{T}}(\boldsymbol{x}_e)\boldsymbol{f}(\boldsymbol{x}_e)}{\|\boldsymbol{\nu}(\boldsymbol{x}_e)\|^2\|\boldsymbol{x}_e\|_{\boldsymbol{r},2}^d}.$$

A trajectory of the projection system with initial condition $\boldsymbol{x}_p$ is plotted in Figure 4.4 in red color. Note that this particular solution coincides with the projection solutions of the trajectories with initial conditions lying on the homogeneous ray passing through the Euler sphere at $\boldsymbol{x}_p$, e.g. $\boldsymbol{x}_a$ and $\boldsymbol{x}_b$. The projection of the homogeneous eigenvectors onto the Euler sphere are points which are denoted as $\boldsymbol{e}_1$ and $\boldsymbol{e}_2$ in the example in Figure 4.4, i.e., $\boldsymbol{e}_1$ and $\boldsymbol{e}_2$ are equilibrium points of the projection system. The solution of the projection system and therefore also the projection solutions converge to the point $\boldsymbol{e}_2$, that means trajectories converge to a homogeneous eigenvector as $t \to \infty$ and eventually to the origin, which proofs asymptotic stability. The formal proof is given in [122]. In summary: if there exist real homogeneous eigenvalues and all homogeneous eigenvalues are negative then the planar homogeneous system is asymptotically stable. The stability proof for the third-order system can be carried out essentially in the same way. However, one has to proof that no cyclic motions exist on the Euler sphere.

The results presented in [122] are restricted to continuous homogeneous systems. However, the considered system is discontinuous only on $x_1 = x_2 = 0$. Therefore the results are also valid for this system. Anyway, the discontinuous system, i.e., $d = -1$, $r_1 = 2$, $r_2 = 1$ can be transformed into a homogeneous system of degree $d = 0$ by a time scale transformation. To achieve this, the system is multiplied by the homogeneous norm $\|\boldsymbol{x}\|_{\boldsymbol{r},2}$ which gives

$$\|\boldsymbol{x}\|_{\boldsymbol{r},2}\frac{\mathrm{d}\boldsymbol{x}}{\mathrm{d}t} = \begin{bmatrix} 0 & \|\boldsymbol{x}\|_{\boldsymbol{r},2} \\ -k_1 r_1 r_2 \|\boldsymbol{x}\|_{\boldsymbol{r},2}^{-1} & -k_2 r_2 \end{bmatrix} \boldsymbol{x}.$$

Introducing

$$\frac{\mathrm{d}\theta}{\mathrm{d}t} = \|\boldsymbol{x}\|_{\boldsymbol{r},2}^{-1},$$

provides for the degree zero system in the new time variable θ, i.e.

$$\frac{\mathrm{d}\boldsymbol{x}}{\mathrm{d}\theta} = \begin{bmatrix} 0 & \|\boldsymbol{x}\|_{\boldsymbol{r},2} \\ -k_1 r_1 r_2 \|\boldsymbol{x}\|_{\boldsymbol{r},2}^{-1} & -k_2 r_2 \end{bmatrix} \boldsymbol{x}. \tag{4.30}$$

It can be verified that the degree zero system (4.30) has the same homogeneous eigenvalues (up to a scaling with the homogeneous norm) as the original system. Furthermore, the degree zero system has the same trajectories in the phase space as the original system. Hence the original system is asymptotically stable if and only if the corresponding degree zero system is asymptotically stable. The obtained degree zero system is continuous on $\mathbb{R}^2$ and therefore, results provided in [122], are applicable.

In the $r-$sliding homogeneous system the internal stability implies external stability, i.e., the closed-loop system is robust against small external perturbations [124]. Unfortunately, the results regarding the sufficient stability criteria cannot be extended to higher dimensional systems in a straightforward way. However, the proposed approach allows to easily construct HOSM controllers and the homogeneous eigenvalue analysis yields necessary conditions for global asymptotic stability. In the following Section, novel arbitrary-order SM controllers are proposed. The construction relies on homogeneous eigenvalue assignment.

4.4.2 Higher-Order Sliding Mode Controllers

Before considering the arbitrary order case, a chain of three integrators

$$\dot{x}_1 = x_2, \quad \dot{x}_2 = x_3, \quad \dot{x}_3 = u,$$

is considered. Following the previous approach, the controller structure is

$$u = -h_1(\boldsymbol{x})x_1 - h_2(\boldsymbol{x})x_2 - h_3(\boldsymbol{x})x_3.$$

To ensure that the closed loop system is a weighted homogeneous system, the degree of the controller u has to satisfy

$$\deg(u) \stackrel{!}{=} r_1 + 3d, \tag{4.31}$$

with $d \geq -\min\{r_1, r_2, r_3\}$ where

$$r_2 = r_1 + d, \quad r_3 = r_2 + d.$$

Thus,

$$\deg(h_1) \stackrel{!}{=} 3d, \quad \deg(h_2) \stackrel{!}{=} 2d, \quad \deg(h_3) \stackrel{!}{=} d. \tag{4.32}$$

If this holds, the closed-loop system is homogeneous and its homogeneous eigenvalues are the roots of the polynomial

$$\tilde{\lambda}^3 + \frac{1}{r_3}h_3(\boldsymbol{w})\tilde{\lambda}^2 + \frac{1}{r_2 r_3}h_2(\boldsymbol{w})\tilde{\lambda} + \frac{1}{r_1 r_2 r_3}h_1(\boldsymbol{w}) = 0.$$

By substituting $\tilde{\lambda} = \lambda\|\boldsymbol{w}\|_{\boldsymbol{r},2}^d$ and multiplying by $\|\boldsymbol{w}\|_{\boldsymbol{r},2}^{-3d}$ one gets

$$\lambda^3 + \frac{1}{r_3}h_3(\boldsymbol{w})\|\boldsymbol{w}\|_{\boldsymbol{r},2}^{-d}\lambda^2 + \frac{1}{r_2 r_3}h_2(\boldsymbol{w})\|\boldsymbol{w}\|_{\boldsymbol{r},2}^{-2d}\lambda + \frac{1}{r_1 r_2 r_3}h_1(\boldsymbol{w})\|\boldsymbol{w}\|_{\boldsymbol{r},2}^{-3d} = 0. \tag{4.33}$$

In the same manner as has been done for the second-order system, the controller is designed s.t. the homogeneous eigenvalues are constant and located at $\lambda_i = p_i$, $p_i \in \mathbb{R}$, $i = 1, 2, 3$. The selection

$$h_1(\boldsymbol{x}) = r_1 r_2 r_3 k_1 \|\boldsymbol{x}\|_{\boldsymbol{r},2}^{3d}, \quad h_2(\boldsymbol{x}) = r_2 r_3 k_2 \|\boldsymbol{x}\|_{\boldsymbol{r},2}^{2d}, \quad h_3(\boldsymbol{x}) = r_3 k_3 \|\boldsymbol{x}\|_{\boldsymbol{r},2}^{d} \tag{4.34}$$

simplifies the polynomial (4.33) to

$$\lambda^3 + k_3\lambda^2 + k_2\lambda + k_1 = 0, \tag{4.35}$$

that means the homogeneous eigenvalues are the roots of the polynomial (4.35), provided that the roots $p_i \in \mathbb{R}$. The functions h_1, h_2, h_3 given in (4.34) can be verified to satisfy the requirements on the degree, written in (4.32). By using Vieta's rule for the calculation of the gains, i.e.,

$$k_1 = -p_1 p_2 p_3, \quad k_2 = p_1 p_2 + p_1 p_3 + p_2 p_3, \quad k_3 = -(p_1 + p_2 + p_3)$$

it is ensured that the homogeneous eigenvalues are located at $\lambda_i = p_i$, $i = 1, 2, 3$. The homogeneous eigenvectors are

$$\boldsymbol{w}_1 = \begin{bmatrix} \frac{\|\boldsymbol{x}\|_{\boldsymbol{r},2}^{-2d}}{p_1^2 r_1 r_2} \\ \frac{\|\boldsymbol{x}\|_{\boldsymbol{r},2}^{-d}}{p_3 r_2} \\ 1 \end{bmatrix}, \quad \boldsymbol{w}_2 = \begin{bmatrix} \frac{\|\boldsymbol{x}\|_{\boldsymbol{r},2}^{-2d}}{p_2^2 r_1 r_2} \\ \frac{\|\boldsymbol{x}\|_{\boldsymbol{r},2}^{-d}}{p_3 r_2} \\ 1 \end{bmatrix}, \quad \boldsymbol{w}_3 = \begin{bmatrix} \frac{\|\boldsymbol{x}\|_{\boldsymbol{r},2}^{-2d}}{p_3^2 r_1 r_2} \\ \frac{\|\boldsymbol{x}\|_{\boldsymbol{r},2}^{-d}}{p_3 r_2} \\ 1 \end{bmatrix}.$$

The particular choice $d = -1$ and $\boldsymbol{r} = \begin{bmatrix} 3 & 2 & 1 \end{bmatrix}$ gives the 3-sliding controller

$$u = \frac{-6k_1 x_1 - 2k_2 x_2 \sqrt{|x_1|^{2/3} + |x_2| + |x_3|^2} - k_3 x_3 \left(|x_1|^{2/3} + |x_2| + |x_3|^2\right)}{\left(|x_1|^{2/3} + |x_2| + |x_3|^2\right)^{3/2}}.$$

Note that, according to (4.31), this choice ensures that the degree of u satisfies $\deg(u) = 0$. Also this controller produces a control signal which is continuous everywhere except in the origin.

This design approach is now generalized to a chain of n integrators subject to a matched perturbation, i.e.,

$$\begin{cases} \dot{x}_j = x_{j+1}, & j = 1, \ldots, n-1 \\ \dot{x}_n \in u + [-L,\, L]. \end{cases} \tag{4.36}$$

Proposition 4.1

Let $d \in [-1,\, 0]$, $r_i = r_n - (n-i)d$ with $r_n = 1$ and the controller parameters $k_1, \ldots k_n$ of the control law

$$u = -\sum_{i=1}^{n} k_i h_i(\boldsymbol{x}) x_i, \quad \text{where} \quad h_i(\boldsymbol{x}) = \|\boldsymbol{x}\|_{\boldsymbol{r},2}^{(n+1-i)d} \prod_{l=i}^{n} r_l \tag{4.37}$$

be chosen such that the roots p_i, of the polynomial

$$\lambda^n + k_n \lambda^{n-1} + \ldots + k_2 \lambda + k_1 \tag{4.38}$$

are real. Then the closed-loop system formed by the plant (4.36) and the controller (4.37) is homogeneous of the degree d and weights $\boldsymbol{r} = \begin{bmatrix} 1-(n-1)d & \ldots & 1-d & 1 \end{bmatrix}$ and the roots $p_i \in \mathbb{R}$ are the homogeneous eigenvalues of the closed-loop system.

Proof. Computing the homogeneous eigenvalues of (4.36) according to (4.11) gives

$$\begin{aligned} x_{j+1} &= \lambda \|\boldsymbol{x}\|_{\boldsymbol{r},2}^{d} r_j x_j \quad j = 1, \ldots, n-1 \\ u &= \lambda \|\boldsymbol{x}\|_{\boldsymbol{r},2}^{d} r_n x_n \end{aligned} \tag{4.39}$$

Substituting the control law (4.37) into the second equation in (4.39) yields

$$-\sum_{i=1}^{n} k_i \|\boldsymbol{x}\|_{\boldsymbol{r},2}^{(n+1-i)d} \prod_{l=i}^{n} r_l x_i = \lambda \|\boldsymbol{x}\|_{\boldsymbol{r},2}^{d} r_n x_n. \tag{4.40}$$

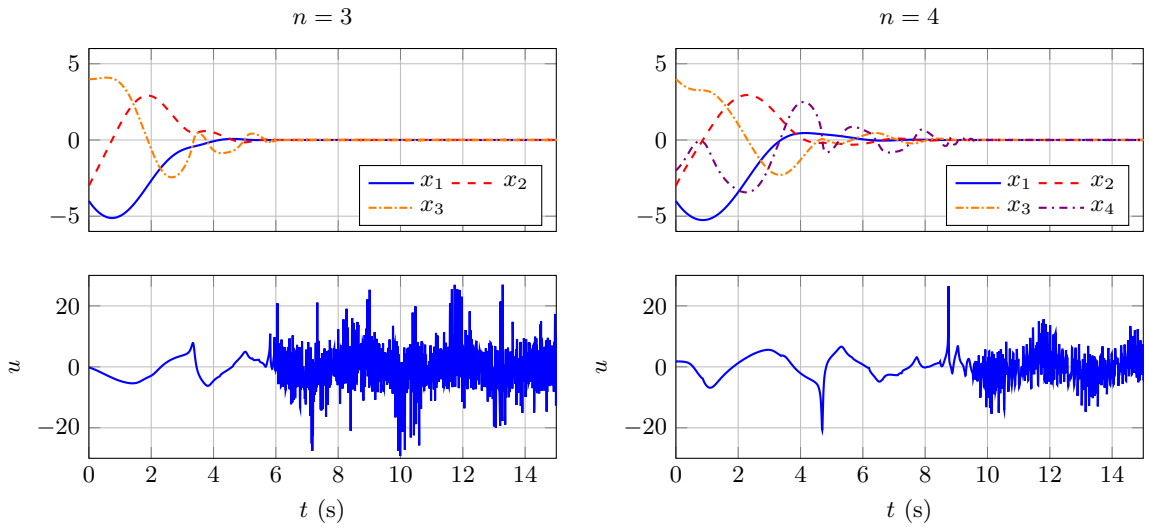

Figure 4.5: Simulation of a 3-sliding and a 4-sliding controller generated by homogeneous eigenvalue assignment.

The first equation in (4.36) is expressed in terms of the first state variable x_1, i.e.

$$x_i = \lambda^{i-1} \|\boldsymbol{x}\|_{\boldsymbol{r},2}^{(i-1)d} \prod_{l=1}^{i-1} r_l x_1. \tag{4.41}$$

Inserting (4.41) into (4.40) eventually gives

$$\lambda^n \|\boldsymbol{x}\|_{\boldsymbol{r},2}^{nd} \prod_{l=1}^{n} r_l x_1 + \sum_{i=1}^{n} k_i \lambda^{i-1} \|\boldsymbol{x}\|_{\boldsymbol{r},2}^{nd} \prod_{l=1}^{n} r_l x_1 = 0 = \lambda^n + \sum_{i=1}^{n} k_i \lambda^{i-1}$$

which asserts the Proposition. □

A necessary condition for asymptotic stability of the closed-loop system is that the roots $p_i \in \mathbb{R}^-$. It is emphasized that this condition is not sufficient for systems of order $n > 2$.

Controllers for systems of order $n = 2$ and $n = 3$ have been presented above. For the scalar system, the $r-$sliding controller generated by (4.37) is the conventional FOSM controller $u = -\text{sign}(x_1)$. A simulation example for the r-sliding controllers $r = n = 3$ and $r = n = 4$ is provided in Figure 4.5. The perturbation is selected as $\varphi(t) = 3\sin(2t)$. The controller gains are chosen s.t. the homogeneous eigenvalues are located at $p_1 = -4$, $p_2 = -2$, $p_3 = -1$ for the 3-sliding controller and $p_1 = -4$, $p_2 = -2$, $p_3 = -1$ $p_4 = -0.5$ for the 4-sliding controller respectively. The discretization time is chosen to $T_\text{s} = 1$ ms. It can be seen, that with this particular parameter choice both controllers ensure convergence of the state variables to zero.

The r-sliding controllers generated by (4.37) are continuous on $\mathbb{R}^n \setminus \mathbf{0}$ and globally bounded. In the origin, the control signal is discontinuous. In this regard, the r-sliding controllers are termed quasi-continuous controllers, see, e.g., [125] for other quasi-continuous controllers. It is noteworthy, that the control law (4.37) basically matches the structure of the sliding mode

controllers derived in [126]. In this work the authors also derive sufficient conditions for robust stability and also propose Lyapunov functions for the closed-loop system. If the norm, which appears in the functions $h_i(\boldsymbol{x})$, is replaced by a so-called canonical homogeneous norm (see [126]) then it is sufficient for global asymptotic stability to choose the gains k_i as a stabilizing linear state feedback controller, i.e., (4.38) is a Hurwitz polynomial. The drawback is, that the canonical homogeneous norm is defined implicitly. For practical reasons it is therefore desirable to replace the canonical homogeneous norm by some explicitly defined norm. A possible explicit selection is also given in [126].

A Lipschitz continuous control signal may be generated by introducing an integrator in the input channel and then designing the controller for the augmented system, see, e.g., [125] for this approach. On the other hand, one may only feed the discontinuous part of the controller through an integrator. In the following, the second-order controller is extended in this direction. The proposed controller solves the same problem statement as the continuous-twisting algorithm, see [127].

4.4.3 Second-Order Integrating State Feedback Controller

The perturbed double integrator (4.18) is considered. The task is to steer the state variables x_1, x_2 to zero by means of a continuous control signal despite the perturbation φ. In contrast to the previous Section, it is assumed that φ has a known global Lipschitz constant. A controller of structure

$$\begin{aligned} u &= -h_1 x_1 - h_2 x_2 + \nu, \\ \dot{\nu} &= -h_\mathrm{i} x_1 \end{aligned} \tag{4.42}$$

is chosen where $h_1 : \mathbb{R}^3 \mapsto \mathbb{R}$, $h_2 : \mathbb{R}^3 \mapsto \mathbb{R}$ and $h_\mathrm{i} : \mathbb{R}^3 \mapsto \mathbb{R}$. The closed-loop dynamics are

$$\dot{\boldsymbol{x}} = \begin{bmatrix} 0 & 1 & 0 \\ -h_1(\boldsymbol{x}) & -h_2(\boldsymbol{x}) & 1 \\ -h_\mathrm{i}(\boldsymbol{x}) & 0 & 0 \end{bmatrix} \boldsymbol{x} + \begin{bmatrix} 0 \\ 0 \\ 1 \end{bmatrix} \dot{\varphi} =: \boldsymbol{M}(\boldsymbol{x})\boldsymbol{x} + \boldsymbol{e}_3 \dot{\varphi}, \quad \boldsymbol{M} : \mathbb{R}^3 \mapsto \mathbb{R}^{3\times 3}$$

where the augmented state vector is $\boldsymbol{x} := \begin{bmatrix} x_1 & x_2 & x_3 \end{bmatrix}$ with $x_3 := \nu + \varphi$. To end up with a 3-sliding controller, the weights are fixed to $\boldsymbol{r} = \begin{bmatrix} 3 & 2 & 1 \end{bmatrix}$ and $d = -1$. The homogeneous eigenvalue equation then is given by

$$\left(\boldsymbol{R}^{-1}\boldsymbol{M}(\boldsymbol{w}) - \tilde{\lambda}\boldsymbol{I}\right)\boldsymbol{w} = \boldsymbol{0}, \quad \boldsymbol{R} = \begin{bmatrix} 3 & 0 & 0 \\ 0 & 2 & 0 \\ 0 & 0 & 1 \end{bmatrix}.$$

The characteristic equation of $\boldsymbol{R}^{-1}\boldsymbol{M}(\boldsymbol{w})$ is

$$\tilde{\lambda}^3 + \frac{1}{2}h_2(\boldsymbol{w})\tilde{\lambda}^2 + \frac{1}{6}h_1(\boldsymbol{w})\tilde{\lambda} + \frac{1}{6}h_\mathrm{i}(\boldsymbol{w}) = 0$$

or

$$\lambda^3 + \frac{1}{2}h_2(\boldsymbol{w})\|\boldsymbol{w}\|_{\boldsymbol{r},2}\lambda^2 + \frac{1}{6}h_1(\boldsymbol{w})\|\boldsymbol{w}\|^2_{\boldsymbol{r},2}\lambda + \frac{1}{6}h_\mathrm{i}(\boldsymbol{w})\|\boldsymbol{w}\|^3_{\boldsymbol{r},2} = 0. \tag{4.43}$$

When it comes to the selection of the nonlinear functions h_1, h_2 and h_i one has to bear in mind that only the state variables x_1 and x_2 are assumed to be available for the purpose of controller design. The variable x_3, which is a combination of the unknown perturbation and the controller state ν is unknown. Therefore it is not possible to achieve constant homogeneous eigenvalues. One may choose

$$h_1(\boldsymbol{x}) = 6k_1\Phi^2, \quad h_2(\boldsymbol{x}) = 2k_2\Phi, \quad h_\mathrm{i}(\boldsymbol{x}) = 6k_3\Phi^3 \tag{4.44}$$

where $\Phi(\boldsymbol{x}) : \mathbb{R}^3 \mapsto \mathbb{R}$ represents a homogeneous function of degree $d = -1$. Substituting the functions (4.44) into (4.43) and calculating the roots gives

$$\lambda_i = p_i\Phi(\boldsymbol{w})\|\boldsymbol{w}\|_{\boldsymbol{r},2}, \quad i = 1, 2, 3,$$

where p_1, p_2 and p_3 are the roots of the polynomial

$$p^3 + k_2p^2 + k_1p + k_3 = 0.$$

The controller (4.42) is composed of the nonlinear functions h_1, h_i and h_2 which are multiplied with the state variables x_1 and x_2 respectively. To generate a bounded control signal, the nonlinear functions are again chosen as a homogeneous function of the state variables x_1 and x_2. In particular

$$\Phi(\boldsymbol{x}) = \left(|x_1|^{\frac{2}{3}} + |x_2|\right)^{-\frac{1}{2}}.$$

The resulting controller

$$\begin{aligned} u &= -\frac{6k_1x_1}{|x_1|^{\frac{2}{3}} + |x_2|} - \frac{2k_2x_2}{\left(|x_1|^{\frac{2}{3}} + |x_2|\right)^{\frac{1}{2}}} + \nu, \\ \dot{\nu} &= -\frac{6k_3x_1}{\left(|x_1|^{\frac{2}{3}} + |x_2|\right)^{\frac{3}{2}}} \end{aligned} \tag{4.45}$$

ensures that the closed loop system is 3-sliding homogeneous and the control signal u is continuous.

A simulation example with this controller is given in Figure 4.6. It can be seen that the state variables x_1 and x_2 converge to the origin despite the disturbance $\varphi(t) = 6\sin(2t)$. The controller gains are $k_1 = 5$, $k_2 = 4$ and $k_3 = 2$. Hence, $p_1 = p_2 = -1$ and $p_3 = -2$. Note that a necessary condition for stability is $6k_3 > \sup_t |\dot{\varphi}|$, which holds in the present example. The controller variable ν tracks the external disturbance φ, i.e, $x_3 \equiv 0$. Due to the negative homogeneity degree, it is expected that the state variables converge in finite time.

Also here, negative homogeneous eigenvalues are a necessary condition for stability of the origin $x_1 = x_2 = x_3 = 0$. To obtain a sufficient stability criterion one has to show that no cyclic motions exist on the Euler sphere. Under those circumstances it is ensured that trajectories eventually converge to a homogeneous eigenvector (in the unperturbed case), and converge to the origin along this eigenvector, see [123].

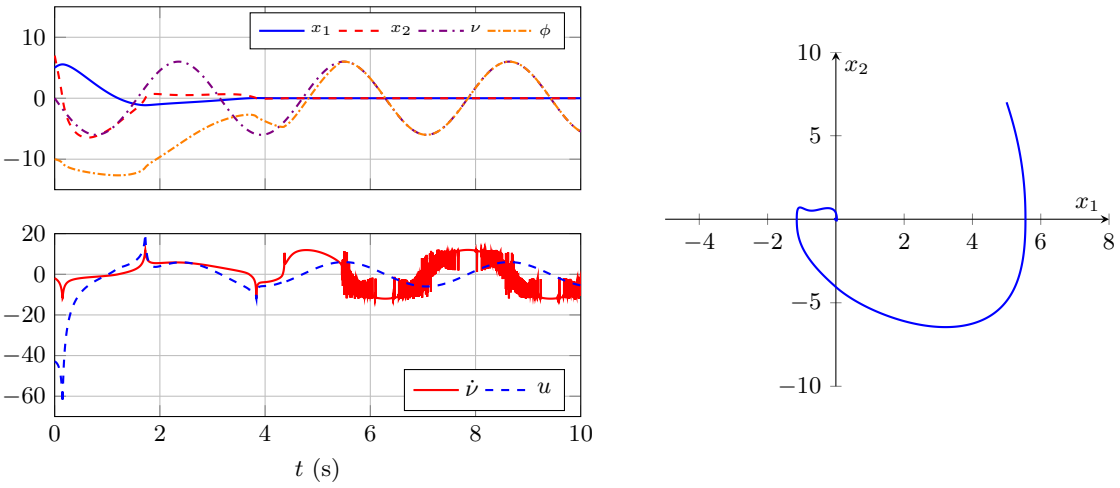

Figure 4.6: Trajectories of the double integrator (4.18) controlled by the nonlinear integrating state feedback controller (4.45) obtained by an eigenvalue assignment.

4.5 Application to Linear Time-Invariant Systems

So far the analysis was restricted to systems described by a chain of n integrators. Many nonlinear systems can be transformed to such a structure by feedback linearization, see, e.g., [128]. In the case of an LTI system, the application of the approach is straightforward and does not entail any significant differences compared to the design of a linear state feedback controller.

4.5.1 Theoretical Considerations

Consider a LTI system given by

$$\dot{\boldsymbol{x}} = \boldsymbol{A}\boldsymbol{x} + \boldsymbol{b}\,(u + \varphi)\,, \quad y = \boldsymbol{c}^{\mathrm{T}}\boldsymbol{x}, \quad \boldsymbol{x} \in \mathbb{R}^n. \tag{4.46}$$

The pair $(\boldsymbol{A}, \boldsymbol{b})$ is assumed to be controllable. The control goal is to steer the state variables $\boldsymbol{x}$ to zero in finite time despite the unknown disturbance φ. The problem may be solved in a straightforward manner by applying the techniques developed in the previous sections. Therefore, the system at hand is transformed to controllable canonical form by means of the state transformation

$$\boldsymbol{z} = \boldsymbol{T}\boldsymbol{x}, \tag{4.47}$$

where

$$\boldsymbol{T} = \begin{bmatrix} \boldsymbol{t}_1^{\mathrm{T}} \\ \boldsymbol{t}_1^{\mathrm{T}}\boldsymbol{A} \\ \dots \\ \boldsymbol{t}_1^{\mathrm{T}}\boldsymbol{A}^{n-1} \end{bmatrix}, \tag{4.48}$$

and $\boldsymbol{t}_1$ is the last row of the inverse of the controllability matrix, i.e.,

$$\boldsymbol{t}_1^{\mathrm{T}} = \begin{bmatrix} 0 & 0 & \dots & 1 \end{bmatrix} \boldsymbol{S}_{\mathrm{u}}^{-1}, \quad \text{with} \quad \boldsymbol{S}_{\mathrm{u}} := \begin{bmatrix} \boldsymbol{b} & \boldsymbol{A}\boldsymbol{b} & \dots & \boldsymbol{A}^{n-1}\boldsymbol{b} \end{bmatrix}.$$

In the transformed state variables, the system dynamics (4.46) read as

$$\dot{\boldsymbol{z}} = \boldsymbol{T}\boldsymbol{A}\boldsymbol{T}^{-1}\boldsymbol{z} + \boldsymbol{T}\boldsymbol{b}\left(u + \varphi\right), \quad y = \boldsymbol{c}^{\mathrm{T}}\boldsymbol{T}^{-1}\boldsymbol{z},$$

where the dynamic matrix has the structure

$$\boldsymbol{T}\boldsymbol{A}\boldsymbol{T}^{-1} = \begin{bmatrix} 0 & 1 & \dots & 0 \\ \vdots & \ddots & \ddots & \vdots \\ 0 & \dots & \dots & 1 \\ -\alpha_0 & -\alpha_1 & \dots & -\alpha_{n-1} \end{bmatrix} \quad \text{and} \quad \boldsymbol{T}\boldsymbol{b} = \begin{bmatrix} 0 \\ \vdots \\ 0 \\ 1 \end{bmatrix}.$$

The controller design is now carried out in two steps. In the first step, a linear state feedback control law

$$u_0 = -\boldsymbol{k}_0^{\mathrm{T}}\boldsymbol{z}$$

is designed such that the dynamic matrix of the closed-loop system, i.e., $\boldsymbol{T}\boldsymbol{A}\boldsymbol{T}^{-1} - \boldsymbol{T}\boldsymbol{b}\boldsymbol{k}_0^{\mathrm{T}}$, describes a chain of n integrators. Exploiting (4.48), the controller that achieves this goal can be written as

$$u_0 = -\boldsymbol{k}_0^{\mathrm{T}}\boldsymbol{z} = -\boldsymbol{e}_n^{\mathrm{T}}\boldsymbol{T}\boldsymbol{A}\boldsymbol{T}^{-1}\boldsymbol{z} = -\boldsymbol{t}_1^{\mathrm{T}}\boldsymbol{A}^n\boldsymbol{T}^{-1}\boldsymbol{z}.$$

Then, in the second step, the control law given in (4.37) is applied in order to assign desired homogeneous eigenvalues to the closed-loop system. The overall control law is given by

$$u = -\boldsymbol{t}_1^{\mathrm{T}}\boldsymbol{A}^n\boldsymbol{T}^{-1}\boldsymbol{z} - \sum_{i=1}^{n} k_i h_i(\boldsymbol{z}) z_i, \quad h_i(\boldsymbol{z}) = \|\boldsymbol{z}\|_{\boldsymbol{r},2}^{(n+1-i)d} \prod_{l=i}^{n} r_l$$

or, by rewriting the sum as a vector multiplication one gets

$$u = -\bar{\boldsymbol{k}}^{\mathrm{T}}(\boldsymbol{z})\boldsymbol{z} := \left[\boldsymbol{t}_1^{\mathrm{T}}\boldsymbol{A}^n\boldsymbol{T}^{-1} + \boldsymbol{k}_{\mathrm{h}}^{\mathrm{T}}(\boldsymbol{z})\right]\boldsymbol{z},$$

with

$$\boldsymbol{k}_{\mathrm{h}}^{\mathrm{T}}(\boldsymbol{z}) := \begin{bmatrix} k_1 h_1(\boldsymbol{z}) & k_2 h_2(\boldsymbol{z}) & \dots & k_n h_n(\boldsymbol{z}) \end{bmatrix},$$

The closed-loop system results in

$$\dot{\boldsymbol{z}} = \boldsymbol{T}\left[\boldsymbol{A}\boldsymbol{T}^{-1} - \boldsymbol{b}\bar{\boldsymbol{k}}^{\mathrm{T}}(\boldsymbol{z})\right]\boldsymbol{z} + \boldsymbol{T}\boldsymbol{b}\varphi. \tag{4.49}$$

The homogeneous eigenvalues of the closed-loop system are the roots p_i of the polynomial

$$\lambda^n + k_n\lambda^{n-1} + \ldots + k_2\lambda + k_1,$$

In this regard, a necessary condition for asymptotic stability of the closed-loop system (4.49) is, that the roots $p_i \in \mathbb{R}^-$. Note that, $\lim\limits_{t\to\infty} \boldsymbol{z}(t) = \boldsymbol{0} \Leftrightarrow \lim\limits_{t\to\infty} \boldsymbol{x}(t) = \boldsymbol{0}$, which follows directly from (4.47). In the original state variables the control law reads as

$$u = -\boldsymbol{k}^{\mathrm{T}}(\boldsymbol{x})\boldsymbol{x} := -\left[\boldsymbol{t}_1^{\mathrm{T}}\boldsymbol{A}^n + \boldsymbol{k}_{\mathrm{h}}^{\mathrm{T}}(\boldsymbol{T}\boldsymbol{x})\boldsymbol{T}\right]\boldsymbol{x}. \tag{4.50}$$

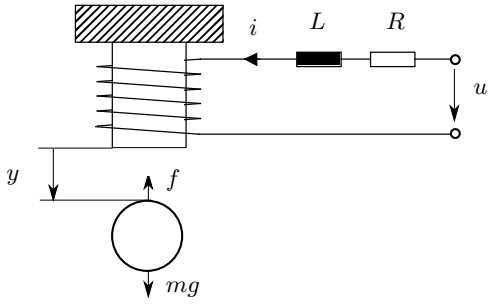

Figure 4.7: Schematic diagram of the magnetic levitation system.

4.5.2 Application to Magnetic Levitation System

The magnetic levitation system is a highly nonlinear system which is open-loop unstable. Therefore, it is in particular interesting for the validation of nonlinear and robust controllers. A schematic drawing of the magnetic levitation system is provided in Figure 4.7. The system input is the supplied voltage u, the position of the steel ball is considered as output y. The state vector is defined as $\mathbf{x} := \begin{bmatrix} y & \dot{y} & i \end{bmatrix}^{\mathrm{T}}$. In [129], the mathematical model

$$\dot{\boldsymbol{x}} = \boldsymbol{f}(\boldsymbol{x}, u) \begin{bmatrix} x_2 \\ g_\mathrm{c} - \frac{c}{m}\frac{x_3^2}{x_1^2} \\ -\frac{R}{L}x_3 + \frac{2c}{L}\frac{x_2 x_3}{x_1^2} \end{bmatrix} + \begin{bmatrix} 0 \\ 0 \\ \frac{1}{L} \end{bmatrix} u, \qquad y = x_1$$

is proposed to describe the dynamical behavior of such a system. The model parameters for the system at hand are: $g_\mathrm{c} = 9.81\ \mathrm{m/s^2}$, $c = 1.005 \cdot 10^{-4}\ \mathrm{kgm^3 s^{-2} A^{-2}}$, $m = 0.06687\ \mathrm{kg}$, $L = 1.08\ \mathrm{H}$ and $R = 18\,\Omega$. The control task is to make the ball track a given reference position, i.e., to make y track a reference signal y_ref.

The output y has relative degree $r = 3$ with respect to the input u. A controller that achieves the stated control goal may be designed by applying state feedback linearization. The local diffeomorphism

$$\boldsymbol{z} := \begin{bmatrix} z_1 & z_2 & z_3 \end{bmatrix}^{\mathrm{T}} = \boldsymbol{t}(\boldsymbol{x}) = \begin{bmatrix} x_1 - y_\mathrm{ref} & x_2 & g_\mathrm{c} - \frac{c}{m}\left(\frac{x^3}{x_1}\right)^2 \end{bmatrix}^{\mathrm{T}}$$

transforms the system into normal form

$$\begin{aligned} \dot{z}_1 &= z_1 \\ \dot{z}_2 &= z_3 \\ \dot{z}_3 &= \tilde{f}(\boldsymbol{z}) + \tilde{g}(\boldsymbol{z})u, \qquad y = z_1, \end{aligned}$$

with the nonlinear functions

$$\begin{aligned} \tilde{f}(\boldsymbol{z}) &= 2(g_\mathrm{c} - z_3)\left[\frac{R}{L} + \frac{z_2}{z_1 + y_\mathrm{ref}}\left(1 - \frac{2c}{L(z_1 + y_\mathrm{ref})}\right)\right], \\ \tilde{g}(\boldsymbol{z}) &= -\frac{2c}{Lm(z_1 + y_\mathrm{ref})}\sqrt{\frac{m}{c}(g - z_3)}. \end{aligned}$$

The feedback controller

$$u = \frac{1}{g(\boldsymbol{z})}\left(-f(\boldsymbol{z}) + v\right)$$

with the new input v provides for a linear input-output behavior and a stabilizing controller may be designed in a straightforward way by standard methods, e.g., a linear state feedback controller $v = -\boldsymbol{k}^{\mathrm{T}}\boldsymbol{z}$ does the job.

However, in order to demonstrate the applicability of the results from the previous Section, the nonlinear model is linearized. Let $(\boldsymbol{x}_{\mathrm{R}},\, u_{\mathrm{R}})$ denote the equilibrium of the system computed from $\dot{\mathbf{x}} = \mathbf{0} = \mathbf{f}\left(\mathbf{x}_{\mathrm{R}}, u_{\mathrm{R}}\right)$ with the corresponding output y_{R} which computes to

$$\mathbf{x}_{\mathrm{R}} = \begin{bmatrix} y_{\mathrm{R}} \\ 0 \\ y_{\mathrm{R}}\sqrt{\frac{mg}{c}} \end{bmatrix}, \qquad u_{\mathrm{R}} = R y_{\mathrm{R}}\sqrt{\frac{mg}{c}}. \tag{4.51}$$

Then, for small deviations from the equilibrium, the dynamics of the system are described by the LTI system

$$\begin{aligned}
\Delta\dot{\mathbf{x}} &= \boldsymbol{A}\Delta\mathbf{x} + \boldsymbol{b}\Delta u = \begin{bmatrix} 0 & 1 & 0 \\ \frac{2g}{y_{\mathrm{R}}} & 0 & -\frac{2}{y_{\mathrm{R}}}\sqrt{\frac{cg}{m}} \\ 0 & \frac{2}{Ly_{\mathrm{R}}}\sqrt{cmg} & -\frac{R}{L} \end{bmatrix}\Delta\mathbf{x} + \begin{bmatrix} 0 \\ 0 \\ \frac{1}{L} \end{bmatrix}\Delta u, \\
\Delta y &= \boldsymbol{c}^{\mathrm{T}}\Delta\mathbf{x} = \begin{bmatrix} 1 & 0 & 0 \end{bmatrix}\Delta\mathbf{x},
\end{aligned}$$

with the coordinates

$$\Delta\boldsymbol{x} := \boldsymbol{x} - \boldsymbol{x}_{\mathrm{R}}, \quad \Delta u := u - u_{\mathrm{R}}.$$

The system is supposed to track a given reference trajectory $y_{\mathrm{ref}}(t)$ and accordingly $\boldsymbol{x}_{\mathrm{ref}}(t)$. It is assumed that the reference signal is stationary or changes slowly with time, i.e., $\dot{y}_{\mathrm{ref}} \approx 0 = y_{\mathrm{R}}$ and $\dot{\boldsymbol{x}}_{\mathrm{ref}} \approx 0 = \boldsymbol{x}_{\mathrm{R}}$. By setting $\boldsymbol{x}_{\mathrm{R}} = \boldsymbol{x}_{\mathrm{ref}}$ the tracking problem is reduced to the stabilization of $\Delta\boldsymbol{x} = \mathbf{0}$. The control law proposed in (4.50) is adopted as feedback controller. The controller design is carried out for the nominal ball position $y_{\mathrm{R}} = y_{\mathrm{R}}^{*} = 0.012$, i.e., the gains in (4.50) are computed with $\bar{\boldsymbol{A}}$ and $\bar{\boldsymbol{b}}$ where $\bar{\boldsymbol{A}} = \boldsymbol{A}|_{y_{\mathrm{R}}=y_{\mathrm{R}}^{*}}$ and $\bar{\boldsymbol{b}} = \boldsymbol{b}|_{y_{\mathrm{R}}=y_{\mathrm{R}}^{*}}$. Hence, the control law for set-point tracking eventually takes the form

$$u = -\left[\boldsymbol{t}_1^{\mathrm{T}}\bar{\boldsymbol{A}}^{n} + \boldsymbol{k}_{\mathrm{h}}^{\mathrm{T}}(\boldsymbol{T}\Delta\boldsymbol{x})\boldsymbol{T}\right]\Delta\boldsymbol{x} + u_{\mathrm{R}},$$

where

$$u_{\mathrm{R}} = R y_{\mathrm{ref}}\sqrt{\frac{mg}{c}},$$

is a feed-forward control obtained from (4.51),

$$\boldsymbol{t}_1^{\mathrm{T}} = \begin{bmatrix} 0 & 0 & 1 \end{bmatrix}\left[\bar{\boldsymbol{b}} \quad \bar{\boldsymbol{A}}\bar{\boldsymbol{b}} \quad \bar{\boldsymbol{A}}^2\bar{\boldsymbol{b}}\right]^{-1} \quad \text{and} \quad \boldsymbol{T} = \begin{bmatrix} \boldsymbol{t}_1^{\mathrm{T}} \\ \boldsymbol{t}_1^{\mathrm{T}}\bar{\boldsymbol{A}} \\ \boldsymbol{t}_1^{\mathrm{T}}\bar{\boldsymbol{A}}^2 \end{bmatrix}.$$

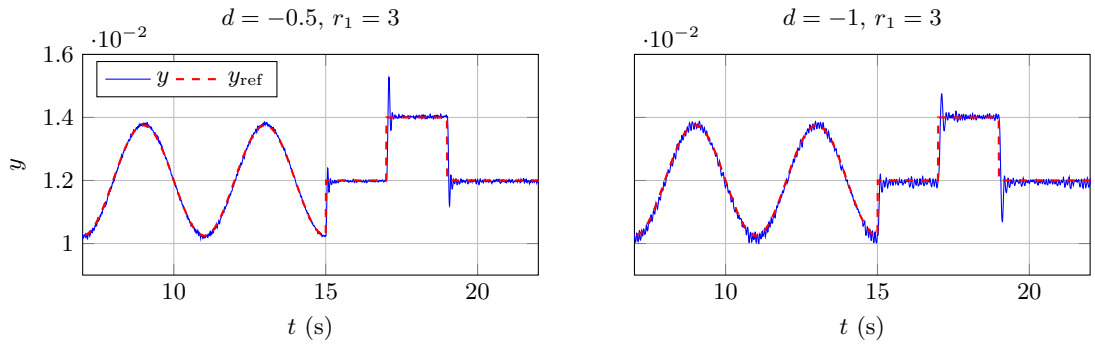

Figure 4.8: Experimental results of the magnetic levitation system. The plots show the ball position which is supposed to track a given reference signal with two different controllers. The controllers have been designed via homogeneous eigenvalue assignment.

The experiment is carried out with two different controller settings. Firstly, the homogeneity degree $d = -0.5$ is selected and the weight of the first variable is chosen as $r_1 = 3$. The homogeneous eigenvalues are selected as $p_1 = p_2 = p_3 = -25$. The second setting, $d = -1$ and $r_1 = 3$, yields a 3-sliding homogeneous controller. The homogeneous eigenvalues are selected as $p_1 = p_2 = p_3 = -2.5$. The static feedback controllers have been directly implemented on the system with sampling time $T_\text{s} = 1$ ms. The results are plotted in Figure 4.8. Both controllers basically ensure accurate tracking of the desired ball position. However, a closer look reveals that the ball oscillates around the reference trajectory when applying the controller with $d = -1$. Note that this controller produces a discontinuous control signal (on $\Delta \boldsymbol{x} = 0$), i.e., the oscillations are the chattering effects. In contrast to that, the controller with $d = -0.5$ produces a continuous control signal and, consequently, less chattering but at the cost of robustness. The choice $d = 0$ will yield a linear state feedback controller. To ensure proper tracking of the reference signal, this controller will demand even larger gains than the homogeneous controller with $d = -0.5$. Such large gains may be of disadvantage as it will lead to the so-called peaking phenomenon, i.e., large overshoots in the step response.

4.6 Equivalent Discrete-Time Controller

By having designed the controller via an eigenvalue assignment, it is straightforward to apply the discretization scheme discussed in the previous chapter. For the sake of simplicity, assume the weight $r_2 = 1$ and $r_1 = 2$ Then the forward Euler discretized closed-loop system(4.20) which is formed by the perturbed double integrator and the second-order controller developed in Section 4.4.1 may also be expressed in terms of the functions $z_i : \mathbb{R} \to \mathbb{R}$, i.e.,

$$\boldsymbol{x}_{k+1} = \begin{bmatrix} 1 & T_\text{s} \\ -\frac{r_1}{T_\text{s}}(z_1 z_2 - z_1 - z_2 + 1) & z_1 + z_2 - 1 \end{bmatrix} \boldsymbol{x}_k + \begin{bmatrix} 0 \\ T_s \end{bmatrix} \varphi_k$$

where

$$z_i = 1 + T_\text{s} s_i, \quad i = 1, 2$$

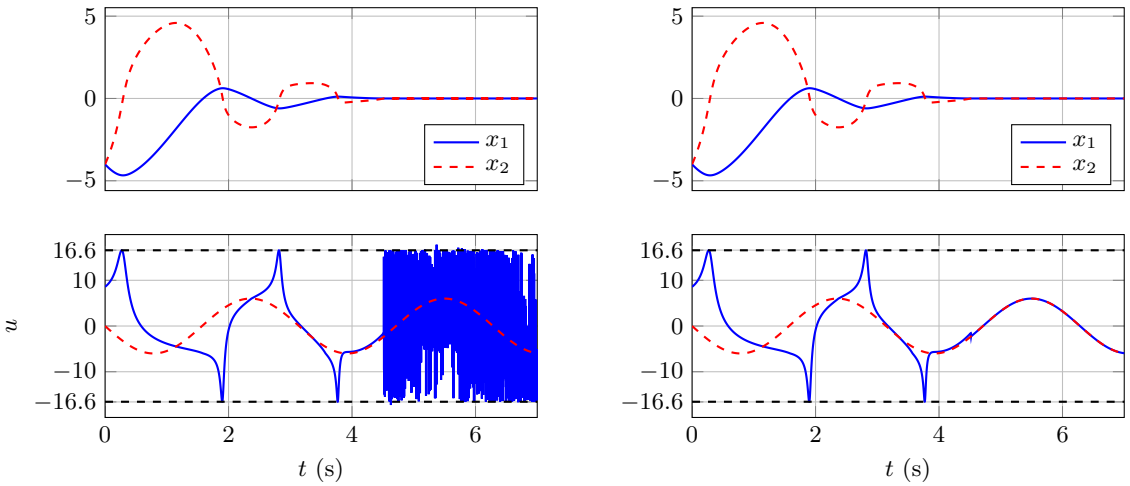

Figure 4.9: Simulation examples comparing results obtained by the explicit Euler discretization and the proposed discretization scheme. The proposed scheme removes the discretization chattering, see plots on the right hand side.

and the homogeneous eigenvalues $\lambda_i \in \mathbb{R}$ scaled by the homogeneous norm, i.e., the functions $s_i : \mathbb{R} \to \mathbb{R}$ given by

$$s_i = \|\boldsymbol{x}\|_{\boldsymbol{r},2}^d \lambda_i.$$

Note that this is just another representation of the closed-loop system (4.20). When performing a simulation of the 2-sliding controller, i.e. $d = -1$ and thus $r_1 = 2$, the discretization chattering effect is clearly visible (see the two plots on the l.h.s. in Figure 4.9). The high frequency components of the control signal contain information about the unknown external disturbance which in this example is selected as $\varphi(kT_\mathrm{s}) = 6\sin(2kT_\mathrm{s})$. The controller parameters are the same as in the simulation performed in Section 4.4.1 which essentially is the same when disregarding the disturbance.

In order to generate an equivalent discrete-time controller which does not suffer from the discretization chattering effect, one simply has to change the mapping z_i to, e.g.,

$$z_i = e^{T_\mathrm{s} s_i}, \quad i = 1, 2, \tag{4.52}$$

or any of the mappings proposed in the previous chapter. The resulting discrete-time controller with the particular mapping (4.52) is

$$u_k = -\frac{2}{T_\mathrm{s}^2}\Big(e^{\frac{T_\mathrm{s}}{\|\boldsymbol{x}_k\|_{\boldsymbol{r},2}}(\lambda_1+\lambda_2)} - e^{T_\mathrm{s}\|\boldsymbol{x}_k\|_{\boldsymbol{r},2}^d\lambda_1} - e^{T_\mathrm{s}\|\boldsymbol{x}_k\|_{\boldsymbol{r},2}^d\lambda_2} + 1\Big)x_{1,k} + \\ + \big(e^{T_\mathrm{s}\|\boldsymbol{x}_k\|_{\boldsymbol{r},2}^d\lambda_1} + e^{T_\mathrm{s}\|\boldsymbol{x}_k\|_{\boldsymbol{r},2}^d\lambda_2} - 2\big)x_{2,k}.$$

A simulation with this controller is presented in the plots on the r.h.s. in Figure 4.9. The lower plot shows the control signal. It does not suffer from the discretization chattering effect and tracks the unknown disturbance without applying any post-processing such as low pass filtering.

4.7 Summary & Concluding Remarks

In this chapter a novel framework that allows to design problem specific robust nonlinear controllers which can be discretized in a simple fashion has been proposed. The approach relies on the assignment of homogeneous eigenvalues to the closed-loop system. Necessary conditions for the stability of the origin are satisfied by an appropriate choice of these homogeneous eigenvalues. For second-order systems, these conditions are sufficient for asymptotic stability of the origin. The robustness against a certain class of perturbations is ensured by assigning a particular homogeneity degree to the closed-loop system. Exploiting this framework, a novel family of arbitrary-order homogeneous state feedback controllers has been proposed. The controllers are parametrized by the homogeneity degree. If the degree $d = 0$ a classical linear state feedback controller is obtained, whenever $d = -1$ one obtains a quasi-continuous SMC. The discretization of the controllers can be carried out by applying techniques developed in the previous chapter. A tutorial example demonstrated the approach for a second-order quasi continuous controller. Simulation examples and the application to a real system demonstrate the effectiveness of the approach. However, further research work is required in order to provide sufficient stability criteria for the arbitrary-order continuous-time system as well as the discretized system.

5 Summary, Conclusion and Outlook

The first part of this thesis was devoted to the analysis of chattering effects in LTI systems controlled by a sliding mode controller or a relay type feedback controller. The control algorithm was assumed to be implemented in a discrete-time environment with equidistant sampling of the system output and reconstruction of the computed control sequence by a zero-order hold element. In the course of this problem setting, the method of so-called sampled describing function analysis was revisited and applied to characterize periodic motions in systems controlled by a second-order sliding mode algorithm. The SDF approach is, equivalent to the classical DF analysis for continuous time systems, a graphical method, that allows to characterize self-sustaining oscillations in the nonlinear unity feedback systems. Therefore, the SDF approach can be used to analyze the combined effects, i.e., chattering due to the discrete-time realization of the controller and chattering due to parasitic dynamics like actuator and sensor dynamics. Furthermore, from a theoretical point of view, this approach also permits to design compensating elements that allow to adjust the frequency and amplitude of the chattering. However, the sampling and hold process adds an additional dimension to the problem which renders the graphical solution unhandy. This issue limits the applicability of the approach and makes it improper for the analysis of dynamic higher-order sliding mode controllers such as super-twisting or continuous-twisting algorithm. In addition, the SDF approach only is of approximative nature.

As an alternative, the extension of the LPRS method to the sampled-data configuration has been studied. Similar to the DF analysis, this approach also yields a graphical solution to the problem of characterizing periodic motions in relay feedback systems, with the advantage that it yields an exact result for the oscillation frequency. A formula for the computation of the LPRS for the sampled-data system has been derived and its application has been demonstrated in a tutorial example. This tutorial example shows that the basin of attraction of limit cycles are possibly disconnected sets in the phase space. An approach that allows to predict the basin of attraction for each limit cycle has been proposed.

The SDF and the LPRS approach can be used to characterize the self-sustaining motions in systems with relay type feedback controllers. This makes them particularly interesting for the analysis of chattering effects in sliding mode control systems. However, the techniques are hardly applicable to dynamic controllers such as the super-twisting algorithm. A possible direction for future research work is to extend the SDF approach in a way that it can be used for the analysis of dynamic controllers in a simple and elegant fashion.

The second part was devoted to the development of discretization schemes for sliding mode controllers that entirely remove the discretization chattering. Such discretization schemes have been developed for the super-twisting algorithm and extended to a family of homogeneous differentiators which also includes the arbitrary-order robust exact differentiator. The new

discretization scheme mainly relies on the pseudo-linear representation of the continuous-time algorithm. The representation permits computing point-wise eigenvalues of the dynamic matrix of the closed-loop system. Discrete-time algorithms have been derived by mapping the continuous-time eigenvalues, which depend on the system state variable, to the discrete-time domain. The resulting discrete-time algorithms have been shown to be numerical schemes for the continuous-time algorithms and, in this regard, also the asymptotic accuracies well-known from the sliding mode of corresponding order are preserved. Local asymptotic stability has been proven for the unperturbed closed-loop system. For the super-twisting algorithm, global stability results have been obtained. Furthermore, it has been shown that the state variables converge with hyper-exponential speed to the origin whenever the perturbation vanishes. Simulation examples revealed, that compared to the forward Euler discretized algorithms, the control/estimation precision is insensitive to overly large gains. In contrast to implicit schemes, the proposed algorithms are given by explicit recursions which render the implementation in a digital environment straightforward. By exploiting the pseudo-linear system representation also for the discrete-time algorithm, it has been shown that the robust exact differentiator can be implemented as a current estimator in an output-feedback configuration. In this configuration, the unknown system state variables, as well as the external matched perturbation, are estimated based on the most recent measurements and consequently more tight control of the output can be achieved. The practical applicability of the approach was demonstrated on a hydraulic test rig.

In addition to the considered algorithms, the proposed discretization scheme seems applicable to other algorithms such as the generalized STA or fixed time convergent algorithms. The investigation of the global stability properties of the discretized homogeneous differentiators forms another open research topic.

The third part dealt with the design of novel continuous-time homogeneous state feedback controllers. The design of the controllers relies on the assignment of homogeneous eigenvalues to the closed-loop dynamics. The resulting family of controllers also includes novel arbitrary-order sliding mode controllers. In the case of a second-order system, the selection of negative homogeneous eigenvalues is necessary and sufficient for global asymptotic stability of the closed-loop system. For higher-order systems, negative homogeneous eigenvalues are necessary for asymptotic stability. The controllers are easy and straightforward to implement in a discrete time environment by adopting the developed approach.

Bibliography

[1] V. I. Utkin, *Sliding modes in control and optimization.* Springer Science & Business Media, 2013.

[2] Y. Shtessel, C. Edwards, L. Fridman, and A. Levant, *Sliding mode control and observation.* Springer, 2014, vol. 10.

[3] A. Sabanovic, L. M. Fridman, and S. K. Spurgeon, *Variable structure systems: from principles to implementation.* IET, 2004, vol. 66.

[4] C. Edwards and S. Spurgeon, *Sliding mode control: theory and applications.* Crc Press, 1998.

[5] V. Utkin, "Variable structure systems with sliding modes," *IEEE Transactions on Automatic control*, vol. 22, no. 2, pp. 212–222, 1977.

[6] K. D. Young, V. I. Utkin, and U. Ozguner, "A control engineer's guide to sliding mode control," *IEEE transactions on control systems technology*, vol. 7, no. 3, pp. 328–342, 1999.

[7] V. Utkin, J. Guldner, and J. Shi, *Sliding mode control in electro-mechanical systems.* CRC press, 2009.

[8] V. Utkin and H. Lee, "Chattering problem in sliding mode control systems," in *Variable Structure Systems, 2006. VSS'06. International Workshop on.* IEEE, 2006, pp. 346–350.

[9] I. Boiko, *Discontinuous control systems: frequency-domain analysis and design.* Springer Science & Business Media, 2008.

[10] A. Levant, "Chattering analysis," *IEEE transactions on automatic control*, vol. 55, no. 6, pp. 1380–1389, 2010.

[11] G. Bartolini, A. Ferrara, and E. Usai, "Chattering avoidance by second-order sliding mode control," *IEEE transactions on Automatic Control*, vol. 43, no. 2, pp. 241–246, 1998.

[12] G. Bartolini, A. Ferrara, A. Levant, and E. Usai, "On second order sliding mode controllers," in *Variable structure systems, sliding mode and nonlinear control.* Springer, 1999, pp. 329–350.

[13] A. Levant, "Sliding order and sliding accuracy in sliding mode control," *International journal of control*, vol. 58, no. 6, pp. 1247–1263, 1993.

[14] ——, "Higher-order sliding modes, differentiation and output-feedback control," *International journal of Control*, vol. 76, no. 9-10, pp. 924–941, 2003.

[15] L. Fridman and A. Levant, "Higher order sliding modes as a natural phenomenon in control theory," in *Robust Control via variable structure and Lyapunov techniques*. Springer, 1996, pp. 107–133.

[16] U. Pérez-Ventura and L. Fridman, "When is it reasonable to implement the discontinuous sliding-mode controllers instead of the continuous ones? frequency domain criteria," *International Journal of Robust and Nonlinear Control*, vol. 29, no. 3, pp. 810–828, oct 2018.

[17] B. Wang, B. Brogliato, V. Acary, A. Boubakir, and F. Plestan, "Experimental comparisons between implicit and explicit implementations of discrete-time sliding mode controllers: Toward input and output chattering suppression," *IEEE Transactions on Control Systems Technology*, vol. 23, no. 5, pp. 2071–2075, Sept 2015.

[18] A. Filippov, *Differential Equations with Discontinuous Righthand Sides - Control Systems*. Berlin Heidelberg: Springer Science & Business Media, 2013.

[19] S. P. Bhat and D. S. Bernstein, "Geometric homogeneity with applications to finite-time stability," *Mathematics of Control, Signals and Systems*, vol. 17, no. 2, pp. 101–127, 2005.

[20] U. Itkis, *Control systems of variable structure*. Wiley New York, 1976.

[21] S. Emelyanov, S. Korovin, and L. Levantovsky, "Higher order sliding regimes in the binary control systems," *Soviet Physics, Doklady*, vol. 31, no. 4, pp. 291–293, 1986.

[22] S. Li, X. Yu, L. Fridman, Z. Man, and X. Wang, *Advances in Variable Structure Systems and Sliding Mode Control—Theory and Applications*, ser. Studies in Systems, Decision and Control. Springer International Publishing, 2017.

[23] W. Hahn, *Stability of motion*. Springer, 1967, vol. 138.

[24] E. Bernuau, D. Efimov, W. Perruquetti, and A. Polyakov, "On homogeneity and its application in sliding mode control," *Journal of the Franklin Institute*, vol. 351, no. 4, pp. 1866–1901, 2014.

[25] A. Levant, "Robust exact differentiation via sliding mode technique," *Automatica*, vol. 34, no. 3, pp. 379 – 384, 1998.

[26] Y. Shtessel, M. Taleb, and F. Plestan, "A novel adaptive-gain supertwisting sliding mode controller: Methodology and application," *Automatica*, vol. 48, no. 5, pp. 759–769, 2012.

[27] I. Castillo, L. Fridman, and J. Moreno, "Super-twisting algorithm in presence of time and state dependent perturbations," *International Journal of Control*, pp. 1–14, 2017.

[28] J. A. Moreno and M. Osorio, "A Lyapunov approach to second-order sliding mode controllers and observers," in *2008 47th IEEE Conference on Decision and Control*, Dec 2008, pp. 2856–2861.

[29] R. Seeber and M. Horn, "Stability proof for a well-established super-twisting parameter setting," *Automatica*, vol. 84, pp. 241–243, 2017.

[30] A. Levant, "Higher order sliding: differentiation and black-box control," in *Decision and Control, 2000. Proceedings of the 39th IEEE Conference on*, vol. 2. IEEE, 2000, pp. 1703–1708.

[31] G. F. Franklin, J. D. Powell, and M. L. Workman, *Digital control of dynamic systems*. Addison-wesley Menlo Park, CA, 1998, vol. 3.

[32] Z. Galias and X. Yu, "Euler's discretization of single input sliding-mode control systems," *IEEE Transactions on Automatic Control*, vol. 52, no. 9, pp. 1726–1730, 2007.

[33] ——, "Complex discretization behaviors of a simple sliding-mode control system," *IEEE Transactions on Circuits and Systems II: Express Briefs*, vol. 53, no. 8, pp. 652–656, 2006.

[34] Y. Yan, Z. Galias, X. Yu, and C. Sun, "Euler's discretization effect on a twisting algorithm based sliding mode control," *Automatica*, vol. 68, pp. 203–208, 2016.

[35] Y. Yan, X. Yu, and C. Sun, "Discretization behaviors of a super-twisting algorithm based sliding mode control system," in *Recent Advances in Sliding Modes (RASM), 2015 International Workshop on*. IEEE, 2015, pp. 1–5.

[36] V. Acary and B. Brogliato, "Implicit euler numerical scheme and chattering-free implementation of sliding mode systems," *Systems & Control Letters*, vol. 59, no. 5, pp. 284–293, 2010.

[37] W. Gao, Y. Wang, and A. Homaifa, "Discrete-time variable structure control systems," *IEEE transactions on Industrial Electronics*, vol. 42, no. 2, pp. 117–122, 1995.

[38] Y. Z. Tsypkin and C. Constanda, *Relay Control Systems*. Cork: Cambridge University Press, 1985.

[39] K. J. Åström, "Oscillations in systems with relay feedback," in *Adaptive Control, Filtering, and Signal Processing*. Springer, 1995, pp. 1–25.

[40] I. Boiko, "Oscillations and transfer properties of relay servo systems—the locus of a perturbed relay system approach," *Automatica*, vol. 41, no. 4, pp. 677–683, 2005.

[41] I. Boiko, L. Fridman, A. Pisano, and E. Usai, "Analysis of chattering in systems with second-order sliding modes," *IEEE transactions on Automatic control*, vol. 52, no. 11, pp. 2085–2102, 2007.

[42] I. Boiko, L. Fridman, and M. Castellanos, "Analysis of second-order sliding-mode algorithms in the frequency domain," *IEEE Transactions on Automatic Control*, vol. 49, no. 6, pp. 946–950, 2004.

[43] I. Boiko, L. Fridman, and R. Iriarte, "Analysis of chattering in continuous sliding mode control," in *American Control Conference, 2005. Proceedings of the 2005*. IEEE, 2005, pp. 2439–2444.

[44] I. Boiko, L. Fridman, A. Pisano, and E. Usai, "On the transfer properties of second-order sliding mode control systems," *IFAC Proceedings Volumes*, vol. 41, no. 2, pp. 3823–3829, 2008.

[45] Y. Shtessel, L. Fridman, A. Rosales, and C. B. Panathula, "Practical stability phase and gain margins concept," in *Advances in Variable Structure Systems and Sliding Mode Control—Theory and Applications*. Springer, 2018, pp. 101–132.

[46] A. Rosales, Y. Shtessel, L. Fridman, and C. B. Panathula, "Chattering analysis of HOSM controlled systems: Frequency domain approach," *IEEE Transactions on Automatic Control*, vol. 62, no. 8, pp. 4109–4115, 2017.

[47] A. Rosales, L. Fridman, and Y. Shtessel, "Smc with linear dynamic compensator design: Performance margins approach," in *Decision and Control (CDC), 2014 IEEE 53rd Annual Conference on*. IEEE, 2014, pp. 4759–4764.

[48] A. Rosales and I. Boiko, "Disturbance attenuation for systems with second-order sliding modes via linear compensators," *IET Control Theory & Applications*, vol. 9, no. 4, pp. 526–537, 2014.

[49] M. Kleindienst, M. Reichhartinger, M. Horn, and E. Usai, "An application of computer aided parameter tuning of a super-twisting sliding mode controller," in *Variable Structure Systems (VSS), 2014 13th International Workshop on*. IEEE, 2014, pp. 1–6.

[50] Z. Galias and X. Yu, "Equivalence of two discretization schemes in a simple sliding mode control system," in *Circuits and Systems, 2007. ISCAS 2007. IEEE International Symposium on*. IEEE, 2007, pp. 1677–1680.

[51] B. Wang, X. Yu, and X. Li, "Zoh discretization effect on higher-order sliding-mode control systems," *IEEE Transactions on industrial electronics*, vol. 55, no. 11, pp. 4055–4064, 2008.

[52] Y. Yan, X. Yu, and C. Sun, "Periodic behaviors of a discretized twisting algorithm based sliding mode control system," in *Variable Structure Systems (VSS), 2014 13th International Workshop on*. IEEE, 2014, pp. 1–6.

[53] W.-C. Su, S. V. Drakunov, and U. Ozguner, "An o (t/sup 2/) boundary layer in sliding mode for sampled-data systems," *IEEE Transactions on Automatic Control*, vol. 45, no. 3, pp. 482–485, 2000.

[54] I. Haskara and U. Ozguner, "Estimation based discrete-time sliding control of uncertain nonlinear systems in discrete strict feedback form," in *Decision and Control, 2000. Proceedings of the 39th IEEE Conference on*, vol. 3. IEEE, 2000, pp. 2599–2604.

[55] M. L. Corradini and G. Orlando, "Variable structure control of discretized continuous-time systems," *IEEE Transactions on Automatic Control*, vol. 43, no. 9, pp. 1329–1334, 1998.

[56] O. Huber, V. Acary, and B. Brogliato, "Enhanced matching perturbation attenuation with discrete-time implementations of sliding-mode controllers," in *ECC-13th European Control Conference*. IEEE, 2014, pp. 2606–2611.

[57] D. Mitic and C. Milosavljevic, "Sliding mode-based minimum variance and generalized minimum variance controls with o (t2) and o (t3) accuracy," *Electrical engineering*, vol. 86, no. 4, pp. 229–237, 2004.

[58] G. Bartolini, A. Ferrara, and V. I. Utkin, "Adaptive sliding mode control in discrete-time systems," *Automatica*, vol. 31, no. 5, pp. 769–773, 1995.

[59] G. Bartolini, A. Pisano, and E. Usai, "Chattering reduction in the variable structure control of nonlinear systems with incomplete state availability," in *Control Conference (ECC), 2001 European*. IEEE, 2001, pp. 3528–3533.

[60] O. Kaynak, K. Erbatur, and M. Ertugnrl, "The fusion of computationally intelligent methodologies and sliding-mode control-a survey," *IEEE Transactions on Industrial Electronics*, vol. 48, no. 1, pp. 4–17, 2001.

[61] D. Munoz and D. Sbarbaro, "An adaptive sliding-mode controller for discrete nonlinear systems," *IEEE transactions on industrial electronics*, vol. 47, no. 3, pp. 574–581, 2000.

[62] O. Huber, V. Acary, B. Brogliato, and F. Plestan, "Implicit discrete-time twisting controller without numerical chattering: Analysis and experimental results," *Control Engineering Practice*, vol. 46, pp. 129–141, 2016.

[63] F. A. Miranda-Villatoro, B. Brogliato, and F. Castaños, "Set-valued sliding-mode control of uncertain linear systems: continuous and discrete-time analysis," *SIAM Journal on Control and Optimization*, vol. 56, no. 3, pp. 1756–1793, 2018.

[64] V. Acary, B. Brogliato, and Y. V. Orlov, "Chattering-free digital sliding-mode control with state observer and disturbance rejection," *IEEE Transactions on Automatic Control*, vol. 57, no. 5, pp. 1087–1101, 2012.

[65] B. Brogliato, A. Polyakov, and D. Efimov, "The implicit discretization of the super-twisting sliding-mode control algorithm," in *Variable Structure Systems (VSS), 2018 15th International Workshop on*. IEEE, 2018, pp. 349–353.

[66] A. Polyakov, D. Efimov, and B. Brogliato, "Consistent discretization of finite-time stable homogeneous systems," in *Variable Structure Systems (VSS), 2018 15th International Workshop on*. IEEE, 2018, pp. 360–365.

[67] I. Boiko, "Analysis of closed-loop performance and frequency-domain design of compensating filters for sliding mode control systems," *IEEE Transactions on Automatic Control*, vol. 52, no. 10, pp. 1882–1891, 2007.

[68] A. Rosales, Y. Shtessel, and L. Fridman, "Performance margins in conventional and second order sliding mode controllers," in *Decision and Control (CDC), 2013 IEEE 52nd Annual Conference on*. IEEE, 2013, pp. 3572–3577.

[69] A. Gelb and W. E. V. Velde, *Multiple-input describing functions and nonlinear system design* -. New York: McGraw-Hill, 1968.

[70] J. T. Tou, *Digital and sampled-data control systems.* McGraw-Hill, 1959.

[71] J. Ackermann, "Beschreibungsfunktionen für die analyse und synthese von nichtlinearen abtast-regelkreisen," *at-Automatisierungstechnik*, vol. 14, no. 1-12, pp. 497–504, 1966.

[72] B. C. Kuo, "The z-transform describing function for nonlinear sampled-data control systems," in *Proc. IRE*, May 1960, pp. 941–942.

[73] F. Geiger, "The application of the describing-function method on sampled-data systems," PhD-thesis, in German, Graz University of Technology, University of Technology Graz, 1998.

[74] K. Barth, "Ein graphisches Verfahren zur Ermittlung der Beschreibungsfunktion eines Abtasters mit Halteglied und Nichtlinearität," *at-Automatisierungstechnik*, vol. 14, no. 1-12, pp. 505–513, 1966.

[75] A. V. Oppenheim, A. S. Willsky, and H. Nawab, *Signals and Systems.* London: Prentice Hall, 1997.

[76] C. L. Phillips, J. M. Parr, and E. A. Riskin, *Signals, systems, and transforms.* Prentice Hall Upper Saddle River, 2003.

[77] W. Vetsch, *Existenz und Stabilität von Grenzzyklen in Pulsregelsystemen.* ETH Zurich, 1972.

[78] J. M. Gonçalves, A. Megretski, and M. A. Dahleh, "Global stability of relay feedback systems," *IEEE Transactions on Automatic Control*, vol. 46, no. 4, pp. 550–562, 2001.

[79] E. G. Gilbert and K. T. Tan, "Linear systems with state and control constraints: The theory and application of maximal output admissible sets," *IEEE Transactions on Automatic control*, vol. 36, no. 9, pp. 1008–1020, 1991.

[80] M. Reichhartinger and S. Spurgeon, "An arbitrary-order differentiator design paradigm with adaptive gains," *International Journal of Control*, vol. 91, no. 9, pp. 2028–2042, feb 2018.

[81] H. K. Khalil and L. Praly, "High-gain observers in nonlinear feedback control," *International Journal of Robust and Nonlinear Control*, vol. 24, no. 6, pp. 993–1015, 2014. [Online]. Available: http://dx.doi.org/10.1002/rnc.3051

[82] P. Kokotovic, H. K. Khali, and J. O'Reilly, *Singular Perturbation Methods in Control - Analysis and Design.* Philadelphia: SIAM, 1999.

[83] O. Huber, V. Acary, and B. Brogliato, "Lyapunov stability and performance analysis of the implicit discrete sliding mode control," *IEEE Transactions on Automatic Control*, vol. 61, no. 10, pp. 3016–3030, 2016.

[84] J. A. Moreno and M. Osorio, "Strict Lyapunov functions for the super-twisting algorithm," *IEEE Transactions on Automatic Control*, vol. 57, no. 4, pp. 1035–1040, April 2012.

[85] T. Sanchez and J. A. Moreno, "A constructive Lyapunov function design method for a class of homogeneous systems," in *53rd IEEE Conference on Decision and Control*, Dec 2014, pp. 5500–5505.

[86] R. Seeber, M. Reichhartinger, and M. Horn, "A Lyapunov function for an extended super-twisting algorithm," *IEEE Transactions on Automatic Control*, 2018.

[87] M. Livne and A. Levant, "Proper discretization of homogeneous differentiators," *Automatica*, vol. 50, no. 8, pp. 2007 – 2014, 2014.

[88] A. N. Michel, L. Hou, and D. Liu, *Stability of Dynamical Systems - Continuous, Discontinuous, and Discrete Systems*, 2008th ed. Berlin Heidelberg: Springer Science & Business Media, 2008.

[89] H. Ghane and M. B. Menhaj, "Eigenstructure-based analysis for non-linear autonomous systems," *IMA Journal of Mathematical Control and Information*, vol. 32, no. 1, pp. 21–40, 2013.

[90] S. Chakrabarty, B. Bandyopadhyay, J. A. Moreno, and L. Fridman, "Discrete sliding mode control for systems with arbitrary relative degree output," in *Variable Structure Systems (VSS), 2016 14th International Workshop on.* IEEE, 2016, pp. 160–165.

[91] C.-T. Chen, *Linear system theory and design.* Oxford University Press, Inc., 1998.

[92] J. Burton and A. S. Zinober, "Continuous approximation of variable structure control," *International journal of systems science*, vol. 17, no. 6, pp. 875–885, 1986.

[93] C.-F. Yung and S.-D. Lin, "New smooth approximation of variable structure systems with application to tracking control," in *Proceedings of 1994 33rd IEEE Conference on Decision and Control*, vol. 2, Dec 1994, pp. 1931–1932 vol.2.

[94] D. Hinrichsen and A. J. Pritchard, *Mathematical systems theory I: modelling, state space analysis, stability and robustness.* Springer Berlin, 2005, vol. 48.

[95] J. B. Hoagg and D. S. Bernstein, "Nonminimum-phase zeros-much to do about nothing-classical control-revisited part ii," *IEEE Control Systems Magazine*, vol. 27, no. 3, pp. 45–57, 2007.

[96] K. E. Atkinson, *An introduction to numerical analysis.* John Wiley & Sons, 2008.

[97] S. Boyd and J. Doyle, "Comparison of peak and rms gains for discrete-time systems," *Systems & Control Letters*, vol. 9, no. 1, pp. 1–6, 1987.

[98] M. L. Hautus, "Strong detectability and observers," *Linear Algebra and its applications*, vol. 50, pp. 353–368, 1983.

[99] D. G. Luenberger, "Observing the state of a linear system," *IEEE Transactions on military electronics*, vol. 8, no. 2, pp. 74–80, 1964.

[100] ——, "An introduction to observers," *IEEE Transactions on automatic control*, vol. 16, no. 6, pp. 596–602, 1971.

[101] R. E. Kalman, "A new approach to linear filtering and prediction problems," *Journal of basic Engineering*, vol. 82, no. 1, pp. 35–45, 1960.

[102] J. Moore, "Optimum differentiation using kalman filter theory," *Proceedings of the IEEE*, vol. 56, no. 5, pp. 871–871, 1968.

[103] M. Mboup, C. Join, and M. Fliess, "Numerical differentiation with annihilators in noisy environment," *Numerical algorithms*, vol. 50, no. 4, pp. 439–467, 2009.

[104] W. Perruquetti, T. Floquet, and E. Moulay, "Finite-time observers: Application to secure communication," *IEEE Transactions on Automatic Control*, vol. 53, no. 1, pp. 356–360, Feb 2008.

[105] E. Cruz-Zavala and J. A. Moreno, "Levant's arbitrary order exact differentiator: A Lyapunov approach," *IEEE Transactions on Automatic Control*, pp. 1–1, 2018.

[106] A. Bacciotti and L. Rosier, *Liapunov Functions and Stability in Control Theory*. Springer Berlin Heidelberg, 2005.

[107] E. Cruz-Zavala and J. A. Moreno, "Lyapunov functions for continuous and discontinuous differentiators," *IFAC-PapersOnLine*, vol. 49, no. 18, pp. 660 – 665, 2016, 10th IFAC Symposium on Nonlinear Control Systems NOLCOS 2016. [Online]. Available: http://www.sciencedirect.com/science/article/pii/S2405896316318213

[108] W. J. Firey, "Remainder formulae in taylor's theorem," *The American Mathematical Monthly*, vol. 67, no. 9, pp. 903–905, 1960. [Online]. Available: http://www.jstor.org/stable/2309469

[109] D. Efimov, A. Polyakov, A. Levant, and W. Perruquetti, "Realization and discretization of asymptotically stable homogeneous systems," *IEEE Transactions on Automatic Control*, vol. 62, no. 11, pp. 5962–5969, nov 2017.

[110] J. P. Barbot, A. Levant, M. Livne, and D. Lunz, "Discrete sliding-mode-based differentiators," in *2016 14th International Workshop on Variable Structure Systems (VSS)*, June 2016, pp. 166–171.

[111] A. Levant and M. Livne, "Weighted homogeneity and robustness of sliding mode control," *Automatica*, vol. 72, pp. 186–193, 2016.

[112] A. M. Dabroom and H. K. Khalil, "Discrete-time implementation of high-gain observers for numerical differentiation," *International Journal of Control*, vol. 72, no. 17, pp. 1523–1537, 1999.

[113] M. Reichhartinger, S. Spurgeon, M. Forstinger, and M. Wipfler, "A robust exact differentiator toolbox for matlab®/simulink®," *IFAC-PapersOnLine*, vol. 50, no. 1, pp. 1711–1716, 2017.

[114] S. Diop, J. Grizzle, P. Moraal, and A. Stefanopoulou, "Interpolation and numerical differentiation for observer design," in *Proceedings of the American Control Conference*, vol. 2, 1994, pp. 1329–1329.

[115] J. Zehetner, J. Reger, and M. Horn, "A derivative estimation toolbox based on algebraic methods - theory and practice," in *2007 IEEE International Conference on Control Applications*, Oct 2007, pp. 331–336.

[116] P. J. Antsaklis and A. N. Michel, *A Linear Systems Primer* -. Berlin Heidelberg: Springer Science & Business Media, 2007.

[117] B. Ayalew and B. T. Kulakowski, "Cascade tuning for nonlinear position control of an electrohydraulic actuator," in *American Control Conference, 2006*, June 2006, pp. 6 pp.–.

[118] M. Jelali and A. Kroll, *Hydraulic servo-systems: modelling, identification and control*. Springer Science & Business Media, 2012.

[119] V. I. Zubov, "Systems of ordinary differential equations with generalized-homogeneous right-hand sides," *Izvestiya Vysshikh Uchebnykh Zavedenii. Matematika*, no. 1, pp. 80–88, 1958.

[120] ——, "Methods of A.M. Lypaunov and their application," ERDA Div. Phys. Res., Tech. Rep., 1961.

[121] J. A. Moreno, "Discontinuous integral control for mechanical systems," in *Variable Structure Systems (VSS), 2016 14th International Workshop on*. IEEE, 2016, pp. 142–147.

[122] H. Nakamura, Y. Yamashita, and H. Nishitani, "Asymptotic stability analysis for homogeneous systems using homogeneous eigenvalues," in *Decision and Control, 2006 45th IEEE Conference on*. IEEE, 2006, pp. 4230–4235.

[123] ——, "Homogeneous eigenvalue analysis of homogeneous systems," in *16th IFAC World Congress*, 2005.

[124] E. Bernuau, A. Polyakov, D. Efimov, and W. Perruquetti, "Verification of iss, iiss and ioss properties applying weighted homogeneity," *Systems & Control Letters*, vol. 62, no. 12, pp. 1159–1167, 2013.

[125] A. Levant, "Quasi-continuous high-order sliding-mode controllers," in *Decision and Control, 2003. Proceedings. 42nd IEEE Conference on*, vol. 5. IEEE, 2003, pp. 4605–4610.

[126] A. Polyakov, "Sliding mode control design using canonical homogeneous norm," *International Journal of Robust and Nonlinear Control*, 2018.

[127] V. Torres-González, T. Sanchez, L. M. Fridman, and J. A. Moreno, "Design of continuous twisting algorithm," *Automatica*, vol. 80, pp. 119–126, 2017.

[128] J.-J. E. Slotine and L. Weiping, *Applied Nonlinear Control* -. New York: Prentice-Hall, 1991.

[129] N. Al-Muthairi and M. Zribi, "Sliding mode control of a magnetic levitation system," *Mathematical Problems in Engineering*, vol. 2004, no. 2, pp. 93–107, 2004.